Synaptic Vulnerability in Spinal Muscular Atrophy

Lyndsay M Murray

A thesis submitted for the degree of PhD at the University of Edinburgh

2009

Declaration

I declare that the work described in this thesis and its composition are entirely my own.

…….

Lyndsay M Murray

Acknowledgements

I would like to thank a number of people for making the last three years really interesting and enjoyable.

First and foremost, I'd like to thank my supervisor Tom Gillingwater. I really appreciate the endless support, motivation and opportunities he has given me, along with his seemingly limitless knowledge and ideas. I would like to thank him for designing a great project, always finding time and continually encouraging me.

I would also really like to thank my second supervisor Simon Parson and all the members of the Gillingwater lab for all their ideas, training and technical expertise and making this a fantastic place to work. In particular, Tom Wishart for his exemplary time-management skills, Laura Comley for being exceedingly happy and letting me rant, and Derek Thomson for knowing everything!

I would, of course, like to thank the Anatomical Society of Great Britain and Ireland for my studentship and all associated opportunities.

I would also like to acknowledge the continual encouragement and enthusiasm from my parents and sister, Kirsty. I would really like to thank David for his constant support, patience and making me dinner. Also thanks to my friends in Edinburgh and beyond, in particular Claire and Kevin for always listening.

Abstract

Mounting evidence suggests that synaptic connections are early pathological targets in many neurodegenerative diseases, including motor neuron disease. A better understanding of synaptic pathology is therefore likely to be critical in order to develop effective therapeutic strategies. Spinal muscular atrophy (SMA) is a common autosomal recessive childhood form of motor neuron disease. Previous studies have highlighted nerve- and muscle-specific events in SMA, including atrophy of muscle fibres and post-synaptic motor endplates, loss of lower motor neuron cell bodies and denervation of neuromuscular junctions caused by loss of pre-synaptic inputs. Here I have undertaken a detailed morphological investigation of neuromuscular synaptic pathology in the *Smn-/-;SMN2* and *Smn-/-;SMN2;Δ7* mouse models of SMA. Results imply that synaptic degeneration is an early and significant event in SMA, with progressive denervation and neurofilament accumulation being present at early symptomatic time points. I have identified selectively vulnerable motor units, which appear to conform to a distinct developmental subtype compared to more stable motor units. I have also identified significant postsynaptic atrophy which does no correlate with pre-synaptic denervation, suggesting that there is a requirement for Smn in both muscle and nerve and pathological events can occur in both tissues independently. Rigorous investigation of lower motor neuron development, connectivity and gene expression at pre-symptomatic time points revealed developmental abnormalities do not underlie neuromuscular vulnerability in SMA. Equivalent gene expression analysis at end-stage time points has implicated growth factor signalling and extracellular matrix integrity in SMA pathology. Using an alternative model of early onset neurodegeneration, I provide evidence that the processes regulating morphologically distinct types of synaptic degeneration are also mechanistically distinct. In summary, in this work I highlight the importance and incidence of synaptic pathology in mouse models of spinal muscular atrophy and provide mechanistic insight into the processes regulating neurodegeneration.

Table of Contents

List of Abbreviations

μm	Micrometer
AAL	Abductor auris longus
ACh	Acetyl choline
AChR	Acetyl choline receptor
ALS	Amyotrophic lateral sclerosis
AS	Auricularis Superior
DeSyn	Delayed synapsing
E	Embryonic day (i.e. E16.5 = embryonic day 16.5)
FaSyn	Fast synapsing
FDB	Flexor digitorum brevis
LAL	Levator auris longus
mg	Milli gram
mM	Milli molar
mnd	motoneuron degeneration mouse model
NMJ	Neuromuscular junction
P	Postnatal (i.e. P6 = postnatal day 6)
PCR	Polymerase chain reaction
Pmn	progressive motoneuropathy mouse model
SMA	Spinal muscular atrophy
Smn/SMN/Smn	Murine/human survival motor neuron *gene/*protein
TVA	Transversus abdominis
Wld^S	Wallerian degeneration slow

Chapter 1: Introduction

1.1 Synaptic vulnerability in neurodegenerative disease

It is now widely recognised that uncovering pathogenic mechanisms occurring during the initial and early stages of disease progression will be key to understanding and treating a wide range of human neurodegenerative disorders affecting the central and/or peripheral nervous systems. Amid the great diversity of neurodegenerative conditions known to exist, there is a growing body of evidence suggesting that synapses and distal axonal compartments are common, early and important sub-cellular pathological targets (Raff *et al.*, 2002; Wishart *et al.*, 2006). It is also clear that mechanisms triggering and regulating neurodegenerative pathways in neurons are very much compartmentalised, with distinct sub-cellular mechanisms regulating the breakdown of synapses, axons and cell bodies (Gillingwater and Ribchester, 2001). This is partly based upon the observation that the spontaneously occurring Wallerian degeneration slow (Wld^{S}) mutation can modify the survival of distal axonal and synaptic compartments in the absence of the cell body (Mack *et al.*, 2001; Gillingwater *et al.*, 2006). The therapeutic relevance of such compartmental degeneration is underlined by studies in which genetic or pharmacological manipulations have conferred significant protection on neuronal cell bodies but failed to provide any protection on synaptic or axonal compartments, resulting in no significant improvement in general outcome measures such as life expectancy (e.g. Sagot *et al.*, 1995; Chiesa *et al.*, 2005; Dewil *et al.*, 2007; Gould *et al.*, 2006).

The list of diseases with known synaptic and/or distal axonal involvement now includes hereditary and sporadic neurodegenerative diseases such as Alzheimer's disease (Selkoe, 2002), Huntington's disease (Li *et al.*, 2003), prion diseases (Cunningham *et al.*, 2003), lysosomal storage disorders such as Batten disease (Kielar *et al.*, 2009), auto-immune conditions such as Guillain-Barré syndrome (Willison, 2005), and also after hypoxic injury (Baxter *et al.*, 2008) or exposure to toxins such as snake venom (Prasarnpun *et al.*, 2005). Thus, mechanisms underlying selective vulnerability of synaptic and distal

axonal compartments of neurons have become the focus of much interest from both basic research and clinical therapeutic perspectives.

This phenomenon of synaptic vulnerability appears to extend to the peripheral nervous system, and may therefore have significant impact upon the pathogenesis in peripheral neuropathies, such as motor neuron disease. A growing number of studies have therefore focussed on the importance of peripheral synapses between lower motor neurons and muscle fibres, known as neuromuscular junctions (NMJ), in motor neuron disease pathogenesis. Additionally, the experimental accessibility of NMJs and availability of numerous different animal models of motor neuron disease provides excellent model systems in which to study synaptic and axonal biology and vulnerability *in vivo*.

In this chapter I will review the current literature available detailing the structure and function of the NMJ during development and maturity, and discuss its potential involvement in motor neuron diseases, with particular focus on the childhood motor neuron disease, Spinal Muscular Atrophy (SMA).

1.2 The neuromuscular junction

1.2.1 Structure

Early studies of the NMJ utilised gold and silver stains coupled with light microscopy to reveal the morphology of neuromuscular connections, while the subsequent development and refinement of electron microscopy techniques added detail about sub-cellular organelles and organisation (Kuhne, 1888; Ranvier, 1889; Robertson, 1956). Such studies have generally stood the test of time, and even following the development of fluorescent labelling technology, ideas regarding the structure of the neuromuscular junction (NMJ) have remained relatively unchanged over the past century. The NMJ is principally made up of 3 cell types: the motor neuron, the muscle and the terminal Schwann cell, although recent reports have identified the presence of a fourth cell type, the kranocyte (Grinnell, 1995; Court *et al.*, 2008; Figure 1.1 A). The motor neuron cell body is situated in the ventral horn of the spinal cord from where it projects axons

through the ventral root of the spinal column to its target muscle. The axon projecting from the spinal cord to the muscle fibre is tightly ensheathed by myelin to facilitate efficient signal transduction, contains structural proteins such as neurofilaments to maintain axonal integrity and microtubules to facilitate both retrograde and anterograde transport to and from the cell body and peripheral synapse. Upon entering the muscle region, an individual axon will undergo a degree of intramuscular branching and will ultimately innervate anywhere between 10 and 2000 muscle fibres depending on the motor unit and muscle function (Bradley, 1987; Conwit *et al*., 1999). At the muscle fibre, the neuron forms the pre-synaptic terminal, becoming highly specialised in both structure and function for neurotransmitter release and contains a large number of mitochondria and synaptic vesicles containing the neurotransmitter acetylcholine (ACh). ACh is an excitatory neurotransmitter which is released and binds to ACh receptors (AChRs) in the post-synaptic membrane of the muscle fibre which form the motor end-plate. The post-synaptic endplate is organised into a series of membrane invaginations, known as post-synaptic folds which function to increase the post-synaptic area and thus increase the area available for AChRs. AChRs are found at a high density within the upper half and crest of the post-synaptic folds, and are associated with the post-synaptic apparatus, a network of structural and signalling proteins specialised for efficient signal transduction (Grinnell *et al*., 1995; Sanes and Lichtman, 1999, Hughes *et al*., 2006). This synapse between the motor neuron and muscle is enveloped by terminal Schwann cells, which are thought to provide a protective ensheathment and trophic support at the NMJ, and modulate synaptic transmission (Feng *et al*., 2005). More recently, an additional cell type, termed kranocytes have been identified at the NMJ, and are thought to have a significant role in synaptic development and regenerative processes (Court *et al*., 2008).

1.2.2 Development

The development of the NMJ involves a series of complex interactions between muscle, nerve and glial cells resulting in structural and functional specialisation within all three cell types (For a detailed review, see Grinnell, 1995 and Sanes and Lichtman 1999).

During the process of embryogenesis, all three cell types originate in distinct locations. Myoblasts, deriving from the embryonic mesenchyme of the somites, fuse to form myotubes which constitute primordial muscle fibres (Grinnell, 1995). Nerve independent signalling events, thought to be primarily directed by muscle derived agrin, induce the formation of acetylcholine receptor clusters (Anderson & Cohen 1977, Frank & Fischbach 1979). Motor neurons arise from the progenitors within the ventral neural tube and after differentiation form axons which project to the muscle (Grinnell 1995, Jacob *et al.*, 2001). Axon path-finding is then directed by a complex array of chemo attractant and repellent guidance cues at defined points along the pathway from the spinal cord to the target muscle (Jacob *et al.*, 2001). Upon reaching the muscle fibre, nerve derived agrin induces further AChR clustering and a primary synaptic contact is established. Schwann cells also originate in the neural crest and follow axon tracts to reach the target muscle and although they do not appear to be necessary for axonal guidance during development, they are crucial for synaptic maintenance (Sanes and Lichtman 1999; Woldeyesus *et al.*, 1999, Wolpowitz *et al.*, 2000). Upon reaching the NMJ, Schwann cells differentiate into terminal Schwann cells, and during the first two post natal weeks, they will increase in number to around 3 or 4 (Feng *et al.*, 2005). At this point, the innervation pattern is highly complex with each muscle fibre innervated by a number of axons. During subsequent weeks the process of developmental synapse elimination results in the pruning of excess inputs until the one-to-one pattern of adult innervation is established. The mechanisms regulating synapse elimination are generally unclear although neuronal activity appears to be sufficient, if not necessary (Gillingwater and Ribchester, 2003; Wyatt and Balice-Gordon, 2003; Buffelli *et al.*, 2004).

Concurrent with synapse elimination, the post-synaptic motor endplate also becomes increasingly specialised (Marques *et al.*, 2000). On initial formation, AChRs are distributed uniformly within the endplate zone, forming a plaque like appearance. During synaptic maturation AChRs become increasingly dense in areas directly opposing pre-synaptic terminal, and increasingly diffuse in areas not directly opposing the pre-synaptic terminal. This initially results in the formation of perforations in the

AChR clusters, and ultimately results in the formation of the adult, 'pretzel' like morphology. Concurrent with this, there is a defined transcriptional switch in the subunit composition of the AChR as the embryonic γ subunit is replaced by the adult ε subunit (Martinou and Merlie, 1991). The switch in subunit results in distinct electrophysiological properties and appears to be fundamental to the formation of post-synaptic folds (Missias *et al*., 1997). Again the processes regulating post-synaptic maturation are relatively undefined, although they appear to involve pre- and post-synaptic communication via synaptic activity and neurotrophic regulation (Fox and Umemori, 2006). The time course of the process of synaptic maturation differs between different species, occurring within the first two post natal weeks in mice and generally being complete by around mid-gestation in humans (Hesselmans *et al.*, 1993; Sanes and Lichtman, 1999).

Interestingly, it has been demonstrated in mice that there are subtypes of motor units which are distinct in regards to their embryonic developmental time course (Fast Synapsing; FaSyn, or Delayed Synapsing; DeSyn). Motor units which conform to a FaSyn subtype display AChR clustering and rudimentary synaptic formation at E14.5, while those categorised as DeSyn did not reach the equivalent stage until E16.5 (Pun *et al*., 2002). These distinct developmental subtypes can be distinguished in adulthood by challenge with paralysis induced by botulinum toxin, which induces significant sprouting and ectopic endplate formation in DeSyn muscles but not in FaSyn muscles. These two subtypes thus retain differential properties in the adult but are morphologically indistinguishable.

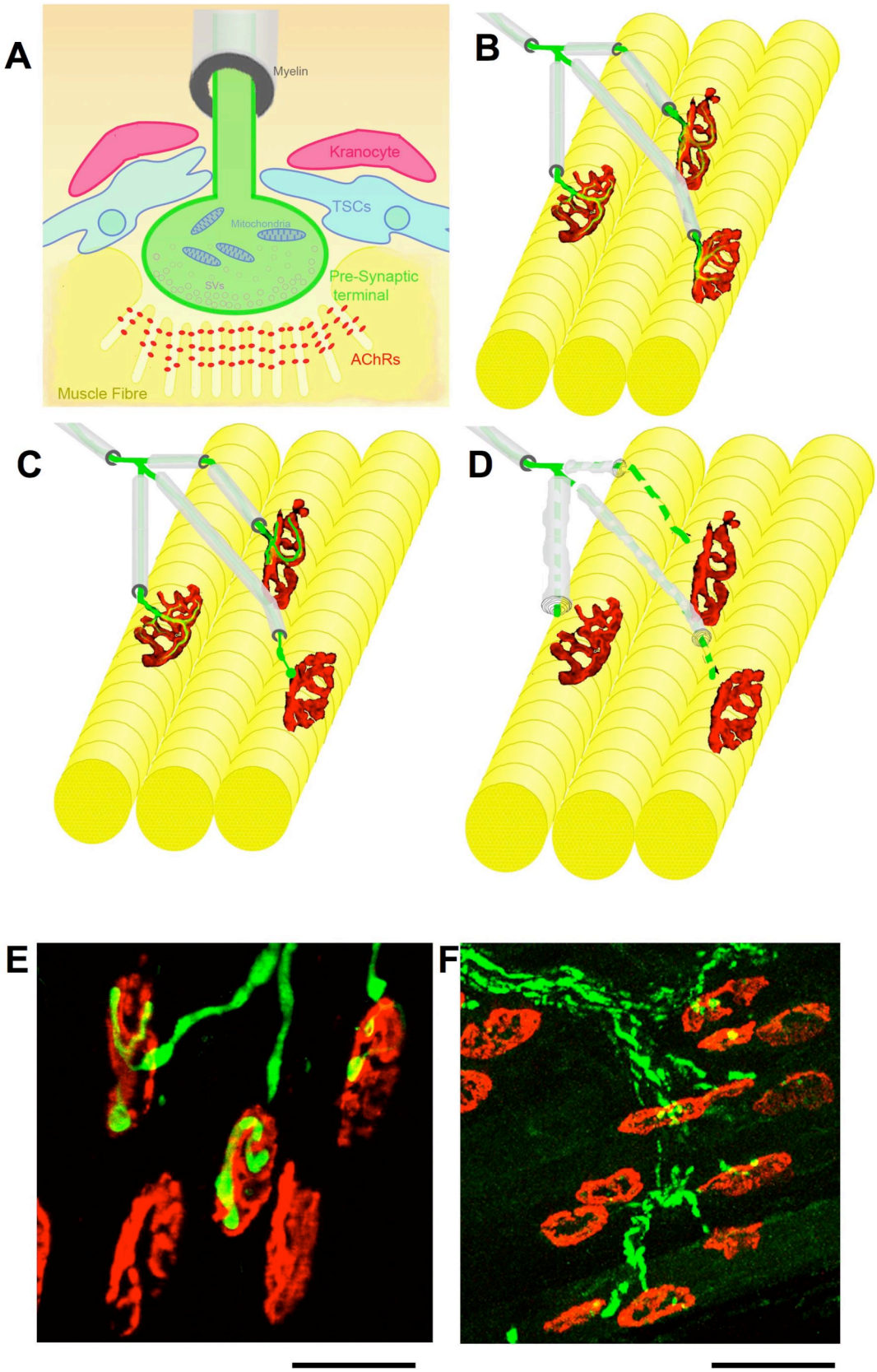
A
Myelin
Kranocyte
TSCs
Mitochondria
SVs
Pre-Synaptic terminal
AChRs
Muscle Fibre
B
C
D
E
F

Figure 1: The neuromuscular junction. A – Schematic diagram illustrating the location of, and relationships between, cell types and organelles at the mammalian NMJ. The distal axon and pre-synaptic motor nerve terminal are shown in green. Note the presence of large numbers of mitochondria and synaptic vesicles in the motor nerve terminal. Also note how the termination of the myelin sheath proximal to the muscle forms the final hemi-node of Ranvier. The post-synaptic muscle fibre is shown in yellow, with characteristic postsynaptic folds and clustering of acetylcholine receptors (AChRs; red). Terminal Schwann cells (TSC) are shown in blue and two NMJ-capping cells (kranocytes) are shown in magenta. B – Schematic diagram illustrating the normal innervation pattern of three muscle fibres (yellow) in an adult mammalian muscle. Note how each muscle fibre is only innervated by a single axon (green; ensheathed by myelin shown in grey) at a single point of synaptic contact (red; AChRs). Also note how each pre-synaptic motor nerve terminal branches at the endplate resulting in a mirror image of the underlying AChRs. C,E – Schematic diagram (C) and representative confocal micrograph (E; taken from a late-symptomatic *wasted* mouse muscle immunohistochemically labeled to reveal 150ka neurofilament proteins, green and AChRs, red) illustrating the morphological correlates of dying-back pathology at the NMJ. Note how there is a gradual retraction of pre-synaptic motor nerve terminals from post-synaptic endplates, rendering muscle fibres denervated in the absence of any major fragmentation of neuronal processes or a breakdown of the myelin sheath. Dying-back pathology occurs over a typical time-course of several days or weeks. D, F - Schematic diagram (D) and representative confocal micrograph (F; taken from a wild-type mouse 24 hours after axotomy immunohistochemically labeled to reveal 150ka neurofilament proteins, green and AChRs, red) illustrating the morphological correlates of Wallerian degeneration at the NMJ. Note how there is a gross, in situ fragmentation of pre-synaptic motor nerve terminals and distal axons as well as a loss of integrity of the myelin sheath. Wallerian degeneration occurs over a typical time-course of several hours. (*Scale bars; 40µm (E), 50µm (F)).*

1.3 The NMJ in motor neuron disease

Due to the observation that synapses appear specifically vulnerable in a range of neurodegenerative diseases, the neuromuscular junction phenotype in motor neuron disease is of great interest. The term motor neuron disease can be used to describe a wide range of heterogeneous disorders resulting from the degeneration of motor neurons and atrophy of associated skeletal musculature. A range of subtypes are observed depending on the motor neuron subset affected, for example purely upper motor neuron involvement, projecting from the motor cortex to the spinal cord (primary lateral sclerosis; Singer *et al*., 2006), purely lower motor neuron involvement, projecting from the spinal cord to muscle (spinal muscular atrophy; Monani *et al*., 2005) or both upper and lower motor neuron involvement (amyotrophic lateral sclerosis; Cleveland and Rothstein, 2001). While a number of atypical subsets of this disease exist, amyotrophic

lateral sclerosis and spinal muscular atrophy remain the most common forms of motor neuron disease and thus the best characterised. In this, and the following section I will review the current literature about amyotrophic lateral sclerosis and spinal muscular atrophy with particular reference to what is known about the involvement of NMJ pathology.

1.3.1 ALS: incidence and aetiology

Amyotrophic lateral sclerosis (ALS) is the most common form of adult onset motor neuron disease, with a typical onset late in adult life (ca.50-60 years old) and a prevalence of 1 in 50,000 (for reviews see Rothstein, 2009). It is a fatal neurodegenerative disease characterised by progressive paralysis resulting from the selective death of both upper and lower motor neurons (Cleveland & Rothstein, 2001). The genetic background to ALS remains complex, with around 5-10% of cases being familial and the remaining 90-95% of sporadic cases having an unknown aetiology (Schymick *et al.*, 2007). However, the underlying genetics of familial ALS cases have begun to shed light on the underlying cellular mechanisms, with numerous genetic mutations now identified as being causative for various different forms of ALS. For example, approximately 20% of familial ALS cases are caused by mutations in the SOD1 gene (Rosen *et al.*, 1993). More recent discoveries have implicated other genes, including TDP-43 (a DNA/RNA binding protein; Sreedharan *et al.*, 2008), FUS (a DNA/RNA binding protein; Vance *et al.*, 2009; Kwiatkowski *et al.*, 2009; Chio *et al.*, 2009) and VAPB (a membrane protein found in plasma and intracellular vesicle membranes; Nishimura *et al.*, 2004; Kanekura *et al*., 2006). The identification of the underlying genetic components of ALS has allowed the development of animal models of the disease (such as mice, rats, zebrafish and *Drosophila*; Gurney *et al.*, 1994; Nagai *et al.*, 2001; Lemmens *et al.*, 2007; Ratnaparkhi *et al.*, 2008), which have been critical for uncovering morphological and molecular pathogenic events *in vivo*. Such models have allowed investigations into the initiating events in disease pathogenesis and there is now mounting evidence that pathological changes at the neuromuscular junction can be detected early in the disease process.

1.3.2 The NMJ as an early pathological target in animal models and human ALS patients

Early studies on human patient material suggested that histological and electrophysiological changes associated with the NMJ were present in ALS (Tsukihata *et al.*, 1984; Maselli *et al.*, 1993). However, it was only with the development and analysis of rodent models of ALS (e.g. the $SOD1^{G93A}$ mouse which displays numerous ALS-associated symptoms; Gurney *et al.*, 1994) that researchers were able to accurately examine the contribution of NMJ breakdown during the early stages of ALS pathogenesis. High-resolution analysis of NMJs in $SOD1^{G93A}$ mice at early- and late-symptomatic stages revealed significant synaptic degeneration prior to the onset of clinical symptoms and motor neuron cell body loss (Fischer *et al.*, 2004). In these mice 40% of motor endplates were devoid of pre-synaptic motor nerve terminals at 47 days old although mice of the same age showed no loss of lower motor neuron cell bodies in the ventral horn of spinal cord and the mice didn't become clinically weak until 80 days old. In addition, microglial and astrocytic activation around motor neurons were not identified until later stages of the disease. These findings, supported by other prior and subsequent studies using $SOD1^{G93A}$ mice; e.g. Frey *et al.*, 2000; Schaefer *et al.*, 2005, led Fischer and colleagues to classify ALS as a "distal axonopathy" (Fischer *et al.*, 2004), with "dying-back" morphological characteristics distinguishing the process from ther neurodegenerative pathways known to be capable of bringing about the breakdown and loss of NMJs (e.g. Wallerian degeneration; see section 1.5).

The early vulnerability of NMJs in mouse models of ALS is not restricted to the $SOD1^{G93A}$ mouse, thus providing strong evidence for the common involvement of NMJs in many forms of ALS. For example, other studies have identified NMJ pathology at early stages of disease progression in motoneuron degeneration (mnd) mice and progressive motoneuropathy (pmn) mice (Frey *et al.*, 2000; Ferri *et al.*, 2003). More recent work on non-rodent models of ALS has provided additional evidence supporting

the notion that NMJs represent important and early pathological targets. For example, analysis of NMJs in dogs with hereditary canine spinal muscular atrophy (HCSMA) has revealed functional deficits at pre-symptomatic ages (Rich *et al.*, 2002). Expression of mutant $SOD1^{G85R}$ in *Caenorhabditis elegans* generates locomotor defects resulting from pathological changes at neuromuscular synapses, including dysfunction of the synaptic vesicle machinery (Wang *et al.*, 2009a). Similarly, studies of VAPB in *Drosophila* have identified important roles in synaptic remodeling and synaptic function at the NMJ (Chai *et al.*, 2008). Depletion of TDP-43 in *Drosophila* has also been shown to induce locomotor defects associated with pathological modifications at the NMJ (Feiguin *et al.*, 2009).

The ability to validate the findings from these animal models in human patients is restricted by the availability of good quality muscle samples (containing NMJs) from human patients at pre- or early-symptomatic stages of the disease. Post-mortem material is almost always from end-stage patients, where it is virtually impossible to identify early and important pathological changes in the neuromuscular system with any accuracy or reliability. However, one case study has been reported from a 58-year-old male ALS patient with a 6-month history of weakness and muscle wasting who died unexpectedly during a minor surgical procedure (Fischer *et al.*, 2004). In this patient, evidence of a "distal axonopathy" was present with denervation characteristics present in muscle alongside an absence of axonal degeneration in ventral roots or degenerative changes in the spinal cord (Fischer *et al.*, 2004).

Taken together, this body of evidence provides strong support for the hypothesis that NMJs are early and important pathological targets in many forms of ALS. However, it should be noted that NMJ vulnerability may not play a key role in all forms of ALS, as evidence has been presented from an ALS mouse model generated via consumption of cycad seed flour, where changes in lower motor neuron soma preceded denervation at the NMJ (Lee *et al.*, 2009).

The clinical relevance of NMJ vulnerability in ALS has been highlighted by several recent *in vivo* studies where a complete therapeutic rescue of lower motor neuron soma or improvement in muscle strength, but failure to concomitantly protect NMJs, offered minimal improvements in overall outcome measures such as lifespan. Both pharmacological and genetic approaches have been used in these experiments, including genetic ablation of the apoptotic regulator bax (Gould *et al.*, 2006), pharmacological inhibition of epigenetic chromatin remodelling (Rouaux *et al.*, 2007), pharmacological inhibition of the stress responsive protein kinase p38MAPK (Dewil *et al.*, 2007), delivery of neurotrophic factors such as GDNF (Suzuki *et al.*, 2007), and treatment with a soluble activin type IIB receptor to prevent myostatin induced muscle growth inhibition (Morrison *et al.*, 2009). These studies underline the importance of treating the site at which pathology originates in order to deliver meaningful therapeutic intervention in ALS. They also offer strong additional support to the idea that NMJs are one of the major sites of early pathological changes in ALS.

1.4 Spinal Muscular Atrophy

1.4.1 Incidence and Aetiology

Spinal muscular atrophy (SMA) is a childhood form of autosomal recessive motor neuron disease caused by mutations in the survival motor neuron (*SMN*) gene. SMA is the most common genetic cause of mortality in children, affecting 1:6000-10,000 live births (Pearn *et al.*, 1978; Wirth *et al*. 2006; Lunn & Wang, 2008). SMA occurs in one of four types which are defined by the age of onset and motor mile stones reached (Monani, 2005; Wirth *et al*., 2006; Farrar *et al*., 2009). SMA type I has an onset under 6 months of age. Affected individuals will never be able to sit unaided and death occurs prior to 2 years of age. SMA type II has an onset of between 6 and 18 months and patients will sit unaided but not walk. SMA type III patients have an onset of between 18 months and early adolescence. Patients are able to initially able stand and walk and although they have a normal lifespan, are likely to be wheelchair bound by adulthood. SMA type IV is characterised by an adult onset and although patients may experience significant muscle weakness later in life, this form of the disease is comparatively mild

and life span is generally normal. A further severe type of SMA has been suggested (type 0), which has a prenatal onset (Russman, 2007). This form of the disease is thought to be rare and as such, has not been extensively described.

In contrast to ALS, SMA is characterised by a specific loss of lower motor neurons (rather than upper and lower motor neurons) and atrophy of the associated skeletal musculature. Clinically, SMA is defined by progressive symmetrical weakness of skeletal musculature in the arms, legs and trunk. Postural muscles in the body trunk are generally more severely affected, with a marked sparing of motor units in the diaphragm and extra-occular muscles (Farrar *et al*., 2009). Alongside locomotor defects, patients experience difficultly sucking and swallowing and respiratory difficulties (Russman, 2007). Cognitive function and sensory neural systems are thought to be spared (von Gontard *et al*., 2002; Farrar *et al*., 2009).

1.4.2 SMA, SMN and animal models

The classification and diagnosis of SMA has been greatly enhanced by the identification of the causative gene: *SMN* (Lefebvre *et al*, 1995). Smn is a ubiquitously expressed protein and its best documented role is in assembly of the essential components of the spliceosomal machinery, required for the removal introns during protein translation (Chari *et al*., 2009). It is currently unclear how reduction of a ubiquitous protein results in neuromuscular specific pathology, although it has been suggested that Smn may have additional axon/muscle specific roles that are critical for neuromuscular function (Burghes, 2008; Burghes and Beattie, 2009). Multiple copies of the *SMN* gene are present in the human genome: one *SMN1* (telomeric copy) and several *SMN*2 (centromeric copies). The two genes are almost identical (differing by only five nucleotides; Lefebvre *et al.*, 1995). *SMN1* encodes a 38kDa protein (Smn) that is widely expressed in tissues throughout the body and localises to the nucleus and cytoplasm of all cells (Francis *et al.*, 1998). The vast majority (~95%) of human SMA cases are caused by a homozygous deletion in *SMN1* (Lefebvre *et al.*, 1995). As complete loss of Smn protein is incompatible with life, the presence of at least one copy of the *SMN*2

gene is required for patients to survive beyond birth. However, *SMN*2 is not capable of fully replacing the loss of *SMN1* as it undergoes alternative splicing producing a truncated mRNA isoform, the transcript of which (mostly lacking exon 7) is rapidly degraded (for review see Burghes & Beattie, 2009). SMA is therefore the result of low levels of Smn protein and the copy number of *SMN*2 therefore determines disease severity.

Our clear understanding of the molecular genetic basis of SMA has facilitated the development of a wide range of different animal models of SMA, including a diverse range of mouse models. A significant problem experienced during the generation of animals models is that all animals, other than humans and higher primates, have only one copy of Smn, with loss being incompatible with life. To circumvent the embryonic lethality due to loss of Smn, two approaches have been commonly employed: conditional loss of Smn directed to specific tissues, or introduction of various Smn transgenes on the Smn knockout background (Table 1.1). Currently, the most commonly used are rodent models genetically engineered to express low levels of Smn protein from a human *SMN*2 transgene whilst silencing endogenous expression from the mouse *SMN* gene, with or without the presence of an additional Δ7 transgene (*Smn-/-;SMN2* mice, Monani *et al.*, 2000; *Smn-/-;SMN2;*Δ*7* mice, Le *et al.*, 2005). These mice model a severe form of SMA, with disease onset occurring around postnatal day 2 (P2) and death by P5/P6 in *Smn-/-;SMN2* mice (Monani *et al.*, 2000). This time-course is extended by around a week in the presence of the Δ7 transgene (Le *et al.*, 2005). Other mouse models have been generated, reducing Smn protein levels by a variety of different means (Table 1.1). More recently, SMA models have been reported in zebrafish (McWhorter *et al.*, 2003; Winkler *et al.*, 2005; Boon *et al.*, 2009), *Drosophila* (Chan *et al.*, 2003; Rajendra *et al.*, 2007; Chang *et al.*, 2008) and *Caenorhabditis elegans* (Briese *et al.*, 2009).

Whilst the genetic basis of SMA is well established, the precise role(s) of *SMN* and its protein product (Smn) in bringing about the selective breakdown of the neuromuscular system remain unknown. The key role played by Smn in pre-mRNA splicing has led to

the suggestion that splicing defects lead to breakdown of the neuromuscular system in SMA (Zhang *et al.*, 2008). However, detailed examination of the temporal characteristics of splicing changes in two mouse models of SMA suggest that splicing defects occur only during late stages of the disease, and are therefore unlikely to contribute to SMA pathogenesis (Baumer *et al.*, under review). Alternative hypotheses for a mechanism of action have also been proposed, some focused on the role of Smn in transport of mRNA in neurons (for review see Burghes & Beattie, 2009), others postulating that Smn has additional neural and/or muscle specific functions (Giavazzi *et al.*, 2006; Rajendra *et al.*, 2007; Setola *et al.*, 2007). The variety of SMA models now available should help elucidate both the cellular function of Smn and the mechanisms by which its loss results in SMA. For example, such models will facilitate studies aimed at identifying the initiating events in SMA pathogenesis and identifying the primary site of pathology. For this reason, defining the involvement of neuromuscular junction pathology will likely be of great importance.

Table 1.1: Available mouse models of SMA

Model	Genetics	Life Span	Reference
Reduced Smn levels			
Smn KO	Disruption of mSmn exon 2 (Schrank *et al*.) or exon 7 (Hseish-Li *et al*.)	~E3.5-6.5	Schrank *et al.*, 1997; Hseish-Li *et al.*, 2000;
Smn+/-	Heterozygous loss of Smn	12 months+	Jablonka *et al.*, 2000
Smn-/-;SMN2^{low}	KO mSmn; insertion of 2 copies of hSMN2	4-6 days	Monani *et al*., 2000
Smn-/-;SMN2 ^{high}	KO mSmn; insertion of 16 copies of hSMN2	300 days+	Monani *et al*., 2000
Smn-/-;SMN2;Δ7	KO mSmn; insertion of 2 copies of hSMN2; Insertion of mSmn lacking exon7	14 days	Le *et al.*, 2005
Smn-/-;SMN2;Smn^{A2G}	KO mSmn; insertion of 2 copies of hSMN2; Insertion of 11 copies of hSMN^{A2G}	227 days	Monani *et al.*, 2003
Smn$^{\Delta7/\Delta7}$;SMN2	Disruption of mSmn exon 7 Insertion of hSMN2	Variable: 10 days – normal survival	Hseish-Li *et al.*, 2000
Tissue specific Smn expression alteration			
Smn^{f7};HSA^{CRE}	Cre-lox excision of Smn exon 7 targeted to muscle	33 days	Cifuentes *et al*., 2001
Smn^{f7};NSE^{CRE}	Cre-lox excision of Smn exon 7 targeted to neurons	25 days	Frugier *et al.*, 2000
Smn-/-;SMN2^{low}; HSA69-SMN$^{+/+}$	*Smn-/-;SMN2*^{low} background with Smn expression restored *exclusively* in muscle	3.5 days	Gavrilina *et al*., 2008
Smn-/-;SMN2^{low}; PRP92-SMN$^{+/+}$	*Smn-/-;SMN2*^{low} background with Smn expression restored *predominantly* in neural tissue	210 days	Gavrillina *et al.*, 2008

***Abbreviations**: KO – knock out; mSmn – murine Smn gene; hSmn – human SMN gene; PRP- human prion protein gene, predominantly neural expression; HSA – Human Skeletal Actin – exclusively muscle expression; NSE - rat neural specific enolase gene.*

1.4.3 *NMJ pathology in SMA*

As for ALS, many early studies on human SMA patient material identified electrophysiological changes consistent with a disruption of NMJ connectivity and denervation of skeletal muscle (Mishra *et al.*, 2004; Swoboda *et al.*, 2005). Further research to examine the contribution of NMJs to SMA pathogenesis in human material has been hampered by the end-stage nature of post-mortem material as well as a limited

supply of material suitable for high-resolution analyses of NMJ structure and/or function. For this reason, animal models have once again proven to be powerful tools for investigating the incidence and importance of NMJ pathology in SMA (Swoboda *et al.*, 2005).

Experimental evidence that a breakdown of connectivity at the NMJ may occur in SMA came from important initial studies using mouse models. A significant denervation of NMJs (evidenced by vacant post-synaptic endplates on skeletal muscle fibres) was reported in mice at the end-stage of disease, alongside significant accumulations of neurofilament proteins in distal axons and motor nerve terminals (Frugier *et al.*, 2000; Cifuentes-Diaz *et al.*, 2002). However, the ability to draw parallels between these findings and events likely to be occurring in human patients was compromised by the fact that this mouse model (*Smn*^{F7}/*Smn*$^{\Delta 7}$, *NSE-Cre*$^{+}$) carries a deletion of *SMN* exon 7 directed to neurons using the Cre–loxP system, thereby having a genetic status distinct from that which causes human SMA. Interestingly however, the morphological correlates of motor nerve terminal loss reported in the *Smn*^{F7}/*Smn*$^{\Delta 7}$, *NSE-Cre*$^{+}$ mouse models of SMA appear very similar to those described in ALS mouse models (c.f. Cifuentes-Diaz *et al.*, 2002; Fischer *et al.*, 2004; Schaefer *et al.*, 2005;). This suggests that both forms of motor neuron disease are distal axonopathies, potentially united by the presence of "dying-back" pathways. Despite this correlation, there is a clear lack of detailed studies regarding the incidence and importance of NMJ pathology in SMA. Additionally, there are a number of outstanding questions in SMA research, specifically, in which tissue does pathology originate - muscle or nerve, and to what extent does abnormal development of the neuromuscular system contribute to neuromuscular pathology. Together these questions will be fundamental in increasing our understanding of SMA pathogenesis and in the development of viable and effective therapeutic strategy.

1.4.4 Nerve or muscle?

A fundamental and ongoing question in SMA research is which tissue is the primary target: muscle and/or nerve (Vrbová, 2008). The development and survival of motor neurons and muscle are highly integrated, with each tissue being mutually dependant on the other for maintenance (for review see Navarrette and Vrbová, 1993). This inevitably makes identifying the primary site of pathology in SMA a great challenge.

A logical experiment is the creation of transgenic animals which selectively lose Smn expression in either muscle or nerve. Initial attempts at this, employing cre-lox technology to selective ablate Smn expression in either muscle or nerve, indicated Smn was required in both tissues and deletion in either tissue led to a severe degenerative phenotype (Frugier 2000; Cifuentes 2001; Table 1.1). However, due to the general house keeping functions of Smn and the embryonic lethality of Smn knockouts, it is perhaps not surprising that complete ablation of Smn expression in given tissue results in associated pathological changes. More recent attempts have been based upon restoring Smn function to specific tissues on the *Smn-/-;SMN2* background (Gavrilina *et al.*, 2008). The introduction of high levels of Smn in muscle had minimal phenotypic affects, suggesting a loss of Smn in muscle cannot be solely responsible for the neuromuscular degeneration in SMA. Restoring Smn expression in neural tissue resulted in a significant improvement in life span, with mice which survived up to 210 days. While this result demonstrates a clear requirement for Smn in motor neurons, a modest increase in Smn expression was also seen in muscle, meaning a simultaneous requirement for Smn in muscle and nerve cannot be eliminated (Table 1.1).

Studies utilising *drosophila* models of SMA have indicated that Smn is found post-synaptically at the NMJ and is also sarcomeric protein with a significant role in myofibril formation (Rajendra *et al.*, 2007; Chang *et al.*, 2008). To study the intrinsic properties of SMA muscle, myoblasts from patients have been cultured in both the presence and absence of motor neurons. Samples from type I patients display abnormalities which are consistent with abnormal muscle growth and development (Guettier-Sigrist *et al*., 2001; Arnold *et al*., 2004; Martínez-Hernández *et al*., 2009; see

section 1.4.4). Culture of myoblasts from SMA patients with rat embryonic motor neurons resulted in a significant reduction in survival compared with cultures from other peripheral neuropathies and controls subjects (Braun *et al.*, 1995). Interestingly they noted that cultures of SMA muscle induced apoptotic cell death of rat embryonic motor neurons, underlining the fact that defects in muscle could conceivable cause the SMA phenotype (Guettier-Sigrist *et al.*, 2002). The authors speculate that there may be some deficiency in nerve-muscle trophic signalling which prevents NMJ maintenance (Guettier-Sigrist *et al.*, 2001).

The experiments detailed above may perhaps imply that loss of Smn can cause pathology in both muscle and nerve. Studies in *drosophila* SMA models have revealed significant NMJ defects when Smn is lost from either muscle or nerve (Chan *et al.*, 2008). There is therefore a potential requirement for Smn in both tissues, but further work is required to directly address this question.

1.4.5 Developmental or degenerative disorder?

Given the early onset of SMA in its most severe form, developmental pathways could potentially play an important role in neuromuscular vulnerability. It is possible that developmental abnormalities could *precede* pathological onset and lead to intrinsic abnormalities to the neuromuscular system structure and function which pre-disposes the system to post-natal degeneration. Studies investigating the expression of Smn protein report high levels during cellular differentiation, thus suggesting Smn could have a role in developmental pathways (Gabanella *et al.*, 2005). Using cultured neurospheres from *Smn-/-;SMN2* mice, Shafey and colleagues demonstrated low Smn levels result in defects in neuronal differentiation and neuritogenesis (Shafey *et al.*, 2008). Additional work in vitro has shown Smn accumulates in growth cones (Fan and Simard, 2002) and that reduced levels decrease axon outgrowth and growth cone size, and have attributed this to defective B-actin transport (Rossoll *et al.*, 2003). Together this data suggests that reduced Smn levels could cause defects motor neuron outgrowth and path-finding making it possible that these defects underlie pathology in SMA. Work in both

zebrafish and xenopus SMA models supports this theory, noting abnormalities such as truncations and increased axon branching (McWhorter *et al.*, 2003, Ymlahi-Ouazzani *et al.*, 2009).

A more limited body of work has investigated muscle development in spinal muscular atrophy. Work on cultured myoblasts from SMA patients has shown that myoblast fusion into myotubes is delayed in samples from SMA patients compared to samples from other peripheral neuropathies and normal controls, with a reduction in acetylcholine receptor clustering in response to agrin (Guettier-Sigrist *et al.*, 2001; Arnold *et al.*, 2004). Furthermore, a recent study on human embryonic muscle reported a general decrease in myotube diameter in samples from SMA patients (Martínez-Hernández *et al.*, 2009). Myotube growth and maturation did not follow the same patterns seen in control samples, indicating muscle development may be abnormal. This work suggests that there may be intrinsic abnormalities in muscle development in SMA which may have post-natal implications for the stability of the neuromuscular system.

Together these findings highlight the requirement for studies on pre-symptomatic neuromuscular development in mammalian systems, to ascertain whether low Smn levels can cause developmental defects which can, to some degree, account for the post natal degenerative phenotype observed.

1.5 Complexity of different cellular pathways resulting in NMJ loss: dying-back pathology versus Wallerian degeneration

To aid our understanding of the mechanisms of neurodegenerative disease, including motor neuron disease, there is a clear requirement to understand the mechanisms regulating and perturbing synaptic vulnerability. Despite the fact that many different neurodegenerative diseases are united by synaptic vulnerability, there are a number of quite morphologically distinct processes by which a synapse can degenerate, i.e. Wallerian Degeneration and dying-back neuropathy (Figure 1.1 C-F). For example, several different motor neuron diseases and sensory neuropathies are thought to

primarily occur via dying-back pathways (Schmalbruch *et al.*, 1991; Frey *et al.*, 2000; Cifuentes-Diaz *et al.*, 2002; Fischer *et al.*, 2004; Keswani *et al.*, 2006), whereas conditions such as multiple sclerosis and degeneration after traumatic nerve injury are more commonly associated with Wallerian degeneration (Ferguson *et al.*, 1997; Perry and Anthony, 1999; Gillingwater and Ribchester, 2001). Wallerian degeneration is characterised by rapid axonal and synaptic fragmentation associated with disruption and loss of organelles and plasma membranes, breakdown of the axonal myelin sheath, and phagocytosis of synaptic and axonal debris (Figure 1.1 D,F). In stark contrast, dying-back neuropathies are characterised by a wave of degeneration beginning at the distal extremities of the neuron and are devoid of the gross fragmentation associated with Wallerian degeneration (Figure 1.1 C,E).

Despite obvious morphological discrepancies, it has been suggested that common mechanisms regulate morphologically distinct types of synaptic and axonal degeneration (Coleman, 2005). This suggestion is based partly upon the fact that the spontaneous neuroprotective Wallerian Degeneration Slow (Wld^S) mutation (see below) can be protective in a range of conditions, including both traumatic injury (a process which induces traditional Wallerian degeneration of distal axons and synapses) and in characteristic dying-back neuropathies (Mack *et al.*, 2001, Ferri *et al.*, 2003; Gillingwater *et al.*, 2006b). The degree of mechanistic commonality is fundamental when attempting to understand the processes regulating synaptic breakdown. The ability to decipher such mechanisms could potentially allow functional categorisation of neuropathies and broaden the scope of pathogenic insight and therapeutic potential.

1.6 The neuro-protective Wld^S model

Although most studies investigating the mechanisms of synaptic vulnerability are centred around neurodegenerative models, we can also gain great insight by utilising models of neuro-protection. One such neuro-protective model is the spontaneously arising Wallerian degeneration slow (Wld^S) mutant. The Wld^S mutation was identified in 1989 after distal axonal compartments failed to undergo highly characteristic

degeneration following a traumatic nerve injury (Lunn *et al.*, 1989). Subsequent work demonstrated that NMJs were also preserved and retained synaptic function up to 2 weeks after nerve injury (Ribchester *et al.*, 1995). The mutation was ultimately found to be a spontaneous triplication resulting in the formation of a novel chimeric protein comprising the N-terminal fragment of ubiquitination factor E4B (Ube4b) fused to the whole coding region of nicotinamide mononucleotide adenylyltransferase (Nmnat) as well as eighteen amino acids normally contained in the 5' untranslated region (Mack *et al.*, 2001). The resultant chimeric protein has been shown to be neuro-protective in both the central and peripheral nervous systems, in a range animals and culture based models and in response to a wide range of traumatic, toxic and genetic insults (Wang *et al.*, 2001; Ferri *et al.*, 2003; Samsam *et al.*, 2003; Fischer *et al*, 2004; Gillingwater *et al.*, 2006a; Hasbani and O'Malley 2006). The mechanisms by which this nuclear protein can confer synaptic protection to distal axonal and synaptic compartments, even when physically separated from the cell body remain undefined and controversial. For example, even though it is generally accepted that Wld^s is acting through downstream modifications of subcellular pathways that are in some way affecting the persistence of axons and synapse, opinions vary in relation to which component of the Wld^s mutation is specifically responsible i.e. the NMNAT1 portion of the mutation or the N70 UBE4b fragment. Despite this controversy, the Wld^s mutation is of interest for several reasons. Firstly, this mutation clearly demonstrates that synapses and distal axon compartment can control their own fate when physically removed from the cell body. Secondly, due to the diversity of insults it can protect against, it suggests that there is a degree of commonality in the pathways mediating synaptic and axonal degeneration. Finally, it is clearly of interest for its therapeutic potential as if it could be applied exogenously, either via virus or direct application of the protein, it could feasible inhibit neurodegenerative processes. The Wld^s mutation is therefore a useful tool when attempting to understand the mechanisms regulating synaptic vulnerability.

1.7 Aims

From the above introduction covering the current literature available it is clear that there is a rationale and requirement for studies on NMJ pathology in SMA. In this study, I therefore aim to address the following aspects of SMA pathology using established mouse models.

Hypothesis 1: Synaptic pathology is an early and significant event in SMA.

AIM 1: Investigate the incidence and importance of NMJ pathology in mouse models of SMA

a. Examine the occurrence of NMJ loss and NMJ morphology during disease progression in a selection of muscle groups reflecting different subtypes and body locations.
b. Investigate potential selectively vulnerable populations of NMJs in different muscles/muscle areas
c. Investigate and correlate the occurrence and relationship of pre- and post-synaptic pathology in nerve and muscle

Hypothesis 2: Abnormal pre-symptomatic development of the lower motor neuron connectivity pre-disposes the neuromuscular system to subsequent degeneration in SMA.

AIM 2: Determine the contribution of abnormal lower motor neuron development to subsequent degenerative events.

a. Examine pre-symptomatic development of lower motor neuron connectivity with regards to axonal path-finding, branching and establishment of innervation patterns
b. Examine pre-symptomatic gene expression by microarray analysis.

Hypothesis 3: Pathological changes occurring in SMA result in altered gene expression

AIM 3: Attempt to identify pathways contributing to the degeneration of lower motor neurons by microarray analysis of spinal cord at end-stage time points.

Hypothesis 4: Common molecular mechanisms regulate morphologically distinct types of synaptic degeneration.

AIM 4: Investigate the relationship between pathways controlling dying-back neuropathy and Wallerian degeneration

a. Define NMJ phenotype in the *wasted* mouse model of early onset neurodegeneration.
b. Investigate progression of Wallerian degeneration in response to nerve injury in *wasted* mice.

Hypothesis 5: Wld^s mice can give mechanistic insight into degenerative pathways in SMA

AIM 5: Investigate potential correlates between the Wld^s mouse model of neuro-protection and a mouse model of SMA

a. Investigate if proteomic changes identified in Wld^s mice occur in an opposite direction in a mouse model of SMA.
b. Investigate if proteins identified as being altered in Wld^s to can be used toidentify potential biomarkers and gauge pathological progression in SMA?

Chapter 2: Materials and methods

2.1 Colony management

2.1.1 Mouse maintenance

C57Bl/6 and YFP-H mice were maintained as breeding colonies in the animal care facilities in Edinburgh under standard SPF conditions. *Smn*$^{+/-}$*;SMN*2 mice (Jackson labs strain no. 005024) were also maintained as heterozygote breeding pairs in animal care facilities in Edinburgh. *Smn*$^{+/-}$*;SMN*2*;Δ7* (Jackson labs strain no. 005025) breeding pairs were maintained in animal care facilities in Oxford. For this strain, basic dissection of muscle groups was performed by Nick Parkinson and Dirk Bäumer in Oxford and shipped to Edinburgh. All genotyping of this colony was performed in Oxford by Nick Parkinson. Pairs of heterozygous *wasted* mice were kindly provided by Dr Cathy Abbott and a breeding colony was established. Breeding colonies of *YFP-H* mice (Feng *et al.*, 2000) were already established in animal care facilities at the University of Edinburgh and were crossed with *wasted* mice in order to obtain homozygous and heterozygous *wasted* mice, as well as wild-type littermates, endogenously expressing yellow fluorescent protein (YFP) in a subset of neurons. Wld^{s} mice were bought in from Harlan UK. All animal procedures and breeding were performed in accordance with Home Office and institutional guidelines. All mice were housed in a semi-barrier facility and were fed a standard chow diet. Mice older than P6 were sacrificed by intra-peritoneal injection of sodium pentabarbitol or overdose of isofluorane. Mice younger than P6 were chilled on ice and decapitated. All animal procedures were performed in accordance with the licensed authority of the UK Home Office.

2.*1.2 Genotyping*

Wasted and Smn-/-;SMN2 mice were genotyped using the following primers (product sizes in bases pairs are shown in brackets):

Smn knockout (neomycin insert) (280BP)	Forward: CTTGGGTGGAGAGGCTATTC Reverse: AGGTGAGATGACAGGAGATC
Smn wild-type (420 BP)	Forward: TTTTCTCCCTCTTCAGAGTGAT Reverse: CTGTTTCAAGGGAGTTGTGGC
SMN2 (530 BP)	Forward: GCGATAGAGTGAGACTCCATCT Reverse: GACATAGAGGTCTGATCTTTAGCT
Wasted wild-type (450 BP)	Forward: TAGTGGCTCCTTGGAACAG Reverse: CTACTCTCCCTGAATGCCTT
Wasted knockout (320 BP)	Forward: ATAAGCTCCCCAATGGTAGAGAA Reverse: CGCGCCATTCTTGTATTGTT

Product amplification was performed using the following thermocycler programme:

Smn knockout, Smn wild-type, SMN2

Step	Temperature (°C)	Time (Seconds)
1	94	120
2	94	30
3	61	30
4	72	45
		(go to step 2 x 27)
5	72	120

Wasted knockout and wild-type

Step	Temperature (°C)	Time (Seconds)
1	94	300
2	94	15
3	55	30
4	68	40
		(Go to step 2 x 34)

Products were separated by gel electrophoresis and genotype assigned by presence or absence of a band of appropriate size.

YFP (yellow fluorescent protein) status was ascertained by examining ear punches for evidence of YFP-labelled neurons.

Real time quantitative PCR was used to assess copy number of Wld^s and SMN2. The following primers and probes were used for Wld^s and SMN2 genes along with endogenous controls.

Wld^S (NMNAT portion)	Forward: GGCAGTGACGCTCAGAAATTC Reverse: GTTCACCAGGTGGATGTTGCT Probe: 6FAM-TCTACGAGTCCGATGTGCTGTGGAGACA-TAMRA
B-Tubulin:	Forward: GTTCCTGCCATGTTCCGG Reverse: GCCTCGGTGAACTCCATCTC Probe:VIC- CAAGGCTTTCCTGCACTGGTACA-TAMRA
SMN2:	Forward: TTTAGACAAAATCAAAAAGAAGGAAGG Reverse: CACTTTCATAATGCTGGCAGACTT Probe: 6FAM-CTCACATTCCTTAAATTAAG-MGB
Endogenous mouse Smn (exon 1):	Forward: CCAGAAGAAAACCTGCCAAGAA Reverse: GGTTAAATCAATCTATCACCTGTTTCAA Probe: 6FAM- AAGAATGCCACAACTC-MGB

For Wld^S copy number analysis, primers and probes specific to Wld^S and Tubulin were combined within 1 well (Wishart *et al.*, 2007a). For SMN2 copy number analysis primers and probes specific to SMN2 and mouse endogenous Smn were amplified in neighbouring wells. Amplification was performed using the following thermocycler programme.

Stage	Temperature (°C)	Time (Seconds)
1	50	120
2	95	600
3	95	15
4	60	60
		Go to step 3 x40

Relative copy number was established by measuring the cycle number difference for equivalent fluorescence between the gene of interest and control gene during the linear phase of amplification (Wishart *et al*., 2007a).

2.1.3 Nerve axotomy

Mice were anesthetized by inhalation of isofluorane (2% in 1:1 N_2O/O_2). A 2mm incision in the skin was made just above the heel to expose the tibial nerve. Blunt dissection was used to tease away overlying muscle, taking care not to damage neighboring blood vessels. A 1–2mm section of the tibial nerve was then removed which denervates the flexor digitorum brevis and deep lumbrical muscles. The incision was closed with a single suture. Mice were allowed to recover from anesthetic before being returned to standard

cages. All surgical procedures were carried out with the licensed authority of the UK Home Office.

2.*1.4 Paralysis with Botulinum toxin type A*

Botulinum toxin type A (0.5µl/g of a 5ng/ml solution; Sigma) or vehicle control (non-sprouting buffer) was repeatedly injected subcutaneously above each levator auris longus muscle (LAL) at postnatal days 15, 19, 22, 26 and 29 (as previously described; Pun *et al.*, 2002). Technical assistance for these experiments was provided by Derek Thomson. Mice were sacrificed and muscles analysed at P45. Muscles were quantified for presence/absence of collateral terminal sprouting and percentage of ectopic endplates (as described below).

2.2 Muscle preparation and staining

2.2.*1 Whole mount muscle preparation*

The levator auris longus (LAL; from the dorsal surface of the neck), adductor auris longus (AAL; from the dorsal surface of the neck, deep to the LAL); auriculars superior (AS; from the dorsal surface of the neck, deep to the LAL); lumbricals (from the plantar surface of the hind-paw); flexor digitorum brevis (FDB; from the plantar surface of the hind-paw) and/or transversus abdominis (TVA; from the antero-lateral abdominal wall) muscles were dissected in oxygenated mammalian physiological saline (mM: NaCl 120, KCl 5, $CaCl_2$ 2, $MgCl_2$ 1, NaH_2PO_4 0.4, $NaHCO_3$ 23.8, D-glucose 5.6). Muscles were exposed to α-bungarotoxin (BTX), conjugated to tetramethyl-rhodamine isothiocyanate (TRITC-α-bungarotoxin; 5mg/ml, Molecular Probes) or AlexaFluor-647 (5mg/ml, Molecular Probes), to label AChRs for 10 minutes and fixed in 0.1M PBS containing 4% Paraformaldehyde (Electron microscopy science) for 15 minutes.

2.2.2 *Preparation of sectioned muscles*

For muscles sectioned in cross section, muscles were dissected and fixed as described above and embedded in 3% agarose gel. Muscles were then embedded in wax, sectioned on a wax microtome at 10um and mounted on poly-lysine coated slides. Sections were

dewaxed in xylene and rehydrated in ascending alcohol series before processing for immunofluorescence on slides.

2.2.*3 FM4-64FX labelling of neuromuscular synaptic function*

Freshly dissected LAL muscles were loaded with the styryl dye FM4-64FX (FM4-64FX, 2mg/ml: Molecular Probes) using a high K^+ stimulus (Baxter *et al*., 2008). Muscle preparations were exposed to a fixable form of the styryl dye FM4-64 in 95%:5% O_2:CO_2 sparged, high K^+ Krebs' Solution (102 mM Na^+, 50 mM K^+, 2 mM Ca^{2+} , 2 mM Mg^{2+} , 132 mM Cl^-, 23.8 mM HCO^{3-} , 0.4 mM $H_2PO_4^{2-}$, 5 mM D-glucose, 5.5mM HEPES: pH 7.2-7.4) for 10mins. Following rigorous washing, muscles were fixed in 4% formaldehyde/PBS solution (Electron Microscopy Science, Pennsylvania).

2.2.*4 Electrophysiology*

Electrophysiological records were conducted with the technical support of Derek Thomson. FDB muscles were used to obtain intracellular recordings of evoked endplate potentials (EPPs) and spontaneous miniature endplate potentials (mEPPs). Isolated muscles were pinned out in a Sylgard (VWR International, Poole, UK) lined bath and perfused with oxygenated mammalian physiological saline. Muscle contractions were reduced or eliminated by bathing the muscles in 2.5μM μ-conotoxin (μ-CTX) GIIIB (Scientific Marketing Associates, UK) for 30–45 min. 10 muscle fibres per muscle were sampled using microelectrodes filled with 5M potassium acetate (impedance ≈ 40 MΩ), according to standard techniques. Spontaneous and evoked endplate potentials were recorded using Axoclamp 2B amplifiers (Axon Instruments) and stored and analysed on a PC using WinWCP v3.9.5 software (developed and distributed by Dr John Dempster, Strathclyde University).

2.2.*5 Immunocytochemistry*

Whole mount muscles were blocked in 4% bovine serum albumin (BSA) and 1% TritonX in 0.1M PBS for 30min before incubation in primary antibodies (150kDa neurofilament proteins - 1:350 dilution, Chemicon International) overnight. After

washing for 30min in 0.1M PBS, muscles were incubated for 4h in a 1:40 dilution of secondary antibody (swine anti-rabbit FITC: swine anti-rabbit TRITC; Goat anti-mouse FITC; all 1:50, Dako). Muscles were then whole-mounted in Mowoil® (Calbiochem) on glass slides and cover-slipped for subsequent imaging.

Sectioned muscles were processed as above but procedures were carried out on slides and incubation times were reduced to 2 hours (Myosin slow/fast – 1:50, AbCam) and 1 hour (Rabbit anti-mouse FITC, 1:50, Dako). Slides were coverslipped using Mowoil® (Calbiochem) for subsequent imaging.

2.3 Image analysis and quantification

2.3.1 Imaging

Muscle preparations were viewed using either a phase contrast microscope (for muscle measurements), a standard epi-fluorescence microscope equipped with a chilled CCD camera (x10 0.3NA, x40 0.6NA lens; Nikon IX71 microscope; Hammamatsu C4742-95), and/or a laser scanning confocal microscope (BioRad Radiance 2000, x40 1.3NA oil immersion lens; Zeiss Axioskop, x40 1.3NA, x63 1.4NA oil immersion lenses). TRITC-α-BTX-labeled preparations were imaged using 543nm excitation and 590nm emission optics and FITC-labeled preparations utilised 488nm excitation and 520nm emission optics. For confocal microscopy, 488nm, 543nm and 633 laser lines were used for excitation and confocal Z-series were merged using Lasersharp (Biorad) or Image J software. All images were then assembled using Adobe Photoshop.

2.3.2 Montages and reconstructions

Reconstructions of immunocytochemically labelled and YFP-H labelled muscle preparations were produced in Adobe Photoshop software by layering and combining multiple micrographs covering the entire muscle. Individual motor neurons were traced and pseudo-coloured manually in Adobe Photoshop software.

2.3.3 Quantification and statistics

A minimum of 80 endplates from a minimum of 3 fields of view per muscle/muscle band were assessed. Muscles with poor staining and/or damage were excluded from further analysis. Wherever possible, all analysis was performed without the operator knowing the status of the material. For basic occupancy counts, the occupancy of individual NMJs was evaluated by categorising endplates as either fully occupied (neurofilament entirely overlies endplate), partially occupied (neurofilament partially overlies endplate) or vacant (no neurofilament overlies endplate). For correlated pre- and post-synaptic measurements, calibrated individual images of NMJs were imported into ImageJ software (NIH, USA) and split into red (endplate) and green (axon and motor nerve terminal) channels. Each endplate and corresponding motor nerve terminal were manually outlined in ImageJ (see Figure 3.3 A-B) and the software used to calculate total areas. To evaluate the number of neural inputs, the number of axons converging on a single motor endplate were counted. Collateral terminal sprouts were identified by the presence of nerve terminal projections exceeding 2µm in length to exclude the possibility that sprouting was due to ongoing synaptic reorganisation. Ectopic endplates were identified by clusters of acetylcholine receptors under 5µm in diameter. Individual muscle fibre diameters were measured in ImageJ using regions of the muscle where teased fibres were present. Only isolated fibres with no overlapping fibres obscuring their profile were included in these analyses. The number of endplates per axon was quantified by evaluating axon number from deconvolved images. Images were taken approximately 100µm from the endplate area of interest to minimise variability introduced from axon branching occurring adjacent to sites of innervation. All muscles in which the complete area of innervation could not be seen, or additional axons branches were present, were excluded from further analysis. Axon numbers were counted by visualisation in the X-Y plane and scanning up and down through the z-series. This was done at three pre-defined points per image with images re-blinded between each measurement. The average of each three counts was divided by the total number of endplates innervated by the axon bundle to give the average number of axons per endplate. To quantify sprouting, sprouts were categorised as ‘small sprouts’ (those

less than 150μm) or 'super sprouts' (those exceeding 150μm). Sprouts were defined as a neurofilament positive process that did not project to a cluster of AChR receptors. Small sprouts were quantified by counting the number of sprouts in a given field of view expressed in relation to the number of endplates present. A minimum of three fields of view were evaluated for each muscle (AAL/AS) or muscle band (LAL). Super sprouts were quantified by counting the total number of sprouts in a muscle region and divided by the total number of endplates in the relevant region. Endplate maturation was evaluated by categorising endplates as either uniform (even distribution of AChRs), folded (bright bands within the AChR region) or perforated (holes within the AChR staining; see Figure 4.11). Any endplate which was difficult to quantify due to orientation or proximity of other endplates was excluded from further analysis. All data were collected and analysed using GraphPad Prism software.

2.4 Electron microscopy

Muscle/nerve preparations were dissected and pinned out on dental wax before being immersion fixed in 0.1M phosphate buffer containing 4% formaldehyde (electron microscopy sciences) and 2.5% glutaraldehyde (sigma) for 4 hours before post-fixation in 1% osmium tetroxide (sigma) for 45 minutes. Preparations were dehydrated in ascending alcohol series (50%, 70%, 90%, 100%x2) and propylene oxide. Preparations were embedded in Durcupan resin. Ultra-thin sections (75-90nm) were cut and collected on formvar-coated grids (Agar Scientific, UK), stained with uranyl acetate and lead citrate in a LKB 'Ultrostainer' and then viewed in a Philips CM12 transmission electron microscope (TEM).

2.5 Quantitative fluorescent (Li-COR) western blots

Total protein was isolated from the spinal cord of late-symptomatic *wasted* mice and control littermates as well as spinal cord, skin and muscle of *Smn-/-;SMN2* mice and control littermates. Total protein was drawn through a decreasing size of needle (spinal cord) or homogenised with mortar and pestle (skin and muscle). Protein levels were quantified by use of a BCA protein quantification kit according to manufacturers

instructions. Protein was separated by SDS/Polyacrylamide gel electrophoresis on 4-20% pre-cast NuPage 4-12% Bis Tris gradient gels (Invitrogen) and then transferred to PVDF membrane overnight. The membranes were blocked using Odyssey blocking buffer (Li-COR) and incubated with primary antibodies as per manufacturers instructions (BRCA2 – AbCam; βSNAP – BioMol International; DRP2 – courtesy of Calum Sutherland, Dundee University; cABL - AbCam; GDI – ProteinTech Europe; Tubulin - Abcam; UBE1 - AbCam; SMN1 – BD Bioscience; STI – BD Transduction Labs; VDAC1 – GeneTex Inc; ZPR1 – BD Bioscience; all 1:10,000). Odyssey secondary antibodies were added according to manufacturers instructions (Goat anti rabbit IRDye 680 and Goat anti mouse IRDye 800). Blots were imaged using an Odyssey Infrared Imaging System (Li-COR Biosciences). Scan resolution of the instrument ranges from 21-339μm and in this study blots were imaged at 169μm. Quantification was performed on single channels with the analysis software provided. Bands were identified according to their relative molecular and delineated using Odyssey software and the arbitrary fluorescence intensity calculated by the software. For each membrane, scans were carried out at three different intensities in order to minimise possible user error in determining correct scan intensities or over-saturation of the membrane. The average of these three separate scans (giving an N of 1 per membrane) was used for analysis.

2.6 RNA isolation and microarray

Whole spinal cords were removed and RNA was extracted using an RNEasy micro kit (Qiagen) and RNA samples were shipped to the microarray facilities in Oxford where subsequent procedures and analysis was conducted by Sheena Lee. Any genomic DNA was removed using an on column digest. The quality and integrity of RNA was assessed on a BioAnalyzer; all samples had a RNA Integrity Number (RIN) $\geq$ 9 (Agilent Laboratories, US). 1μg starting RNA was ribosome depleted using the Ribominus Human/MouseTranscriptome Isolation kit (Invitrogen). Labelled sense ssDNA for hybridization was generated with the Affymetrix GeneChip WT sense target labelling and control reagents kit (Affymetrix, UK) according to the manufacturer's instructions.

Sense ssDNA was fragmented and the distribution of fragment lengths was measured on the BioAnalyser. The fragmented ssDNA was labelled and hybridized to the Affymetrix GeneChip Mouse Gene 1.0 ST Array (Affymetrix). Chips were processed on an Affymetrix GeneChip Fluidics Station 450 and Scanner 3000. The core genes on the arrays were RMA normalized in GeneSpring GX 9 and differentially expressed genes were identified using an unpaired t-test with a p-value cut off of ≤ 0.05 and a fold change difference between SMNMu and WT of ≥ 1.5. The genes were sorted according to their gene ontology using GenMAPP's GO-Elite. Only MAPPFinder ontologies with ≥ 3 genes showing changes and a permuted p-value ≤ 0.05 were selected.

Chapter 3: NMJ pathology in mouse models of spinal muscular atrophy

Summary

Based on the hypothesis that synapses are specifically vulnerable in neurodegenerative disease, I have investigated synaptic pathology at the neuromuscular junction in two mouse models of SMA. I have used immunocytochemistry, confocal microscopy and electron microscopy to investigate synaptic pathology in a range of muscles (levator auris longus, transversus abdominis, deep lumbrical muscles) in the $Smn^{-/-}$;SMN2 and $Smn^{-/-}$;SMN2;$SMN^{\Delta 7}$ mouse models of SMA during disease progression.

Results detailed in this chapter show that:

1. Pre-synaptic degeneration of the NMJ was an early and significant event in mouse models of SMA, being present at pre-symptomatic time points in the most severely affected muscle groups.
2. There was significant inter-muscle heterogeneity in regards to pre-synaptic pathology, with postural, slow twitch muscles of the trunk being more affected than fast twitch muscles.
3. Significant post synaptic shrinkage of muscle fibres and endplates was apparent but appears to be dissociated with pre-synaptic degeneration.
4. Pre-synaptic pathology in *Smn-/-;SMN2;Δ7* mice was reduced compared to *Smn-/-;SMN2* mice at late-symptomatic time-points, although post-synaptic pathology was equally severe.
5. Selectively vulnerable pools of motor units exist within the caudal band of the LAL muscle and appear to belong to a developmentally distinct subtype.

3.1 Introduction

As mounting evidence suggests that synaptic compartments of neurons are specifically vulnerable to a range of pathogenic triggers, I have investigated whether the NMJ was a primary pathological target in SMA. Prior to this study, a number of studies based on human patients (Soubourillard *et al.*, 1996; Mishra *et al.*, 2004, Swoboda *et al.*, 2005) and animal models (Cifuentes-diaz *et al.*, 2002; Chan *et al.*, 2003; Monani *et al.*, 2003; Le *et al.*, 2005) have suggested that NMJ defects are an important aspect of SMA pathology. Findings include electrophysiological abnormalities associated with denervation (Mishra *et al.*, 2004), vacant endplates (Cifuentes-diaz *et al.*, 2002; Le *et al.*, 2005) and terminal and nodal sprouting associated with denervation-induced re-innervation (Monani *et al.*, 2003). Despite this work, we still lack fundamental details of the morphological defects and time course of the pathological events occurring at the NMJ. A more detailed understanding of such pathological events could give important insights into the disease mechanisms underlying SMA. For example, despite evidence suggesting that both neuron-specific and muscle-specific events can occur during SMA (see introduction), no studies to date have addressed whether muscle atrophy occurs as a direct result of synaptic denervation at the mammalian NMJ. Teasing apart the nerve- and/or muscle-specific roles of SMN will be important for developing therapeutic strategies that target all pathological sites in SMA. Similarly, it is not known whether certain intrinsic characteristics of motor neurons (e.g. fast-fatigable, fast fatigue-resistant and slow phenotypes) can lead to modifications in their susceptibility to SMA-induced disease stimuli. The identification of intrinsic factors that make subpopulations of motor neurons particularly vulnerable or resistant to SMA is likely to highlight critical molecular and cellular targets for the development of new therapies and treatments.

Here I have undertaken a detailed analysis of synaptic pathology at the NMJ in two different mouse models of SMA: the *Smn-/-;SMN*2 mouse model of severe SMA (Monani *et al.*, 2000) and the *Smn-/-;SMN*2*;Δ7* mouse model with a modified, less severe phenotype (Le *et al.*, 2005). I have used immunocytochemistry, fluorescence/confocal microscopy and electron microscopy to demonstrate that

neuromuscular synapses are grossly disrupted in late symptomatic (P5-6) *Smn-/-;SMN*2 mice, with postural muscles in the trunk being more severely affected than the fast-twitch muscles in both the trunk and lower limbs. The morphology of synaptic degeneration showed correlates to a dying-back neuropathy, with gradual proximal to distal withdrawal and minimal axonal fragmentation. Synaptic abnormalities were present in severely-affected muscles at pre-symptomatic time-points (P2) indicating synapse loss is an early event in disease progression. *Smn-/-;SMN*2*;Δ7* mice also showed signs of synaptic disruption at early/mid-symptomatic time-points (P7), but in late symptomatic mice (P14) post-synaptic pathology had progressed significantly but pre-synaptic pathology had not extended much beyond the modest levels observed at P7. Together these findings support the hypothesis that synapses are vulnerable in SMA. I also show that shrinkage of post-synaptic motor endplates does not correlate with pre-synaptic motor nerve terminal loss, suggesting that pre- (neuronal) and post- (muscular) synaptic pathology can occur independently of one another. Finally, my investigations of neuromuscular pathology in the LAL muscle identified selectively vulnerable subpopulations of motor neurons, with those conforming to a 'Fast Synapsing' (FaSyn) phenotype (Pun *et al*., 2002) likely to be more susceptible in SMA than those with a 'Delayed Synapsing' (DeSyn) phenotype.

3.2 Results

3.2.1 Motor nerve terminal loss, neurofilament accumulation and muscle fibre shrinkage in Smn-/-;SMN2 mice

Neuromuscular pathology was investigated in a range of muscles from the trunk and hind limbs of the mouse, with each muscle allowing assessment of the entire synaptic innervation of the muscle in a whole-mount preparation. Synaptic pathology was examined at the NMJ in the transversus abdominis (TVA) a postural muscle from the anterior abdominal wall innervated by lower intercostal nerves, known to be affected in other mouse models of motor neuron degeneration (Newbery *et al.*, 2005), levator auris longus (LAL), a pure fast-twitch muscle from the dorsal surface of the head innervated by the facial nerve (Angaut-Petit *et al.*, 1987; Erzen *et al.*, 2000) and deep lumbrical muscles, fast-twitch muscles from the hind-paw innervated by terminal branches of the tibial nerve. These preparations allowed us to quantify and correlate pre- and post-synaptic pathology in muscle groups taken from several anatomical regions of the mouse, whilst also providing the ability to compare pathology in predominantly slow- (TVA) versus fast-twitch (LAL and lumbricals) muscles as well as between muscles innervated by nerves with long (lumbricals) and short (TVA/LAL) nerve stumps.

NMJs were labelled in whole-mount TVA, LAL and lumbrical preparations from late-symptomatic (P5-P6) *Smn-/-;SMN2* mice with a severe SMA phenotype. Care was taken during dissection to make sure that the muscle and its nerve supply were removed in their entirety, especially for the LAL which has two constituent muscle bands (rostral and caudal; see below). Pre-synaptic axons and motor nerve terminals were labelled using antibodies directed against 150kDa neurofilament proteins (green; Figure 3.1 A) and post-synaptic acetylcholine receptors were labelled using rhodamine-conjugated α-bungarotoxin (red; Figure 3.1A). The vast majority of NMJs in control preparations from wild-type littermates were, as expected, fully occupied, with a motor nerve terminal branching over the whole post-synaptic motor endplate. As the muscles were taken from animals at P5-P6, most endplates in control preparations were also contacted by more than one incoming motor axon (polyneuronally innervated), as the process of

developmental synapse elimination (establishing the adult mononeuronal innervation pattern of one axon innervating one muscle fibre) is not complete until approximately two weeks after birth.

In contrast, numerous examples of partially occupied and vacant endplates (Figure 3.1A) were present in all muscle preparations from *Smn*-/-;*SMN*2 mice, indicative of denervation events occurring due to a loss of pre-synaptic motor nerve terminals. The numbers of fully occupied endplates were significantly reduced in all muscles compared to wild-type littermates, albeit with the slow-twitch, postural TVA being more affected (63% fully occupied at P5) than the fast-twitch LAL and lumbricals (77% and 73% respectively fully occupied at P5; Figure 3.1 B-D).

Concurrent to nerve terminal loss, numerous examples was found of pre-synaptic nerve terminals with abnormal accumulations of neurofilament proteins (Figure 3.2). This data supports similar findings from a previous study of NMJs in a different mouse model of SMA, suggesting that neurofilament accumulation in motor nerve terminals is a pathological feature of SMA (Cifuentes-Diaz *et al*., 2002).

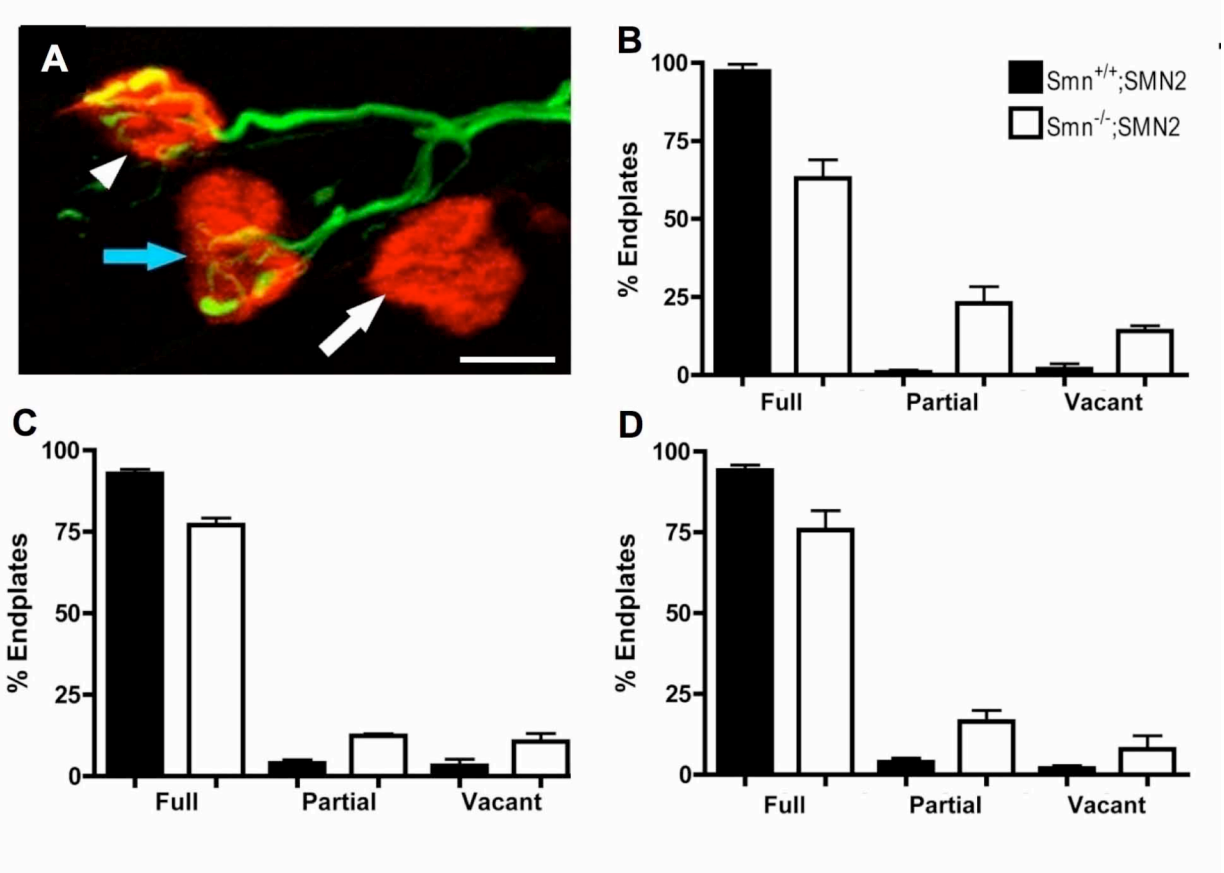

Figure 3.1: Synaptic pathology at the neuromuscular junction in late-symptomatic (P5-6) *Smn-/-;SMN2* mice. A – Confocal micrograph showing three neuromuscular junctions in an immunohistochemically labelled TVA muscle preparation from a P5 *Smn-/-;SMN2* mouse (green = 150kDa neurofilaments; red = post-synaptic acetylcholine receptors labelled with TRITC-α-bungarotoxin). The white arrowhead is identifying a fully occupied endplate, the blue arrow a partially occupied endplate, and the white arrow a vacant (denervated) endplate. B-D – Quantification of synaptic pathology in late-symptomatic (P5-6) *Smn-/-;SMN2* mice. Panels show the percentages of fully occupied, partially occupied and vacant endplates in the TVA (B), LAL (C) and deep lumbrical (D) muscles from SMA mice (white bars) compared to control littermate controls *(black bars; mean±SEM; n=4 per muscle control, n=6 per muscle). Scale bar = 10μm (A)).*

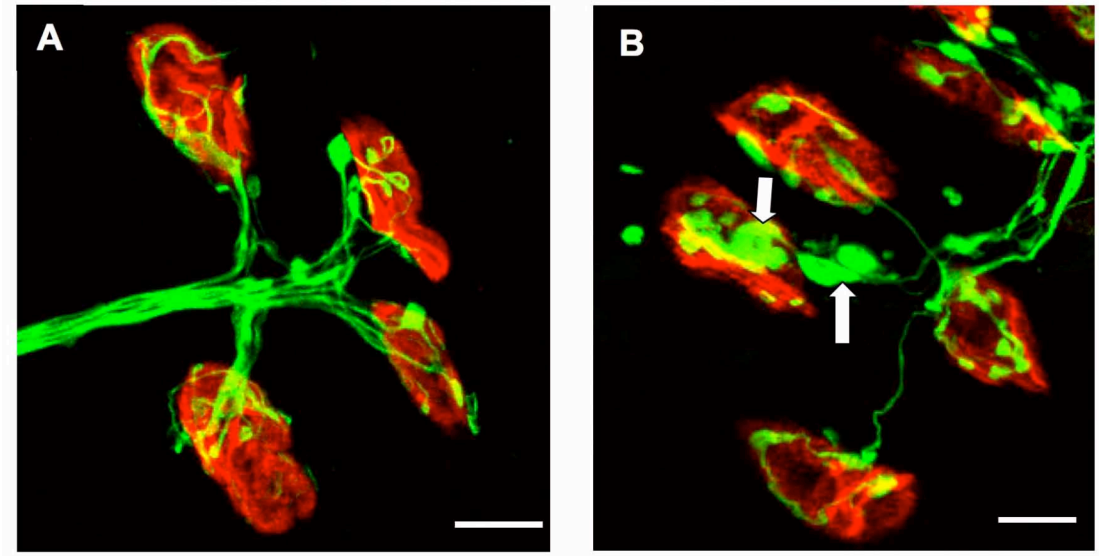

Figure 3.2: Neurofilament accumulation at the neuromuscular junction in late-symptomatic (P5-6) *Smn-/-;SMN2* mice. A,B - Confocal micrographs showing abnormal accumulations of neurofilament at *Smn-/-;SMN2* neuromuscular junctions (B; white arrows) compared to littermate controls (A) in an immunohistochemically labelled LAL muscle preparation from a P5 *Smn-/-;SMN2* mouse (*green = 150kDa neurofilaments; red = post-synaptic acetylcholine receptors labelled with TRITC-α-bungarotoxin; scale bar = 10μm (A,B))*.

As previous studies have identified shrinkage of post-synaptic motor endplates alongside muscle fibre atrophy in SMA (Le *et al.*, 2005), motor endplate size and muscle fibre diameter were examined in the TVA and LAL of *Smn-/-;SMN*2 mice (Figure 3.3). Quantitative analysis confirmed that motor endplate areas were significantly reduced in the TVA and LAL of *Smn-/-;SMN*2 mice (Figure 3.3 B). Measurements of muscle fibre diameter revealed significant shrinkage in the TVA (average muscle fibre diameter of 11 *Smn-/-;SMN*2 *vs* 17 control, P<0.001 ANOVA with Tukeys post hoc test; Figure 3.3 C,D), with the LAL much less affected (average muscle fibre diameter of 12μm *Smn-/-;SMN*2 *vs* 13μm control, non-significant, ANOVA with Tukeys post hoc test; Figure 3.3 C,D).

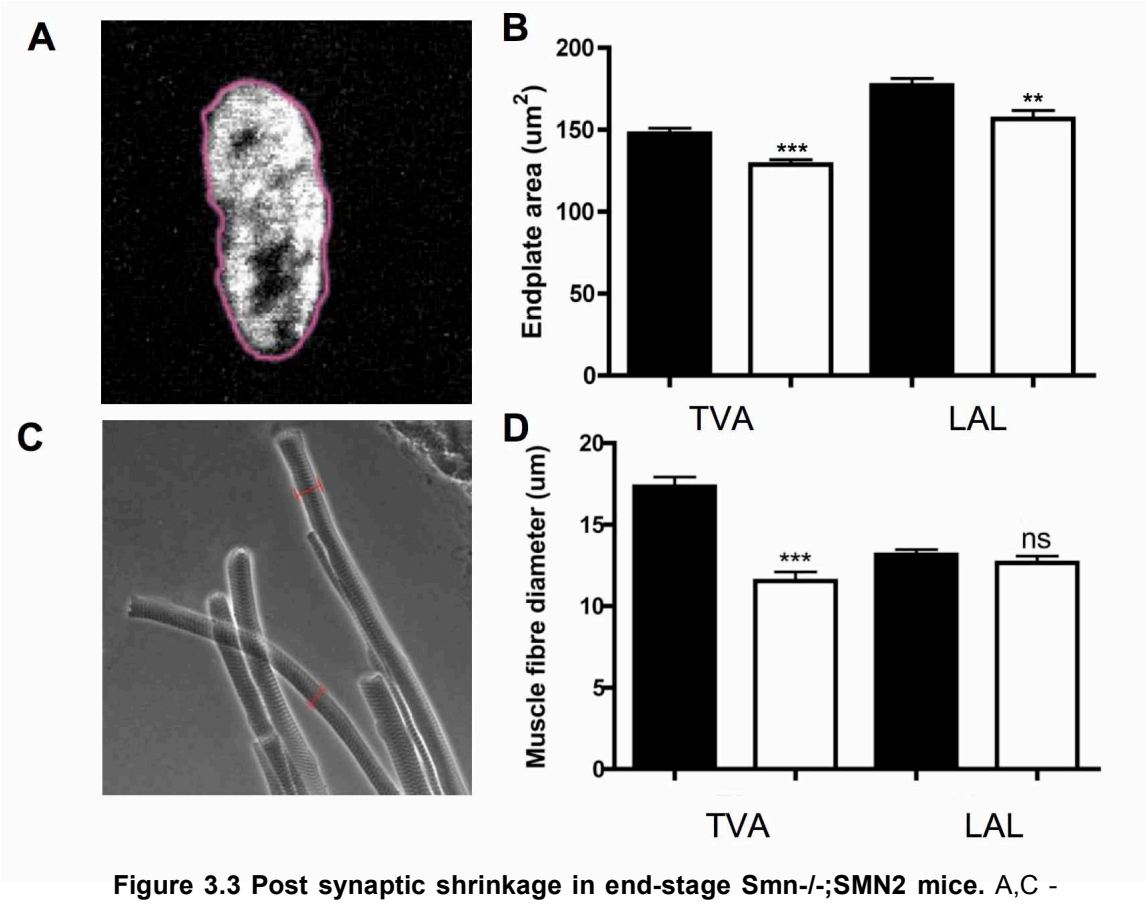

Figure 3.3 Post synaptic shrinkage in end-stage Smn-/-;SMN2 mice. A,C - endplates area (A) and muscle fibre diameter (C) were measured using image J software as shown (pink outline (A); red line (C)). B,D - Bar charts showing the mean endplate area (B) and muscle fibre diameters (D) in the TVA and LAL from SMA mice (white bars) compared to control littermate controls (black bars). *(mean±SEM; n=4 per muscle control, n=6 per muscle; ANOVA with Tukey's Post Hoc test; ***P<0.001; **P<0.01; ns- non significant).*

The data discussed above suggest that NMJs are primary pathological targets in SMA and also indicate that significant levels of inter-muscle variability exist within affected individuals, with slow-twitch postural muscles more affected than fast-twitch phasic muscles.

The morphological correlates of nerve terminal loss appeared distinct from those occurring during more Wallerian-like degenerative processes (Miledi and Slater, 1970; Gillingwater *et al.*, 2003), suggesting that a 'dying-back' process is more likely to be responsible for removing nerve terminals. In order to confirm this, intramuscular nerves and NMJs were examined in deep lumbrical muscles from late-symptomatic (P5-P6) *Smn-/-;SMN*2 mice using transmission electron microscopy. All intramuscular nerves examined were devoid of classical markers of Wallerian degeneration (e.g. myelin debris and plasma membrane breakdown; Miledi and Slater 1970; Gillingwater *et al.*, 2003), with intact myelin sheaths, neurofilaments and microtubules (Figure 3.4 A). Modest accumulations of neurofilament in some axons confirmed the occasional neurofilament accumulations observed using immunocytochemistry (Figure 3.4 A). At the qualitative level, intact myofibrils were present in all skeletal muscle fibres examined (Figure 3.4 B). Immature NMJs could be identified (devoid of the adult ultrastructural characteristics such as large post-synaptic folds), and many contained large accumulations of neurofilaments, presenting as neurofilament whorls within the body of the motor nerve terminal (Figure 3.4 C). These whorls are likely to be the ultrastructural equivalents of neurofilament accumulations observed using immunocytochemistry (c.f. Figure 3.2 B) and are similar to those previously reported in other mouse models of SMA (Cifuentes-Diaz *et al.*, 2002). No evidence of membrane breakdown, organelle fragmentation or phagocytosis by terminal Schwann cells was present, suggesting the involvement of a mechanism distinct from Wallerian or Wallerian-like degeneration (Gillingwater and Ribchester, 2003). This data suggests that the morphology of synaptic degeneration in SMA is more akin to a 'dying-back' type degeneration, as observed in other models of motor neuron degeneration (Frey *et al.*, 2000; Fischer *et al.*, 2004)

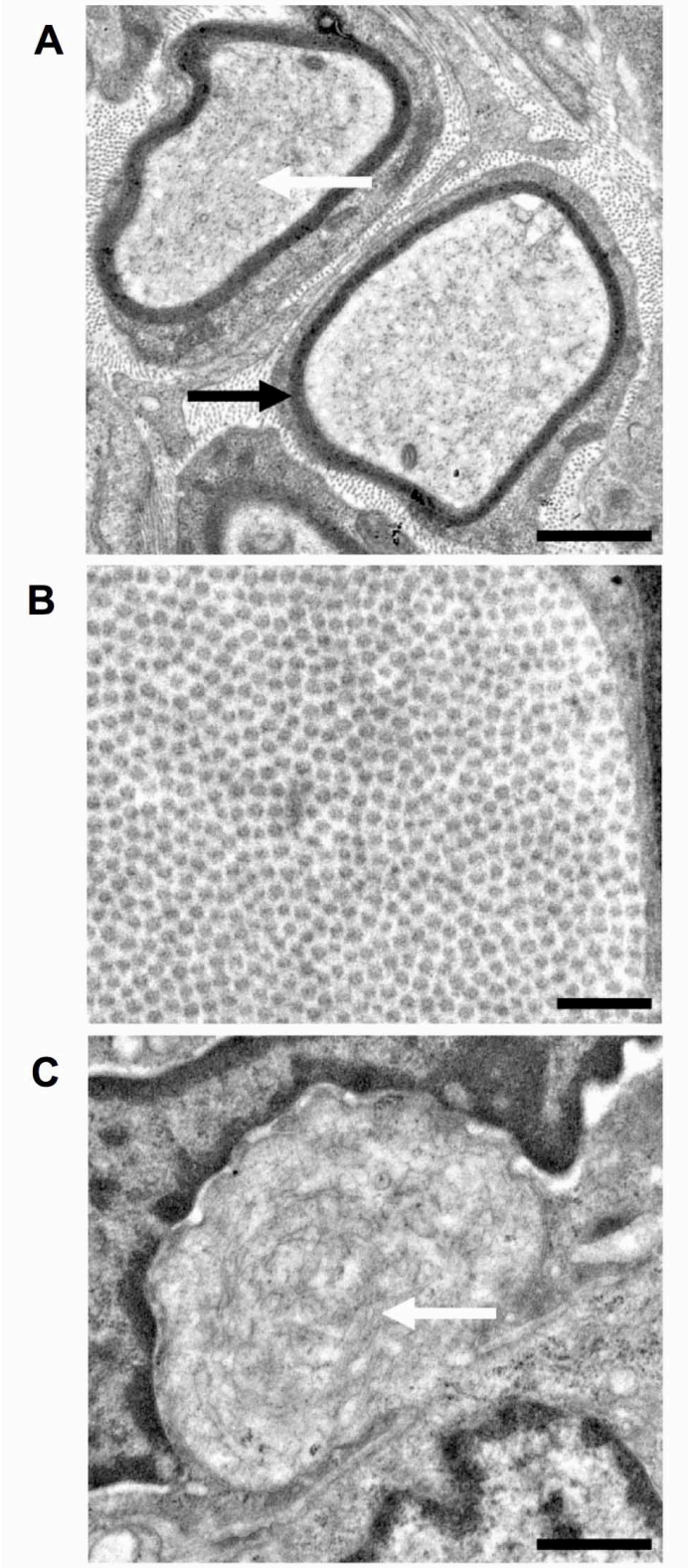

Figure 3.4: Ultrastructural correlates of synaptic pathology at the neuromuscular junction in late-symptomatic (P5-6) *Smn-/-;SMN2* mice. A – Electron micrograph showing a pair of intramuscular axons in a lumbrical muscle from a P6 *Smn-/-;SMN2* mouse. Note how the gross ultrastructure is retained, with intact myelin sheaths (black arrow) and neurofilaments/microtubules. Both axons have low-level accumulations of neurofilaments (white arrow). B – High power electron micrograph showing intact myofibrils in a lumbrical muscle from a P6 *Smn-/-;SMN2* mouse. C - Electron micrograph showing a motor nerve terminal at a neuromuscular junction in a lumbrical muscle from a P6 *Smn-/-;SMN2* mouse. Note how the nerve terminal bouton is filled with abnormally large accumulations of neurofilaments in the form of neurofilament whorls. Note that ultrastructural features normally associated with mature, adult neuromuscular junctions (e.g. post-synaptic folds, large numbers of clustered synaptic vesicles) are not present in mice of this age due to their developmental stage. *(Scale bar = 1μm (A), 0.1μm (B), 0.5μm (C)).*

3.2.2 Occupancy counts underestimate levels of synaptic pathology at the NMJ in Smn-/-;SMN2 mice

Despite clear evidence of synaptic pathology provided by counts of fully occupied, partially occupied and denervated endplates (Figure 3.1), I investigated whether or not the presence of multiple axonal inputs converging on individual endplates - due to ongoing developmental synapse elimination (see above) – resulted in underestimation of pre-synaptic nerve terminal loss. The numbers of individual axonal inputs converging on fully-occupied endplates were examined (i.e. classified as 'normal' in previous analysis) in the TVA and LAL of late-symptomatic *Smn-/-;SMN2* mice and control littermates (Figure 3.5). In the TVA, the mean number of inputs converging on endplates was significantly reduced (1.28 Smn-/-;SMN2 vs 1.65 control; P<0.01 Mann Whitney test). The same trend existed in the LAL muscle (1.75 Smn-/-;SMN2 vs 1.64 control) although due to high intramuscular variability (see below), this did not reach statistical significance. Thus, more pre-synaptic inputs were being lost than previously estimated from denervation counts alone.

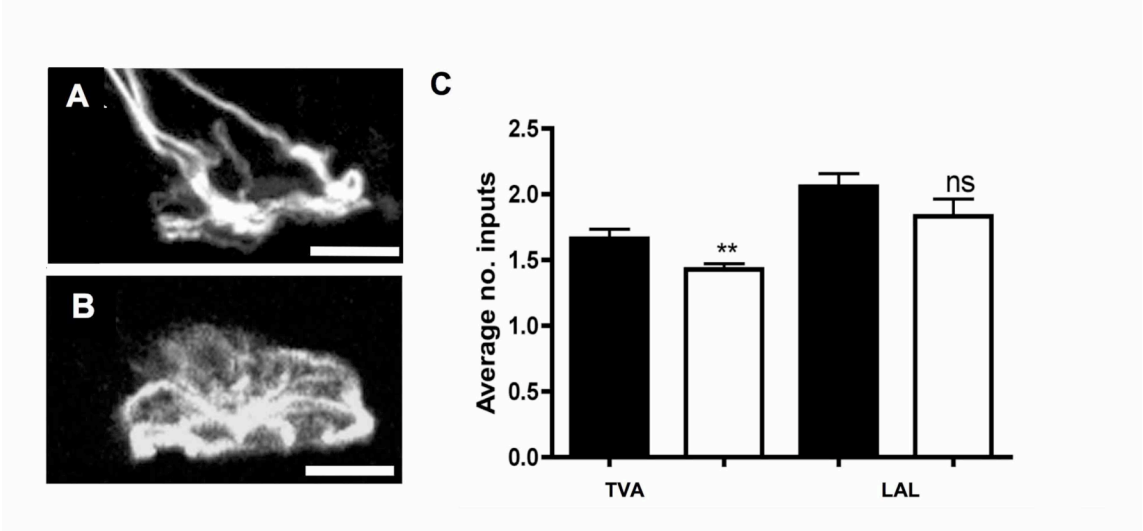

Figure 3.5: Synaptic pathology at the neuromuscular junction is underestimated when based on occupancy counts alone. A,B – Confocal micrographs showing a single polyneuronally innervated neuromuscular junction (A, pre-synaptic axons and nerve terminal; B, post-synaptic acetylcholine receptors) in an immunocytochemically labelled LAL from a P6 *Smn-/-;SMN2* mouse. Note how three axons are converging on this single endplate. C – Bar chart showing the average number of axonal inputs innervating individual neuromuscular junctions classified as fully occupied (see Figure 3.1) in the TVA and LAL of late-symptomatic (P5-6) *Smn-/-;SMN2* mice compared to control littermates. *(mean±SEM; Mann Whitney test, two-tailed; **P<0.01, ns non significant; n=6 per muscle Smn-/-;SMN2 Scale bar = 5μm).*

It is possible, however, that reduced numbers of synaptic inputs could also result from defective synapse formation, leading to hypo-innervation of NMJs before the onset of pathology. To rule out this possibility, analysis of synaptic pathology was performed in the TVA and LAL of P2 *Smn-/-;SMN*2 mice (Figure 3.6). From a qualitative perspective, no discernable differences could be identified between neuromuscular innervation in the LAL muscle from P2 (i.e. pre-symptomatic) *Smn-/-;SMN*2 mice versus control littermates (Figure 3.6 A-B). Quantification of innervation (Figure 3.6 C) supported qualitative observations that the LAL was devoid of denervation pathology at P2. Similarly, quantification of the average number of inputs and muscle fibres diameters in the LAL confirmed that synapses were being formed in a similar manner to control littermates (Figure 3.7 B,D). By P4, synaptic pathology was evident in the LAL, although not to the extent observed in late-symptomatic P6 mice (Figure 3.6C).

A similar analysis of TVA from P2 *Smn-/-;SMN*2 mice showed evidence of low levels of pre-symptomatic synaptic pathology (Figure 3.6 C). The average number of inputs per synapse were also decreased at P2, although post-synaptic muscle fibre shrinkage was not yet evident (Figure 3.7 A,C). As in the LAL, synaptic pathology in the TVA progressively worsened with time and was always more severe than in LAL at any given time-point (Figure 3.6 C).

The above results indicate that NMJ pathology in the form of pre-synaptic degeneration, neurofilament accumulation and post-synaptic shrinkage, is an early and significant event in pathology in the Smn-/-;SMN2 mouse model. Significant inter-muscle heterogeneity is apparent and pathological changes can be identified in the most severely affected muscles prior to symptom onset. While these changes were a clear feature within this severe mouse model, the extent to which they are general feature of SMA, as oppose to specific to this mouse model, was unclear.

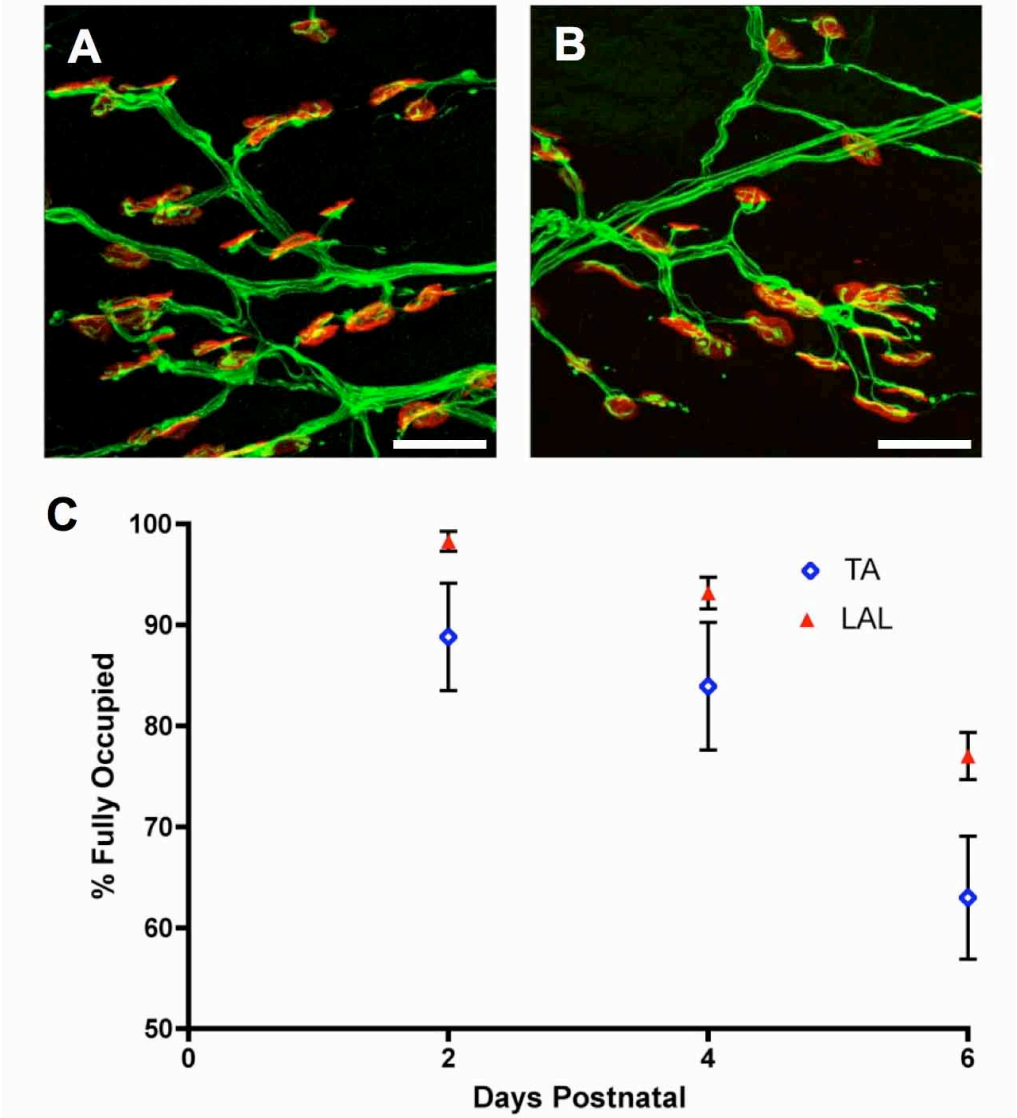

Figure 3.6: Synapses form normally, but synaptic pathology can occur pre-symptomatically in severely affected muscles, in *Smn-/-;SMN2* mice. A/B – Confocal micrographs showing neuromuscular junctions in the LAL muscle from control (A) and *Smn-/-;SMN2* mice (B). Innervation levels were qualitatively indistinguishable between the two genotypes in this muscle. C – Graph showing the onset and progression of pre-synaptic pathology in the TVA and LAL muscles from *Smn-/-;SMN2* mice at P2 (pre-symptomatic), P4 (mid-symptomatic) and P6 (late-symptomatic). Note how the LAL is almost entirely free from synaptic pathology at P2, with pathology first appearing at P4. By contrast, the TVA is affected, albeit at modest levels, at P2 with more severe synaptic pathology present at P4 and P6). The vast majority of endplates (>95%) were fully occupied in the TVA and LAL from control littermates at the same time-points (data not shown). *(n=4/5/6 muscles per P2/P4/P6 time-point; scale bar = 20μm).*

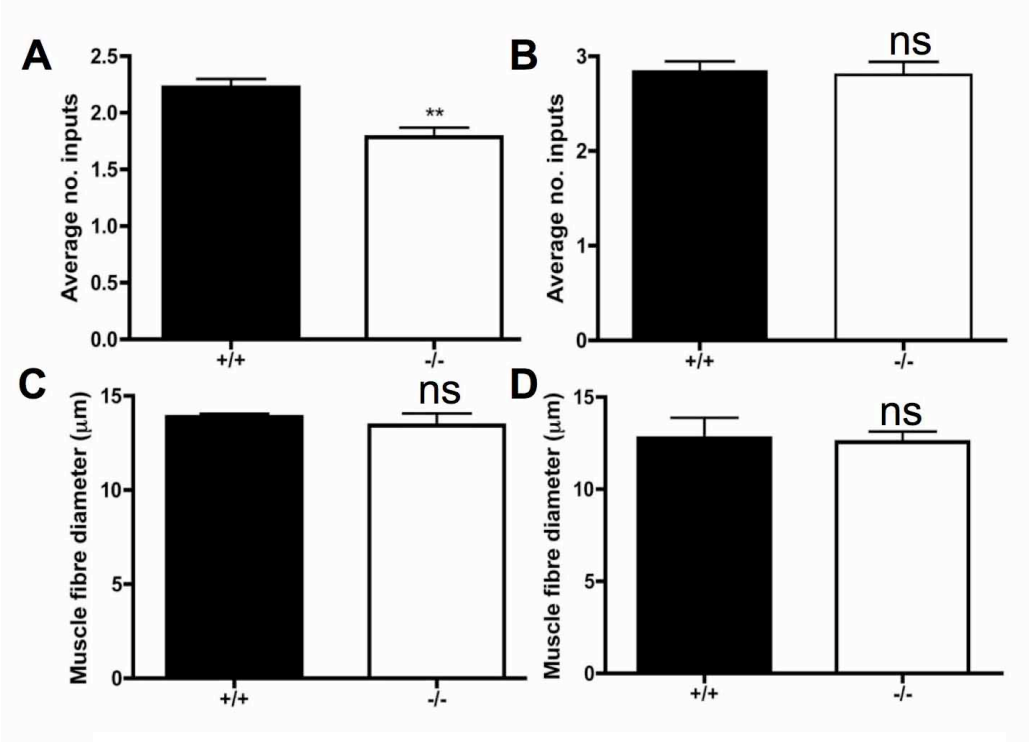

Figure 3.7: Pathology can occur pre-symptomatically in severely affected muscles in *Smn-/-;SMN2* mice. A-D - Bar charts showing the average number of inputs per synapse (A,B) and mean muscle fibre diameter (C,D) in the TVA (A,C) and LAL (B,D) muscles from *Smn-/-;SMN2* mice at P2 (pre-symptomatic). (*Mann Whitney test, two-tailed; ** P<0.01, ns non significant; n=5 muscles per genotype).*

3.2.3 Motor nerve terminal loss, neurofilament accumulation and muscle fibre shrinkage in Smn-/-;SMN2;Δ7 mice

In order to determine that the synaptic events detailed above were not specific to *Smn-/-;SMN*2 mice, NMJ morphology was quantified in early/mid symptomatic (P7) and late-symptomatic (P14) *Smn-/-;SMN2;Δ7* mice. As in the *Smn-/-;SMN*2 mice, synaptic pathology was evident in all muscle groups examined at both P7 and P14, evidenced by partially occupied endplates and vacant endplates (Figure 3.8). Again the presence of motor nerve terminals with abnormal accumulations of neurofilaments was noted (Figure 3.9). Interestingly, neurofilament accumulation appeared to be even more severe in *Smn-/-;SMN2;Δ7* mice than previously observed in *Smn-/-;SMN*2 mice, particularly in the TVA (Figure 3.9 C).

The numbers of fully occupied endplates were significantly reduced in the TVA compared to control littermates in early/mid symptomatic (P7) mice (reduction in percentage of fully occupied endplates of 9% *Smn-/-;SMN2;Δ7* vs control, P<0.01 Mann Whitney test; Figure 3.8 B). There was only a subtle decrease in the numbers of fully occupied endplates in the LAL compared to control littermates (reduction in percentage of fully occupied endplates of 6% *Smn-/-;SMN2;Δ7* vs control, non-significant Mann Whitney test; Figure 3.8 B). This result confirms findings in *Smn-/-;SMN2* mice showing that the LAL is less affected in SMA than the TVA. In line with the data on pre-synaptic pathology, muscle fibre shrinkage was also pronounced in TVA but not LAL (average muscle fibre diameter of 16/13μm *Smn-/-;SMN2;Δ7 vs* 21/14μm control in TVA/LAL respectively, P<0.001 TVA, non-significant LAL, ANOVA with Tukeys post hoc test; Figure 3.10 A).

Surprisingly, equivalent analysis of synaptic pathology in end-stage (P14) *Smn-/-;SMN2;Δ7* revealed synaptic degeneration had not progressed significantly in either the TVA or LAL muscles (reduction in the percentage of fully occupied endplates of 7% and 15% *Smn-/-;SMN2;Δ7* compared to controls in TVA and LAL respectively; Figure 3.8 C). However, post-synaptic muscle fibre shrinkage was more pronounced in both the TVA and LAL at P14 compared to both earlier time points and end-stage Smn-/-;SMN2 mice (average muscle fibre diameter of 13/12μm *Smn-/-;SMN2;Δ7 vs* 23/18μm control in TVA/LAL respectively, P<0.001 ANOVA with Tukeys post hoc test; Figure 3.10 B) suggesting that the attenuation of pre- and post-synaptic pathology may be differentially modulated by the *SMNΔ7* transgene.

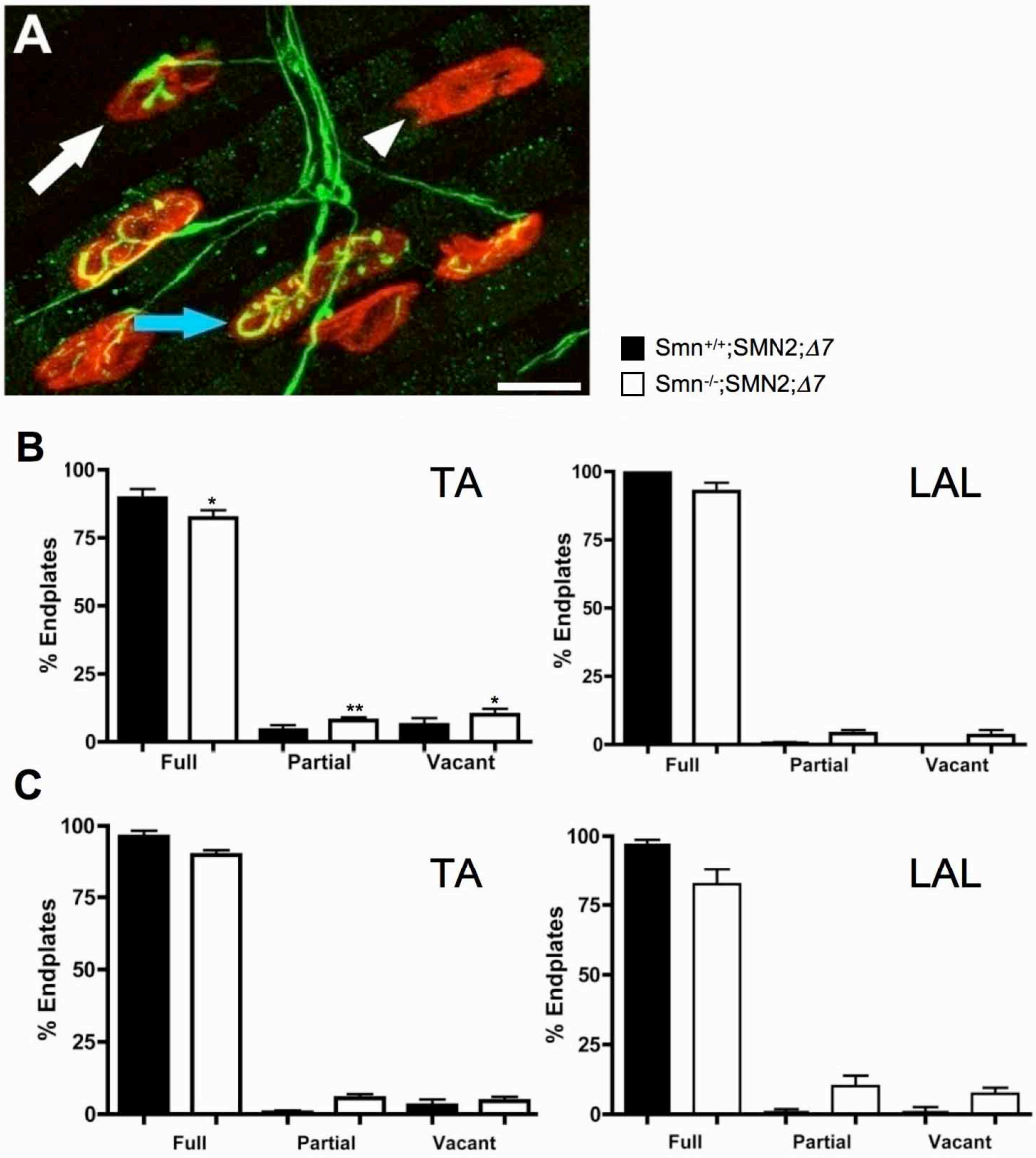

Figure 3.8: Synaptic pathology at the neuromuscular junction in early/mid-symptomatic (P7) and late-symptomatic (P14) *Smn-/-;SMN2;Δ7* mice. A – Confocal micrograph showing neuromuscular junctions in an immunocytochemically labelled LAL muscle preparation from a P14 *Smn-/-;SMN2;Δ7* mouse (green = 150kDa neurofilaments; red = post-synaptic acetylcholine receptors labelled with TRITC-α-bungarotoxin). The white arrowhead is identifying a vacant endplate, the blue arrow a fully occupied endplate, and the white arrow a partially occupied endplate. B,C – Quantification of synaptic pathology in early/mid-symptomatic (P7; B) and late-symptomatic (P14; C) *Smn-/-;SMN2;Δ7* mice in the TVA (left panel) and LAL (right panel) *(black bars = control littermate; white bars = Smn-/-;SMN2;Δ7; mean±SEM; Mann Whitney test, 2 tailed; *P<0.05, **P<0.00; n=6 per muscle control, n=10 per muscle Smn-/-;SMN2;Δ7 at P7; n=2 per muscle/genotype at P14; Scale bar = 15μm (A))*.

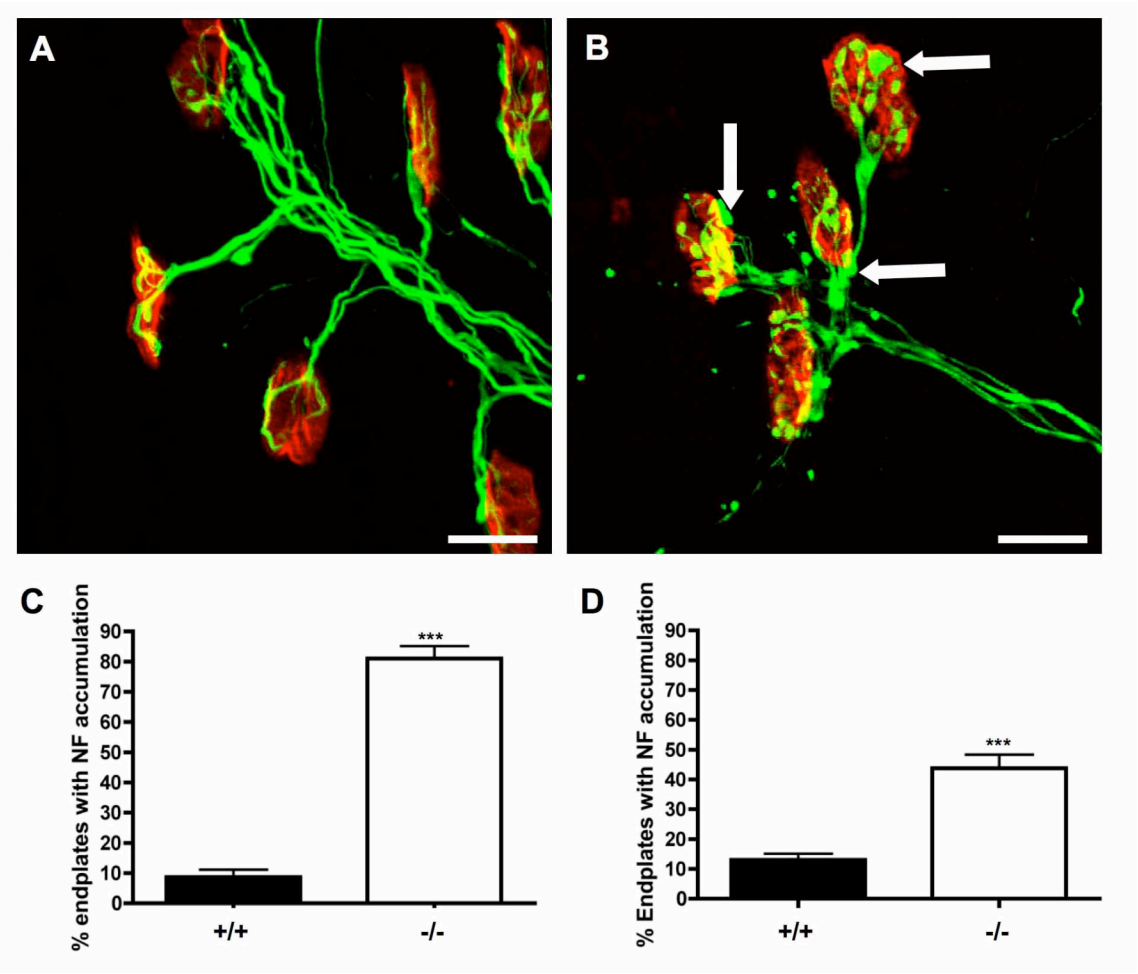

Figure 3.9: Abnormal accumulation of neurofilaments in *Smn-/-;SMN2;Δ7* mice. A,B – confocal micrographs showing neuromuscular junctions from P7 control (A) and *Smn-/-;SMN2;Δ7 (B)* LAL muscles (green = 150kDa neurofilaments; red = post-synaptic acetylcholine receptors labelled with TRITC-α-bungarotoxin). Note the abnormal accumulations of neurofilament present at axon terminals (white arrows). C,D – bar charts show percentage of neuromuscular junctions with accumulation of neurofilaments in TVA (C) and LAL (D) muscles. *(mean±SEM; Mann-Whitney test; *** P<0.001; n=6 per muscle control, n=10 per muscle Smn-/-;SMN2;Δ7; Scale bar = 20μm (A,B)).*

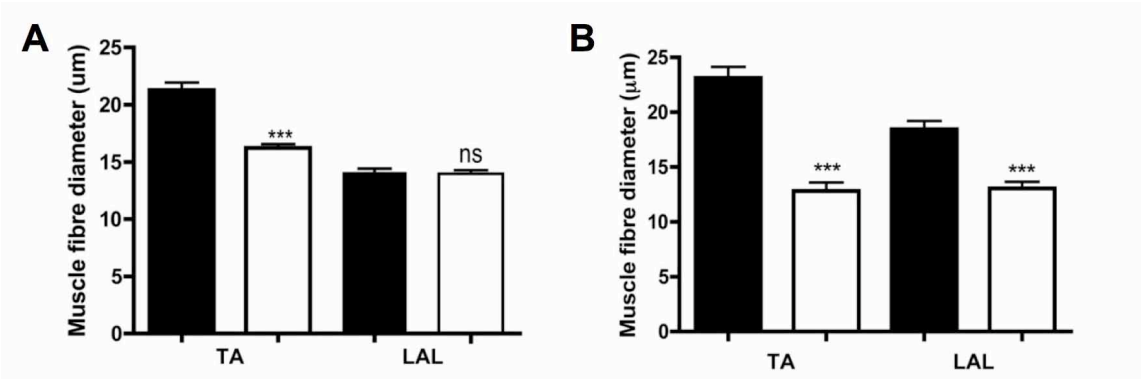

Figure 3.10: Post-synaptic pathology in early/mid-symptomatic (P7) and late-symptomatic (P14) *Smn-/-;SMN2;Δ7* mice. A,B – Bar charts showing muscle fibre diameter in P7 (A) and P14 (B) *Smn-/-;SMN2;Δ7* mice. *(mean ±SEM; Black bars = control, white bars = Smn-/-;SMN2; ANOVA with tukeys post-hoc test; *** P<0.001; ns non-significant; n=6 per muscle control, n=10 per muscle Smn-/-;SMN2; Δ7 at P7; n=2 per strain/genotype at P14).*

3.2.4 Post-synaptic endplate shrinkage and pre-synaptic nerve terminal loss can occur independently at the NMJ

The results detailed above have described the observed pre-synaptic degeneration alongside post-synaptic atrophy. However it was unclear whether these changes were interdependent, i.e. neural pathology resulted in post-synaptic atrophy or vice versa, or whether pathological changes were occurring independently. In order to examine whether post-synaptic changes occurred as a direct result of the loss of innervation at individual NMJs, the percentage occupancy of individual endplates with their area was analysed and compared (Figure 3.11). There was no correlation between endplate area and occupancy (r2=0.006018*;* Figure 3.11 D). As a result, endplates with any given area were just as likely to be fully occupied as partially occupied or vacant. Of particular note, an equivalent spread of endplates areas was observed in both vacant and fully occupied endplates, indicating endplate shrinkage does not correlate with pre-synaptic degeneration. The data suggest that post-synaptic changes at motor endplates are not simply a reaction to pre-synaptic pathology.

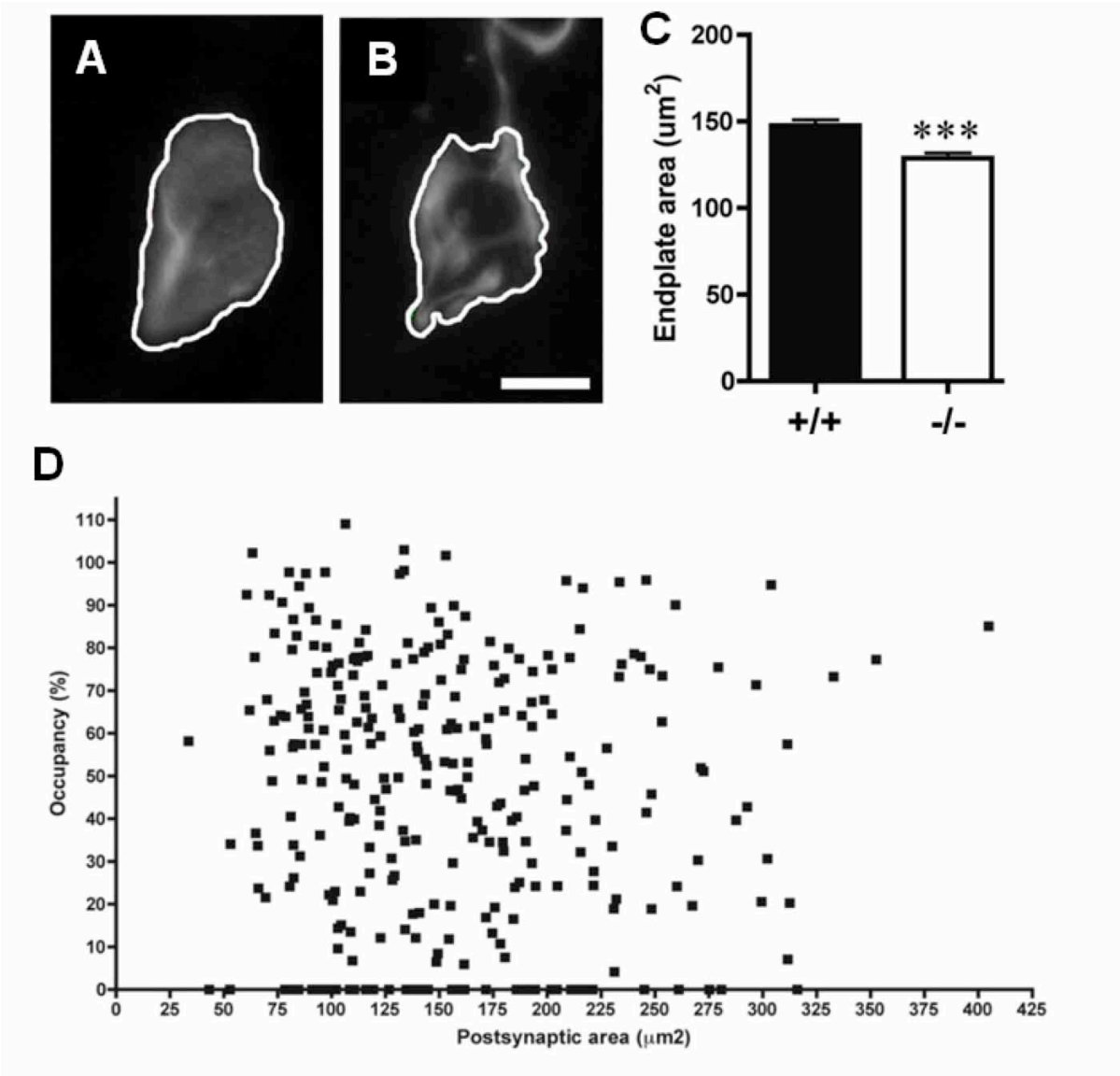

Figure 3.11: Dissociation of pre- and post-synaptic pathology at the neuromuscular junction in late-symptomatic *Smn-/-;SMN2* mice. A,B – Fluorescence micrographs showing a single neuromuscular junction from the TVA of a P6 *Smn-/-;SMN2* mouse immunocytochemically labelled to show the post-synaptic endplate (A) and pre-synaptic axon and motor nerve terminal (B). The highlighted edges of the endplate and motor nerve terminal illustrate how measurements were taken to calculate endplate area and percentage endplate occupancy (area of motor nerve terminal divided by area of endplate x 100). C – Bar chart showing a significant reduction in the mean endplate area in P6 *Smn-/-;SMN2* TVA (white column) compared to control littermates (black column). *(unpaired t test, two-tailed; ***P<0.001; n=4 per muscle control, n=6 per muscle Smn-/-;SMN2 Scale bar = 7.5mm A,B).* D – Scatterplot showing no correlation between endplate area and endplate occupancy in P6 *Smn-/-;SMN2* TVA muscles. Occupancy levels had no effect on endplate size, showing that post-synaptic endplate shrinkage does not occur as a direct result of pre-synaptic pathology. *(P=0.1802, r^2=0.006018, N=6 muscles, n=300 endplates (D))*. *Some* d*ata acquired by Laura Comley during a BSc honours project*

3.2.5 Selective vulnerability of a subpopulation of motor neurons in the LAL muscle

Whilst quantifying synaptic pathology in LAL, it became apparent that there appeared to be higher levels of nerve terminal loss in the thinner, caudal band of the muscle compared to the neighbouring rostral band. This was the case in both strains of mouse and at all time-points examined (Figure 3.12). Quantification of synaptic pathology (using both occupancy counts and assessment of the average number of inputs) confirmed that neuromuscular pathology was indeed widespread in the caudal band of LAL, but was almost absent in the rostral band of the muscle in both *Smn-/-;SMN*2 (Figure 3.12 C,D) and *Smn-/-;SMN*2*;Δ7* mice (Figure 3.12 E,F).

Correlation analysis of post-synaptic endplate areas and pre-synaptic occupancy in both the caudal and rostral bands of LAL again confirmed post-synaptic shrinkage was not associated with pre-synaptic retraction (Figure 3.13). Furthermore, comparisons of endplate area and muscle fibre diameter showed no significant difference between the rostral and caudal bands of LAL (Figure 3.14). This data further supports the hypothesis Figure 3.11) that pre-synaptic nerve terminal loss (which is widespread in the caudal band of LAL but not the rostral band) is not correlated with post-synaptic endplate shrinkage (which shows no difference between the two muscle bands).

This observed selective vulnerability of NMJs in the caudal band of the LAL muscle presents a useful tool to investigate factors which influence synaptic vulnerability. Any intrinsic differences between the two muscle bands are therefore of great interest. Previous studies have demonstrated that both rostral and caudal portions of LAL are composed of a homogenous population of fast-twitch muscle fibres, with predominance of fast twitch fibres and almost complete absence of slow-twitch fibres (Erzen *et al.*, 2000). Therefore fibre type is unlikely to account for the differing vulnerabilities observed.

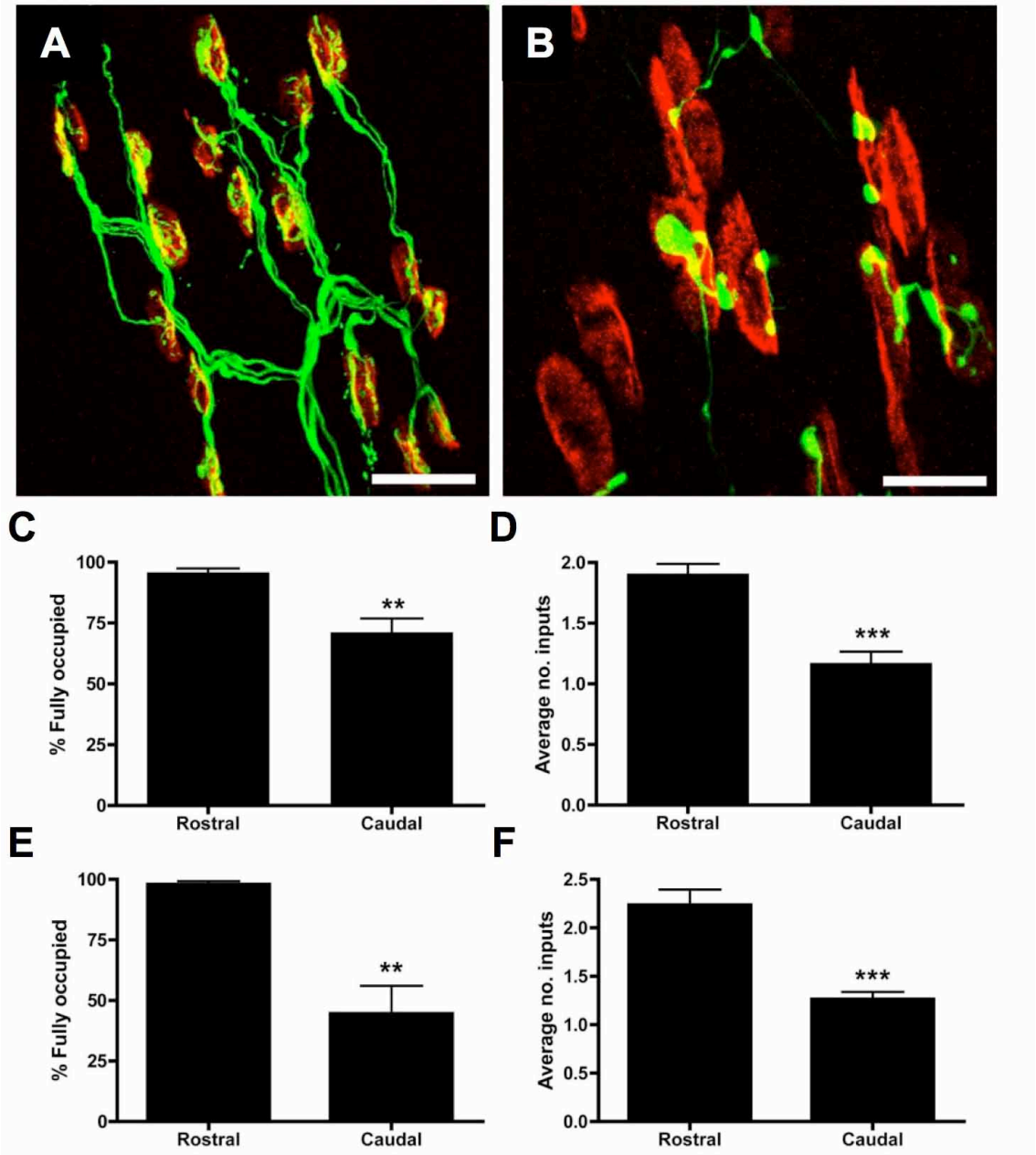

Figure 3.12: Selective vulnerability of synapses in the caudal band of LAL in *Smn-/-;SMN2* mice and *Smn-/-;SMN2;Δ7* mice. A,B – Confocal micrographs showing immunocytochemically labelled neuromuscular junctions (green = 150kDa neurofilaments; red = post-synaptic acetylcholine receptors labelled with TRITC-α-bungarotoxin) from the rostral band (A) and caudal band (B) of the same LAL from a P7 *Smn-/-;SMN2;Δ7* mouse. Note how most endplates in the rostral band are fully occupied (and often polyneuronally innervated) whereas endplates in the caudal band are mainly partially occupied or vacant. C-F – Bar charts showing quantification of synaptic pathology (assessed using occupancy and average number of inputs criteria) in the rostral and caudal bands of LAL from late-symptomatic (P5-6) *Smn-/-;SMN2* mice (C,D) and *Smn-/-;SMN2;Δ7* (E,F) mice. Both assessment criteria revealed significantly more pathology in the caudal band compared to the rostral band (*Mann Whitney test(C,E) or unpaired t-test (D,F); **P<0.01, *** P<0.001; n=3 muscles per assessment C,D; n= 5 muscles per assessment E,F; Scale bars = 40 μm (A), 25μm (B)).*

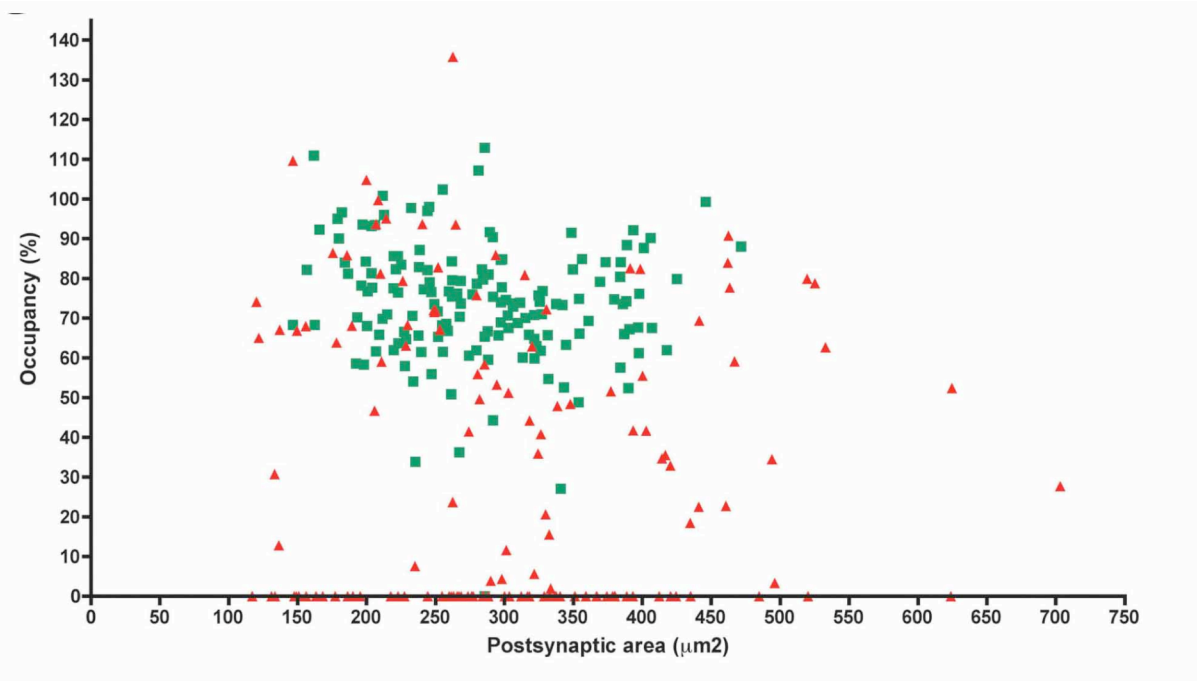

Figure 3.13: Dissociation of pre- and post- synaptic pathology in caudal and rostral bands of the LAL of *Smn-/-;SMN2;Δ7 mice*. Scatterplot showing no correlation between endplate area and endplate occupancy in either the caudal band (red triangles) or rostral band (green squares) from P7 *Smn-/-;SMN2;Δ7* LAL muscles as in the *Smn-/-;SMN2* TVA (see Fig 3.11), pre-synaptic occupancy levels did not correlate with post-synaptic endplate size. *(caudal band, P=0.4457, r2=0.004314, N=5 muscles, n=137 endplates; rostral band, P=0.1406, r2=0.01433, N=5 muscles, n=153 endplates). Some data acquired by Laura Comley during a BSc honour project*

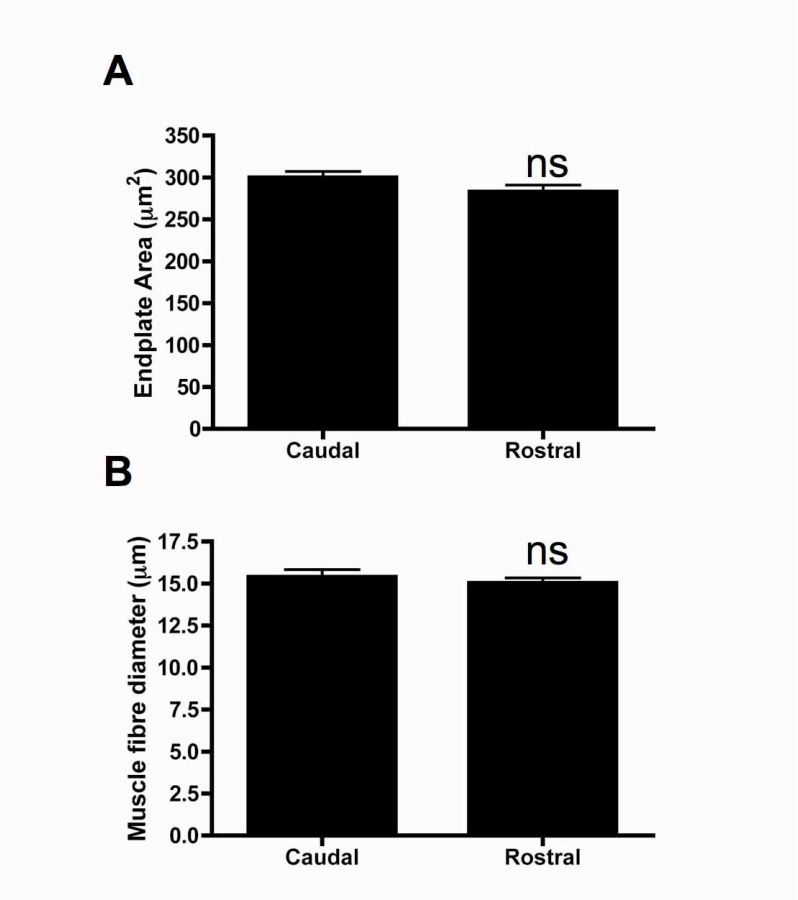

Figure 3.14: No change in post synaptic parameters in rostral and caudal bands of the LAL in *Smn-/-;SMN2;Δ7* mice. A/B – Bar charts showing no difference in endplate area (A) or muscle fibre diameter (B) between the caudal and rostral bands of the LAL muscle in P7 *Smn-/-;SMN2;Δ7* mice *(mean±SEM; unpaired students t-test; ns – non significant; n=10 muscles).* As pre-synaptic pathology differs between rostral and caudal bands, this supports data indicating that pre and post synaptic pathology occur independently.

In order to try and identify the nature of the selective vulnerability of motor neurons and neuromuscular synapses in the caudal band of LAL, innervation patterns of immunocytochemically labelled LAL muscles from wild-type mice were mapped (Figure 3.15). Every muscle of over 40 examined conformed to a consistent pattern of innervation as shown in Figure 3.15 C. The thin caudal band consistently had two clusters of NMJs (C1 and C2), located at lateral and medial ends of the muscle respectively. The thicker rostral band consistently had five clusters of NMJs (R1 to R5), which were arranged in two groups (R1 and R2 together and R3-R5 together).

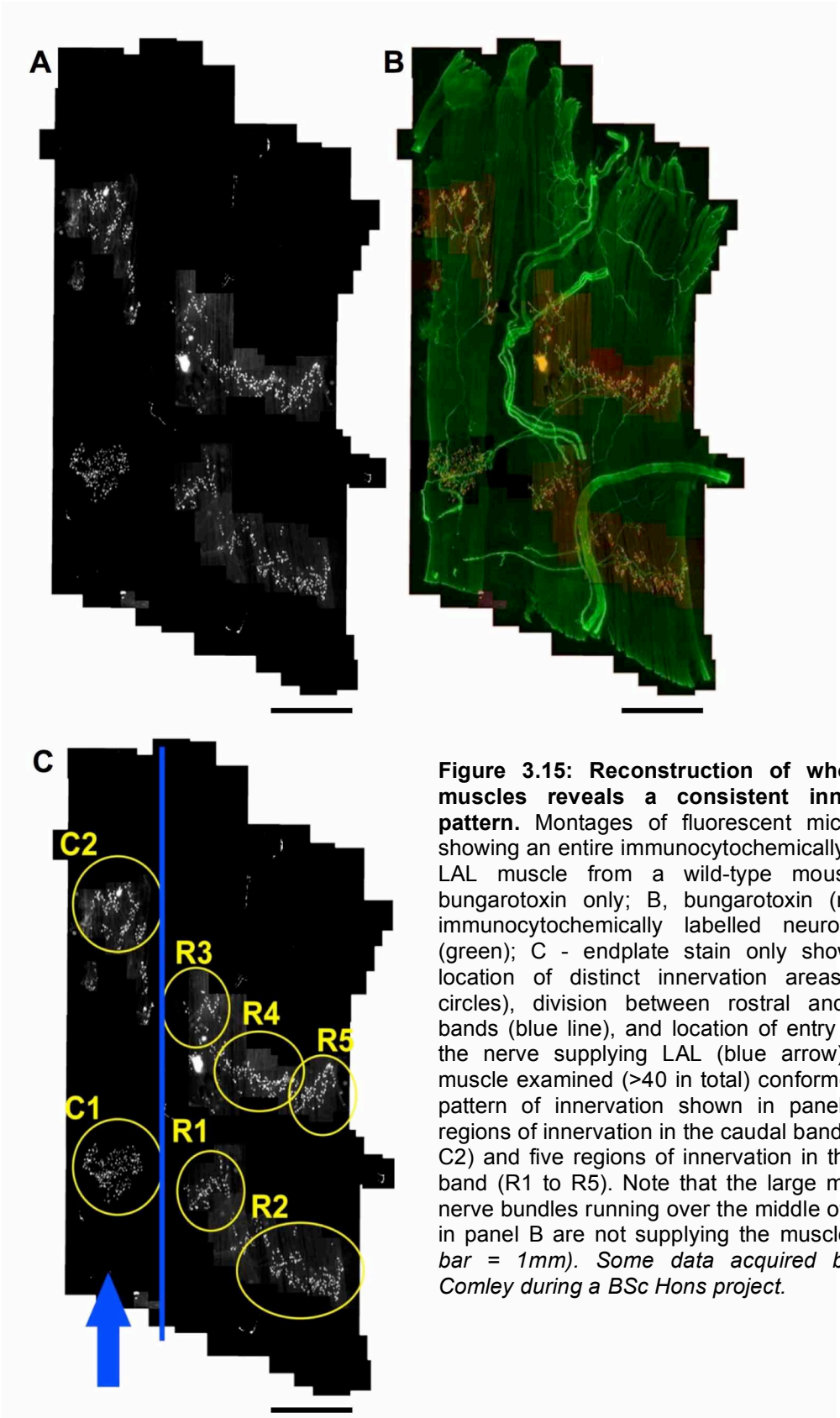

Figure 3.15: Reconstruction of whole LAL muscles reveals a consistent innervation pattern. Montages of fluorescent micrographs showing an entire immunocytochemically labelled LAL muscle from a wild-type mouse (A,C, bungarotoxin only; B, bungarotoxin (red) and immunocytochemically labelled neurofilaments (green); C - endplate stain only showing the location of distinct innervation areas (yellow circles), division between rostral and caudal bands (blue line), and location of entry point for the nerve supplying LAL (blue arrow)). Every muscle examined (>40 in total) conformed to the pattern of innervation shown in panel C: two regions of innervation in the caudal band (C1 and C2) and five regions of innervation in the rostral band (R1 to R5). Note that the large multi-axon nerve bundles running over the middle of the LAL in panel B are not supplying the muscle. *(Scale bar = 1mm). Some data acquired by Laura Comley during a BSc Hons project.*

In order to investigate whether the rostral and caudal bands shared pools of innervating motor neurons, or whether they were composed of distinct and separate motor units individual, immunocytochemically labelled motor neuron axons were traced from the point at which they entered the muscle (via a single muscle entry point; arrow in Figure 3.15 C) through to their ultimate termination in one of the NMJ clusters in LAL (Figure 3.16). In every muscle examined, motor units exclusively supplied either the rostral *or* the caudal band. No motor units were found that had synaptic terminals in both bands. To confirm this observation, 16 LAL muscles from YFP-H mice in which only a small number of motor neurons (usually one or two) expressed endogenous yellow fluorescent protein were examined (Feng *et al.*, 2000). In each case, individually labelled motor units innervated either the caudal band or the rostral band, but never both (Figure 3.16 B). These experiments show that distinct populations of motor neurons supply the rostral and caudal bands of LAL. The preferential loss of innervation in the caudal band of *Smn-/-;SMN*2 and *Smn-/-;SMN*2*;Δ7* mice is therefore likely to represent innervation from a selectively vulnerable population of motor neurons.

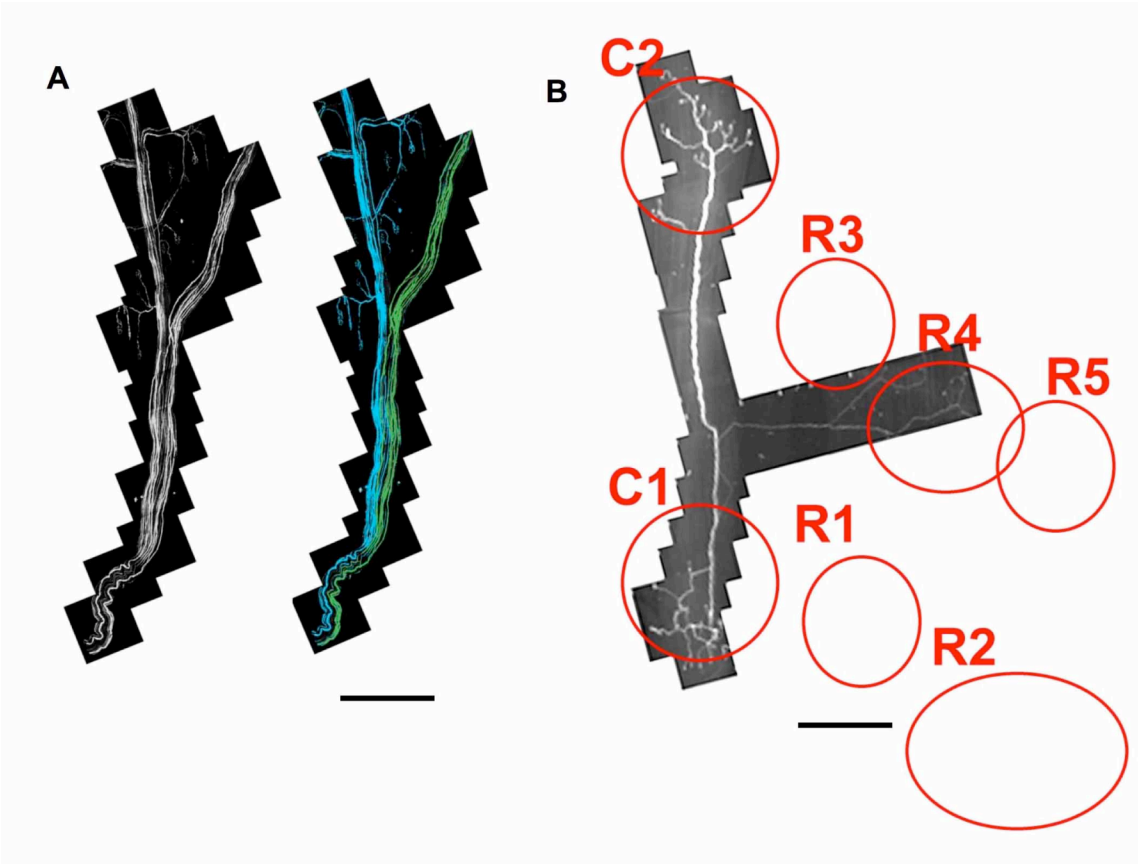

Figure 3.16: Reconstruction of muscle innervation in the LAL reveals distinct subpopulations of motor neurons supplying the rostral and caudal bands of the muscle. A - Montages of fluorescent micrographs showing immunocytochemically labelled axons entering a LAL muscle from a wild-type mouse (equivalent location to the arrow in figure 15C). The right panel is a pseudo-coloured version of the axons shown in the left panel which have been manually traced to identify whether they innervate the caudal band (blue; some endplates in area C1 can be seen at the top of the panel) or rostral band (green). We never found any examples of a single axon that innervated both rostral and caudal bands of the muscle. B - Montage of fluorescent micrographs showing two distinct YFP-labelled motor neurons (one bright and one faint) innervating the LAL muscle in a thy1.1-YFP-H mouse with innervation regions superimposed from figure 15C. Note how the bright motor neuron only innervates the caudal band (synapses formed in both C1 and C2) whereas the faint motor neuron innervates only the rostral band (R4 only). In all of the YFP-H muscles examined (N=16 muscles), individually labelled motor units were only seen to innervate either the caudal band, or the rostral band alone. Thus, distinct subpopulations of motor neurons innervate the rostral and caudal bands of the LAL with no overlap in innervation. *(Scale bars = 200μm (A), 750μm (B).) Some data acquired by Laura Comely during a BSc Hons project.*

3.2.6 Selectively vulnerable motor neurons conform to a FaSyn phenotype

One possible explanation for the selective vulnerability of synapses in the caudal band of LAL was that these motor units were larger (and hence had a more severe demand on intrinsic resources required to maintain viability following a degenerative stimulus) than motor units innervating the rostral band. However, quantitative analysis of motor unit sizes in the rostral and caudal bands of the LAL, using YFP-H mice to label the entire synaptic cohort of individual motor units, showed no difference between the two muscle bands (average motor unit size of 18/19 in rostral/caudal band respectively, non-significant students T test; Figure 3.17). Similarly, a previous study of motor neuron vulnerability in SOD1 mouse models of amyotrophic lateral sclerosis demonstrated that axons of fast-fatiguable motor neurons are more vulnerable than slow motor neurons (Pun *et al*., 2006). However, as the LAL muscle is composed of an entirely homogenous population of fast-twitch muscle fibres (see above), it is unlikely that the selective vulnerability of motor neurons innervating the caudal band is due to a difference in the fast/slow status of motor neurons between the two bands of the muscle.

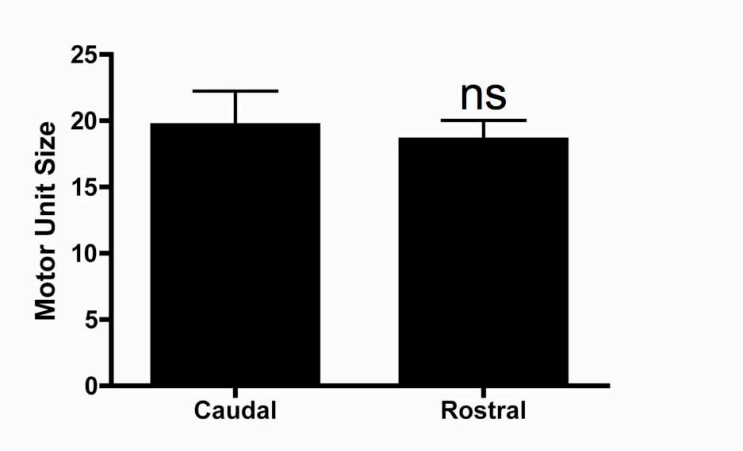

Figure 3.17: There is no difference in motor unit size between rostral and caudal bands of the LAL. Bar chart showing the motor unit size (number of endplates innervated by a given motor neuron) in rostral and caudal bands of the LAL. *(mean±SEM; unpaired students t-test; ns – non significant; n=10 muscles).*

I therefore examined whether motor neurons innervating the caudal band differed from those innervating the rostral band with respect to their FaSyn/DeSyn characteristics (Pun *et al*., 2002; see section 1.2.2). In particular, NMJs conforming to a 'Delayed Synapsing' (DeSyn) phenotype have been shown to undergo dramatic collateral sprouting and the formation of ectopic endplates following prolonged paralysis with BotA, whilst 'Fast Synapsing' (FaSyn) NMJs remain largely unaffected.

To test whether neuromuscular synapses in the caudal band of LAL differed from those in the rostral band with respect to their FaSyn/DeSyn characteristics, in wild-type the LAL muscle was paralysed for 1 month with repeated subcutaneous injections of BotA (see materials and methods). Subsequent quantitative analysis of collateral sprouting from nerve terminals and ectopic endplate formation in immunocytochemically stained LAL muscles revealed striking differences between the two bands (Figure 3.18). In the caudal band of the muscle, very few motor nerve terminals (<5%) showed any signs of collateral sprouting (Figure 3.18 E). In contrast, more than 20% of endplates in the rostral band showed clear evidence of terminal collateral sprouting (Figure 3.18 E). Similarly, there were significantly fewer ectopic endplates formed in the caudal band compared to the rostral band (Figure 3.18 F). In addition, the differential disruption of post-synaptic acetylcholine receptor clusters, previously reported in FaSyn/DeSyn muscles in response to BotA (Pun *et al*., 2002), was observed in the rostral and caudal bands, with the former undergoing significant post-synaptic disassembly and the latter less affected (Figure 3.18 C,D). These experiments reveal that motor neurons supplying the caudal band of the LAL are more FaSyn-like than their counterparts in the rostral band. Motor neurons with FaSyn-like characteristics may therefore be more likely to be vulnerable to SMA-induced synapse loss than those with DeSyn characteristics.

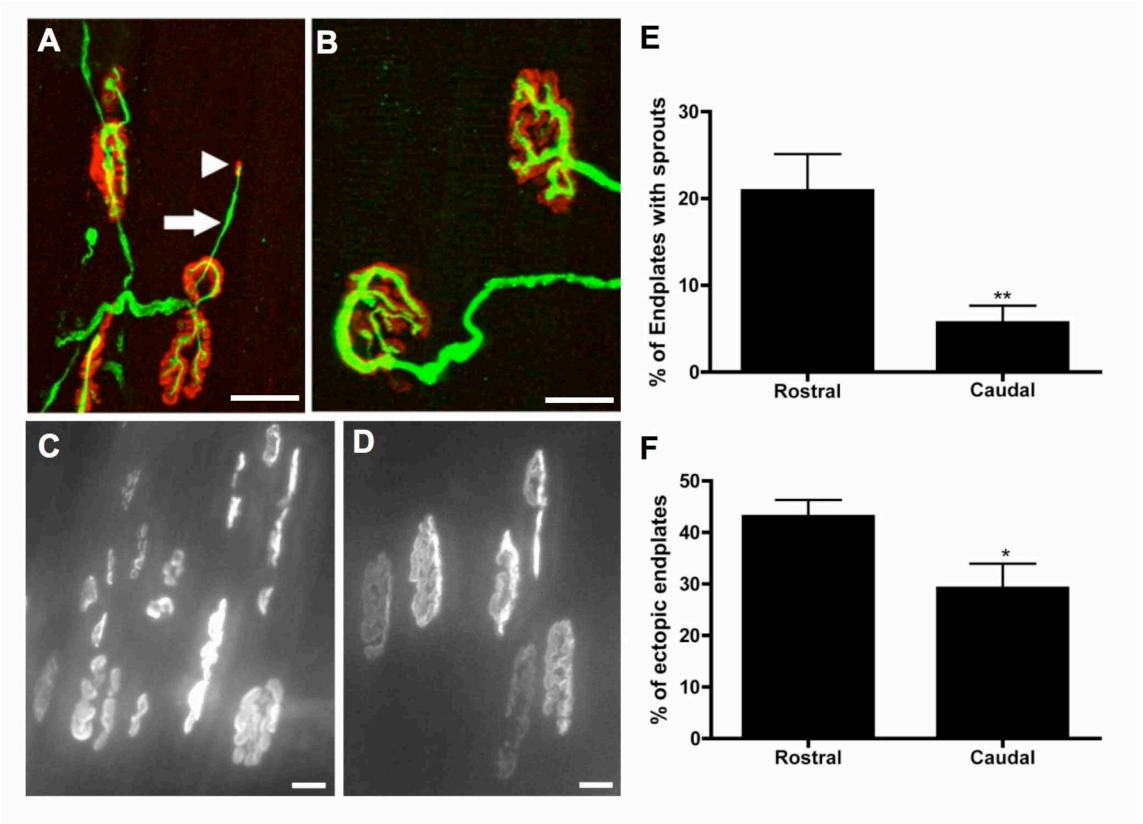

Figure 3.18: Selectively vulnerable motor neurons in the caudal band of LAL conform to FaSyn characteristics. A/B – Confocal micrographs showing neuromuscular junctions in the caudal (A) and rostral (B) portions of an immunocytochemically labelled LAL from a wild-type mouse muscle paralysed for 1 month with repeated injections of BotA (green = 150kDa neurofilaments; red = post-synaptic acetylcholine receptors labelled with TRITC-α-bungarotoxin). The white arrow is identifying a collateral terminal sprout induced by paralysis and the white arrowhead is highlighting an ectopic endplate innervated by a collateral sprout. C,D - Fluorescent micrographs showing significant post-synaptic disassembly in the rostral band (C) of the LAL compared to the reduced levels observed in the caudal band (D) (Post-synaptic AChR's labeled with TRITC-α-bungarotoxin) E – Bar chart showing significantly fewer collateral terminal sprouts in paralysed neuromuscular junctions from the caudal band of LAL compared to the rostral band. F - Bar chart showing significantly fewer ectopic endplates (expressed as a percentage of total enplates) in paralysed neuromuscular junctions from the caudal band of LAL compared to the rostral band *(Mean ± SEM; Mann Whitney test, two tailed; *P<0.05, **P<0.01; n=10 muscles; Scale bars = 20 μm (B), 15μm (A,C,D)).*

3.3 Discussion

The findings of this chapter confirm that NMJs are early and significant targets in SMA and provide novel insights into neuromuscular pathology. I first demonstrated that neuromuscular pathology was prominent in muscle groups taken from different locations throughout the body of two SMA mouse models. Consistently, the postural TVA was more severely affected than fast-twitch LAL and lumbrical muscles, suggesting that muscle fibre-type and body location are likely to be important determining factors in regulating synaptic vulnerability during SMA. The morphological and ultrastructural correlates of nerve terminal loss support the hypothesis that SMA demonstrates characteristics consistent with a dying-back neuropathy. Second, I showed that synapses form normally in SMA mouse models, but that in the most severely affected muscles (e.g. TVA) pre-synaptic pathology occurs early on in the disease course. Third, I identified differences in the time-course and severity of neuromuscular pathology between *Smn-/-;SMN*2 and *Smn-/-;SMN*2*;Δ7* mice. Severe pre-synaptic pathology in late-symptomatic *Smn-/-;SMN*2 mice was not mirrored in late-symptomatic *Smn-/-;SMN*2*;Δ7* mice. Post-synaptic pathology, however, appeared to be much more severe in late-symptomatic *Smn-/-;SMN*2*;Δ7* mice, suggesting that the *Δ7* transgene does not simply delay the neuropathology observed in *Smn-/-;SMN*2 mice. Rather, it appears that the *Δ7* transgene has an affect in attenuating pre-synaptic pathology. Fourth, I demonstrated that post-synaptic changes resulting in shrinkage of motor endplates do not correlate with pre-synaptic pathology (loss of nerve terminals). Thus, pre- and post-synaptic changes can occur independently of one another at any given NMJ. And finally, I have identified a selectively vulnerable population of motor neurons innervating the caudal band of the LAL muscle. These motor neurons conform to a FaSyn phenotype when challenged with paralysis (Pun *et al*., 2002) suggesting that FaSyn motor neurons may be particularly vulnerable in SMA.

3.3.1 Differences in neuromuscular pathology progression in Smn-/-;SMN2 and Smn-/-;SMN2;Δ7 mouse models

An important finding from this study is the difference in pre-synaptic pathology observed between the two mouse models investigated. Significant and progressive pre-synaptic denervation was observed in Smn-/-;SMN2 mice in all muscles investigated, albeit at varying levels, with denervation being apparent from pre-symptomatic time points. This finding has since been corroborated by another group who observed denervated endplates in intercostal muscles at late embryonic time points (McGovern *et al.*, 2008). In contrast, in the Smn-/-;SMN2;Δ7 model, although denervation was observed at early symptomatic time points, degeneration was not progressive leaving NMJs surprisingly intact at end-stage time points. It is unclear why such discrepancies exist but it is perhaps worth considering given the implications such differences could have. Due to the prolonged life span of the Smn-/-;SMN2;Δ7 model, it is used by many groups as a model for therapeutic strategy. Therapeutic approaches that facilitate retrograde transport, and/or synaptic protection are perhaps more likely to be successful in a system in which there is minimal denervation. Further study is therefore required to determine, firstly why pre-synaptic denervation is attenuated in the Smn-/-;SMN2;Δ7 model, and secondly what level of denervation is observed in human patients.

3.3.2 Pre- and post- synaptic pathology can occur independently

The data presented above showed a clear dissociation of pre- and post-synaptic pathology in all muscle groups examined, and in both mouse models of SMA. These findings provide strong support for the hypothesis that pre- and post-synaptic pathology can occur independently of one another in SMA. One possible explanation for this, which the current study has not been able to directly address, is that SMN gene activity may be required in both neuronal and muscle tissue in order to alleviate the pathological phenotype (Chan *et al.*, 2003). Neuron-specific functions of SMN are well documented, and are supported by data in the current study, with SMN being shown to be important

for events including axon outgrowth, path-finding and neuronal maintenance (McWhorter *et al.*, 2003; Rossoll *et al.*, 2003; Ferri *et al.*, 2004; Gavrilina *et al.*, 2009). The muscle-specific role of SMN is rather less clear, although deletion of SMN exon 7 in mouse muscle is known to cause severe muscular dystrophy (Cifuentes-Diaz *et al.*, 2001) and a study utilising another *Drosophila* model of SMA has identified an important role for SMN protein in the form and function of muscle sarcomeres (Rajendra *et al.*, 2007; Walker *et al.*, 2008). A way to address this question would be to repeat the current set of experiments in mouse models in which SMN levels have been reduced, but not completely abolished, in a tissue specific fashion in muscle or nerve individually. Attempts have been made to create such mouse models, and although they demonstrate a clear requirement for Smn in motor neurons, a concurrent increase in the expression levels of Smn in muscle mean that the importance on Smn in muscle cannot be eliminated (Gavrilina *et al.*, 2008). Another possible explanation for the apparent dissociation of pre- and post-synaptic pathology could be that muscle fibre pathology was a consequence of pre-synaptic inactivity - resulting in deficient neuromuscular transmission - occurring in the absence of pre-synaptic degeneration. However, the finding that some nerve terminals were removed from corresponding muscle fibres devoid of any pathology suggests that pre-synaptic inactivity is likely to play, at most, a minor role in regulating post-synaptic pathology.

3.3.3 Selective vulnerability of NMJ pathology in SMA

The finding that motor neurons innervating the TVA (a predominantly slow-twitch muscle) appear to be more susceptible in SMA models than the LAL and lumbrical muscles (exclusively fast-twitch muscles) is in contrast to studies of adult onset motor neuron diseases and provides a potential explanation for the proximal distribution of muscle weakness in SMA (Farrar *et al.*, 2009). Studies of SOD1 mouse models of adult-onset motor neuron disease have demonstrated that phasic, fast-twitch motor neurons are selectively vulnerable with slow-twitch motor neurons reported to be resistant and even capable of initiating regenerative responses (Pun *et al.*, 2006). This contrasting data is

likely to reflect the different cellular stimuli and neuronal environments (e.g. age of disease onset) present in SMA and ALS, but it also highlights the fact that motor neurons cannot be grouped into those that are generically vulnerable and those that are not. Motor neurons that are particularly vulnerable in one form of motor neuron disease may not be vulnerable in another.

The surprising result that motor neurons innervating the caudal band of the LAL muscle are more susceptible than those innervating the rostral band supports the hypothesis that not all pools of motor neurons are affected in the same way and at the same time in different motor neuron diseases (Frey *et al.*, 2000; Ferri *et al.*, 2004; Schaefer *et al.*, 2005). Whereas differences in vulnerability based around different motor neuron properties (e.g. fast-fatiguable, fast-fatigue resistant) and muscle fibre types are certain to exist, the current study demonstrates that motor neurons within a single muscle consisting of a homogeneous population of muscle fibres can also be differentially vulnerable in motor neuron disease. The result here have identified a correlation between vulnerable motor units and FaSyn characteristics. Whilst these experiments do not directly demonstrate a causal link between FaSyn characteristics and selective vulnerability (genetic tools to experimentally manipulate FaSyn and DeSyn characteristics are unfortunately not yet available), the hypothesis is strongly supported by the selective vulnerability of muscle groups present in human SMA patients. For example, the diaphragm (a DeSyn muscle; Pun *et al.*, 2002) is relatively spared whilst the intercostal muscles (FaSyn muscles; Pun *et al.*, 2002) are severely affected (Dubowitz, 1999). These results might suggest that developmentally distinct motor units populations are specifically more vulnerable to pathology in SMA and implicate developmental process with SMA pathogenesis. Alternatively, they may indicate that the greater degree of plasticity observed in DeSyn motor units is somehow neuroprotective. This finding would be consistent with the observation that slow twitch fibres, which are known to retain a higher degree of plasticity than fast twitch fibres, are selectively less vulnerable in mouse models of ALS (Pun *et al.*, 2006).

This is the first time that FaSyn and DeSyn characteristics have been identified in subpopulations of neurons innervating the same muscle. The data suggest that further studies providing insights into the mechanisms through which motor neurons and their synapses are specified to be, and develop into, FaSyn or DeSyn motor units may provide important insights into vulnerability of motor neurons in SMA. The ability to identify factors associated with the more resistant DeSyn synapses may provide new targets for therapeutic intervention. The neuroanatomical map of LAL innervation and the identification of its differential neuronal susceptibility provided in the current study is likely to provide a useful model system with which to explore the differences between FaSyn and DeSyn synapses, and their vulnerability in SMA, in more detail.

Chapter 4: Pre-symptomatic development of lower motor neuron connectivity in SMA

Summary

Based on the hypothesis that Smn is required for normal neuronal development, I have used immunocytochemical labelling and confocal microscopy to allow analysis of pre-symptomatic (P1) LAL and AS/AAL muscles from *Smn-/-;SMN2* mice. I have compared the developmental morphology of pathologically vulnerable and stable motor units to determine whether abnormal development of lower motor neuron connectivity underlies neuromuscular vulnerability. Together with pre-symptomatic micro-array analysis of the spinal cord, results suggest that abnormal pre-symptomatic development does not underlie pathogenesis in SMA.

Results detailed in this chapter show that:

1. Innervation patterns form normally in both vulnerable and stable regions of the LAL muscle
2. Axon guidance and branching are unaltered in both vulnerable and stable motor units.
3. Significant developmental sprouting exists in control P1 muscles but is unaltered in vulnerable and stable SMA motor units.
4. Post-synaptic maturation occurs normally in both vulnerable and stable muscle regions.
5. There are minimal changes in gene expression in the spinal cord of P1 *Smn-/-;SMN2* mice.

4.1 Introduction

Given the early onset of SMA in its more severe form, it has been postulated that abnormal pre-symptomatic development could render motor units vulnerable and pre-empt degeneration. This finding would be consistent with the observation that motor units conforming to distinct development subtypes are differentially vulnerable in SMA mouse models (see chapter 3). Several studies have suggested that reduced Smn protein levels can have a significant influence on neuro-developmental processes in lower motor neurons (see section 1.4.5). Although a failure to establish the neuromuscular system during embryogenesis appears unlikely to contribute to any developmental phenotype (McGovern *et al.*, 2008), it is possible that deficiencies in motor unit development (controlling factors such as motor unit branching, size, pruning and function) may play a major role in conferring pre-symptomatic vulnerability upon lower motor neurons.

These ideas have led to the suggestion that SMA may be caused by the incorrect development of the neuromuscular system, which confers an intrinsic vulnerability upon lower motor neurons during the early stages of growth and maturation before the onset of neurodegenerative events. If this were the case, then attempts to rescue the neuromuscular system after birth (e.g. by elevating levels of Smn protein using gene therapy or pharmaceutical approaches; Azzouz *et al.*, 2004; Avila *et al.*, 2007) would have significant limitations. However, if pre-symptomatic developmental abnormalities are not a major feature of SMA, the neuromuscular system may remain intact until the postnatal onset of symptoms and therefore be more amenable to rescue.

To directly address whether alterations in pre-symptomatic development of lower motor neurons and motor neuron connectivity contribute to SMA pathogenesis *in vivo*, I have undertaken a combined analysis of pre-symptomatic neuromuscular morphology and gene expression in the *Smn-/-;SMN2* mouse model of SMA (Monani *et al.*, 2000). I have taken advantage of the novel observation that selectively vulnerable populations of lower motor neurons and NMJs in the caudal band of the mouse LAL muscle have neighbouring stable populations in the rostral band of the same muscle (see chapter 3).

This has allowed us to investigate and compare pre-symptomatic lower motor neuron development and connectivity in both vulnerable and non-vulnerable motor units supplying the same muscle, testing the hypothesis that pre-symptomatic developmental dysfunction is a pre-requisite for subsequent neuromuscular pathology. I show that perturbations in pre-symptomatic developmental pathways are neither present nor necessary for subsequent lower motor neuron pathology in SMA *in vivo*. Parallel gene expression analyses of pre-symptomatic spinal cord from *Smn-/-;SMN2* and *Smn-/-;SMN2;Δ7* mice confirmed the absence of any disruption of developmental pathways.

4.2 Results

4.2.1 Innervation patterns form normally in both vulnerable and stable motor units of the LAL in Smn-/-;SMN2 mice

To establish whether pre-symptomatic developmental abnormalities are a significant feature of SMA *in vivo* morphological correlates of lower motor neuron connectivity were examined in the *Smn-/-;SMN2* mouse model of severe SMA at pre-symptomatic ages (post-natal day 1; P1). At this time point there is no evidence of pre-synaptic degeneration or post-synaptic atrophy within this muscle (see chapter 3). The LAL muscle provided us with an excellent model system with which to study selectively vulnerable populations of lower motor neurons in these mice, allowing a direct comparison of neighbouring populations of differentially-affected motor units whilst eliminating variables such as nerve stump length, muscle fibre type and muscle function (see chapter 3). Whole mount LAL muscles from P1 *Smn-/-;SMN2* and litter-mate control mice (*Smn*+/+;*SMN*2,) were labelled with antibodies against 150kDa neurofilament to reveal axonal and synaptic morphology and rhodamine-conjugated α-bungarotoxin to label post-synaptic acetylcholine receptors at the NMJ.

Fluorescent micrograph montages of the whole LAL muscle (incorporating both caudal and rostral bands) allowed analysis of the gross muscle innervation pattern in pre-symptomatic P1 mice (Figure 4.1). No differences were observed between the gross innervation patterns of either the rostral (non-vulnerable motor units) or caudal (vulnerable motor units) bands of the LAL in *Smn-/-;SMN2* and litter-mate control mice (N=8 control muscles; N=14 *Smn-/-;SMN2* muscles). Endplates were clustered into distinct and highly characteristic innervation bands in all muscles examined: C1 and C2 in the caudal band and R1-5 in the rostral band (see figure 3.15). Axons consistently entered adjacent to region C2. Analysis of axon branching patterns in the caudal band of the LAL revealed some variability in the number and distribution of branch points within genotypes (Figure 4.2). Despite this, no consistent abnormality between genotypes was observed. Quantification of the numbers of neuromuscular synapses in medially situated endplate bands (regions C2 and R3-5, selected because these areas

were least likely to suffer damage during muscle dissection) revealed no differences in either caudal or rostral bands between *Smn-/-;SMN2* and control mice (Figure 4.3). This was in agreement with previous studies that reported no obvious discrepancy in the initial embryonic establishment of neuromuscular innervation patterns in SMA mice (McGovern *et al*., 2008).

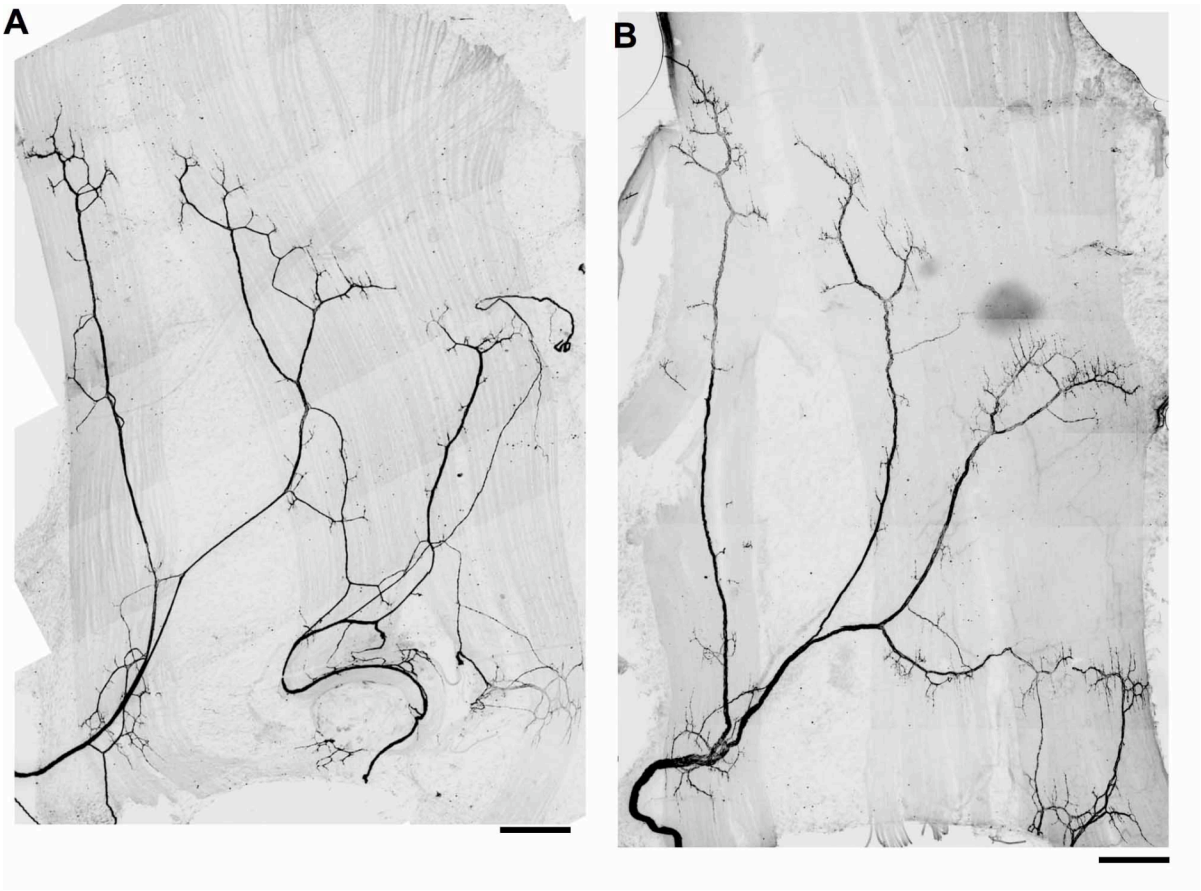

Figure 4.1: Gross anatomy of the LAL muscle at P1 shows normal innervation patterns in *Smn-/-;SMN2* mice. A,B – montaged fluorescent micrographs from immunocytochemically labelled LAL muscles (Black = 150kDa neurofilaments) showing innervation pattern in P1 control (A) and *Smn-/-;SMN2* (B) LAL muscles. Individual fluorescent micrographs were montaged and photo-inverted in adobe photoshop. *(Scale bar = 400μm).*

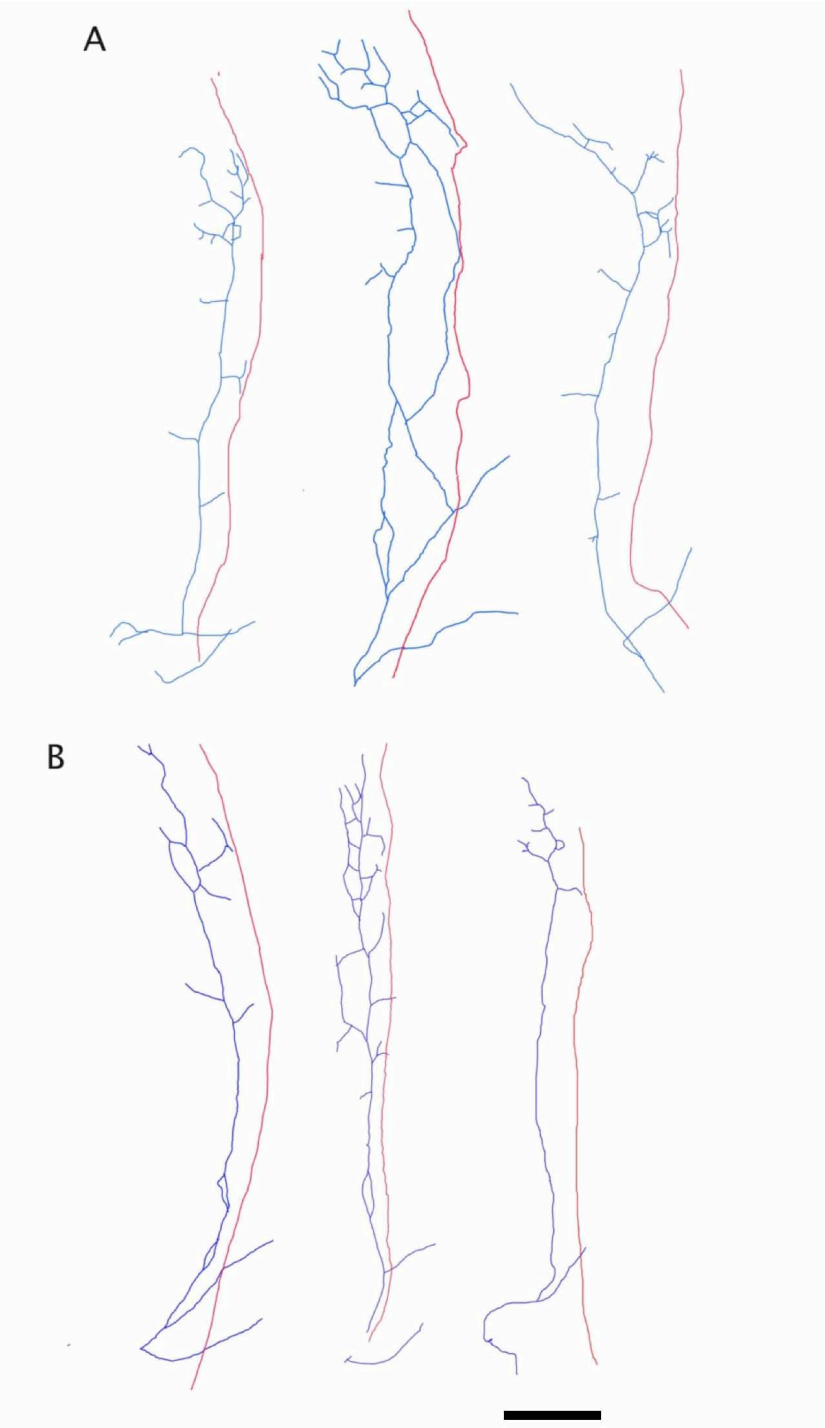

Figure 4.2: Despite variability in axon branching patterns in the caudal band of the LAL, no consistent abnormality was observed. A,B – Example axon traces of branching patterns (blue) in the caudal band (limit shown in red) revealed significant variability in the number and location of axon branches in both control (A) and *Smn-/-;SMN2* muscles (B). Most caudal bands had a intermediate level of axon branching (left) while examples of muscle bands with a high amount of branching (middle) or reduced about of branching (right) could be observed in both genotypes. Despite this, no consistent abnormality could be observed between genotypes. *(Scale bar = 400μm)*

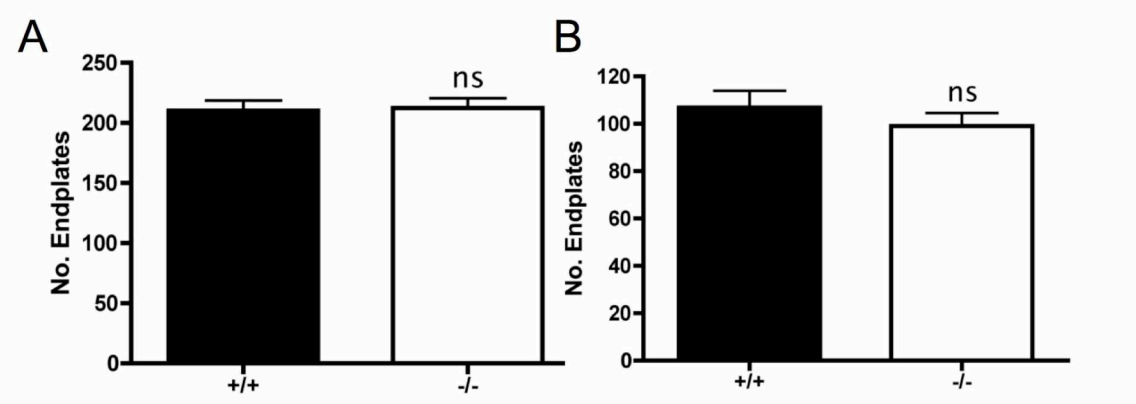

Figure 4.3: There is no change in the number of endplates in the LAL muscle from P1 *Smn-/-;SMN2* mice. A,B - Bar charts (Mean ±SEM) showing the number of endplates in regions R3-5 (A) and C2 (B) in LAL muscles from P1 control *(+/+; black bars)* and *Smn-/-;SMN2 (-/-; white bars)* mice. *(students T-test; ns non-significant; N=7/8 per control rostral/caudal band; N=14/12 per Smn-/-;SMN2 rostral/caudal band.)*

4.2.2 Axon branching and path-finding occur normally in both vulnerable and stable motor units in the LAL muscle of pre-symptomatic Smn-/-;SMN2 mice.

It is possible that pre-symptomatic changes in lower motor neuron branching and path-finding could lead to excessive demands being placed on individual lower motor neurons (e.g. functionally and/or energetically), thereby damaging the cell and pre-disposing it to subsequent degeneration. Such defects in axonal path-finding and/or branching would most likely manifest as alterations in the number of axons present in intramuscular nerve bundles. Axon number was therefore quantified in intramuscular nerve bundles innervating regions C2 and R3 (two anatomically highly-consistent areas of the LAL muscle) in P1 *Smn-/-;SMN2* and control mice. Axons were only quantified in areas of the muscle where the complete endplate band could be seen in order to ensure that no other axon branches were entering the endplate band from a different nerve bundle. Initial attempts to quantify the numbers of individual axons in intramuscular nerve bundles by undertaking analyses on raw confocal stacks and z-projections proved inconsistent and unreliable (Figure 4.4; Appendix 10.1). To achieve the necessary resolution required for accurate and robust analysis, confocal stacks were subjected to deconvolution analyses (Figure 4.4; Appendix 10.1). Quantification of axon numbers normalised to the number of endplates innervated revealed no difference in the numbers

of axons innervating either C2 or R3 regions of *Smn-/-;SMN2* or control mice (Figure 4.5).

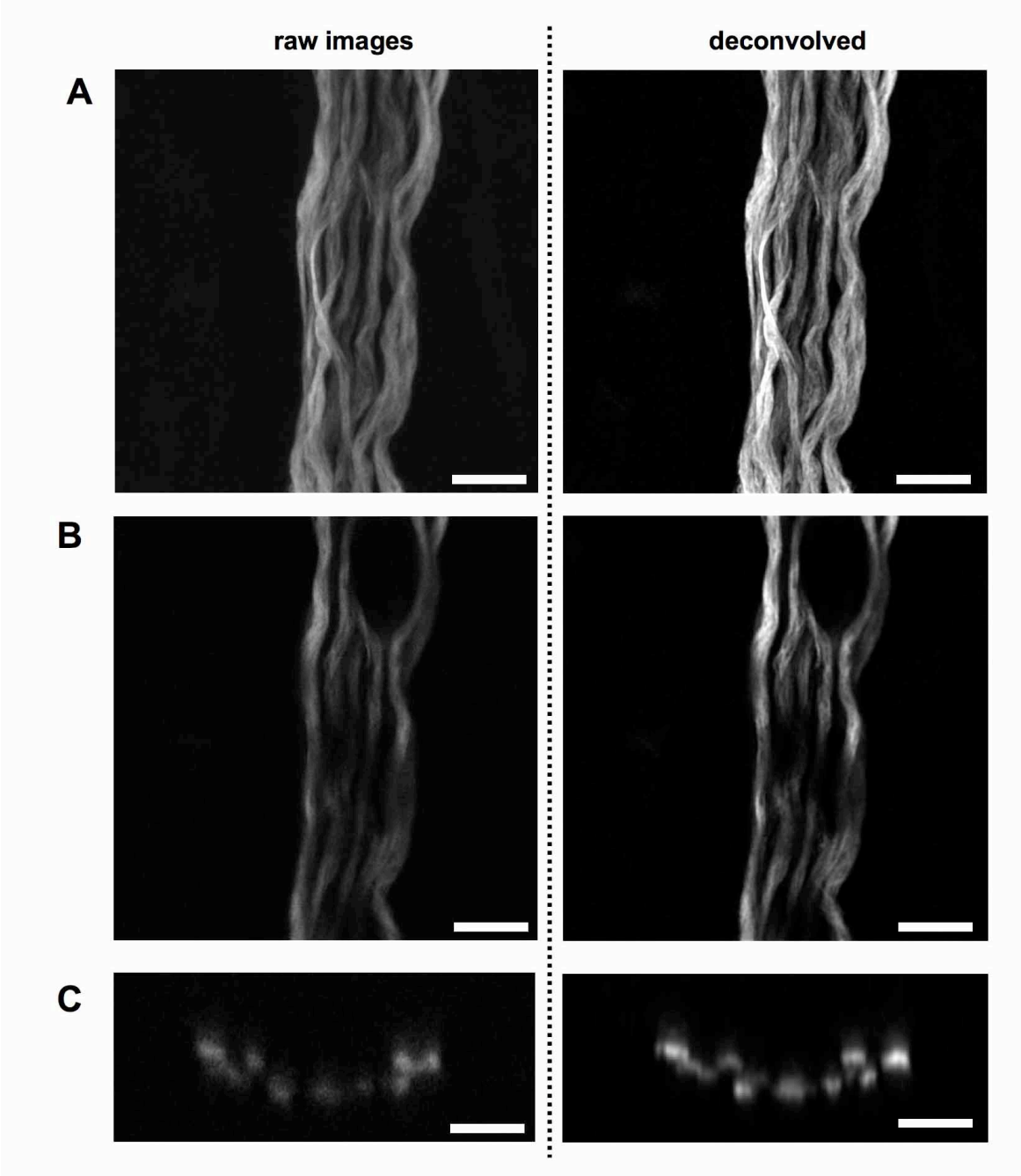

Figure 4.4: Deconvolution as a tool to count axon number in axon bundles. Panels show a confocal micrograph of a neurofilament labelled axon bundles visualised as a z-projection (A), single slice (B) or cross-sectional slice (C). Images on the left show raw images obtained from the confocal microscope. Images on the right are the equivalent images which have undergone deconvolution analysis. *(Scale bar = 10μm (A,B), 5μm (C)).*

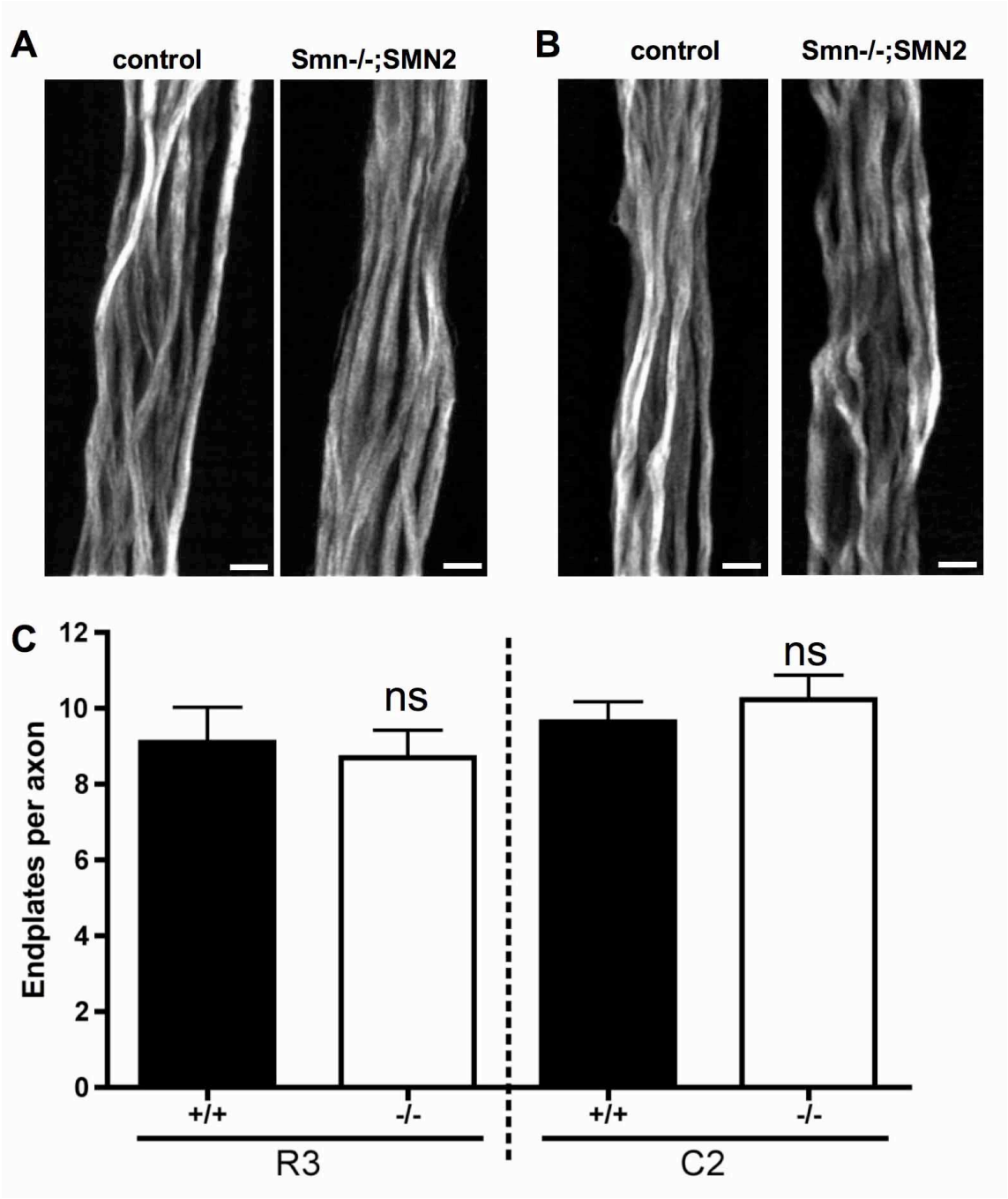

Figure 4.5: There is no change in the number of axons innervating regions R3 or C2 in LAL muscles from P1 *Smn-/-;SMN2* mice. A,B - Deconvolved confocal micrograph Z-projections of axons bundles innervating region R3 (A) and C2 (B) in muscles from control and *Smn-/-;SMN2* mice C – Bar chart (Mean ± SEM) showing number of endplates per axon in regions R3 and C2 from control littermate *(+/+;black bars)*, and *Smn-/-;SMN2 (-/-;white bars)* mice. *(ANOVA; ns non significant; N=4/5 per control rostral/caudal band; N=10/10 per Smn-/-;SMN2 rostral/caudal band;* scale *bar = 8μm (A,B)).*

Although there appears to be no change in axonal branching or pathfinding within intramuscular nerves, it remains possible that excessive branching distal to this point results in an increase in motor unit size. Such changes may increase the energetic demands and thus the vulnerability status of a given motor unit. Such alterations would likely result in an increase in the number of axonal inputs per endplate. To address this possibility the number of axon collaterals converging on individual post-synaptic endplates at NMJs were quantified in both bands of the LAL muscle from *Smn-/-;SMN2* and control mice at P1. Note that at this age, NMJs are normally poly-neuronally innervated, as the process of developmental synapse elimination is ongoing. No significant differences were found in the average number of inputs converging on endplates in either rostral or caudal bands between genotypes (Figure 4.6). There was a small, but noticeable, trend towards an increased number of inputs in *Smn-/-;SMN2* mice compared to Smn+/+;SMN2 controls. However, as this small increase was present in both bands of the LAL, and equivalent levels were also observed in heterozygote controls (Smn+/-;SMN2), these small differences are unlikely to contribute to subsequent selective neuromuscular vulnerability in the caudal band of the LAL.

Therefore no changes could be detected which would be consistent with an alteration in axonal pathfinding or branching. It therefore seems unlikely that such defects could account for either the pre-synaptic vulnerability in SMA, or for the differential vulnerability observed between the caudal and rostral bands of the LAL at end-stage time points.

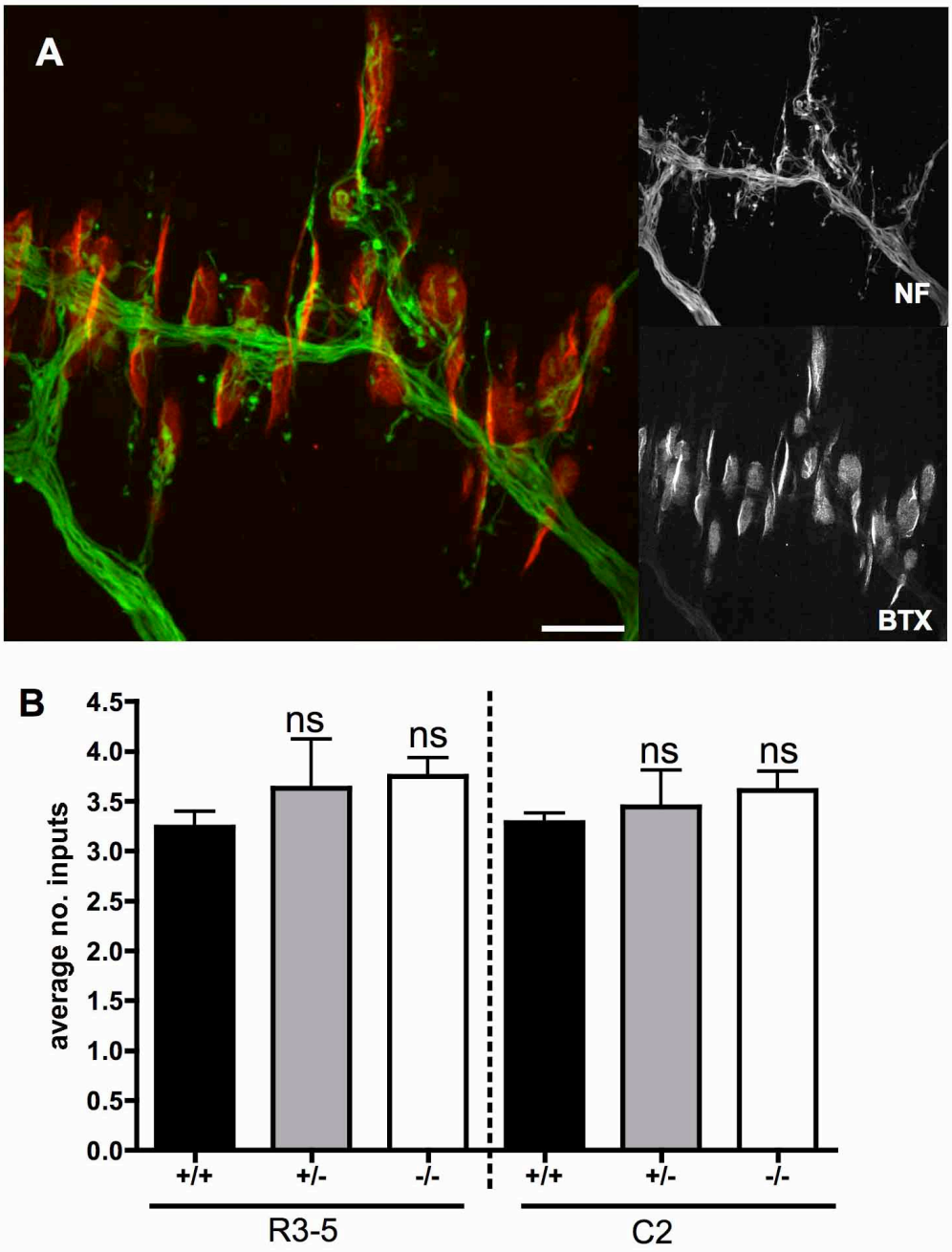

Figure 4.6: No significant change in the number of axonal inputs per endplate in *Smn-/-;SMN2* mice. A – Representative confocal micrograph of an LAL muscle from a P1 control littermate mouse, labelled with antibodies against 150kDa neurofilaments (green, upper left panel) and TRITC-α-bungarotoxin (red, lower left panel), illustrating the type of images used for the quantification of axonal inputs. Note the complexity of innervation patterns at this age and high degree of poly-neuronal innervation (i.e. multiple axons converging on a single motor endplate). B – Bar chart showing no significant difference in the number of inputs per endplate in either the rostral or caudal band of the LAL muscle between P1 *Smn-/-;SMN2 mice (-/-;white bars)* and either Smn+/-;SMN2 *(+/-;grey bars)* or Smn+/+;SMN2 *(+/+; black bars)* littermate controls. *(mean ± SEM; ANOVA; ns non-significant; n=6/6 per rostral/caudal band Smn+/+;SMN2, N=3/3 per Smn+/-;SMN2 rostral/caudal band; n=8/8 per rostral/caudal band Smn-/-;SMN2; Scale bar = 30μm)*

4.2.3 Exuberant terminal sprouting is present in all muscles and unchanged in Smn-/-;SMN2 LAL muscles

During analysis of P1 muscles, numerous axon sprouts extending from pre-synaptic motor nerve terminals were observed that have not been previously reported in the literature. These sprouts were consistently present in all bands of all muscles analysed, including both *Smn-/-;SMN2* and litter-mate control mice. Sprouts ranged in size from under 5μm to over 250μm. Such sprouts could potentially put significant energy demands on the motor unit.

To establish that this was a natural phenomenon and not occurring due to the presence of the *SMN*2 transgene, P1 muscles from wild-type CD1 mice (a completely unrelated genetic strain) were examined. Terminal sprouts were present in CD1 mice (Figure 4.7) and were indistinguishable from those observed in *Smn-/-;SMN2* and control mice at the same age (Figure 4.8; 4.9). These observations warrant further investigation in future studies of normal neuromuscular development. However, neither the numbers of small (<150μm; see methods) nor larger 'super sprouts' (those >150μm in length) were modified in pre-symptomatic *Smn-/-;SMN2* mice (Figure 4.8; 4.9).

These findings indicate that excessive axonal growth in the form of terminal sprouting is unlikely to contribute to synaptic vulnerability in the LAL muscle. They further show that the developmental processes regulating axonal growth are unaltered in *Smn-/-;SMN2* muscles. Taken together, the data above show that pre-symptomatic development of lower motor neuron connectivity occurs normally in both affected and non-affected motor units in severe SMA mice.

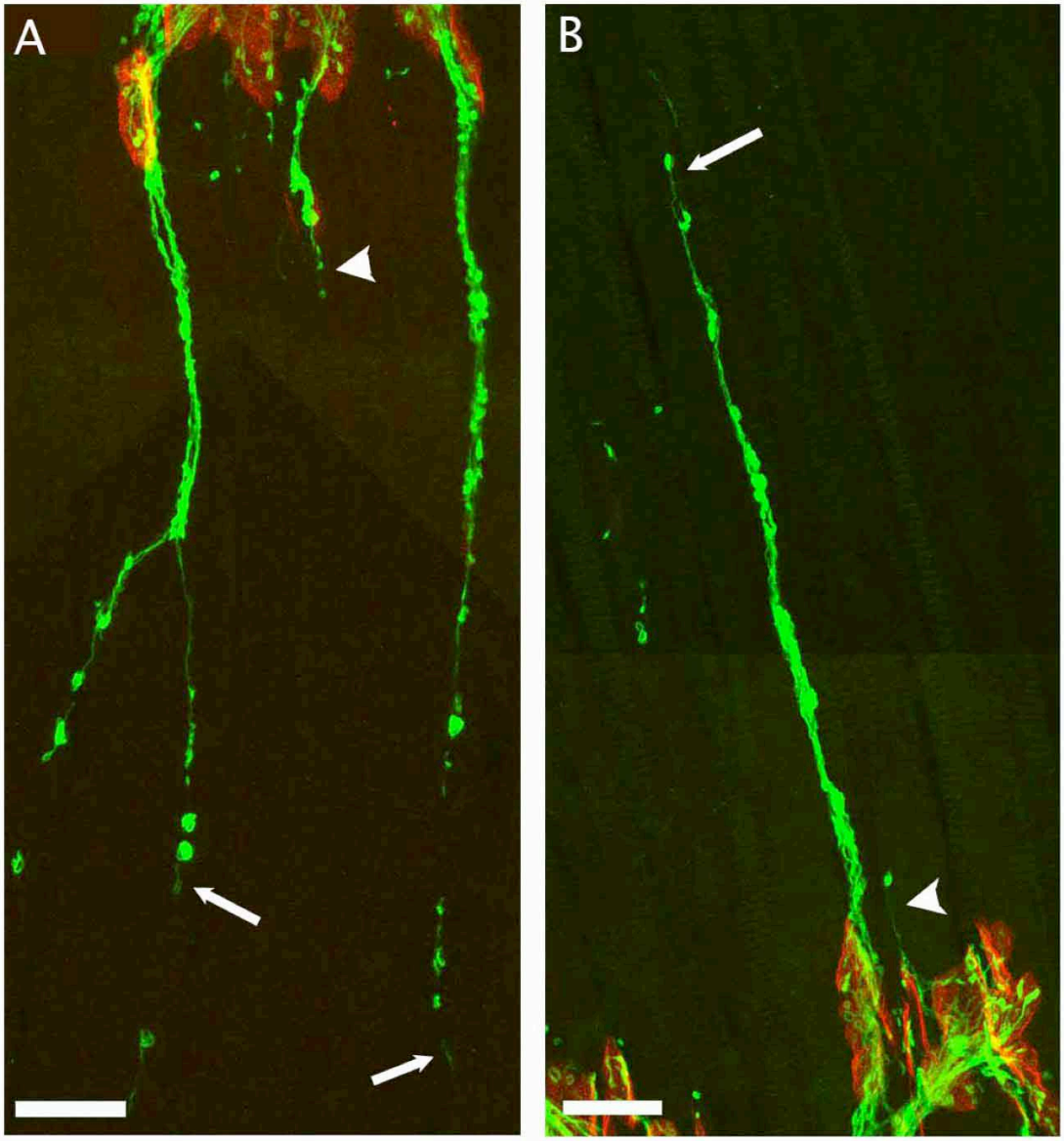

Figure 4.7: Nerve terminal sprouts are neither strain specific nor an aberrant response to the expression of *SMN2*. A,B – Montaged confocal micrographs from an immunohistochemically labelled LAL muscle preparation from a wild-type CD1 mouse (green = 150kDa neurofilaments; red = post-synaptic acetylcholine receptors labelled with TRITC-α-bungarotoxin). Note the presence of both long 'super-sprouts' (arrow) and short sprouts (arrowhead) in both rostral (A) and caudal (B) bands. *(Scale bar = 20μm.)*

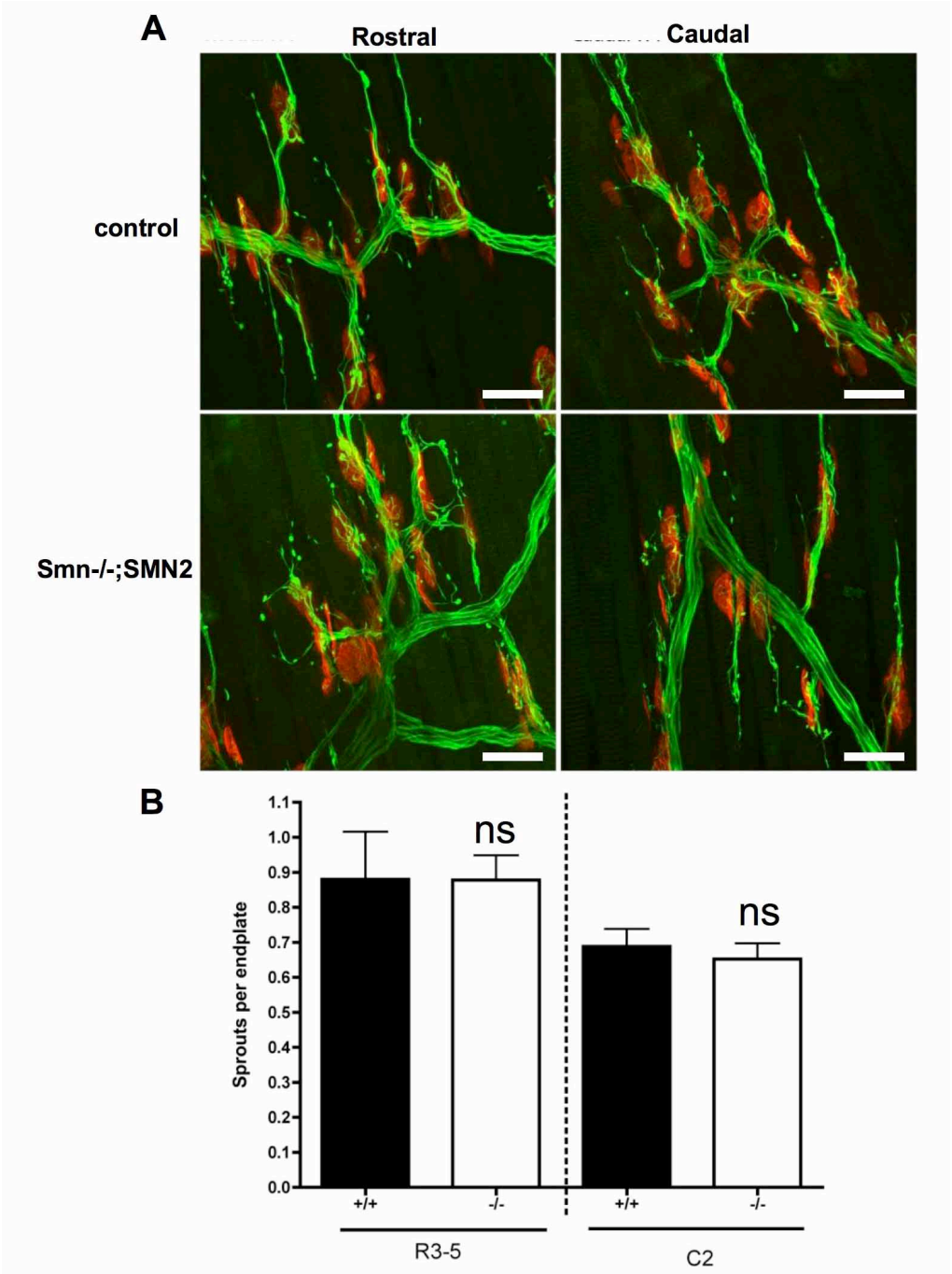

Figure 4.8: Small axonal sprouts were present in both rostral and caudal bands of the LAL muscle at P1, but were unchanged in *Smn-/-;SMN2* mice. A – Representative confocal micrographs from an immunohistochemically labelled LAL muscle preparations (green = 150kDa neurofilaments; red = post-synaptic acetylcholine receptors labelled with TRITC-α-bungarotoxin) showing the presence of small sprouts projecting from nerve terminals in both rostral (left) and caudal (right) muscle bands in both control (upper panels) and *Smn-/-;SMN2* (lower panels) mice at P1. Sprouts were identified as neurofilament positive projections not contacting AChR clusters (see white arrowheads). B – Bar chart showing no change in the number of small sprouts per endplate in *Smn-/-;SMN2* mice *(-/-;white bars)* compared to littermate controls *(+/+; black bars). (mean ± SEM; ANOVA; ns non-significant; n=6/6 per rostral/caudal band control, n=8/8 per rostral/caudal band Smn-/-;SMN2. Scale bar = 30μm (A)).*

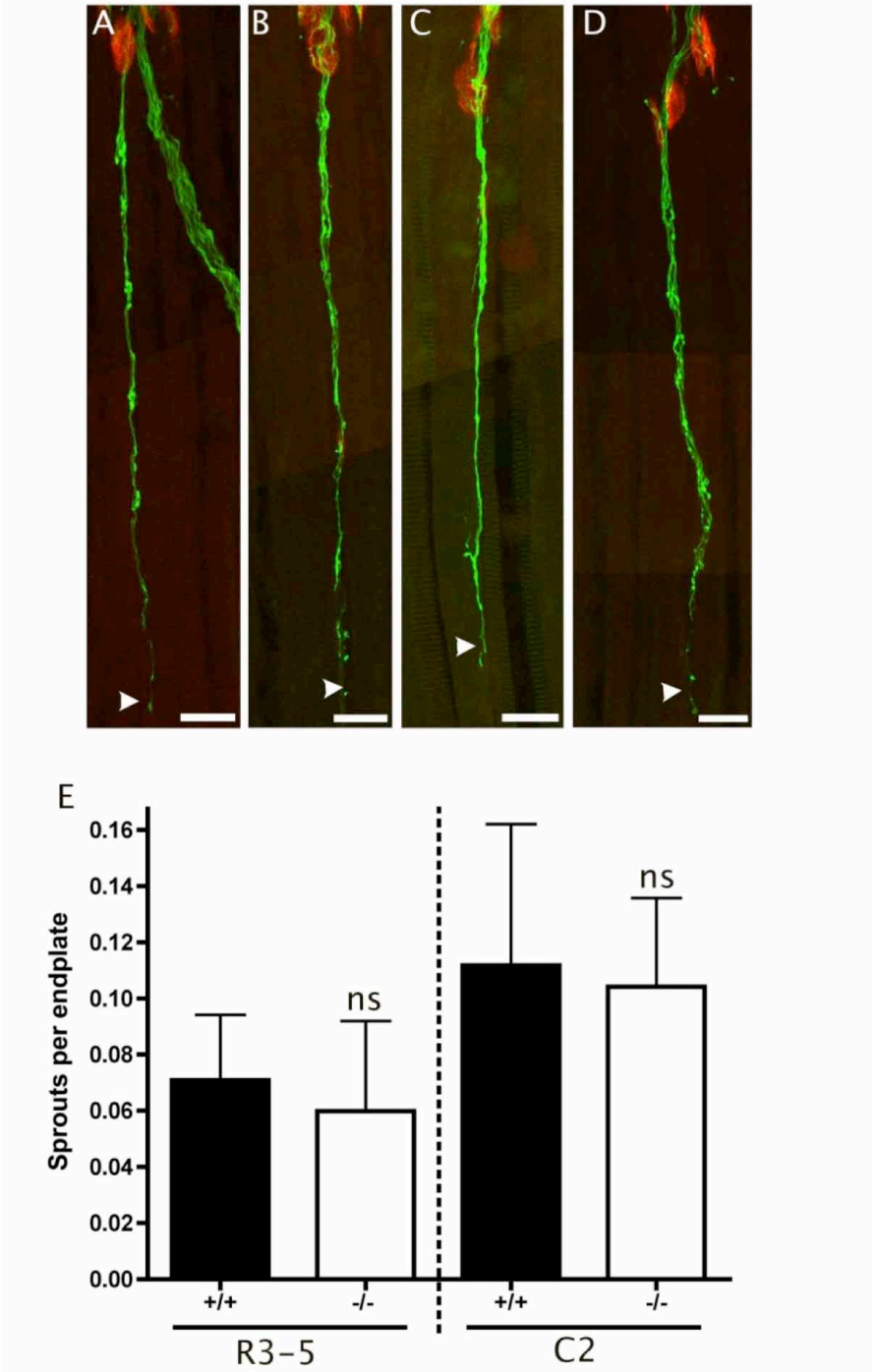

Figure 4.9: Large 'super sprouts' were present in both rostral and caudal bands of the LAL muscle but were also unchanged in *Smn-/-;SMN2* mice. A-D – Representative confocal micrograph reconstructions showing large super sprouts (axonal projections exceeding 150μm in length; white arrowheads) in rostral (A,B) and caudal (C,D) bands from immunohistochemically labelled LAL muscle preparations from P1 control (A,C) and *Smn-/-;SMN2* (B,D) mice *(green = 150kDa neurofilaments; red = post-synaptic acetylcholine receptors labelled with TRITC-α-bungarotoxin; Scale bar = 20μm)*. E – Bar chart showing no significant difference in the numbers of super sprouts (normalised to the number of endplates) present in regions R3-5 and C2 of the LAL muscle of *Smn-/-;SMN2* mice*(-/-; white bars)* compared to littermate controls (*+/+; black bars). (Mean ± SEM; ANOVA; ns non-significant; n=8/8 per rostral/caudal band control, n=15/14 per rostral/caudal band Smn-/-;SMN2)*.

4.2.4 Post-synaptic maturation was unaltered in Smn-/-;SMN2 mice

As lower motor neuron morphology and connectivity were unaffected in *Smn-/-;SMN2* mice at pre-symptomatic stages, I next investigated whether changes in post-synaptic development at the NMJ were present and could account for subsequent vulnerability of motor units. In agreement with previous studies, results here have already established that the position and relative number of post-synaptic motor endplates was normal in both caudal and rostral bands of the LAL muscle in *Smn-/-;SMN2* mice (Figure 4.1, 4.3). Quantification of individual endplate areas revealed a similar, normal distribution in *Smn-/-;SMN2* mice (Figure 4.10). As previous work has suggested that endplate maturation may have an impact upon lower motor vulnerability in SMA mice (Biondi *et al*., 2008), a scale to quantify and compare endplate maturation was applied in *Smn-/-;SMN2* and control mice (Figure 4.11 A). Endplates were categorised as either 'uniform', where AChR receptors were evenly distributed within the endplate area, 'folded' where bright bands on the endplate had formed which were indicative of post-synaptic fold formation (a sign of early maturation), or perforated, where holes in the AChR labelling was indicative of the endplate beginning to take on the adult 'pretzel-like' morphology (see Marques *et al*., 2000). Overall, there was no difference in the numbers or proportion of uniform, folded and perforated endplate morphologies between genotypes (Figure 4.11 B). However, there was an observed increase in endplate maturation in the caudal band of the LAL in mice from both genotypes, as evidenced by an increase in the number of folded and perforated endplates. This finding is consistent with motor units in the caudal band conforming to 'FaSyn' characteristics, being developmentally more advanced than their 'DeSyn' neighbours (Pun *et al*., 2002; see chapter 3).

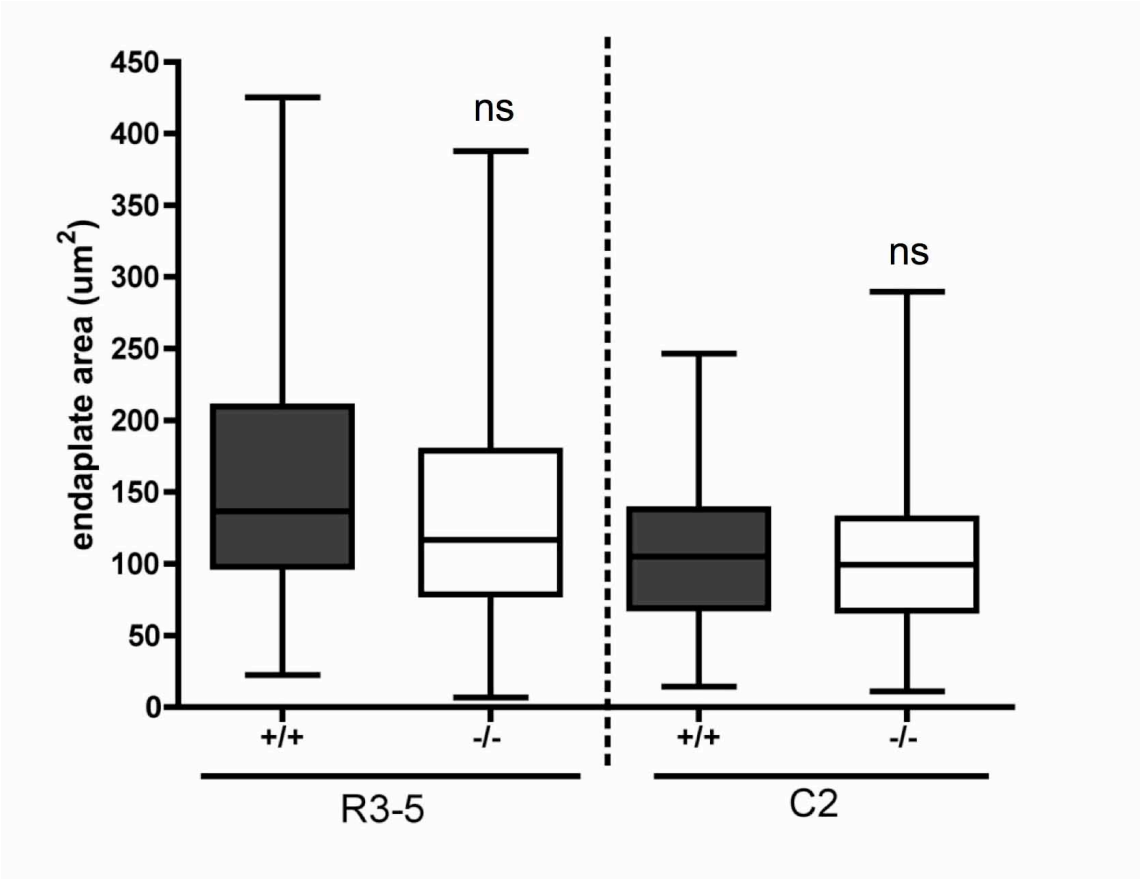

Figure 4.10: There is no difference in endplate area in rostral or caudal bands of the LAL in *Smn-/-;SMN2* mice. Box and whisker plot showing endplate area in regions R3-5 and C2 in LAL muscles from control *(+/+; dark grey boxes)*, and *Smn-/-;SMN2 (-/-;white boxes)* mice. *(Kruskal-Wallis test; ns non significant; N=8/8 per control rostral/caudal band; N=14/14 per Smn-/-;SMN2 rostral/caudal band)*.

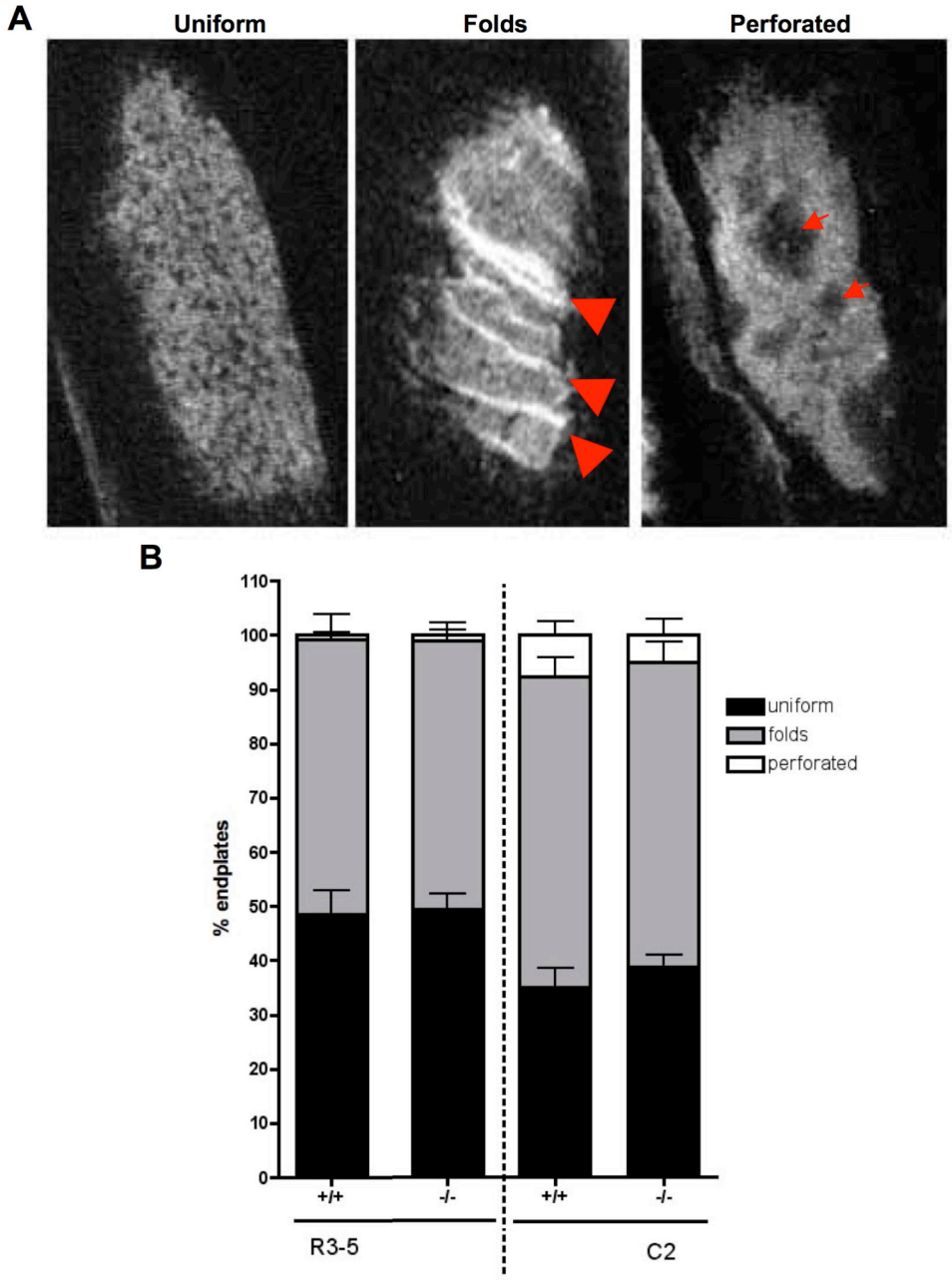

Figure 4.11: There is no difference in endplate maturation in either the rostral or caudal bands of the LAL in *Smn-/-;SMN2* mice. A – confocal micrographs showing example images of endplates in which the bungarotoxin staining is uniformly distributed (left), developed post synaptic folds (red arrowheads, middle) or become perforated (red arrows, right). B – Bar chart showing the percentage of endplates which were categorised uniform (black bars), folded (grey bars) and perforated (white bars) in regions R3-5 and C2 in LAL muscles from *Smn-/-;SMN2 (-/-)* mice compared to control littermates *(+/+). (mean ± SEM; Kruskal-Wallis test; P>0.05; N=8/8 per control rostral/caudal band; N=15/14 per Smn-/-;SMN2 rostral/caudal band).*

4.2.5 There is no alternation in pre-symptomatic development between differentially vulnerable fast-twitch and slow-twitch muscles

The finding that lower motor neuron development occurs normally in both the rostral and caudal bands of the LAL implies that abnormal pre-symptomatic neuromuscular development does not contribute to the increased vulnerability of motor units in the caudal band of the LAL. However, these analyses compared two bands of a homogenous fast-twitch muscle. It therefore remained possible that abnormalities in pre-symptomatic development may contribute to increased vulnerability of lower motor neurons innervating slow-twitch muscles. To investigate this possibility, two additional muscles immediately deep to the LAL muscle were examined: abductor auris longus (AAL) and auricularis superior (AS). The AAL is a predominantly fast-twitch muscle whilst the AS is predominantly slow-twitch (Figure 4.12 A). These muscles were chosen for comparison because of their close proximity and function to one another (and the LAL) as well as their common innervation by the facial nerve (eliminating variables such as nerve stump length and body position, while still allowing whole mount analysis of the complete innervation pattern within a muscle). In late-symptomatic (P5) *Smn-/-;SMN2* mice, there was approximately 25% denervation in the AS muscle while the AAL remained relatively unaffected (Figure 4.12 B,C). The increased vulnerability of slow-twitch muscles at late-symptomatic stages was therefore reflected in the increased pathology observed in the AS muscle.

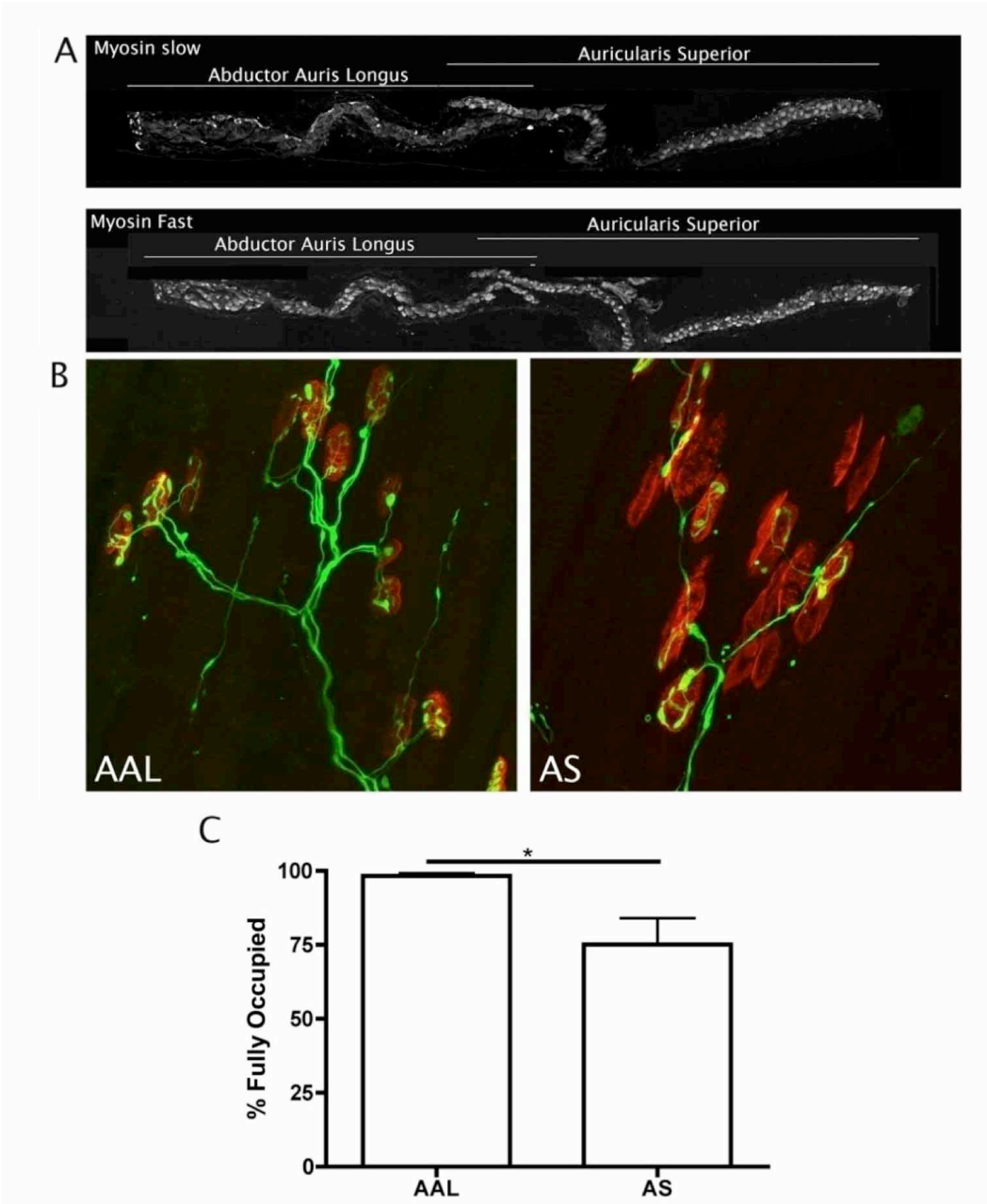

Figure 4.12: Selective vulnerability of motor units in the predominantly slow twitch auricularis superior muscle compared to the fast twitch abductor auris longus muscle in late-symptomatic (P5) *Smn-/-;SMN2* mice. A – Representative micrographs of AAL and AS muscles sectioned coronally and stained with antibodies against either slow myosin (upper panel) or fast myosin (lower panel). Note how the AAL muscle is composed of predominantly fast twitch fibres while the AS muscle is composed of predominantly slow twitch fibres (albeit with fast-twitch fibres also present). B – Confocal micrographs from immunohistochemically labelled AAL (left) and AS (right) muscles from P5 *Smn-/-;SMN2* mice (green = 150kDa neurofilaments; red = post-synaptic acetylcholine receptors labelled with TRITC-α-bungarotoxin) showing large numbers of denervated endplates in the AS muscles while the AAL muscle remained relatively spared. C – Bar chart (mean ± SEM) showing the percentage of fully occupied endplates from P5 *Smn-/-;SMN2* AAL and AS muscles. Note that only 75% of endplates in the AS muscle remain fully innervated at this stage of the disease whereas nearly 100% of connections remained in the AAL muscle. (*Mann Whitney test; * P<0.01; n = 6/6 per AAL/AS muscle and genotype; Scale bar = 100μm (A), 15μm (B))*.

Comparable analyses of pre-symptomatic development to those detailed above for the LAL muscle revealed no significant differences in gross innervations patterns in either the AAL or AS muscle (Figure 4.13). Quantification of endplate numbers revealed no difference in either muscle (Figure 4.14). There was also no change in the levels of poly innervating in either muscle between *Smn-/-;SMN2* mice and control littermates (Figure 4.15).

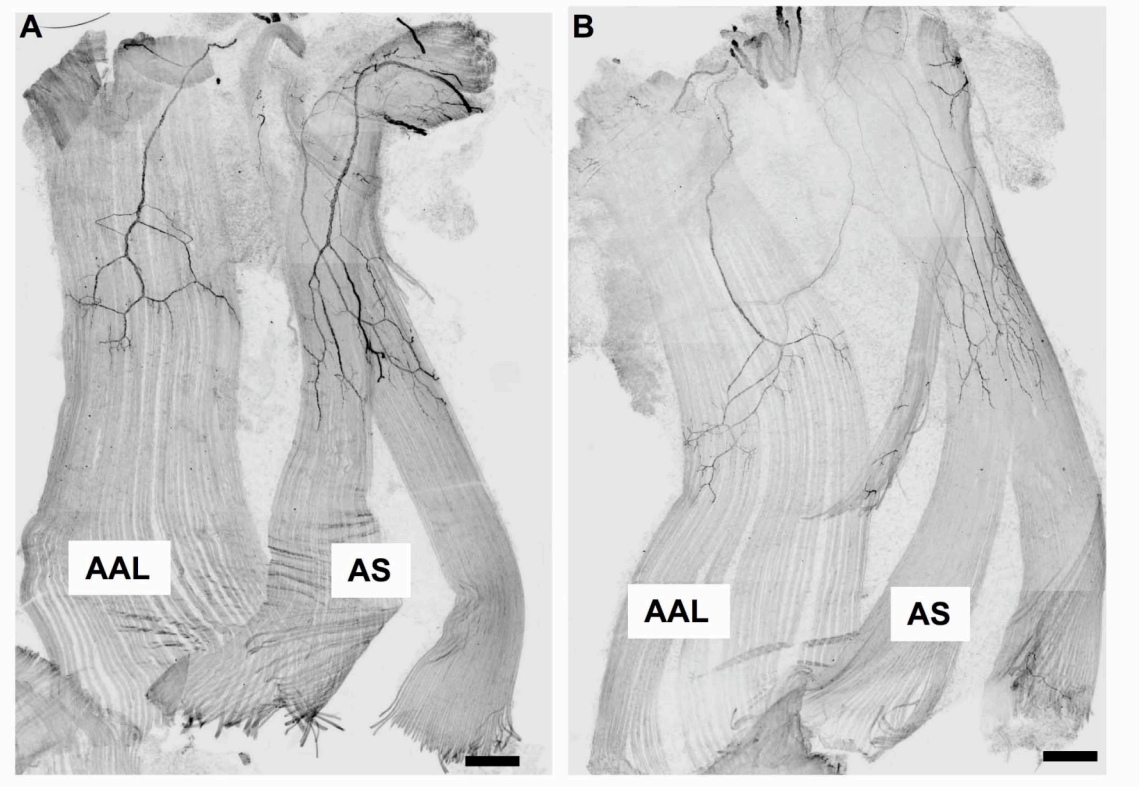

Figure 4.13: Gross anatomy of the AAL and AS muscles at P1 shows normal innervation patterns. A,B – montaged fluorescent micrographs from immunocytochemically labelled AAL/AS muscles (Black = 150kDa neurofilaments) showing innervation pattern in P1 control littermate (A) and *Smn-/-;SMN2* (B) AAL and AS muscles. Individual fluorescent micrographs were montaged and photo-inverted in adobe photoshop. *(Scale bar = 400μm).*

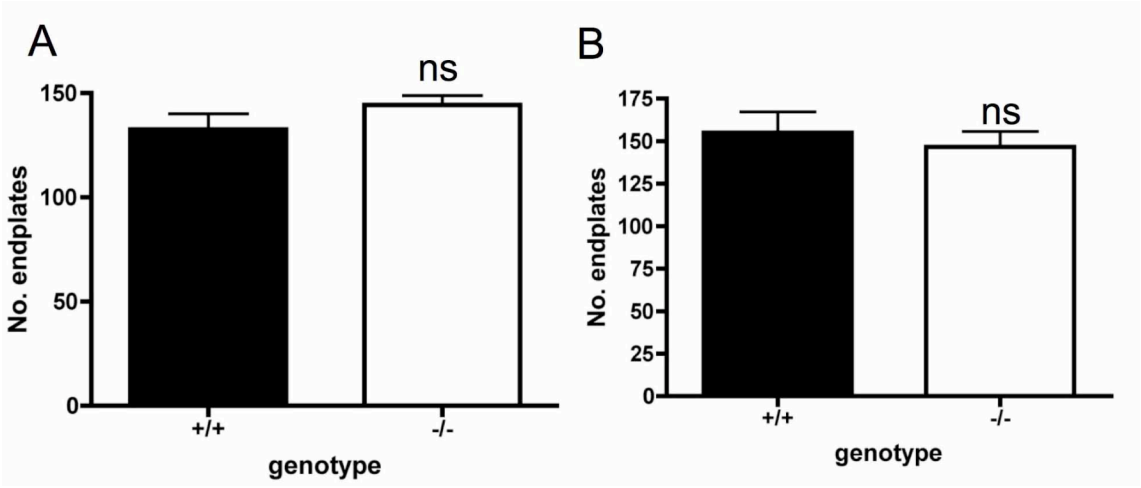

Figure 4.14: There is no change in the number of endplates in either the AS or AAL muscle from P1 *Smn-/-;SMN2* mice. A,B - Bar charts (mean ±SEM) showing the number of endplates in the AAL (A) or AS (B) muscle P1 *Smn-/-;SMN2* mice *(-/-; white bars)* compared to control littermates *(+/+; black bars). (students T-test; ns non-significant; N=10/9 per control AAL/AS muscle; N=9/7 per Smn-/-;SMN2 AAL/AS muscle).*

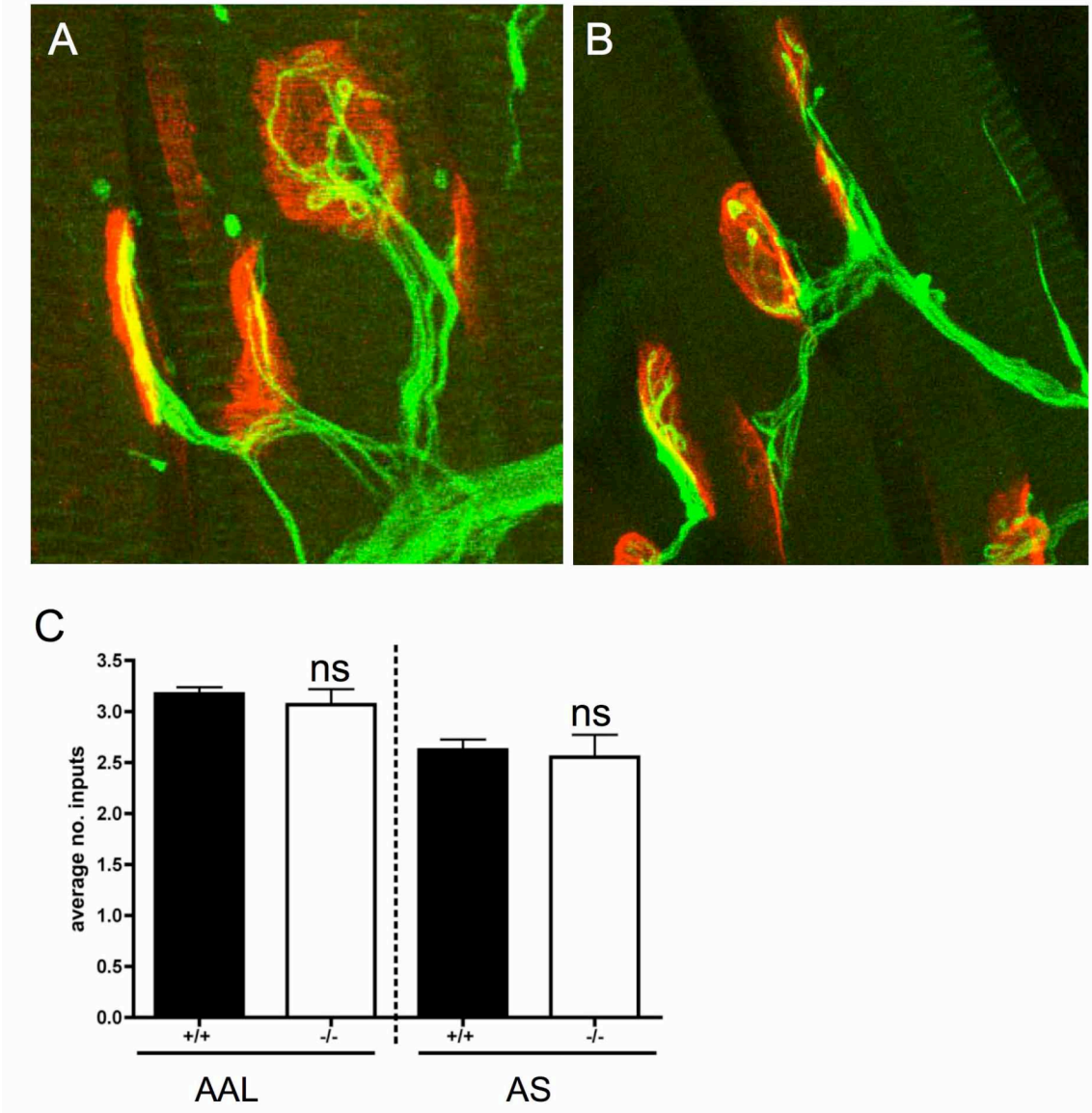

Figure 4.15: No change in the number of axonal inputs per endplate in either AAL or AS muscles from *Smn-/-;SMN2* mice. A,B – Representative confocal micrographs of AAL muscles from a P1 control littermate (A) and *Smn-/-;SMN2* (B) mouse, labelled with antibodies against 150kDa neurofilaments (green) and TRITC-α-bungarotoxin (red), illustrating the type of images used for the quantification of axonal inputs. C – Bar chart showing no significant difference in the number of inputs per endplate in either the AAL or AS muscles between P1 *Smn-/-;SMN2 (-/-; white bars)* and litter mate controls (*+/+; Black bars). (mean ± SEM; ANOVA; ns - non significant; N=10/9 per control AAL/AS muscle; N=9/7 per Smn-/-;SMN2 AAL/AS muscle; Scale bar = 30μm (A,B))*.

There was again, high variability in the levels of both small and 'super' terminal sprouts but over all there was no difference between genotypes in either muscle. Although there was no significant difference in the *level* of sprouting between the AS or AAL muscle (Figure 4.16; 4.17), there did appear to be subtle differences in sprout morphology. Sprouts in the AAL muscle generally appear fine and minimally branched, while those in the AS muscle commonly contained spherical neurofilament accumulations and an increase in branching (Figure 4.16; 4.17). As these differences in morphology were present in both *Smn-/-;SMN2* mice and littermates controls, it is unlikely that they are a result of or contributor to pathology, however these observations do raise the possibility that these sprouts are dynamically distinct (see discussion).

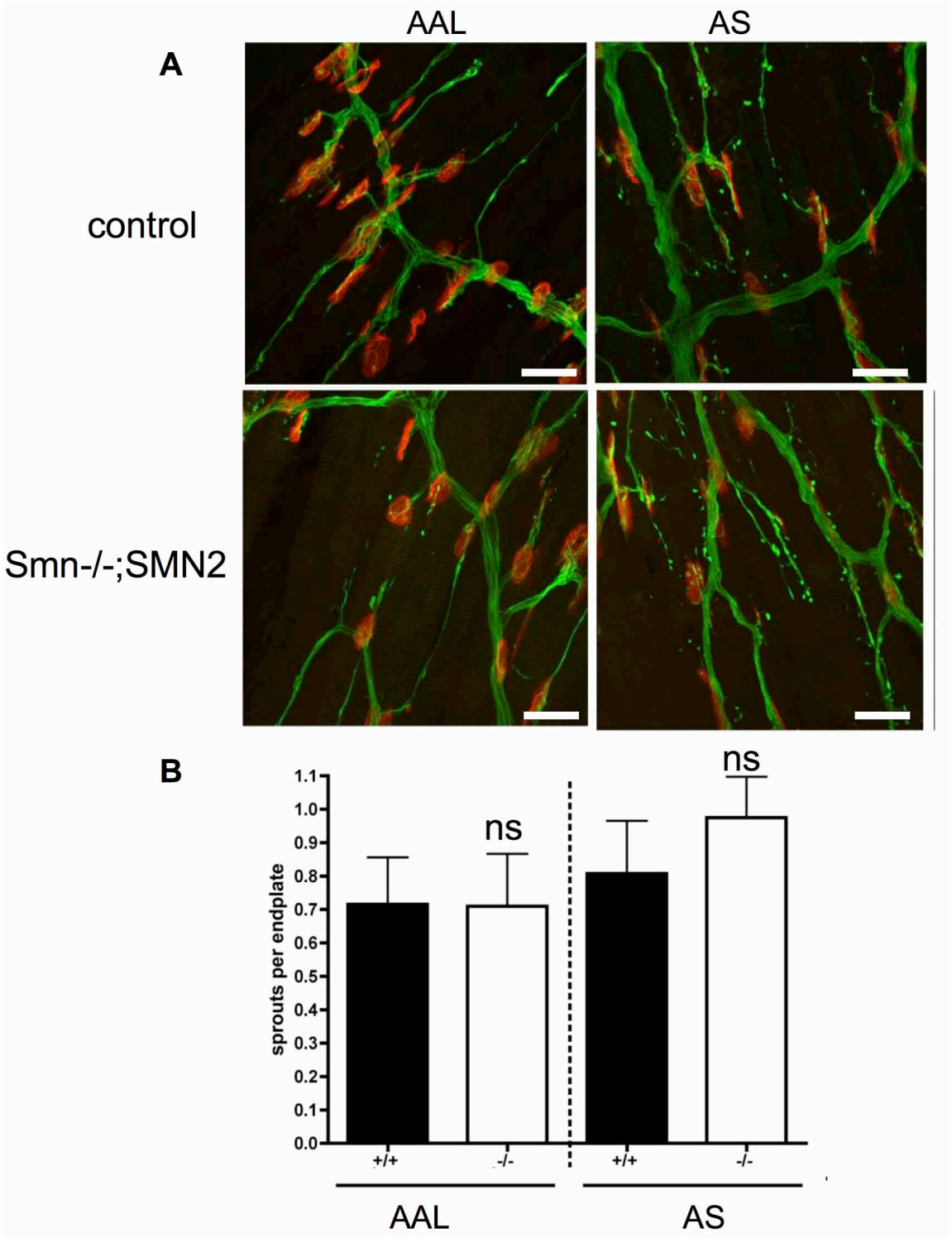

Figure 4.16: There is no difference in the number of small sprouts in either AAL or AS muscles P1 *Smn-/-;SMN2* mice. A – confocal micrographs of neuromuscular preparations (green = 150kDa neurofilaments, red = TRITC-α-bungarotoxin) showing the presence neuronal sprouts present in AAL and AS muscles in both litter mate controls and *Smn-/-;SMN2* mice. B - Bar chart showing the number of sprouts per endplate in AAL and AS muscles from control *(+/+; black bars)* and *Smn-/-;SMN2 (-/-; white bars)* mice. *(mean ± SEM; ANOVA; ns non significant. N=8/6 per control AAL/AS muscle; N=8/9 per Smn-/-;SMN2 AAL/AS muscle. Scale bar = 30μm(A)).*

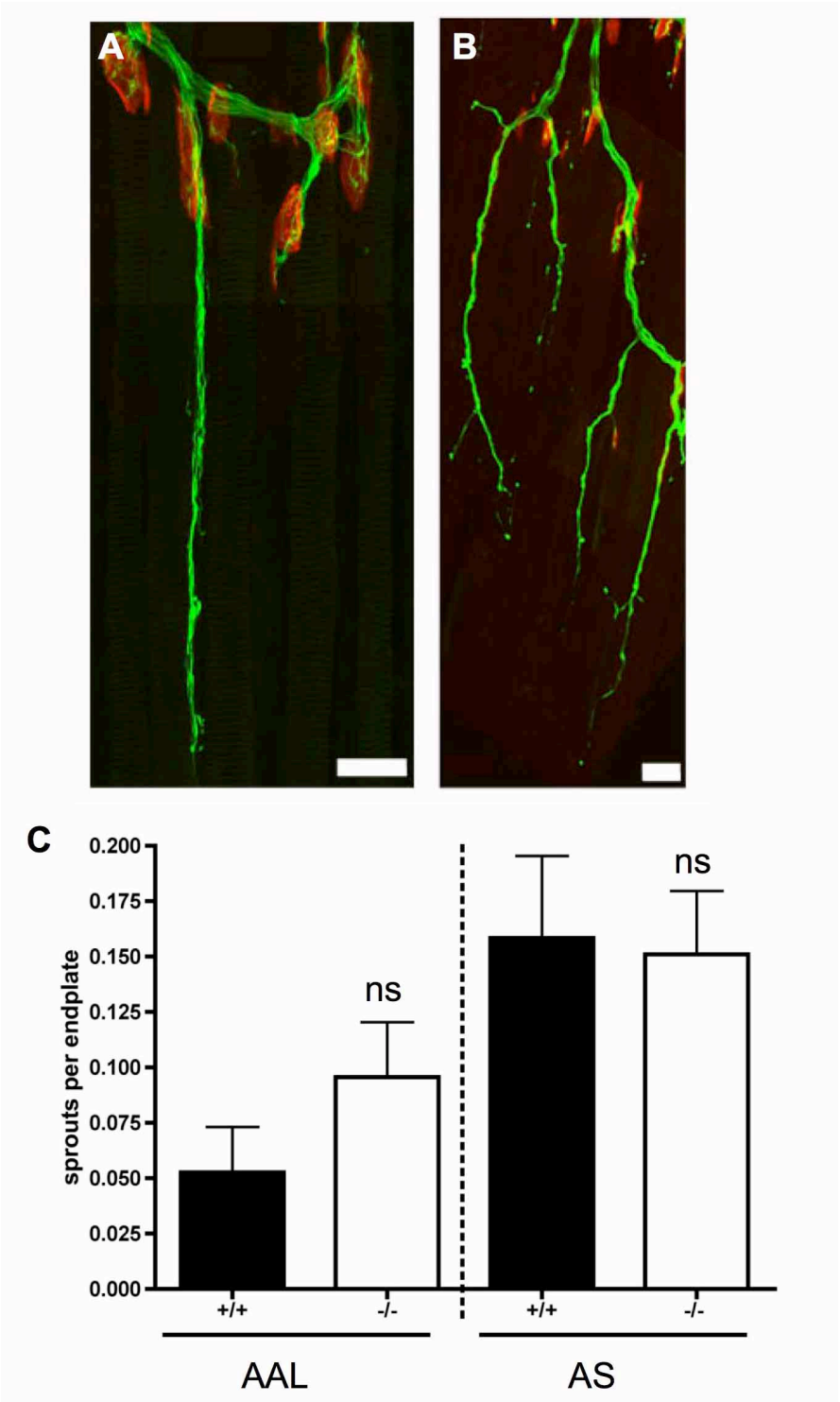

Figure 4.17: There is no difference in the number of super sprouts in either AAL or AS muscles P1 *Smn-/-;SMN2* mice. A,B – montaged confocal micrographs of neuromuscular preparations (150kDa neurofilaments (green) and TRITC-α-bungarotoxin (red)) showing the presence large super sprouts in both AAL (A) and AS (B) muscles in *Smn-/-;SMN2* mice. (C) Bar chart showing the number of super sprouts per endplate in AAL and AS muscles in control *(+/+; black bars)* and *Smn-/-;SMN2 (-/-; white bars)* mice. *(mean ± SEM; ANOVA; ns non significant; N=8/6 per control AAL/AS muscle; N=8/9 per Smn-/-;SMN2 AAL/AS muscle. Scale bar = 20μm (A,B)).*

Again, no difference was observed in endplate area or maturation in either AAL or AS muscle compared to littermate controls, although interestingly, more advanced endplate maturation was observed in the less vulnerable AAL muscle compared to the AS muscle (Figure 4.18). This is in contrast to increased maturation being present in the more vulnerable caudal band of the LAL muscle. This result implies that while there are different time courses of endplate maturation in distinct muscles/muscle bands, it is unlikely to be a direct contributor to pathology.

This data therefore indicates that, at pre-symptomatic time points, development of lower motor neuron connectivity in differentially vulnerable fast and slow twitch muscles fibres proceeds normally. These findings are therefore in agreement with results from the LAL muscle, suggesting that abnormal neuromuscular development cannot account for neuromuscular pathology in SMA.

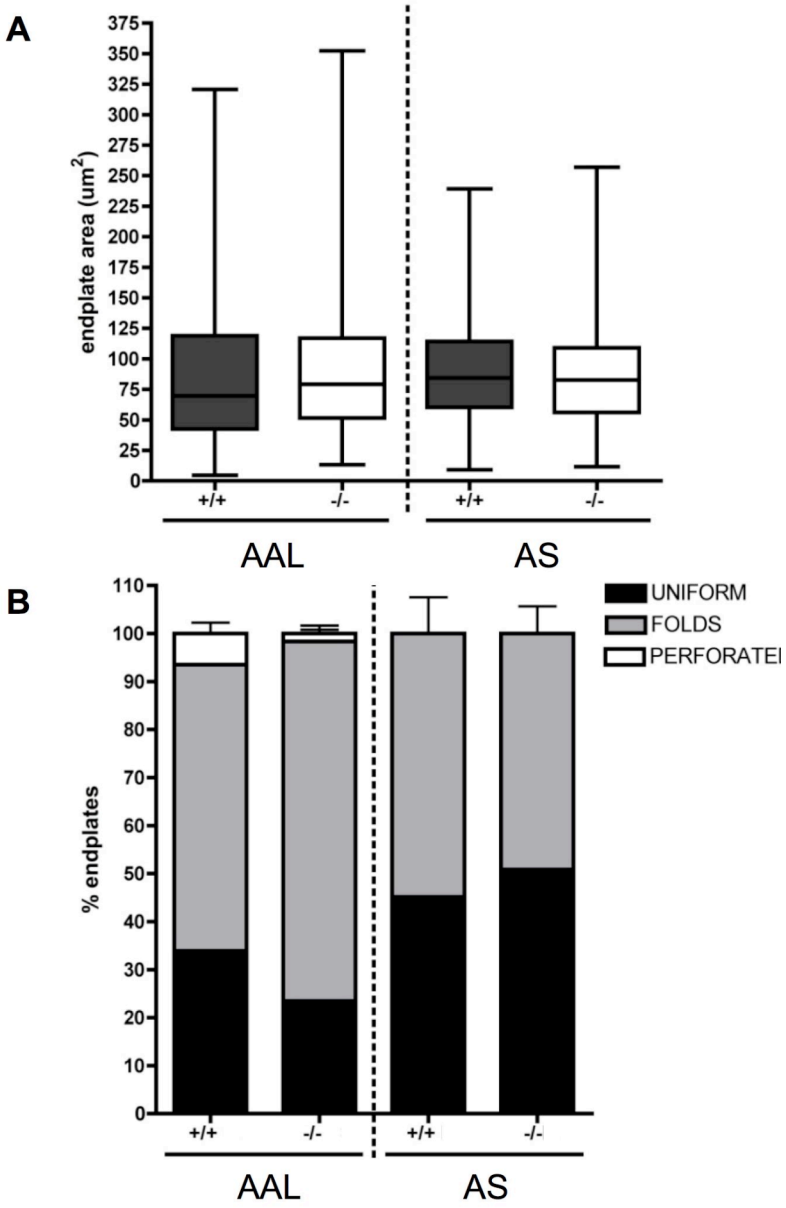

Figure 4.18: There is no difference in post synaptic area of maturation in either the AS or AAL muscle *Smn-/-;SMN2* mice. A - Box and whisker plot showing no change in the distribution of endplate areas between control *(+/+; black boxes*) and *Smn-/-;SMN2 (-/-; white boxes)* mice in either AAL or AS muscles *(ANOVA; P>0.05 for all comparisons, N=10/9 per control AAL/AS muscle; N=9/7 per Smn-/-;SMN2 AAL/AS muscle). B* -Bar chart (mean ± SEM) showing the percentage of endplates which were categorised uniform (black bars), folded (grey bars) and perforated (white bars) in AAL or AS muscles from *Smn-/-;SMN2 (-/-)* mice compared to control littermates *(+/+). (Kruskal-Wallis test; P>0.05; N=8/6 per control AAL/AS muscle; N=8/9 per Smn-/-;SMN2 AAL/AS muscle.)*

4.2.6 Minimal alterations in developmental gene expression at pre-symptomatic time-points in mouse models of SMA

The experiments detailed above indicate that lower motor neurons develop normally until the onset of degenerative symptoms in SMA mice. Although there was no evidence of abnormal pre-symptomatic morphological development in the neuromuscular system, it remained possible that developmental changes at the level of gene expression could impact on lower motor neuron vulnerability without modifying morphology. To investigate this possibility, gene expression analyses was undertaken in pre-symptomatic (P1) *Smn-/-;SMN2* mouse spinal cord compared to control littermates (*Smn*+/+*;SMN*2; N=4 mice per genotype, littermate matched). Affymetrix Mouse Exon ST arrays (see methods) were used to identify any genes showing more than 1.5 fold changes in expression levels. Out of 16,755 genes examined at P1, only 3 were significantly changed i.e >1.5 fold (Table 4.1). The largest change observed was in expression levels of *Smn*, providing an internal control for the sensitivity of the experiment. The other two genes identified fell close to the margin of the 1.5 fold cut off (1.6 fold down regulation and 1.7 fold up-regulation; Table 4.1) but to date neither are considered important for development of the neuromuscular system. Equivalent microarray analysis was performed in a collaboration with colleagues in Oxford on the *Smn-/-;SMN2*;Δ7 mouse model of SMA. Results implied that there were again minimal changes in gene expression in pre-symptomatic time points, with only small magnitude changes observed in a small number of genes (Table 4.2).

Table 4.1: Gene expression changes >1.5 fold in pre-symptomatic (P1) *Smn-/-;SMN2* mouse spinal cord compared to litter-mate controls.

Gene Title	Gene Symbol	Fold change	Regulation
survival motor neuron 1	Smn1	2.7	down
olfactory receptor 1288	Olfr1288	1.6	down
developmental pluripotency associated 5A	Dppa5a	1.7	up

Table 4.2: Gene expression changes >1.5 fold in pre-symptomatic (P1) *Smn-/-;SMN2;Δ7* mouse spinal cord compared to litter-mate controls.

Gene Title	Gene Symbol	Fold change	Regulation
survival motor neuron 1	Smn1	3.4	down
histone cluster 1, H1c	Hist1h1c	1.8	up
histone cluster 1, H2bc *et al*	Hist1h2bc	1.8	up
glycoprotein 49 A /// leukocyte immunoglobulin-like receptor, subfamily B, member 4	Gp49a /// Lilrb4	1.8	up
olfactory receptor 1393 /// olfactory receptor 1392	Olfr1393 /// Olfr1392	1.6	down
laminin, alpha 2	Lama2	1.6	up
olfactory receptor 978	Olfr978	1.6	down
kallikrein 1-related peptidase b21 *et al*	Klk1b21	1.6	up
polymerase (RNA) II (DNA directed) polypeptide H	Polr2h	1.6	down
ribosomal protein L14 /// RIKEN cDNA 5830454E08 gene	Rpl14 /// 5830454E08Rik	1.5	down
Adrenomedullin	Adm	1.5	down

4.3 Discussion

The data presented in this chapter have generated two important findings. Firstly, reduced *Smn* expression does not significantly modify pre-symptomatic development of lower motor neuron morphology and connectivity *in vivo*. Abnormal pre-symptomatic development is therefore not a pre-requisite for subsequent lower motor neuron vulnerability in SMA. Secondly, lower motor neurons and their neuromuscular synaptic connections have no pre-existing abnormalities when degenerative changes and symptoms begin to occur. This suggests that there is a "therapeutic time-window" which extends into the postnatal period for many motor units. Significantly, during this period the neuromuscular system may be in a state amenable to rescue. This study therefore highlights a need to focus on the role of Smn protein in maintaining the neuromuscular system once formed, rather than its role in regulating motor neuron outgrowth and axonogenesis, for understanding SMA pathogenesis.

The data suggest that the developmental effects of reduced Smn levels reported *in vitro* as well as in zebra fish and *Xenopus* models *in vivo* (Fan and Simmard, 2002; McWhorter *et al.*, 2003, Rossoll *et al.*, 2003; Shafey *et al.*, 2008; Ymlahi-Ouazzani *et al.*, 2009) are not mirrored in mammalian SMA models *in vivo*. Whilst it remains possible that Smn protein can influence developmental pathways including axon outgrowth and path-finding under some experimental conditions, the data presented here demonstrate that such changes are not sufficient to cause defects in motor neuron development in mouse models *in vivo* and are not a major contributing factor to SMA pathogenesis. As a result, efforts to understand the role of Smn protein in the triggering and progression of SMA pathology would likely be better served by focussing on events occurring during and around the onset of motor neuron degeneration and symptom onset. The data also suggest that modifier genes which influence disease severity in SMA, such as plastin 3 (Oprea *et al.*, 2008), are more likely to work through stabilising the neuromuscular system (e.g. by modifying actin dynamics) rather than by influencing pre-symptomatic developmental pathways such as axonogenesis (c.f. Oprea *et al.*, 2008).

Whilst development of lower motor neuron connectivity is unlikely to be a contributor to pathology in SMA, this study has not investigated the contribution of muscle development. Studies which employ human muscle cell cultures have reported that myoblast fusion into myotubes can be significantly delayed in cells from SMA type I patients and that ACh receptor clustering in response to agrin was reduced (Guettier-Sigrist 2001; Arnold *et al.*, 2004). Analysis of human embryonic muscle development also revealed changes which are consistent with abnormal muscle growth and development (Martínez-Hernández *et al.*, 2009). These studies together suggest that there may be intrinsic abnormalities in muscle development which may have profound influences on early NMJ formation. Further studies into the contribution of muscle development to pathology in SMA are therefore required.

4.3.1 Morphological discrepancies between distinct muscles/muscle regions

While pre-symptomatic development of lower motor neurons was not modified by SMA, some subtle differences between neuromuscular development of the rostral and caudal bands of the LAL, and between the AS and AAL muscles were observed. The finding that endplate maturation was occurring faster in the caudal band of the LAL muscle is in agreement with previous findings that motor units in this muscle band belong to the developmentally more advanced fast-synapsing ('FaSyn') subtype (Pun *et al.*, 2002; chapter 3). Whilst this may indicate that increased maturation is linked to increased vulnerability, advanced endplate maturation was also seen in the relatively non-vulnerable AAL muscle compared to the less mature endplates in the vulnerable AS muscle. These results indicate that the rate of endplate maturation does not impact upon motor unit vulnerability in SMA. This is in contrast to recent published findings suggesting that increasing endplate maturation by exercise stabilises the NMJ and confers neuroprotection (Biondi *et al.*, 2008). In light of the findings presented here, it may be appropriate to revise these conclusions to state that, while exercise can clearly be

neuroprotective, endplate maturation is likely to be a by-product of the exercise regime and is not likely to have a direct effect on lower motor neuron vulnerability.

The results also indicated that, while there was overall no significant change in the level of sprouting between *Smn-/-;SMN2* mice and control littermates, there was a tendency for increased numbers of 'super sprouts' in more affected muscles/muscle bands (i.e. caudal band of the LAL and AS muscle) compared to neighbouring more stable regions. While this is unlikely to be a pathological event as it is also seen in control littermates, it may indicate increased demands upon these motor neurons and increase their vulnerability. There was also subtle differences in sprout morphology between the AS and AAL muscles. The consequence of these morphological discrepancies is currently unclear although it possibly reflects differences in the dynamic status of the sprouts. Without performing real-time imaging of sprout morphology, it is not possible to discern whether these sprouts are actively growing, stable or undergoing retraction. These processes could have significant impacts upon the energy demands of the motor unit and developmental status of the motor unit.

4.3.2 Minimal gene expression changes in pre-symptomatic SMA mice

One remarkable finding of this study was that pre-symptomatic analyses of lower motor neuron gene expression failed to identify any major changes in either mouse model prior to symptom onset. This is true even in the severe mouse model of SMA where the disease kills the animals by P5-P6. Although no gross changes in gene expression were identified, these results must be interpreted with caution as the analysis performed does not account for genes in which a high degree of variability caused them to be discounted from the results. It is also important to remember that this analysis is on whole spinal cord, not just motor neurons, let alone selectively vulnerable populations. Such experiments would not be practically possible in such severe mouse models at such young ages. Despite these caveats, should there have been a disruption in the normal development of lower motor neurons at pre-symptomatic time points, it might be

reasonable to expect to observe a degree of change in gene expression. The minimal changes observed here are further emphasised when results are compared to the wide spread gene expression changes occurring at end-stage time points (see chapter 5).

Together with the morphological data, these results highlight the rapid progression of neuromuscular breakdown that can occur as a result of reduced Smn levels, but also gives great encouragement for the development of post-natally delivered treatments for SMA in human patients. Had there been evidence for disrupted pre-symptomatic development of lower motor neurons, leading to subsequent neuronal vulnerability, it would be difficult to envisage how this could be fully remedied by post-natal treatment options alone. By contrast, the results suggest the existence of a pre-symptomatic therapeutic time window in which lower motor neurons and neuromuscular synaptic connections remain intact, extending into post-natal days even in a mouse model of severe SMA where death occurs by P5-P6. This work therefore provides encouragement for current efforts to treat SMA post-natally, using strategies such as increasing Smn levels in the nervous system (Azzouz *et al.*, 2004; Foust *et al.*, 2009) or increasing full-length splicing from the preserved *SMN*2 gene (Lim and Hertel, 2001; Madocsai *et al.*, 2005; Baughan *et al.*, 2006; Avila *et al.*, 2007; Coady *et al.*, 2007; Ting *et al.*, 2007; Hua *et al.*, 2008; Baughan *et al.*, 2009).

Chapter 5: Microarray analysis in end-stage *Smn-/-;SMN2* mice

Summary

Further to results suggesting that there are minimal changes in gene expression prior to symptom onset, I have investigated what cellular pathways are mis-regulated during disease progression in SMA. Microarray analysis has been performed on spinal cord from P5 *Smn-/-;SMN2* and P14 *Smn-/-;SMN2*;Δ7 mice and compared gene expression levels to littermate controls.

Results detailed in this chapter show that:

1. A large number genes are altered in end-stage SMA mice highlighting the minimal extent of changes observed at pre-symptomatic time points
2. Pathways involved in growth factor signalling and extracellular matrix integrity are altered in end-stage SMA mice.

5.1 Introduction

In this study, I have thus far demonstrated that neuromuscular pathology is a progressive event in SMA, with synaptic loss being apparent early in the disease time course. I have further shown that abnormalities in pre-symptomatic lower motor neuron connectivity do not underlie neuromuscular pathology and that at pre-symptomatic time points there are minimal changes in gene expression in the spinal cord. This result is somewhat striking, indicating that the neuromuscular system remains physically and functionally intact up to P1, at which point an unidentified trigger causes rapid and progressive neural muscular pathology causing death within 4 days in the *Smn-/-;SMN2* model. This work therefore leads to the question: what cellular and molecular pathways are responsible for the initiation and progression of neuromuscular breakdown?

To begin to address this question, high stringency microarray analysis has been performed on spinal cord tissue from end-stage (P5) *Smn-/-;SMN2* mice. This analysis identified a large number of genes which show altered expression in end-stage *Smn-/-;SMN2* mice, further emphasising the minimal changes observed at P1. Use of GO-Elite MAPPFinder software for pathways analysis revealed significant alterations in pathways implicated in growth factor signalling and extracellular matrix integrity.

5.2 Results

5.2.1 Significant changes in gene expression were present in late-symptomatic Smn-/-;SMN2 mice

In an attempt to gain insights into the pathways controlling pathological progression in SMA, microarray expression analysis was applied to late-symptomatic (P5) spinal cord from *Smn-/-;SMN2* mice (N=4 mice per genotype, littermate matched). Of the 16,755 individual genes investigated, 160 were significantly changed greater than 1.5 fold (Table 5.1). The biggest single change was found for a gene in the myelination pathway, where there was a significant 6.5 fold decrease in expression of myelin protein zero.

These results were in stark contrast to the P1 results (a 53 fold increase in the number of changed genes), underlining the minimal changes seen pre-symptomatically (see chapter 4). A comparison of P1 and P5 data also clearly underlined the scale and rapid progression of pathological changes that occur in the neuromuscular system in this severe model of SMA.

5.2.2 Pathway mapping software implicates pathways involved in cell extracellular matrix integrity and growth factor signalling in SMA pathology

Utilisation of GO-Elite MAPPFinder software to further investigate the potential function of genes shown to have modified expression levels identified 35 different cellular pathways which were modified in late-symptomatic (P5) *Smn-/-;SMN2* spinal cord (Table 5.2). This *in silico* analysis highlighted changes in pathways relating to extracellular matrix integrity (shown in blue) and growth factor signalling (shown in green) in SMA pathology. Equivalent microarray analysis has been performed collaboratively with colleagues in Oxford, on the *Smn-/-;SMN2*;Δ7 mouse model (Baumer *et al.*, under review). Results from the *Smn-/-;SMN2*;Δ7 mouse model reveal a very similar pattern of gene expression changes, with very few changes pre-symptomatically (11 genes statistically altered) and large numbers of changes at end-

stage time points (142 genes statistically altered). Equivalent G0 pathway analysis on microarray results from P14 *Smn-/-;SMN2*;Δ7 spinal cord revealed that gene changes did not coincide with known cellular pathways to the extent observed in Smn-/-;SMN2 mice, but again pathways involved in growth factor signalling were highlighted (Table 5.3).

Table 5.1: Gene expression changes >1.5 fold in late-symptomatic (P5) *Smn-/-;SMN2* mouse spinal cord compared to litter-mate controls.

Gene Title	Gene Symbol	Fold change	Regulation
myelin protein zero	Mpz	6.5	down
decorin	Dcn	4.2	down
microfibrillar-associated protein 4	Mfap4	3.8	down
peripheral myelin protein 22	Pmp22	3.7	down
osteoglycin	Ogn	3.7	down
periostin, osteoblast specific factor	Postn	3.6	down
lumican	Lum	3.5	down
survival motor neuron 1	Smn1	3.5	down
prostaglandin D2 synthase (brain)	Ptgds	3.4	down
collagen, type III, alpha 1	Col3a1	3.0	down
collagen, type I, alpha 1	Col1a1	2.9	down
histocompatibility 2, *et al*	H2-T22	2.7	down
procollagen C-endopeptidase enhancer protein	Pcolce	2.7	down
ATP-binding cassette, sub-family A (ABC1), member 8a	Abca8a	2.6	down
thrombomodulin	Thbd	2.5	down
fibronectin 1	Fn1	2.5	down
reticulocalbin 3, EF-hand calcium binding domain	Rcn3	2.4	down
dipeptidylpeptidase 4	Dpp4	2.3	down
collagen, type I, alpha 2	Col1a2	2.3	down
asporin	Aspn	2.3	down
immunoglobulin superfamily containing leucine-rich repeat	Islr	2.3	down
dermatopontin	Dpt	2.2	down
solute carrier family 6 (neurotransmitter transporter, GABA), member 13	Slc6a13	2.2	down
serine (or cysteine) peptidase inhibitor, clade G, member 1	Serping1	2.2	down
collagen, type XII, alpha 1	Col12a1	2.2	down
gap junction protein, beta 2	Gjb2	2.2	down
cadherin 5	Cdh5	2.2	down
nidogen 2	Nid2	2.1	down
AE binding protein 1	Aebp1	2.1	down
Rho GTPase activating protein 19	Arhgap19	2.1	down
solute carrier family 7 (cationic amino acid transporter, y+ system), member 11	Slc7a11	2.1	down
histone cluster 1, H2bb	Hist1h2bb	2.1	down
solute carrier family 13 (sodium/sulfate symporters), member 4	Slc13a4	2.1	down
vesicle-associated membrane protein 5	Vamp5	2.0	down
vitronectin	Vtn	2.0	down
insulin-like growth factor 2	Igf2	2.0	down
serine (or cysteine) peptidase inhibitor, clade D, member 1	Serpind1	2.0	down
CD93 antigen	Cd93	2.0	down
laminin, alpha 2	Lama2	2.0	down
family with sequence similarity 107, member A	Fam107a	1.9	up
angiotensinogen (serpin peptidase inhibitor, clade A, member 8)	Agt	1.9	up
lymphatic vessel endothelial hyaluronan receptor 1	Lyve1	1.9	down
disabled homolog 2 (Drosophila)	Dab2	1.9	down
epithelial membrane protein 3	Emp3	1.9	down
mannose receptor, C type 1	Mrc1	1.9	down

H19 fetal liver mRNA	H19	1.9	down
transforming growth factor, beta induced	Tgfbi	1.9	down
solute carrier family 38, member 5	Slc38a5	1.9	down
proteoglycan 4 (megakaryocyte stimulating factor, articular superficial zone protein)	Prg4	1.9	down
alcohol dehydrogenase 1 (class I)	Adh1	1.9	down
laminin B1 subunit 1	Lamb1-1	1.9	down
peptidylprolyl isomerase C	Ppic	1.9	down
endothelial-specific receptor tyrosine kinase	Tek	1.9	down
folate hydrolase	Folh1	1.8	up
RIKEN cDNA 2810417H13 gene	2810417H13 Rik	1.8	down
crystallin, alpha B	Cryab	1.8	down
nephroblastoma overexpressed gene	Nov	1.8	down
forkhead box C2	Foxc2	1.8	down
laminin, alpha 4	Lama4	1.8	down
collagen, type VI, alpha 3	Col6a3	1.8	down
insulin-like growth factor binding protein 4	Igfbp4	1.8	down
metallothionein 2	Mt2	1.8	up
follistatin-like 1	Fstl1	1.8	down
cyclin-dependent kinase inhibitor 2C (p18, inhibits CDK4)	Cdkn2c	1.8	down
microfibrillar associated protein 5	Mfap5	1.8	down
fibulin 5	Fbln5	1.8	down
apolipoprotein D	Apod	1.8	down
integrin, beta-like 1	Itgbl1	1.8	down
angiopoietin-like 2	Angptl2	1.8	down
periaxin	Prx	1.7	down
discoidin domain receptor family, member 2	Ddr2	1.7	down
insulin-like growth factor binding protein 6	Igfbp6	1.7	down
coagulation factor XIII, A1 subunit	F13a1	1.7	down
histone cluster 1, H1b	Hist1h1b	1.7	down
aldehyde dehydrogenase family 1, subfamily A1	Aldh1a1	1.7	down
actin, alpha 2, smooth muscle, aorta	Acta2	1.7	down
coatomer protein complex, subunit zeta 2	Copz2	1.7	down
EF hand domain containing 1	Efhd1	1.7	down
collagen, type VI, alpha 2	Col6a2	1.7	down
aldehyde dehydrogenase family 1, subfamily A2	Aldh1a2	1.7	down
Nik related kinase	Nrk	1.7	down
bone morphogenetic protein 5	Bmp5	1.7	down
fibrillin 1	Fbn1	1.7	down
leptin receptor	Lepr	1.7	down
inter-alpha trypsin inhibitor, heavy chain 2	Itih2	1.7	down
monooxygenase, DBH-like 1	Moxd1	1.7	down
collagen, type VI, alpha 1	Col6a1	1.7	down
histone cluster 1, H2ac	Hist1h2ac	1.7	up
integral membrane protein 2A	Itm2a	1.7	down
G protein-coupled receptor 182	Gpr182	1.7	down
palmitoyl-protein thioesterase 1	Ppt1	1.7	up
collagen, type XV, alpha 1	Col15a1	1.7	down
annexin A2	Anxa2	1.6	down
acyl-CoA thioesterase 11	Acot11	1.6	up
zinc finger protein 458 /// zinc finger protein 457	Zfp458 ///	1.6	down

	Zfp457		
pleckstrin homology-like domain, family B, member 2 /// phosphatidylinositol-specific phospholipase C, X domain containing 2	Phldb2 /// Plcxd2	1.6	down
collectin sub-family member 12	Colec12	1.6	down
lipopolysaccharide binding protein	Lbp	1.6	down
cathepsin H	Ctsh	1.6	down
Friend leukemia integration 1	Fli1	1.6	down
solute carrier family 22 (organic anion transporter), member 8	Slc22a8	1.6	down
apelin receptor	Aplnr	1.6	down
platelet factor 4	Pf4	1.6	down
carbonic anhydrase 13	Car13	1.6	down
Rho GTPase activating protein 29	Arhgap29	1.6	down
EH-domain containing 2	Ehd2	1.6	down
small nuclear ribonucleoprotein polypeptide A'	Snrpa1	1.6	up
glypican 3	Gpc3	1.6	down
RIKEN cDNA 2310046A06 gene	2310046A06 Rik	1.6	down
RAN binding protein 3-like	Ranbp3l	1.6	down
v-erb-b2 erythroblastic leukemia viral oncogene homolog 3 (avian)	Erbb3	1.6	down
biglycan	Bgn	1.6	down
calponin 2	Cnn2	1.6	down
inter-alpha (globulin) inhibitor H5	Itih5	1.6	down
ATP-binding cassette, sub-family A (ABC1), member 9	Abca9	1.6	down
cellular retinoic acid binding protein II	Crabp2	1.6	down
RIKEN cDNA 1110032E23 gene	1110032E23 Rik	1.6	down
claudin 5	Cldn5	1.6	down
cysteine-rich protein 1 (intestinal)	Crip1	1.6	down
ASF1 anti-silencing function 1 homolog B (S. cerevisiae)	Asf1b	1.6	down
thrombospondin 2	Thbs2	1.6	down
gliomedin	Gldn	1.6	down
tubulin, beta 6	Tubb6	1.6	down
glycophorin C	Gypc	1.6	down
chemokine (C-C motif) ligand 11	Ccl11	1.6	down
olfactomedin-like 3	Olfml3	1.6	down
EGF-like domain 8	Egfl8	1.6	down
SET domain containing (lysine methyltransferase) 8	Setd8	1.6	down
early growth response 2	Egr2	1.6	down
sema domain, immunoglobulin domain (Ig), short basic domain, secreted, (semaphorin) 3B	Sema3b	1.6	down
perlecan (heparan sulfate proteoglycan 2)	Hspg2	1.6	down
zinc finger protein 458 /// zinc finger protein 457	Zfp458 /// Zfp457	1.6	up
epidermal growth factor-containing fibulin-like extracellular matrix protein 1	Efemp1	1.6	down
PDZ binding kinase	Pbk	1.6	down
cyclin B1	Ccnb1	1.6	down
smoothelin	Smtn	1.5	down
elastin	Eln	1.5	down
odd-skipped related 1 (Drosophila)	Osr1	1.5	down
cell division cycle associated 7	Cdca7	1.5	down
ubiquitin-like, containing PHD and RING finger domains, 1	Uhrf1	1.5	down
ectodysplasin A2 isoform receptor	Eda2r	1.5	up

histone cluster 1, H1a	Hist1h1a	1.5	down
phospholipid transfer protein	Pltp	1.5	down
HtrA serine peptidase 1	Htra1	1.5	up
histocompatibility 2, K1, K region /// histocompatibility 2, Q region locus 2 /// histocompatibility 2, D region /// histocompatibility 2, D region locus 1	H2-K1 /// H2-Q2 /// H2-L /// H2-D1	1.5	up
stabilin 1	Stab1	1.5	down
cyclin A2	Ccna2	1.5	down
src homology 2 domain-containing transforming protein C1	Shc1	1.5	down
myelin and lymphocyte protein, T-cell differentiation protein	Mal	1.5	down
collagen, type V, alpha 2	Col5a2	1.5	down
cadherin 1	Cdh1	1.5	down
epithelial membrane protein 1	Emp1	1.5	down
collagen, type X, alpha 1	Col10a1	1.5	down
protein regulator of cytokinesis 1	Prc1	1.5	down
Fc receptor, IgG, alpha chain transporter	Fcgrt	1.5	down
aldehyde dehydrogenase family 1, subfamily A7	Aldh1a7	1.5	down
regulator of G-protein signaling 5	Rgs5	1.5	down
phospholipase A2, group III	Pla2g3	1.5	up
alpha 1,4-galactosyltransferase	A4galt	1.5	down

Table 5.2: Pathway analysis of late-symptomatic (P5) microarray results.

GOID	GO Name	No. Changed	No. Measured	No. in GO	Percent Changed	Percent Present	Z Score	Permute P	Adjusted P
≥3 genes changing & ≥50% genes changing p0.05									
43256	laminin complex	3	5	7	60	71	12.7	0	0
48407	platelet\-derived growth factor binding	4	8	9	50	89	13.3	0	0
≥3 genes changing and 20-49% genes changing p0.05									
42573	retinoic acid metabolic process	4	10	11	40	91	11.8	0	0
5605	basal lamina	3	8	11	38	73	9.9	0	0
46332	SMAD binding	3	8	10	38	80	9.9	0	0
6776	vitamin A metabolic process	5	15	18	33	83	12.0	0	0
5201	extracellular matrix structural constituent	7	24	24	29	100	13.2	0	0
1523	retinoid metabolic process	3	11	14	27	79	8.3	0	0
16101	diterpenoid metabolic process	3	11	14	27	79	8.3	0	0
30199	collagen fibril organization	4	15	18	27	83	9.5	0	0
6775	fat\-soluble vitamin metabolic process	5	19	25	26	76	10.6	0	0
6721	terpenoid metabolic process	3	13	18	23	72	7.6	0	0
5520	insulin\-like growth factor binding	4	18	20	22	90	8.6	0	0
5581	collagen	4	18	19	22	95	8.6	0	0
44420	extracellular matrix part	13	59	71	22	83	15.5	0	0
≥3 genes changing and 10-19% genes changing p0.05									
6022	aminoglycan metabolic process	3	17	20	18	85	6.6	0	0
30203	glycosaminoglycan metabolic process	3	17	20	18	85	6.6	0	0
19838	growth factor binding	8	50	56	16	89	10.1	0	0
5604	basement membrane	7	44	54	16	81	9.5	0	0
6817	phosphate transport	11	70	80	16	88	11.8	0	0
30198	extracellular matrix organization and biogenesis	7	49	59	14	83	8.9	0	0
16620	oxidoreductase activity\, acting on the aldehyde or oxo group of donors\, NAD or NADP as acceptor	3	22	27	14	81	5.7	0.0005	0.0645
5578	proteinaceous extracellular matrix	31	234	267	13	88	18.0	0	0
31012	extracellular matrix	31	238	271	13	88	17.8	0	0
1871	pattern binding	10	79	93	13	85	9.9	0	0
5539	glycosaminoglycan binding	9	72	79	13	91	9.3	0	0
8201	heparin binding	7	56	62	13	90	8.2	0	0
30247	polysaccharide binding	9	76	86	12	88	9.0	0	0
6720	isoprenoid metabolic process	3	26	35	12	74	5.1	0.0035	0.2485
6334	nucleosome assembly	4	36	94	11	38	5.8	0.0005	0.0645
7160	cell\-matrix adhesion	8	75	85	11	88	8.0	0	0
16903	oxidoreductase activity\, acting on the aldehyde or oxo group of donors	3	30	36	10	83	4.7	0.0015	0.147
7422	peripheral nervous system development	3	30	34	10	88	4.7	0.002	0.176
1656	metanephros development	4	41	51	10	80	5.3	0.0005	0.0645
7596	blood coagulation	5	52	59	10	88	5.9	0.0005	0.0645

Table 5.3: Pathway analysis of late-symptomatic (P14) *Smn-/-;SMN2*;Δ7 microarray results.

GOID	GO Name	No. Chang-ed	No. Measur-ed	No. in GO	Percent Changed	Percent Present	Z Score	Permute P	Adjusted P
≥3 genes changing and >10% genes changing p0.05									
5922	connexon complex	3	16	20	19	80	8	0.0005	0.333
5520	insulin\-like growth factor binding	3	18	20	17	90	7	0	0
5921	gap junction	3	21	26	14	81	7	0.0005	0.333
14704	intercalated disc	4	38	49	11	78	6	0.0005	0.333

5.3 Discussion

In this chapter I have shown that gene expression changes correlating with SMA pathology progress rapidly following the onset of symptoms and the results highlight the involvement of specific cellular pathways, namely extracellular matrix integrity, growth factor signalling and myelination pathways.

The finding that pre-symptomatic developmental pathways do not play a role in SMA pathogenesis suggests that a focus on cellular and molecular pathways active around the time of disease onset and lower motor neuron breakdown will be required for a full understanding of the disease and for the identification of novel therapeutic targets. The late-symptomatic (P5) gene expression data presented in this study provide some initial insights into these pathways. Whilst, at this point it is not possible to dissect gene expression changes *causing* pathology from those *resulting from* pathological changes, the data suggest that extracellular matrix integrity, growth factor signalling and myelination pathways are all significantly modified in SMA.

Although microarray data presented here represent the first attempt to understand gene expression changes in mouse models of severe SMA, equivalent analysis has been performed using a mouse model of a very mild form of the disease (Balabanian *et al.*, 2007). Comparison of the individual expression changes in microarray analysis of the mild model of SMA (Smn+/-) reveal very little overlap with results detailed here - as might be expected given the differing nature of pathological changes between the two models. Despite this, they did observe changes in the expression of genes associated with the extracellular matrix (Balabanian *et al.*, 2007). It is therefore conceivable that therapeutic strategies designed to preserve and support the extracellular matrix (often referred to as peri-neuronal nets in the nervous system; Celio *et al.*, 1998) may help to sustain lower motor neuron form and function by influencing factors such as the maintenance of cellular relationships and adhesion, the control of synaptic plasticity and neurotransmitter receptor localisation, and the concentration of growth factors around

neurons (Celio *et al.*, 1998; Frischknecht *et al.*, 2009). Similarly, the finding that genes associated with growth factor signalling are dys-regulated in late-symptomatic SMA spinal cord suggests that lower motor neurons may be breaking down as a result of abnormal trophic signalling. Trophic factors have long been considered as potential therapeutic agents for SMA (Swoboda *et al.*, 2007), but a comprehensive analysis of the effects of different growth factors on SMA pathology has yet to be undertaken. The identification of changes in retinoic acid metabolic processes is also of significant interest. A role for retinoic acid in neuronal patterning, differentiation and maintenance has been well established (for review see Maden, 2007). Additional studies have suggested that a dietary deficiency of retinoids can cause motor neuron disease like symptoms in rats, and identified disruption in the retinoid signalling pathways in rat models of motor neuron disease and ALS patients (Corcoran *et al.*, 2002; Jokic *et al.*, 2007).

A common theme occurring within the microarray results is the potential for disruption of myelination pathways. The largest change in expression was observed in the myelin protein P0. Over 50% of the genes involved in platelet derived growth factor binding were altered and such pathways have been implicated in oligodendrocyte recruitment in the CNS (Hinks and Franklin, 2000). Furthermore, significant alterations were seen in pathways involved in the laminin complex, which has been implicated in the process of myelination with decreased expression being associated with axon loss and congenital muscular dystrophies in humans (Masaki *et al.*, 2000; Masaki *et al.*, 2003; Pegoraro *et al.*, 1998). Clearly such changes in myelination could be either causative or resultant of pathological events, but further work is clearly required to look at the myelin surrounding axons, perhaps by use of the electron microscope to visualise myelin integrity both within intramuscular nerves and ventral roots during the disease time course.

Chapter 6: Loss of eEF1A2 distinguishes dying-back neuropathy from Wallerian Degeneration *in vivo*

Summary

Results from chapter 3 have suggested that synaptic degeneration in SMA mouse models conformed to a dying-back type morphology, as observed in other models of motor neuron pathology. This morphology is quite distinct to the rapid fragmentation observed in Wallerian degeneration occurring, for example, in response to traumatic injury. Despite clear morphological discrepancies, little is known about the convergence or divergence of mechanisms underlying morphologically distinct types of synaptic degeneration, for example Wallerian degeneration and dying-back neuropathy. I have therefore used the *wasted* mouse model of neurodegeneration to further investigate the retraction process in a characteristic dying-back neuropathy, and have further observed that the progression of Wallerian degeneration is altered in the presence of an existing dying-back neuropathy.

Results detailed in this chapter show that:

1. In *wasted* mice, functional loss at the synapse precedes structural loss, therefore implying degeneration is a dying-back neuropathy.
2. Synapse loss occurs asynchronously within a motor unit, therefore implying degeneration is a dying-back neuropathy.
3. *Wasted* and *Smn-/-;SMN2* mice are united by a shared reduction in ZPR1 levels.
4. Axotomy induced Wallerian degeneration is significantly delayed in *wasted* mice, thus indicating that morphologically distinct types of degeneration are also mechanistically distinct.

6.1 Introduction

Work thus far has indicated that neuromuscular junctions are pathological targets in SMA. This synaptic degeneration does not appear to be based on developmental abnormalities, suggesting degeneration is caused by activation of post-natal degenerative pathways. Although microarray analysis has presented some putative pathways which may be involved in neuromuscular pathology in SMA, the precise mechanisms regulating synaptic degeneration are unclear.

Morphologically, synaptic degeneration in SMA conforms to a dying-back neuropathy, with gradual proximal to distal retraction of the pre-synaptic terminal and an absence of widespread fragmentation (Chapter 3) and is quite distinct when compared to the rapid fragmentation observed in Wallerian degeneration (see introduction, section 1.6). Such dying-back degenerative morphology is consistent with observations in other motor neuron disease models (Frey *et al*., 2000; Fischer *et al*., 2004), however it is not clear whether this shared morphology extends to reflect a commonality in degenerative mechanism. Furthermore, despite these clear morphological differences between dying-back and Wallerian degeneration processes, little is known about convergence or divergence of their underling molecular mechanisms (Coleman, 2005; Hoopfer *et al.*, 2006), although evidence has been presented suggesting that morphologically distinct degenerative pathways can share common mechanistic links (Coleman, 2005; Mi *et al.*, 2005). More detailed knowledge of the cellular events in morphologically distinct types of degeneration and the potential overlap in mechanistic pathways would therefore be of significant importance for our understanding of the healthy and pathological nervous system and may give insight into the degenerative mechanisms in SMA.

Due to the early lethality in models of SMA their use as a model to investigate and compare degenerative mechanisms is somewhat limited. For this reason, I now turn to a different model of neurodegeneration known as the *wasted* mouse. The delayed onset of neurodegenerative events at around P14 in this mouse model allow investigation and

comparison of pathways controlling dying-back neuropathy and Wallerian degeneration while eliminating the contribution of developmental events.

Wasted mice carry a spontaneous mutation in a gene encoding the translation elongation factor *eEF1A*2, which abolishes its expression (Shultz *et al.*, 1982; Chambers *et al.*, 1998). E*EF1A* (of which there are two variant forms; *eEF1A1* and *eEF1A*2) is the second most abundant protein in the cell, constituting 1-2% of total protein and playing an integral role in the elongation stages of protein synthesis during which the polypeptide chain is assembled (Condeelis, 1995). Alongside important roles in protein synthesis, eEF1A proteins have also been postulated to play non-canonical roles in pathways including modification of the cytoskeleton (Condeelis, 1995), the heat shock response (Shamovsky *et al.*, 2006) and synaptic plasticity (Giustetto *et al.*, 2003). Expression patterns of the two variant forms (*eEF1A1* and *eEF1A*2) are mutually exclusive in all cells and tissues examined. The *eEF1A*2 variant is only expressed in neuronal cells and muscle (Pan *et al.*, 2004). However, *eEF1A1* is expressed in nerve and muscle at the time of birth, where its expression declines from the first post-natal week onwards until it is absent by around post-natal day 20-21 (Pan *et al.*, 2004). During this period of declining expression, the role of *eEF1A1* is normally replaced by correlated increasing expression levels of *eEF1A*2 (Chambers *et al.*, 1998), with the latter being the sole translation elongation factor in muscle and nerve by post-natal day 21.

It has previously been shown that loss of *eEF1A*2 results in the degeneration of lower motor neurons in *wasted* mice, characterised by vacuolation and neurofilament accumulation in neuronal soma and denervation of skeletal muscle fibres (Newbery *et al.*, 2005). Importantly, the onset of degeneration correlates precisely with the switch to reliance on *eEF1A*2 expression (Newbery *et al.*, 2005) and it has been conclusively demonstrated that the specific loss of *eEF1A*2 function is solely responsible for these events (Newbery *et al.*, 2007). Recent work from the Gillingwater laboratory has indicated that synaptic degeneration in *wasted* mice conforms to a dying-back pathology

distinct from classic Wallerian degeneration (ultimately published in Murray *et al*, 2008). Pre-synaptic terminals underwent a gradual retraction from the post-synaptic endplate with no apparent fragmentation of pre-synaptic or axonal compartments. This morphology shares striking similarities with synaptic degeneration in SMA mouse models (see chapter 3). Furthermore, ultrastructural studies in *wasted* mice revealed synaptic degeneration occurred in advance of overt axonal pathology and retracting terminals were devoid of structural fragmentation and organelle depletion.

In this chapter I further detail the pathological changes occurring at the neuromuscular junction in *wasted* mice and use them to investigate the mechanistic commonality or divergence between Wallerian degeneration and dying-back neuropathy. Firstly, I have shown that functional loss at the NMJ precedes structural loss in *wasted* mice and that degeneration occurs asynchronously within motor units. Such changes confirm that neurodegeneration in *wasted* mice conforms to a characteristic dying-back neuropathy. Secondly, I have used quantitative protein expression experiments to show that dying-back pathology in *wasted* and SMA mouse models share a common reduction in ZPR1 levels, presenting a common mechanistic link between SMA and *wasted* pathology. Thirdly, I have used nerve axotomy experiments to show that Wallerian degeneration of distal axons and synaptic terminals in *wasted* mice is delayed, with synapses remaining up to 48 hours post nerve injury and retaining functional ability. This demonstrates that *eEF1A*2 is required for the normal initiation and progression of Wallerian degeneration pathways and suggest that divergent mechanism are responsible for the instigation and/or progression of Wallerian degeneration and dying-back neuropathies.

6.2 Results

6.2.1 Dying-back pathology was evident in the LAL muscle and shows mild correlation to axonal length

Previous reports have identified synaptic pathology in *wasted* mice in the TVA and deep lumbrical muscles (Newbery *et al.*, 2005). I extended these observations to include the LAL in which there was significant NMJ loss (Figure 6.1). Closer examination of the distinct endplate regions within rostral and caudal bands of the LAL muscle, revealed no selective vulnerability betweens NMJs in the caudal and rostral band (Figure 6.1 B). This is in contrast to the selective vulnerability seen in SMA mouse models (see chapter 3), suggesting this selective vulnerability of the LAL caudal band is a feature unique to SMA pathology. There was a slight reduction in pathology in the C1 region of the muscle (as evidenced by an increase in partially occupied endplates with a corresponding decrease in vacant endplates). This may indicate that NMJs closer to the point of nerve entry into the muscle are more vulnerable. I therefore sought to determine whether axon length had an impact upon the vulnerability of an NMJ. *Wasted* YFP-H mice (in which only a small subset of motor neurons are labelled with YFP allowing reconstruction of single motor units) were therefore used to assess of the degree of denervation at a given NMJ with the length of the intramuscular axon. This revealed a weak correlation, indicating that an increase in axon length is associated with increased vulnerability of a NMJ (Figure 6.1 C). For this analysis, any endplate that is completely denervated cannot be included and as there is an increased number of vacant endplates in regions further from the point of nerve entry into the muscle, this correlation may be even stronger than suggested by this data.

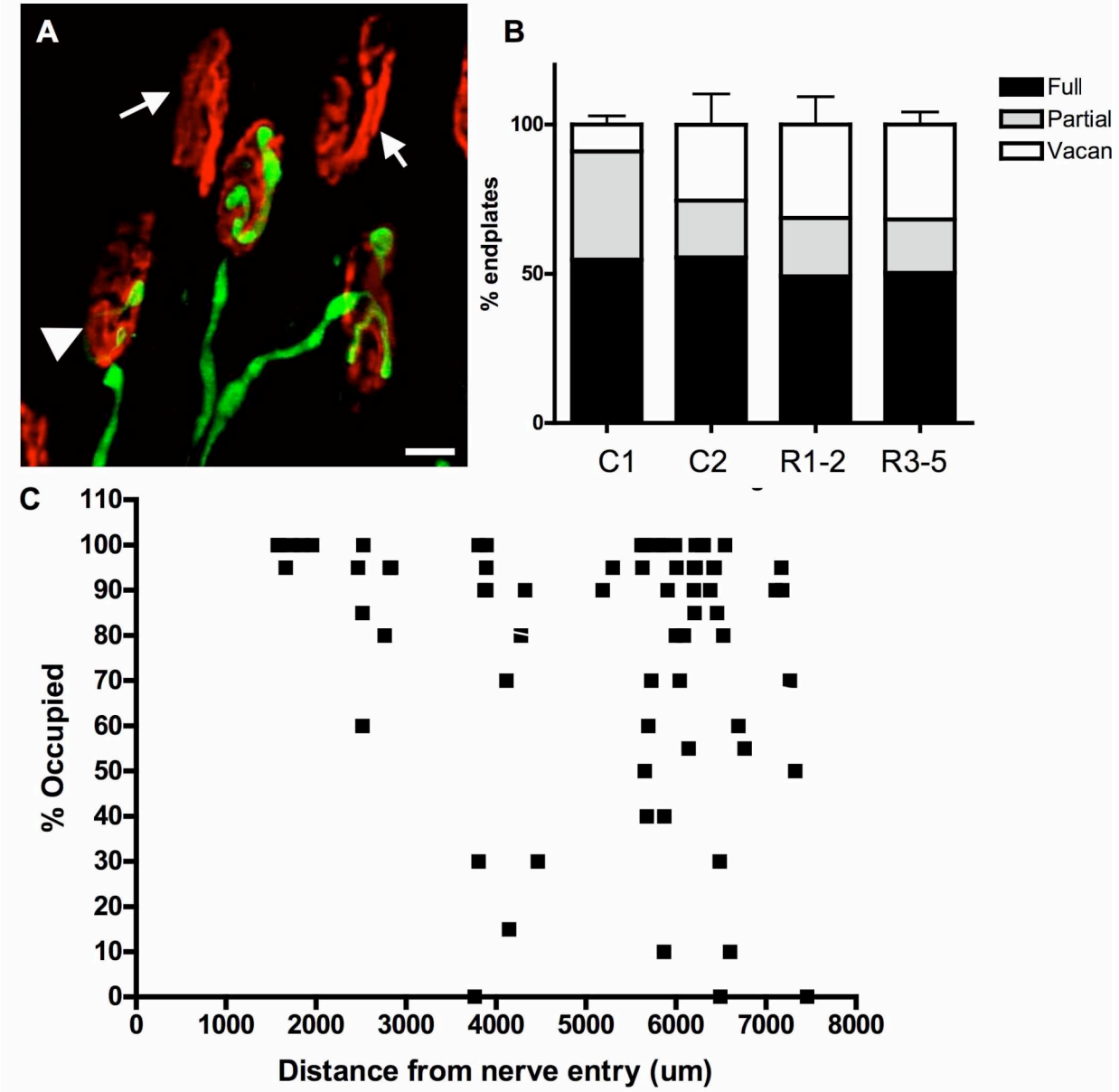

Figure 6.1: Synaptic pathology in the LAL muscle is equivalent in caudal and rostral bands but shows modest correlation to axonal length. A – Confocal micrographs showing neuromuscular junctions in immunohistochemically labelled LAL muscle preparations from P25 *wasted* mice (green = 150kDa neurofilaments; red = post-synaptic acetylcholine receptors labelled with TRITC-α-bungarotoxin). Partially occupied (white arrowhead) and vacant (white arrow) endplates were present throughout the muscle groups, as previously observed in TVA and lumbrical muscles (Figure 1; Newbery et al., 2005) (*Scale bars = 10μm).* B – Bar chart showing the percentage of fully occupied, partially occupied and vacant endplates in LAL muscles from *wasted* mice at P25 in LAL regions C1,C2, R1-2 and R3-5 *(*mean±SEM; *Kruksal Wallis test; all non significant by except for % vacant C1 vs R3-5 where P<0.05; N=4 mice,)*. Note that there is no selective vulnerability of the caudal band compared to the rostral band. C – Scatter plot showing a modest correlation between the degree an endplate is innervated and the distance from the point of nerve entry ($P<0.05$, $r^2 = 0.05970$).

6.2.2 *Functional loss at the NMJ precedes structural loss*

Previous reports of characteristic dying-back neuropathies indicate that functional loss at the synapse precedes structural loss (Balice-Gordon *et al.*, 2000; Pun *et al.*, 2006). Synaptic fuction was therefore investigated in *wasted* mice to investigate whether this feature of a dying-back neuropathy was also present in *wasted* mice.

Interestingly, prior work from the Gillingwater laboratory has identified an accumulation of synaptic vesicles at the NMJ in *wasted* mice (ultimately published in Murray *et al.*, 2008) and such an increase in synaptic vesicle numbers may imply altered synaptic function. Pre-synaptic function at the NMJ in late-symptomatic (P25) homozygous *wasted;YFP-H* mice was examined. The styrl dye FM4-64 was applied in high potassium ringer solution allowing the labelling of functionally active NMJs (see methods). *Wasted;YFP-H* mice allowed us to examine synaptic function at morphologically intact motor nerve terminals, indicated by the presence of YFP label (Feng *et al.*, 2000; see below). While, as expected, all motor nerve terminals showed uptake of FM4-64 in wild-type littermate mice, large numbers of morphologically present motor nerve terminals in *wasted* mice showed no FM4-64 uptake (Figure 6.2). These data suggest that despite the presence of large numbers of synaptic vesicles in motor nerve terminals, the functional machinery required for exocytosis/endocytosis was impaired as part of the dying-back process in *wasted* mice. Thus, functional loss preceded morphological retraction, and degeneration in *wasted* mice is consistent with previous reports for other dying-back neuropathies.

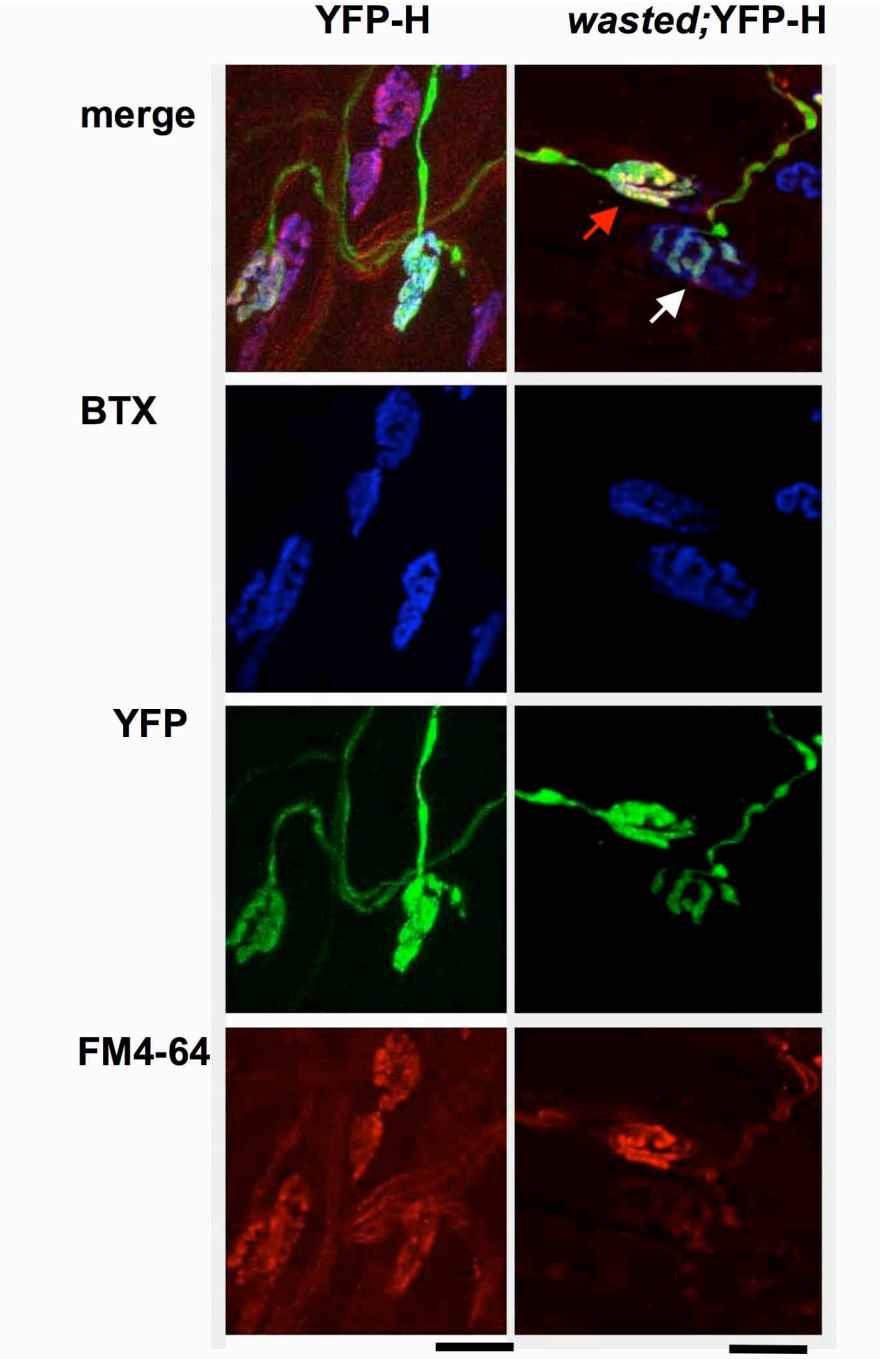

Figure 6.2: Functional loss precedes structural loss at neuromuscular junctions undergoing dying-back pathology in *wasted* mice. Confocal micrographs (merge of all 3 channels in top panels with separate channels shown below) of neuromuscular junctions from a P25 YFP-H and *wasted;YFP-H* mouse LAL muscle. Motor nerve terminals were loaded with FM4-64FX using a depolarising high-potassium solution leading to the selective labelling of functionally-active terminals (i.e. with the retained ability to recycle synaptic vesicles). In control YFP-H muscles (left) FM4-64 labelled all nerve terminals. In the *wasted*YFP-H preparation shown (right), two neuromuscular junctions with motor nerve terminals containing YFP can be seen, but only one of these motor nerve terminals demonstrated retained functional ability (red arrow; note the presence of strong FM4-64FX label in the bottom panel). The junction indicated by the white arrow was present morphologically (as evidenced by the YFP label) but had lost its functional capacity to recycle synaptic vesicles and hence had not taken up the FM4-64FX label. Thus, synaptic function was lost before morphological retraction occurred in *wasted* mice. *(Scale bar = 20μm (YFP-H), 10μm (wastedYFP-H)).*

6.2.3 Synapse loss occurs asynchronously within single motor units in wasted mice

The pattern of synaptic loss within a motor unit can give important information about the factors regulating degeneration. For example, synchronous loss within a motor unit, where all NMJs in a given motor unit degenerate, with all NMJs in a neighbouring motor unit remaining intact, might imply that pathogenic mechanisms are mediated from the cell body. Conversely, if degeneration within the motor unit is asynchronous, where some NMJs from a motor unit degenerate while other remain intact, then it is likely that local factors regulate synaptic vulnerability.

To investigate the synchronicity of synapse loss within motor units, the patterns of synaptic pathology occurring within single YFP-labelled motor units of *wasted*;*YFP-H* mice (Feng *et al.*, 2000) have been examined. Synaptic cohorts of single motor units supplying 5 different LAL muscles from late-symptomatic *wasted*;*YFP-H* mice were reconstructed and analysed (Figure 6.3). Branching diagrams produced by tracing individual, labelled motor units revealed a homogenous response, with all motor neurons seemingly affected to a similar level (i.e. all motor units exhibited clear evidence of synaptic pathology; Figure 6.4). Moreover, each motor unit displayed a wide range of synaptic morphologies, including intact synapses (fully occupied) and synapses at various stages of dismantling (partially occupied). Comparison of the innervation states of neighbouring synapses, sharing a single branch point, showed that synapses were being lost progressively and asynchronously in *wasted* mice. This finding indicates that local mechanisms, resident at individual synapses, are likely to play an important role in determining an individual synapse's response to the effects of a loss of *eEF1A*2. This finding is consistent with results from other dying-back neuropathies (Gillingwater and Ribchester, 2003) which are characterised by a progressive asynchronous loss of nerve terminals and is in contrast to Wallerian degeneration, which is known to bring about a relatively synchronous and rapid (i.e. within several hours) degeneration of NMJs (Miledi and Slater, 1970). The above results therefore further support the hypothesis that degeneration in *wasted* mice conforms to a highly characteristic dying-back neuropathy.

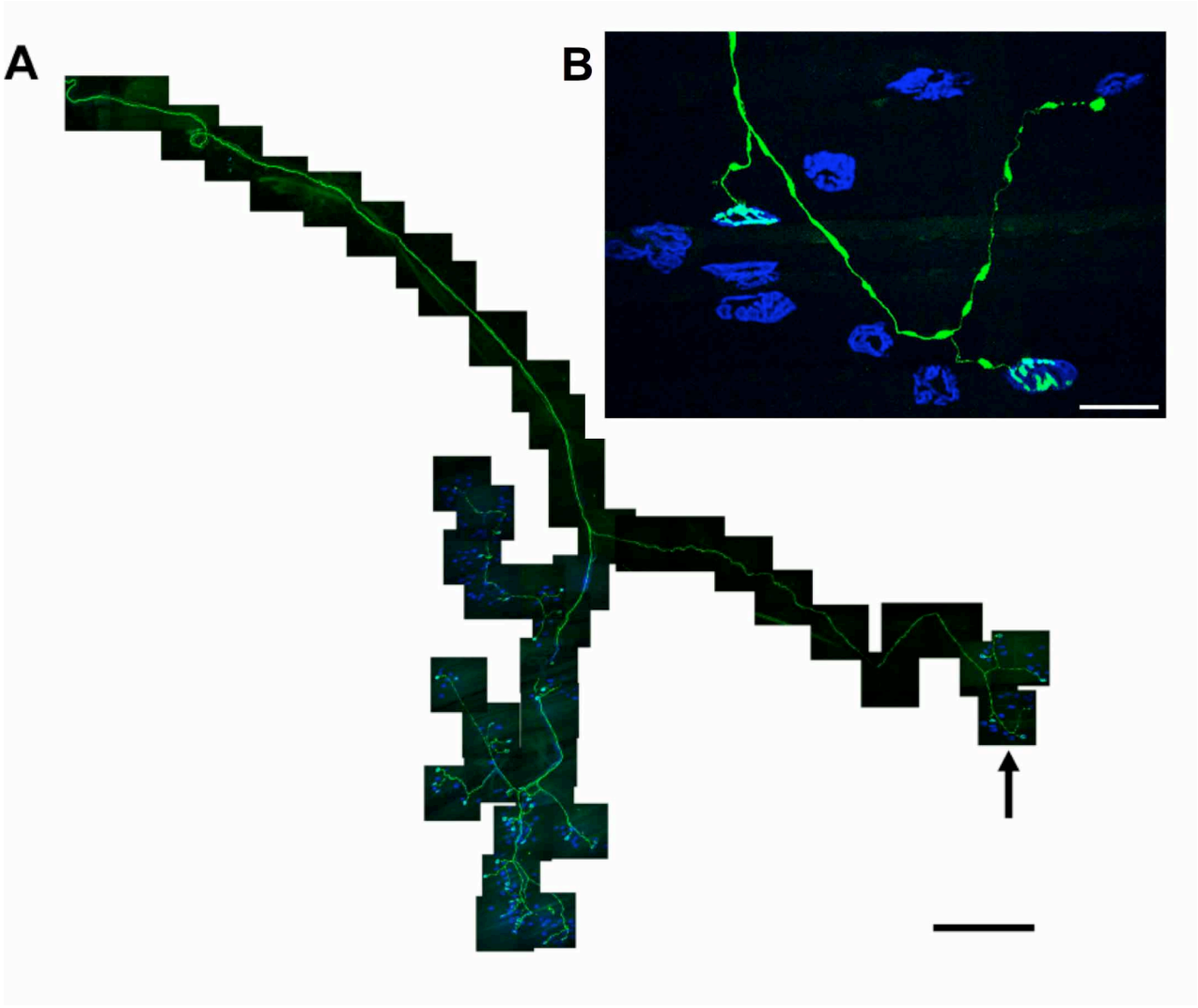

Figure 6.3: Reconstruction of individual YFP-H motor units reveals asynchronous loss of synapses at the NMJ in late-symptomatic *wasted* mice. A – Montage of confocal micrographs showing a single YFP-H labelled motor unit from a P25 *wasted*;*YFP-H* mouse (green = YFP; blue = post-synaptic acetylcholine receptors labelled with α-bungarotoxin). B – Higher power confocal micrograph showing a small region of the larger whole motor unit shown in A (position indicated by black arrow in A). Note how the first (far left) NMJ is fully occupied, the second (lower right) NMJ is partially occupied and the third (upper right) NMJ has lost its pre-synaptic input, remnants of which are left as a retraction bulb. *(Scale bars = 500μm (A), 50μm (B)).*

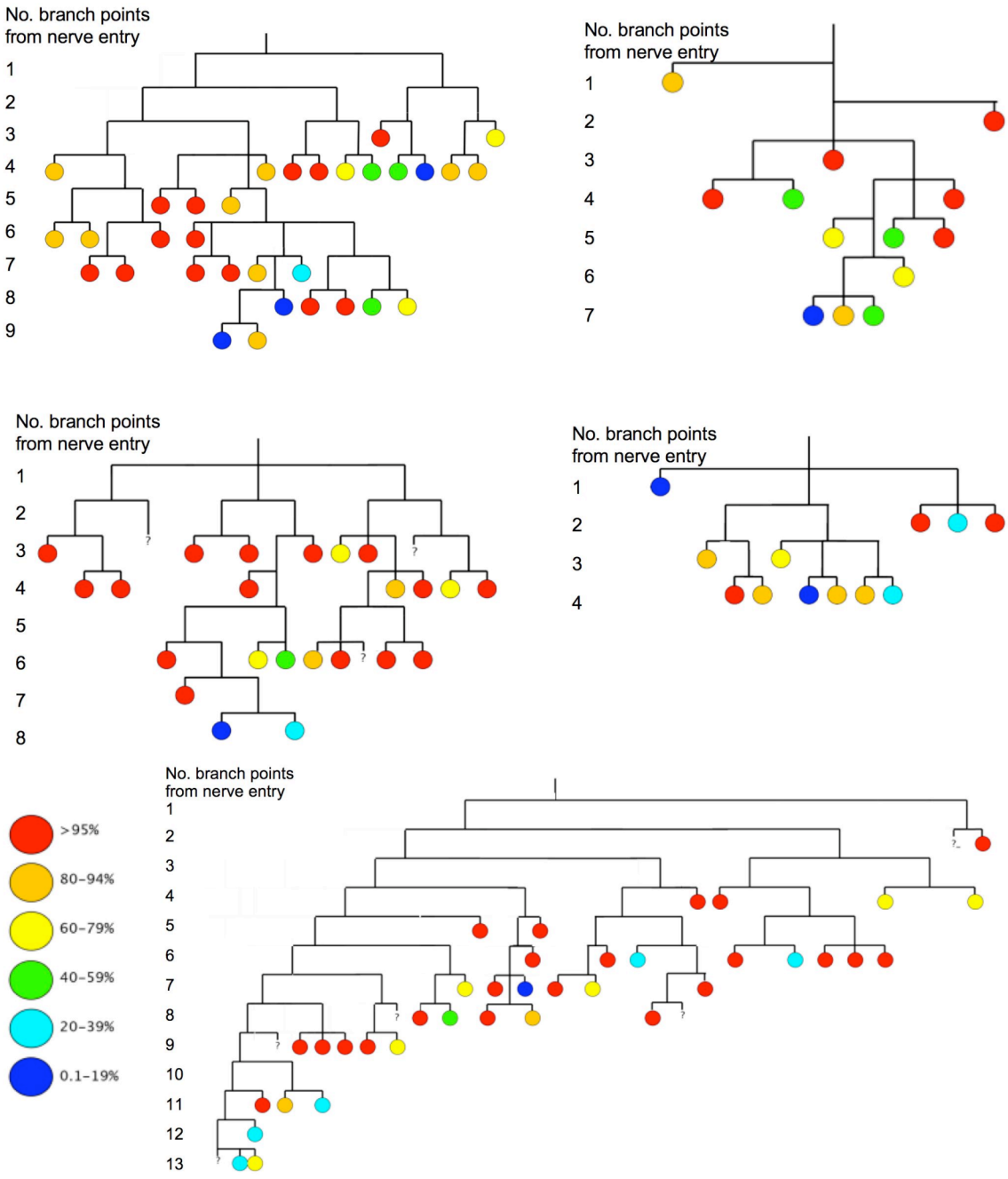

Figure 6.4: Branch diagrams confirm asynchronous loss of synapses at the NMJ in late-symptomatic *wasted* mice. Branch diagrams generated from an analysis of the single motor units (i.e. See figure 4), with each individual NMJ represented as a circle relative to its branch point position within the motor unit. The occupancy status of each NMJ is represented by the colour of the circle (key to colours is at bottom left). Note how synaptic retraction occurred asynchronously throughout the motor units, with a full spread of occupancies present. Note also how fully occupied (i.e. 'normal'; red) NMJs were distributed at locations throughout the motor units, as were almost fully retracted NMJs (blue). NMJs represented by a question mark indicate a point at which it was not possible to trace the motor unit branch any further.

6.2.4 Molecular correlates of dying-back neuropathy: A role for ZPR1?

The degenerative morphology in *wasted* mice shares striking similarities with degeneration in SMA mouse models, with both models displaying characteristic features of dying-back neuropathy. Despite this, the extent to which there is mechanistic commonality between SMA and *wasted* mice is currently unclear. A potential link is created by the observation that eEF1A and Smn proteins both assemble into complexes with the zinc finger protein *ZPR1*, which has also been implicated in motor neuron pathology (Gangwani *et al.*, 1998; Mishra *et al.*, 2007).

To test whether the dying-back pathology in *wasted* mice could simply be accounted for by reduced levels of Smn protein resulting from decreased *eEF1A*2 expression, Smn protein levels were quantified in the spinal cord of late-symptomatic *wasted* mice (P25) and littermate controls using fluorescent (Li-COR) western blots. Smn levels remained relatively stable in homozygous *wasted* mice, and if anything showed a trend towards increased rather than decreased expression levels (Figure 6.5). This was in stark contrast to the significant reduction in Smn levels observed in the spinal cord of late-symptomatic *Smn-/-;SMN2* mice. Thus, the dying-back pathology observed in *wasted* mice could not be simply attributed to downstream changes in Smn protein levels.

Next, a similar question was posed, but this time focussing on levels of ZPR1 protein expression. Interestingly, ZPR1 protein levels were found to be consistently reduced in *wasted* mice (Figure 6.5). Equivalent analysis in *Smn-/-;SMN2* mice revealed ZPR1 levels were reduced to similar levels (Figure 6.5). As reduced ZPR1 levels have been previously been suggested to contribute to dying-back pathology in SMA (Gangwani *et al.*, 2001; Helmken *et al.*, 2003) a comparable reduction in *wasted* mice may provide evidence for a common regulatory role of ZPR1 in regulating dying-back pathways in both *wasted* and *Smn-/-;SMN2* mice.

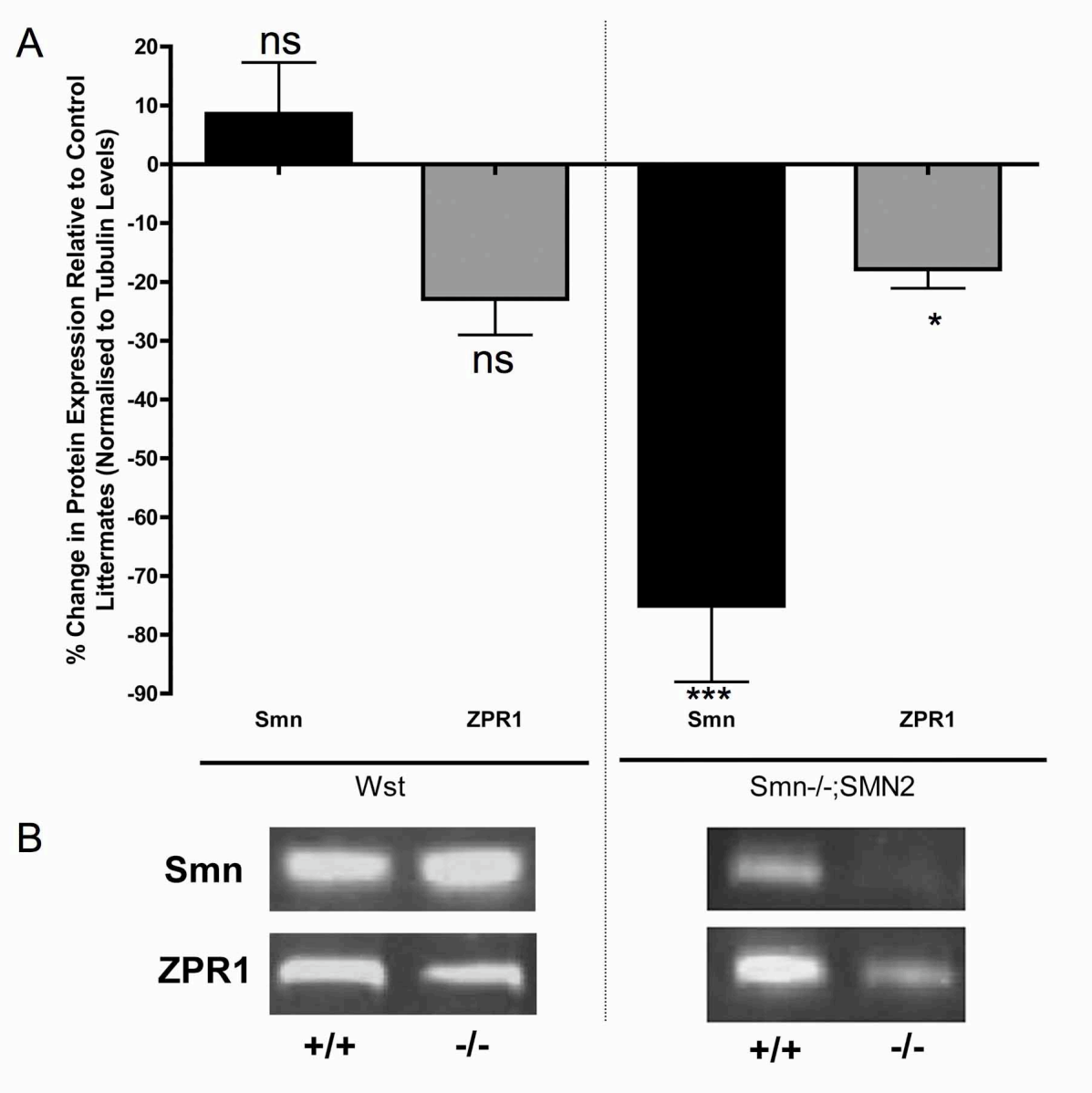

Figure 6.5: Dying-back pathology in *wasted* mice occurs independently of changes in Smn protein expression but correlates with modest reductions in ZPR1 protein levels. A - Bar chart (mean±SEM; upper panel) showing expression levels of Smn and ZPR1 protein in the mid-thoracic spinal cord of late-symptomatic *wasted* (Wst; left bars; P25) and *Smn-/-;SMN2* (right bars; P5) mice compared to respective control littermate mice, quantified using fluorescent western blots (N = 3 mice per genotype). B - Representative fluorescent western blots showing levels of Smn and ZPR1 protein in *wasted* (Wst) mice versus control littermates (left panel) and *Smn-/-;SMN2* mice versus control littermates (right panel). Smn protein levels did not decrease in *wasted* mice (if anything showing a modest increase in expression), but as expected decreased by around 75% in *Smn-/-;SMN2* mice. Thus, dying-back pathology observed in *wasted* mice is not simply occurring due to reduced levels of Smn protein. ZPR1 protein levels, however, were reduced by comparable amounts in both *wasted* and *Smn-/-;SMN2* mice. *(mean ± SEM;data reflect changes normalised to control littermate values, Student unpaired T test for each column compared to control; ***P<0.001, *P<0.05, ns non significant)*

6.2.5 eEF1A2 is required for the normal initiation and progression of axotomy-induced Wallerian degeneration

If, as suggested, Wallerian degeneration and dying-back neuropathy are regulated by common mechanisms (Coleman *et al.*, 2005), then one might expect Wallerian degeneration to be accelerated in neurons already undergoing a dying-back neuropathy. As results to date provide strong evidence that *eEF1A2* is an important regulator of dying-back pathways *in vivo*, the progression of Wallerian degeneration in *wasted* mice was investigated by studying responses to nerve injury in homozygous *wasted*, heterozygous *wasted* and wild-type littermate mice. For these experiments lumbrical muscles were examined following a tibial nerve cut, as synaptic pathology resulting from dying-back pathology is significantly less in these muscles compared to more rostral muscle groups (Newbery *et al.*, 2005), thus minimising the complexity of distinguishing disease-induced changes from those induced by nerve injury. Late-symptomatic (P24) *wasted* and *wasted*;*YFP-H* mice were subjected to a unilateral tibial nerve cut under general anaesthesia. 24 hours later (P25), following recovery and resumption of normal behaviour, mice were sacrificed and their lumbrical muscles and tibial nerves distal to the site of lesion removed.

As expected, nerve lesion in wild-type littermate mice resulted in a complete loss of neuromuscular innervation 24 hours after surgery, occurring via classical Wallerian degeneration pathways characterised by rapid breakdown and fragmentation of pre-synaptic motor nerve terminals and distal axons (Figure 6.6 A). Surprisingly, however, the vast majority (~80%) of motor nerve terminals and their intramuscular axon collaterals remained intact in lumbrical muscles from homozygous *wasted* mice 24 hours after nerve lesion (Figure 6.6 B,C). Similarly, the tibial nerve distal to the site of nerve lesion showed no signs of degeneration in homozygous *wasted* mice assayed using YFP-H and ultrastructural techniques (Figure 6.7). Examination of early axonal ultrastructural indicators of Wallerian degeneration (swelling and damage of mitochondria; Miledi & Slater, 1970; Winlow & Usherwood, 1975) revealed subtle but widespread changes in wild-type nerves (~50% of axons examined showed mitochondrial changes or disruption

of the myelin sheath; Figure 6.7 B), but almost complete absence of any early markers of Wallerian degeneration in *wasted* nerves (only one out of ~200 axons showed signs of disrupted mitochondria; Figure 6.7 C).

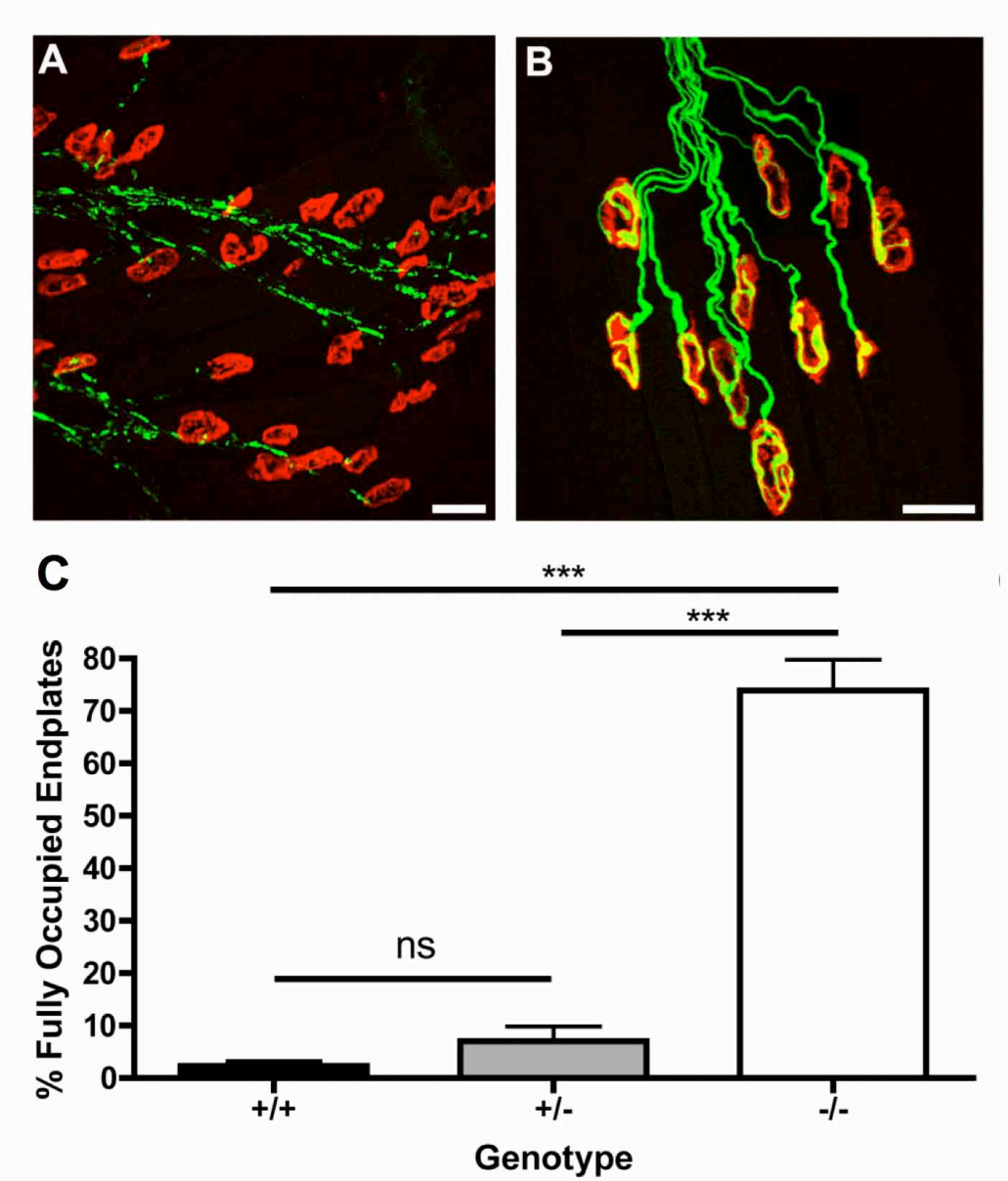

Figure 6.6: *eEF1a2* expression is required for the normal initiation and progression of axotomy-induced synaptic WD. A,B – Confocal micrographs showing NMJs in immunohistochemically labelled lumbrical muscle preparations from P25 wild-type (+/+; A), homozygous *wasted* (-/-; B) mice 24 hours after a tibial nerve cut (green = 150kDa neurofilaments; red = post-synaptic acetylcholine receptors). As expected, axotomy resulted in almost complete WD of motor nerve terminals and distal axon collaterals in lumbrical muscles of wild-type mice (A). Surprisingly, however, axotomy-induced WD was almost completely absent from homozygous *wasted* mice at the same time-point (B). C – Bar chart showing the percentage of NMJs remaining in lumbrical muscles 24 hours post-axotomy. Note how less than 5% of NMJs remain intact in muscles from wild-type mice, whereas ~80% of NMJs remained intact in muscles from homozygous *wasted* mice. *(mean±SEM; Kruskal Wallis test with Dun's post hoc; *** P<0.001; n=57 muscles, N=19 mice +/+; n=36 muscles, N=12 mice +/-; n=36 muscles, N=12 mice -/-; Scale bar = 50μm (A,B)).*

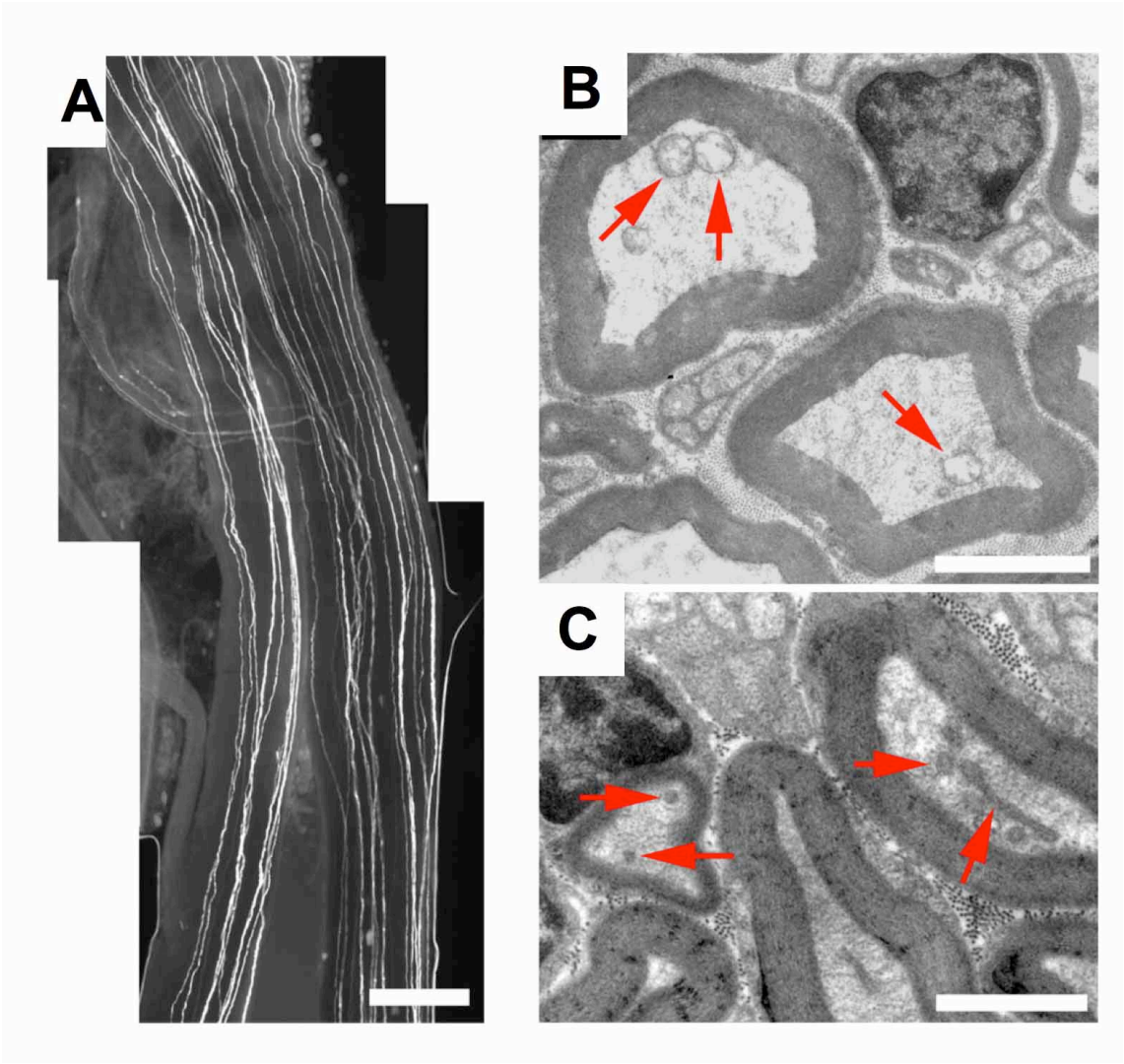

Figure 6.7: *eEF1a2* expression is required for the normal initiation and progression of axotomy-induced axonal Wallerian degeneration. A – Montage of fluorescence micrographs showing YFP-labelled axons in a tibial nerve (supplying the lumbrical muscles) from a P25 *wasted;YFP-H* mouse 24 hours after a tibial nerve cut. Note the complete absence of any axonal pathology at this time-point. B – Electron micrograph showing early ultrastructural signs of WD in +/+ tibial nerves 24 hours after axotomy (swollen and disrupted mitochondria; red arrows). C - Electron micrograph showing lack of early ultrastructural signs of WD in -/- tibial nerves 24 hours after axotomy (mitochondria remained intact; red arrows). *(Scale bars = 200μm (A), 2μm (B,C))*

To investigate whether structurally preserved NMJs were also functional, electrophysiological recordings were made from flexor digitorum brevis (FDB) muscles from both operated and un-operated legs of *wasted* and wild-type mice. FDB muscles are also innervated by the tibial nerve and show significant structural protection 24 hours after nerve cut in *wasted* mice, albeit at a lower level than that observed in lumbrical muscles (Figure 6.8). While in wild-type muscles 24 hours after nerve cut, no endplates show any evoked or spontaneous activity endplate potential in response to a nerve stimulus, significant functional protection was observed in *wasted* mice, with around 50% of NMJs showing spontaneous transmitter release and/or evoked activity (Figure 6.9; 6.10).

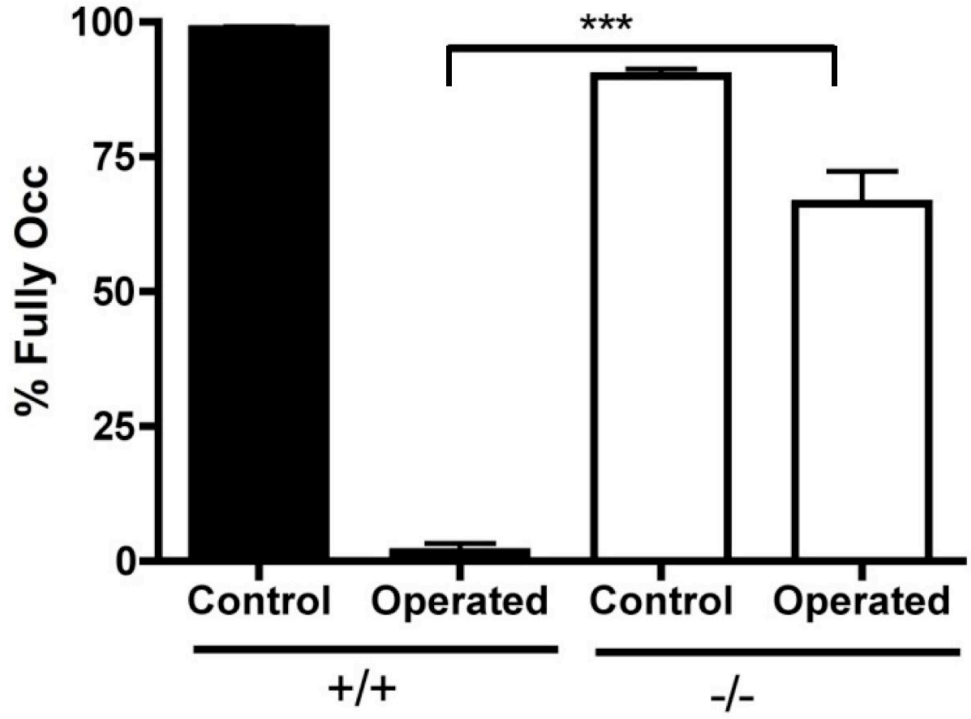

Figure 6.8: Significant delay in synaptic degeneration 24 hours after nerve cut in flexor digitorum brevis muscles. Bar chart showing percentage of fully occupied endplates in wild-type and *wasted* FDB muscles in un-operated control legs, and legs 24 hours after tibial nerve cut. Note NMJ protection still occurs in this muscle, albeit at a slightly lower level than in lumbrical muscles. *(Mean ± SEM; Mann Whitney test; ***P<0.001; N = 2/3 per mouse, 6/9 per muscle wild-type/wasted)*

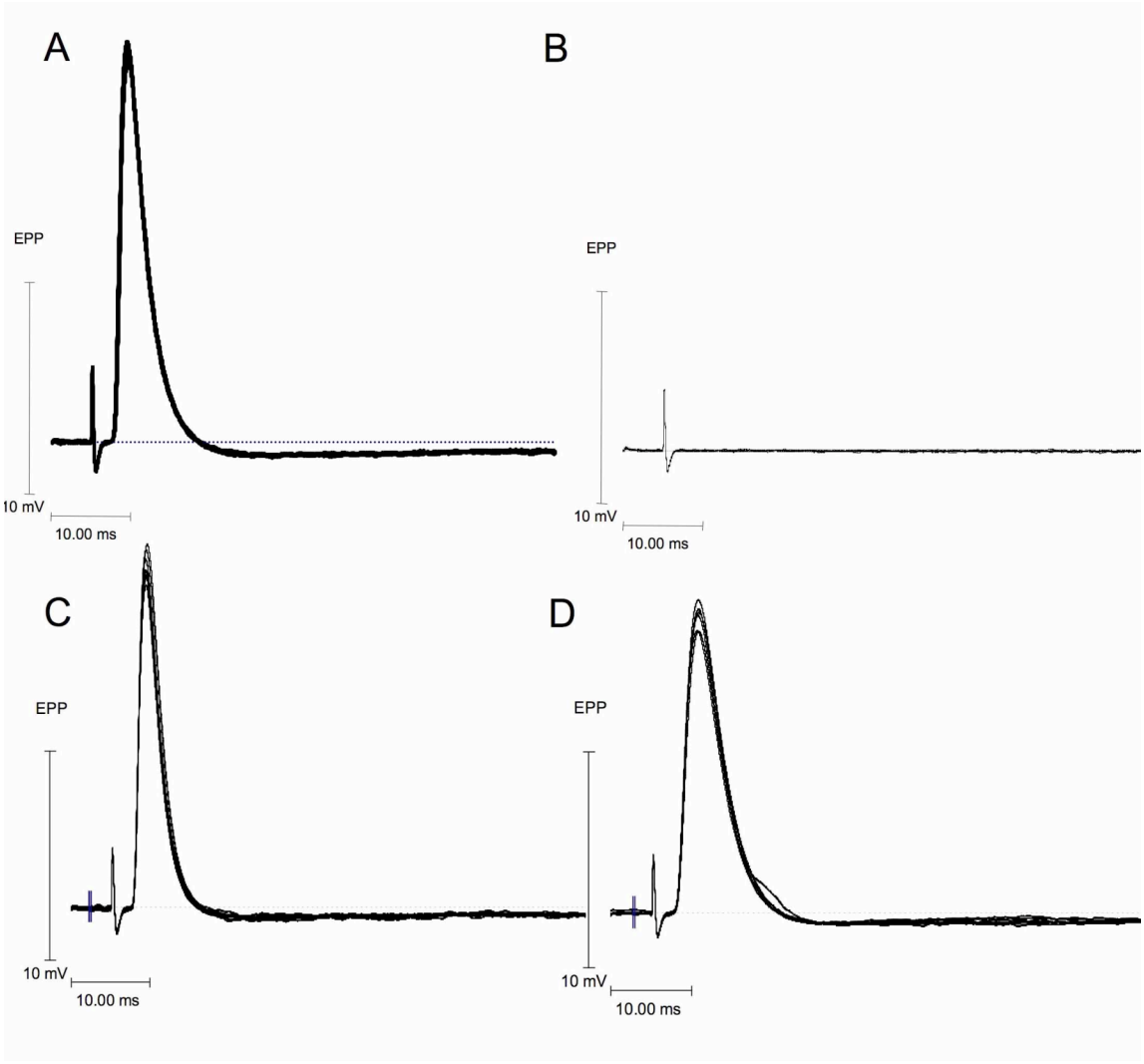

Figure 6.9: Synaptic function is retained in *wasted* NMJs 24 hours post nerve cut. A-D – example electrophysiological traces showing evoked response from nerve stimulation in flexor digitorum brevis muscles from wild-type (A,B) and *wasted* (C,D) mice from both operated (B,D) and control contralateral (A,C) legs . Note muscles from un-operated control legs (A,C) show robust endplate potentials in response to nerve stimulation while no response is seen in wild-type operated legs 24 hours post-nerve cut (B). Muscles from *wasted* operated legs show endplate potentials in response to nerve stimulation (D) implying functional activity is retained 24 hours after nerve transection.

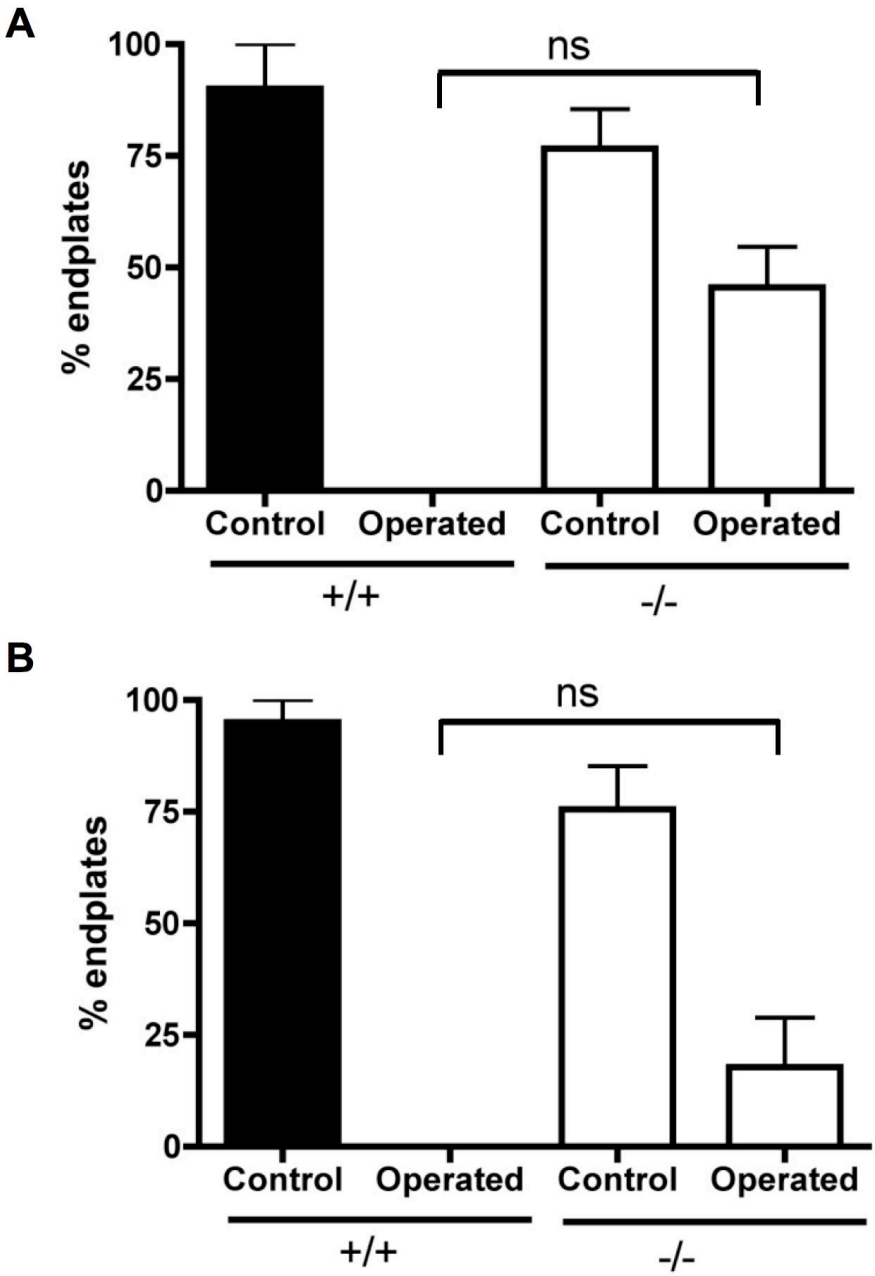

Figure 6.10: Synaptic function is retained in *wasted* NMJs 24 hours post nerve cut. A,B - Bar charts (mean ± SEM) showing the percentage of endplates in the FDB muscle showing spontaneous (B) and evoked (C) activity in wildtype (black bars) and *wasted* mice (white bars) in control un-operated legs and legs 24 hours following tibial nerve cut. Note an increase in the percentage of endplates showing evoked and spontaneous activity in muscles from operated legs in *wasted* mice compared to wild-type. *(Kruskal Wallis test with Dunns multiple comparison, ns non significant. N = 2/3 per mouse, 6/9 per muscle muscle wildtype/wasted)*

In order to confirm that the significant inhibition in Wallerian degeneration found in homozygous *wasted* mice extended beyond the 24 hour period initially examined, synaptic degeneration was quantified morphologically in mice subjected to a unilateral tibial nerve cut at P23 that were sacrificed 48 hours later (P25). Even at 48 hours post-axotomy, around 50% of motor nerve terminals and their intramuscular axon collaterals remained intact in lumbrical muscles from homozygous *wasted* mice (Figure 6.11). As at 24 hours, almost all motor nerve terminals (>95%) had undergone degeneration in wild-type and heterozygous littermates. It was not possible to extend the time-course of investigations much beyond this 48 hour period because the operated mice do not live beyond P26 (due to the severity of dying-back pathological changes in more severely affected rostral muscle groups).

The experiments detailed above demonstrate that *eEF1A*2 is required for the normal initiation and progression of Wallerian degeneration. These data also add further support to the conclusion that the dying-back pathways instigated following disruption of *eEF1A*2 in *wasted* mice are mechanistically distinct from Wallerian degeneration, as Wallerian degeneration pathways are actually inhibited (rather than initiated) in *wasted* mice.

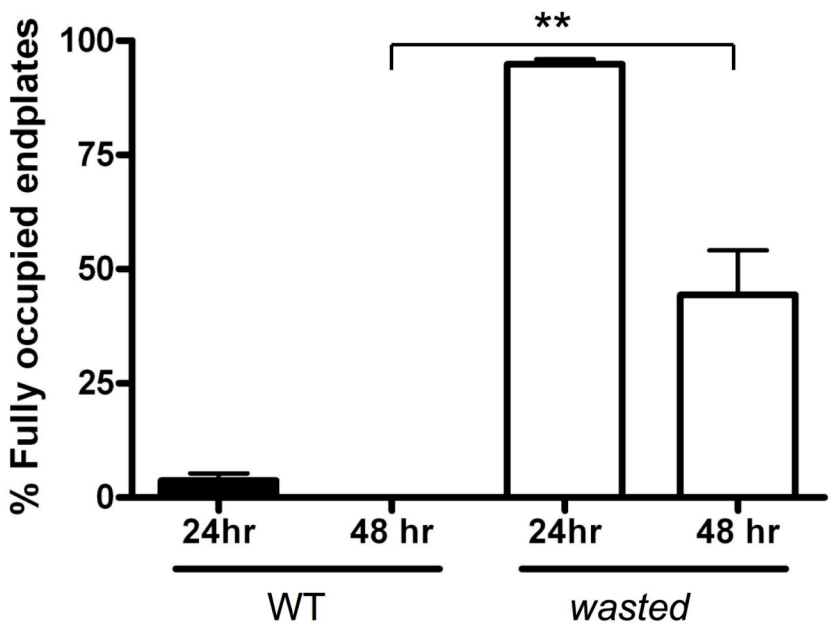

Figure 6.11: Wallerian degeneration remains significantly delayed 48 hours after nerve cut. Bar chart showing the percentage of NMJs remaining in lumbrical muscles from wild-type and homozygous *wasted* mice 24 and 48 hours post-axotomy *(mean±SEM; Unpaired students T-test between WT and wasted at 48hr; ** P<0.01 n=57 muscles, N=19 mice wildtype 24hrs; n=36 muscles, N=12 mice wasted 24 hrs; n=6 muscles, N=2 mice wildtype and wasted 48 hrs; N numbers are insufficient for statistical analysis)*. Note how ~50% of NMJs remained intact in muscles from homozygous *wasted* mice even at 48 hours post-axotomy.

6.2.6 Is the delay in Wallerian degeneration due to a requirement for eEF1A2 or the instigation of dying-back pathways?

In order to investigate whether this protection is a result of a requirement of eEF1A2 during Wallerian degeneration, or due to the instigation of dying-back pathways, tibial nerve cuts were performed in *wasted* mice at P16, prior to the onset of any neuromuscular pathology. Interestingly, although significant synaptic protection was observed in *wasted* mice, equivalent protection was evident in wild-type and heterozygote mice (Figure 6.12). Although it was previously reported that Wallerian degeneration progresses quite differently in neonatal mice, with proximal degeneration being more apparent and distal degeneration being inhibited, it is perhaps not

appreciated that this phenomenon continues to this time point. Although this finding prevents us from further addressing the original question, it does provide a potential explanation for the protection seen in *wasted* mice i.e. if a lack of eEF1A2 impairs neuromuscular development and the system retains an immature phenotype, normal adult progression of Wallerian degeneration could be significantly altered. This finding may be consistent with the preliminary observation that an increase in temperature and/or exercise ameliorated *wasted* pathology and reduced the observed protection from Wallerian degeneration (Appendix 10.2). This theory undoubtedly requires further investigation.

During this study I also made some interesting observations about the progression of Wallerian degeneration in motor neurons labelled with YFP, indicating that either presence of the protein or genetic background may have modifying effects on the time course of NMJ breakdown in response to nerve axotomy (Appendix 10.3). This finding clearly has important implications for the use of fluorescent markers to label cell types and again clearly warrant further investigation.

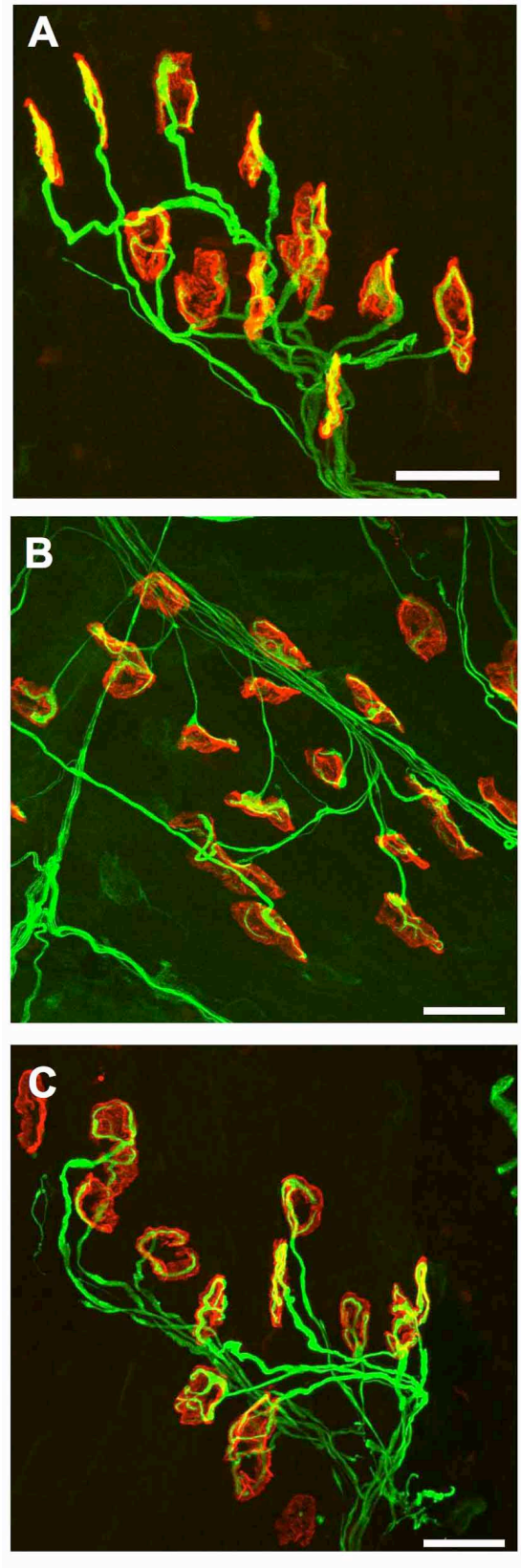

Figure 6.12: Preservation of neuromuscular junctions 24hrs post-nerve cut in wildtype, heterozygous and homozygous *wasted* P17/P18 mice. A-C - Confocal micrographs of immunocytochemically labelled lumbrical muscles from P18 wildtype (A), *wasted* heterozygote (B) and *wasted* (C) mice 24 hours following tibial nerve cut *(green = 150KDa neurofilaments; red = post-synaptic acetylcholine receptors).* Note all neuromuscular junctions in all genotypes remain fully innervated. *(Scale bar = 30μm)*

6.3 Discussion

The results presented in this chapter firstly support the hypothesis that degeneration in *wasted* mice conforms to highly characteristic dying-back neuropathy. Significant NMJ pathology can be identified in the LAL muscle, where a mild correlation between synaptic vulnerability and axonal length was observed. Functional loss preceded structural loss and synapse loss was asynchronous, which is consistent with previous report from other dying-back neuropathies (Balice-Gordon *et al.*, 2000; Pun *et al.*, 2006). Secondly I show that there may be a common molecular linkage between SMA and *wasted* mice, through the mutual down-regulation of ZPR1. This finding may prompt further study into the pathways acting downstream of eEF1A2 and SMN and their regulation in a variety of neurodegenerative conditions. Thirdly, the experiments show that significant divergence exists in the mechanisms regulating degenerative pathways in axons and synapses, where dying-back pathology can be *caused by* deficiencies in *eEF1A*2 whereas Wallerian degeneration *requires eEF1A*2 expression. This finding contradicts, to some extent, an emerging view that many axonal and synaptic degenerative pathways converge onto common underlying mechanisms (c.f. Coleman, 2005; Kielar *et al*., 2009). The observation that *eEF1A*2 expression is required for the normal initiation and progression of Wallerian degeneration also adds significant support to previous experimental studies suggesting that Wallerian degeneration is an active, genetically-regulated process, rather than a simple passive consequence of disconnection from the parent cell body (Mack *et al.*, 2001; Coleman and Perry, 2002).

6.3.1 Can deficiencies in protein synthesis explain the neurodegenerative phenotype in wasted mice?

The most parsimonious explanation for the observed dying-back pathology in *wasted* mice is that defects in protein synthesis, resulting directly from a loss of *eEF1A*2 expression and function, are responsible for triggering dying-back pathways and for the delay in Wallerian degeneration. The fact that deficiencies in *eEF1A* proteins lead to disruption of protein synthesis is not in doubt (Shultz *et al.*, 1982; Chambers *et al.*, 1998;

Pan *et al.*, 2004). Moreover, the protein synthesis machinery is known to influence axonal and synaptic form and function in neuronal cells (Piper and Holt, 2004; Grossman *et al.*, 2006; McCann *et al.*, 2007) and *eEF1A* is known to be important for local protein synthesis determining synaptic stability and function (Giusetto *et al.*, 2003). This also provides mechanistic links to SMA, as the main documented function of Smn is in pre-mRNA slicing, a crucial step in protein translation (Burghes and Beattie, 2009). However, whilst inhibition of protein synthesis has been shown to accelerate neurodegeneration of axons and synapses *in vitro* (Stavisky *et al.*, 2003), the influence of protein synthesis on neurodegenerative mechanisms resident in axons and synapses *in vivo* remains unclear.

It is not currently possible to directly visualise or measure *de novo* protein synthesis occurring in distal axonal and/or neuromuscular synaptic compartments of *wasted* mice *in vivo* with any accuracy, ruling out the possibility of definitively linking the induction of dying-back pathways to deficiencies in protein synthesis. Similarly, the current data do not allow us to directly link the inhibition of Wallerian degeneration with deficiencies in local protein synthesis. However, *wasted* mice are likely to provide an ideal model system within which to further investigate downstream molecular mechanisms, once more sensitive techniques to measure local neuronal protein synthesis become available. Its attractiveness as an experimental model is highlighted by the fact that *eEF1A*2 deficiencies are restricted to neuronal cells and muscle and are only instigated post-natally before progressing over a fairly rapid time-course.

*6.3.*2 *Could non-canonical roles of eEF1A*2 *be responsible for the neurodegenerative phenotype in wasted mice?*

Alternative hypotheses explaining the potential mechanisms underlying modifications in dying-back pathways and Wallerian degeneration in *wasted* mice can be raised in light of other known non-canonical functions of *eEF1A* proteins. For example, several studies have implicated *eEF1A* proteins in assembly and stability of the cytoskeleton, including roles in actin binding and microtubule severing (Yang *et al.*, 1990; Yang *et al.*, 1993;

Shiina *et al.*, 1994). It is possible, therefore, that the dying-back pathways instigated in *wasted* mice occur as a direct result of perturbations in stability of the axonal and synaptic cytoskeleton. Moreover, a loss of ability to transport factors down the distal axon resulting from cytoskeletal disruption may explain the inhibition of Wallerian degeneration pathways. If the latter were found to be true, it would provide experimental support for the hypothesis that Wallerian degeneration is triggered by a signal that passes from the site of injury down to the nerve terminal (Miledi and Slater, 1970). Alternatively, it is possible that perturbations in synaptic plasticity pathways, known to be modulated by *eEF1A* levels (Giustetto *et al.*, 2003), lead to destabilisation of the NMJ and induction of dying-back pathology. However, it should be noted that it has yet to be demonstrated that the *eEF1A*2 variant has the same non-canonical roles previously attributed to non variant-specific *eEF1A* protein. It therefore also remains possible that *eEF1A*2 has as yet unidentified roles that are responsible for the phenotypes described in the current study.

It should also be noted that it is by no means certain that the same down-stream effects resulting from loss of *eEF1A*2 in *wasted* mice are responsible for the dual effects on dying-back pathways and Wallerian degeneration pathways. Further mechanistic experiments are required to distinguish the specific characteristics or molecular targets of *eEF1A*2 required to prevent a dying-back neuropathy and/or inhibit the initiation and progression of Wallerian degeneration.

6.3.3 Potential implications for the stability and vulnerability of lower motor neurons in human motor neuron disease

As highlighted above, although *eEF1A*2 mutations are not currently thought to be directly responsible for any human neurodegenerative conditions, eEF1A proteins are known to assemble into complexes with Smn and *ZPR1 (*Gangwani *et al.*, 1998; Mishra *et al.*, 2007). The finding that dying-back pathology occurring in *wasted* mice closely resembles lower motor neuron pathology occurring in mouse models of SMA and in *ZPR1*-deficient mice (Monani *et al.*, 2000; Monani *et al.*, 2003; Doran *et al.*, 2006)

prompted us to examine whether the pathways modified by loss *of eEF1A*2 converged onto those involving Smn and ZPR1. Results suggest that dying-back pathology in *wasted* mice can not be attributed to corresponding reductions in Smn protein levels, showing that dying-back pathology in *wasted* and *Smn-/-;SMN2* mice are not triggered by the same molecular cues. However, the observation that ZPR1 protein levels were modestly reduced in *wasted* mice, to a similar level found in *Smn-/-;SMN2* mice, raises the possibility of shared mechanistic pathways focussed around ZPR1. As decreasing ZPR1 levels have been shown to correlate with disease severity in SMA patients (Helmken *et al.*, 2003) and ZPR1 is known to be required for the normal maintenance and localisation of Smn protein (Gangwani *et al.*, 2001), it is tempting to speculate that ZPR1 is capable of playing an important role in regulating lower motor neuron vulnerability in SMA and in *wasted* mice. Further investigations into the expression and function of *ZPR1* in *wasted* and *Smn-/-;SMN2* mice may therefore provide novel insights into cellular and molecular cascades regulating the vulnerability of motor neurons in SMA. Moreover, as the current data suggest that *eEF1A*2 is required to prevent pre-synaptic degeneration via a dying-back neuropathy, it may also be worth investigating the possibility of increasing levels of *eEF1A*2, on its own or in combination with ZPR1, as a potential neuroprotective strategy in dying-back neuropathies, such as SMA.

The finding that distinct rostral and caudal bands of the LAL muscle showed comparable levels of synaptic pathology in *wasted* mice is in contrast to observation in SMA mouse models and has potential implications for our understanding of the selective vulnerability of motor neuron pools and neuromuscular synapses in SMA. As similar selective vulnerability does not occur in *wasted* mice, it seems reasonable to conclude that the selective vulnerability observed in SMA mouse models occurs as a direct response to mutations in the *SMN* gene, rather than a more generic neurodegenerative stimulus. These findings also suggest that, whilst there may be potential linkages between *eEF1A*2 and proteins modulating dying-back pathology in SMA (i.e. ZPR1), the selective vulnerability of motor neurons and NMJ sub-types observed in SMA mice must be occurring via mechanisms distinct from *eEF1A*2.

Chapter 7: Potential mechanistic insights in SMA from Wld^s mice

Summary

In addition to using models of neurodegeneration, it is also possible to gain insight into mechanisms which regulate synaptic vulnerability by analysis of models of neuroprotection. In this chapter, I have utilised quantitative fluorescent western blotting to investigate whether proteomic changes occurring in tissue expressing the neuroprotective Wld^s gene which protects axons and synapses can also be observed in *Smn-/-;SMN2* mice. I also describe attempts to cross Smn-/-;SMN2 mice with Wld^s mice to investigate any potential phenotypic rescue. Due to practical issues and time constraints, the results presented within this chapter are not intended to represent a complete or conclusive story, but rather reflect a 'proof of principle' study detailing work in progress.

Results detailed in this chapter show that:

1. Proteomic changes identified in Wld^s mice were observed to occur in an opposite direction in *Smn-/-;SMN2* mice and could potentially be used to identify important regulators of synaptic vulnerability
2. This approach can be used to identify novel biomarkers which can act as indicators of the pathological status of an individual/tissue
3. In *Smn-/-;SMN2* mice with one copy of Wld^s, no protection was observed, with no change in body weight or neuromuscular junction pathology.

7.1 Introduction.

Work presented so far has revealed that NMJs are early and significant targets in SMA and has demonstrated that abnormal development of neural connectivity is unlikely to underlie pathology. While microarray analysis has hinted at some pathways which may be involved in the degenerative processes, the mechanisms regulating synaptic pathology in SMA are broadly unknown. A better understanding of the mechanisms regulating synaptic vulnerability will therefore be important for our understanding of disease pathogenesis and are likely to be key in the development of effective therapeutic approaches.

In order to better understand the mechanisms which regulate synaptic stability, much work to date has been focused on the Wld^s mutation. This spontaneous mutation produced a novel 373 amino acid protein, termed Wallerian Degeneration Slow, or Wld^s, and confers significant synaptic and axonal protection in response to a range of traumatic and pathological insults (Lunn *et al.*, 1989; Perry *et al.*, 1990; Glass *et al.*, 1993; Mack *et al.*, 2001; Ferri *et al.*, 2003; Samsam *et al.*, 2003; Gillingwater *et al.*, 2006). Intriguingly, the Wld^s mutation does not have an influence on the process of developmental synapse elimination (Parson *et al.*, 1997; Hoopfer *et al.*, 2006) thus providing an *in vivo* tool to separate two mechanistically distinct types of synapse loss. Synaptic and axonal protection appears to be proportional to Wld^s protein expression levels i.e. while significant axonal and synaptic protection is observed in homozygote animals, heterozygote animals only show axonal protection (Mack *et al.*, 2001; Wong *et al*., 2009).

The Wld^s mutation is of clear interest due to its potential clinical application and mechanistic insight. Wld^s mice have now been crossed to a range of neurodegenerative models including models of motor neuron diseases, with varying degrees of protection observed (Ferri *et al.*, 2003; Samsam *et al.*, 2003; Vande-Velde *et al.*, 2004; Fischer *et al.*, 2005; Mi *et al.*, 2005; Hasbani and O'Malley, 2006; Beirowski *et al.*, 2008; Gultner *et al.*, 2009). In SMA research, crossing Wld^s mice with the *Smn;SMN2;Δ7* model

revealed no change in motor phenotype or life span (Kariya *et al.*, 2009; Rose *et al.*, 2009). However, as resultant mice were only heterozygous for the Wld^s gene and homozygosity is required for synaptic protection, these studies does not conclusively demonstrate whether or not the Wld^s mutation can confer protection in SMA mice.

Although the precise mechanisms underlying the Wld^s phenotype are currently controversial, several *in vivo* and *in vitro* proteomic and genomic screens have highlighted a number of genes and proteins which show altered expression in the presence of the Wld^s mutation and may therefore be important regulators of synaptic status (Gillingwater *et al.*, 2006b; Wishart *et al.*, 2007b; Wishart *et al.*, 2008). Furthermore, some of these expression changes have been observed to occur in an opposite direction in mouse models of Batten disease (an autosomal recessive childhood neurodegenerative disorder), and these changes occurred in proportion to the levels of pathology present (Kielar *et al.*, 2009). This work implies that the Wld^s mouse model can be used to identify proteins which are differentially regulated in models of neurodegeneration. This approach could potentially provide mechanistic insights into cell death pathways in axons and synapses and identify candidate biomarkers which may be used to assess pathological status and disease progression.

In this chapter I have investigated whether mechanisms regulating synaptic and axonal protection in Wld^s mice can offer any insight into pathological mechanisms in SMA. Due to practical issues and time constraints, the results presented here are not intended to represent a complete or conclusive story, but rather reflect a 'proof of principle' study, where this hypothesis driven approach can give insight into mechanisms regulating neuronal vulnerability in SMA. I have firstly used quantitative western blots to assess levels of proteins altered in Wld^s and have identified a number of proteins which are also altered in SMA. I have also investigated whether any of these proteins can be used as potential biomarkers for SMA disease progression. I finally attempt to cross Wld^s mice with *Smn-/-;SMN2* mice to investigate whether Wld^s can confer any neuroprotection and modify disease phenotype. While this work is ongoing and

consequently currently incomplete, preliminary results imply that this approach can give mechanistic insight into the pathological processes in SMA and potentially yield novel biomarkers to measure disease progression.

7.2 Results

7.2.1 Candidate proteins altered in Wld^s are also differentially regulated in SMA

Previous work using 2D gel electrophoresis to perform proteomic screens on synaptic compartments of Wld^s striatal neurons has identified a number of candidate proteins which may act to regulate synaptic vulnerability (Wishart *et al.*, 2007b). I therefore sought to determine whether any of these proteins were also differentially regulated in tissue from SMA mice. As it is currently not technically viable to investigate protein expression in synaptic compartments of lower motor neurons, quantitative western blotting was used to investigate protein expression levels in whole spinal cord from P1 (pre-symptomatic) and P5 (end-stage) Smn-/-;SMN2 mice compared to littermate controls (for quantification methodology see Appendix 10.4). A neuronal specific loading control (β-Tubulin) was included to ensure results were not due to the decreased proportion of neural cells, especially at the end-stage time point. Of the 8 proteins initially investigated, which have been identified as those which show some of the greatest changes in Wld^s, apparent changes in levels compared to littermate controls were observed in 6 proteins (UBE1, DRP2, βSNAP, VDAC1, GDI, STI; Figure 7.1). In 5 of the 6 proteins a progressive increase in the magnitude of the change was observed from P1 to P5. This therefore indicates that these proteins are strong candidates for indicators of pathological status in SMA.

Of the proteins investigated, UBE1, βSNAP, VDAC1 and DRP2 were of particular interest as significant changes were observed to occur in the opposite direction to those in Wld^s i.e. down regulated in SMA and up-regulated in Wld^s (UBE1, βSNAP, DRP2), or up regulated in SMA and down regulated in Wld^s (VDAC1; Figure 7.2). This further indicates that these proteins could be involved in pathways regulating neuronal survival. Furthermore these proteins could potentially act as makers for altered neuronal vulnerability, and quantification of their levels could act as a 'read-out' for the pathological status of the neuromuscular system.

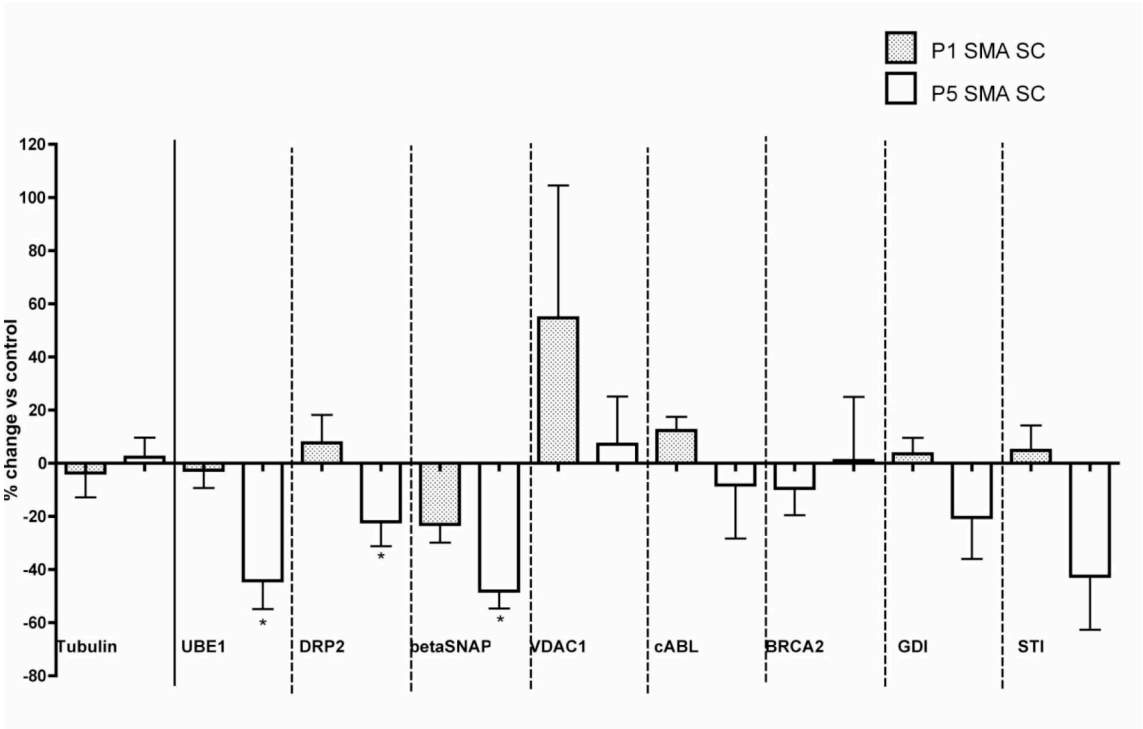

Figure 7.1: Protein level changes observed in P1 and P5 *Smn-/-;SMN2* spinal cord. Bar chart showing the average percentage change in protein levels compared to control littermates as assessed by quantitative western blotting on proteins from whole spinal cord from P1 mice (grey bars) and P5 mice (black bars). *(mean ± SEM;data reflect changes normalised to control littermate values, Student unpaired T test for each column compared to control; *P<0.01 Smn-/-;SMN2 compared to Smn+/+;SMN2 litter mate controls, all other changes were not statisitically significant; N=5/4 (UBE1), 3/5 (DRP2; βSNAP; cABL; BRCA2), 4/5 (VDAC1;GDI), 4/4 (STI1) per P1/P5 mouse respectively).*

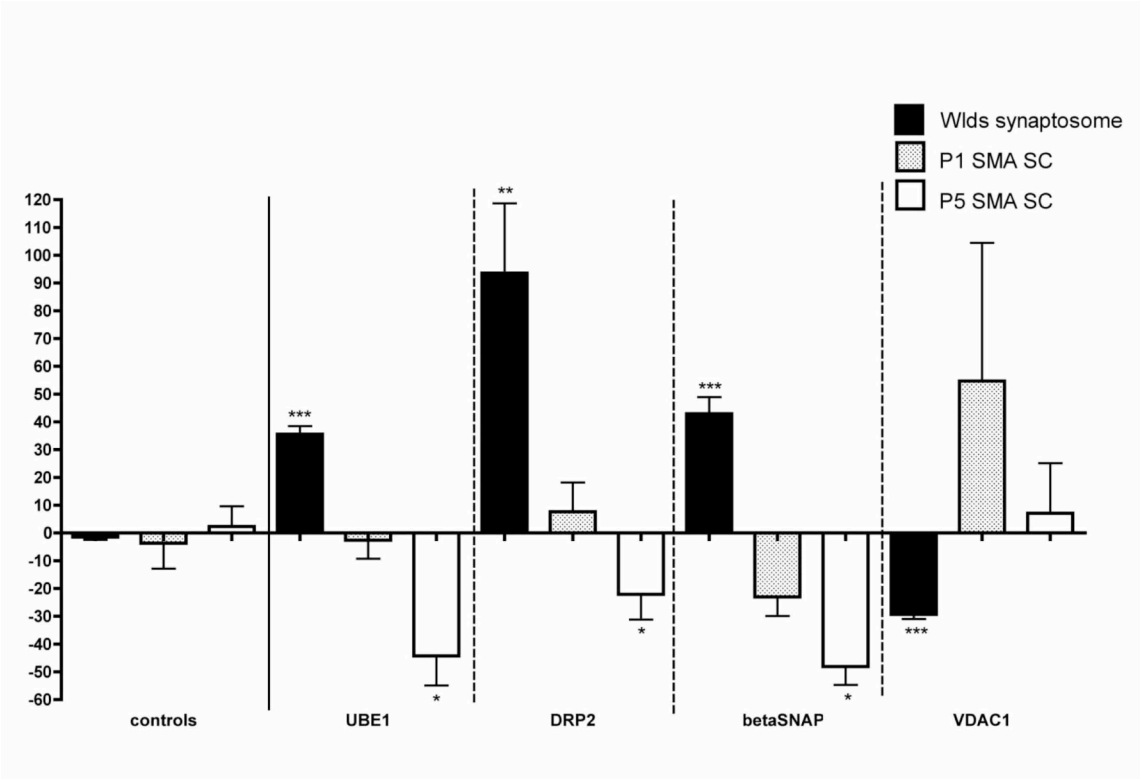

Figure 7.2: Protein changes in *Smn-/-;SMN2* spinal cord which occur in an opposite direction to that seen in Wld^S synaptosomes. Bar chart showing the average percentage change in protein levels in Wld^S striatal synaptosomes (black bars; *Data courtesy of S Meridith and T Wishart)* compared to protein from whole spinal cord from *Smn-/-;SMN2* mice at P1 (grey bars) and P5 (white bars). *(mean ± SEM; data reflect changes normalised to control littermate values, Student unpaired T test for each column compared to control; * P<0.05, ** P<0.01, ***P<0.001 Wld^S/Smn-/-SMN2 mouse compared to control littermates. Non-annotated bars were not statistically significant; N=12/5/4 (UBE1), 9/3/5 (DRP2; βSNAP), 12/4/5 (VDAC1) per Wld^S/P1/P5 mouse respectively).*

7.2.2 Identification of potential biomarkers for outcome measures in SMA

The identification of novel proteins which are altered in SMA tissue in a manner that is proportional to the pathological status of the individual and/or tissue would be a great value to SMA research. Such proteins could be used as biomarkers to indicate disease progression and be used as an outcome measure in clinical trials. As a number of proteins have been identified which are altered in SMA tissue, I investigated whether any of these proteins might posses the profiles required of suitable biomarkers, such as relevant changes in clinically accessible material, minimal inter-individual variability and progressive changes associated with pathological status.

Firstly, I have investigated whether the changes observed in the spinal cord, are also apparent in other tissues. For this analysis, proteins which have either shown high magnitude (VDAC1) or highly consistent (βSNAP, DRP2) changes in the spinal cord were chosen. Quantitative western blots for these proteins in muscle and skin samples show that similar changes in protein levels for VDAC1, βSNAP and DRP2 in both tissues can be detected and the direction of these changes correlates well with what was observed in spinal cord (Figure 7.3). The magnitude of change of protein level observed in VDAC1, βSNAP and DRP2 in skin samples was observed to increase from P1 to P5. This finding suggests that protein levels are associated with pathological status.

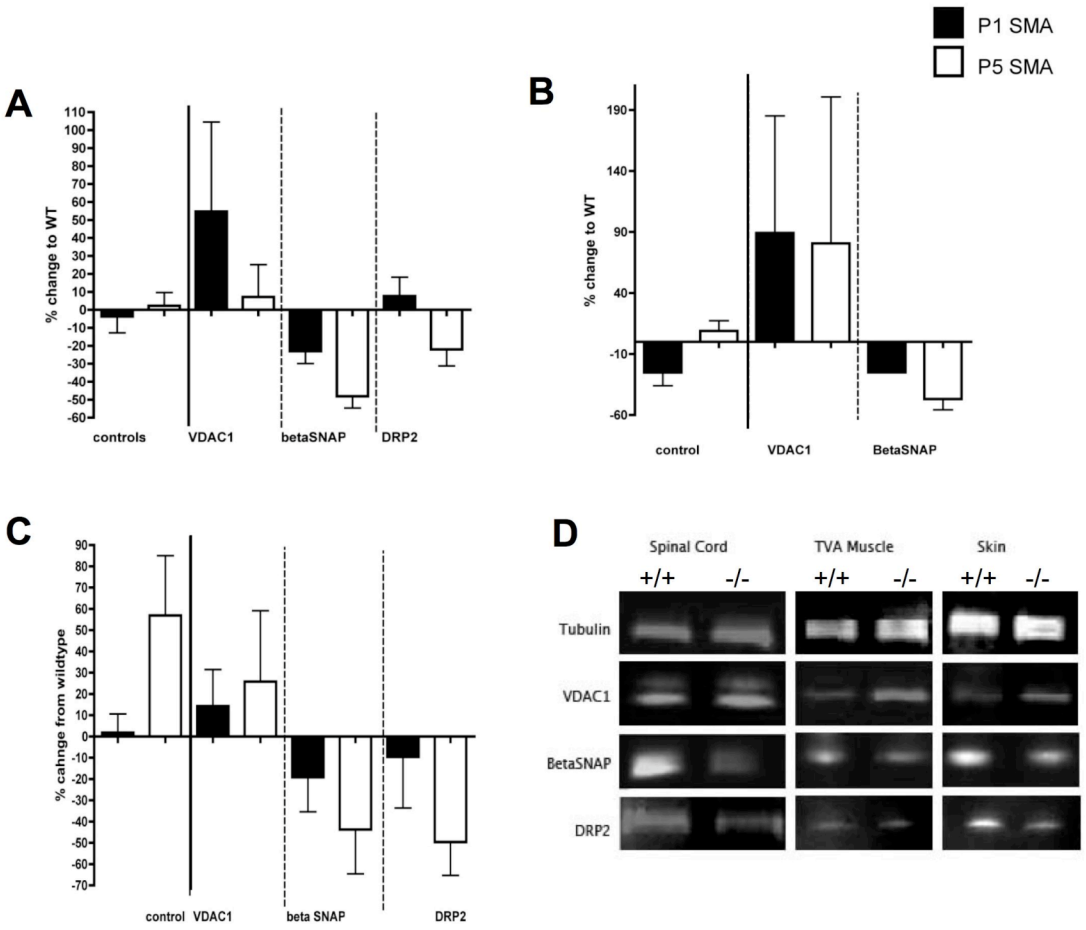

Figure 7.3: Protein changes observed in spinal cord are also observed in muscle and skin from *Smn-/-;SMN2* mice. A – Bar chart showing percentage change in levels of VDAC1, βSNAP and DRP2 protein from spinal cord from P1 (black bars) and P5 (white bars) *Smn-/-;SMN2* mice. B,C – Bar chart showing equivalent protein analysis in total protein extracted from the transversus abdominis muscle (B) and skin sample (C). D - Example images from western blots used for quantification of levels of VDAC1, βSNAP and DRP2. Tubulin (spinal cord) or *β*actin (muscle,skin) was included as a loading control. Note how changes in protein expression observed in spinal cord are also observed in muscle and skin. *(mean ±SEM, N = 4/5 (VDAC1); 3/5 (DRP2; βSNAP), per P1/P5 mouse respectively* (A); *2/3 (VDAC1; βSNAP) per P1/P5 mouse respectively* (B); *4/2 (VDAC1); 3/2 (βSNAP); 2/2 (DRP2), per P1/P5 mouse respectively* (C)).

For clinical application, protein biomarkers would be measured over time and protein levels compared to previous levels observed within the individual. As the approach used here relies upon comparing protein levels between *Smn-/-;SMN2* mice to littermates, one might expect that variability in this system will be higher than when levels are compared

at different time points within the same individual. Despite this, an appropriate biomarker should show relatively consistent changes between individuals, with at least the direction of the change being reliable. Comparison of the changes observed in VDAC1 reveals substantial variability in both magnitude and direction between individuals (Figure 7.4). This was apparent at both P1 and P5, in both the TVA muscle and skin sample. Equivalent analysis of βSNAP revealed that although there was significant variability in the magnitude of observed changes, particularly in skin samples, the direction of the change was consistent (Figure 7.5). Furthermore, in the TVA, the changes appeared of greater magnitude at P5 compared to P1. Results therefore suggest that while VDAC1 appears to be subject to high fluctuation and therefore may not be appropriate for use as a biomarker, β-SNAP may be a good potential candidate for further study.

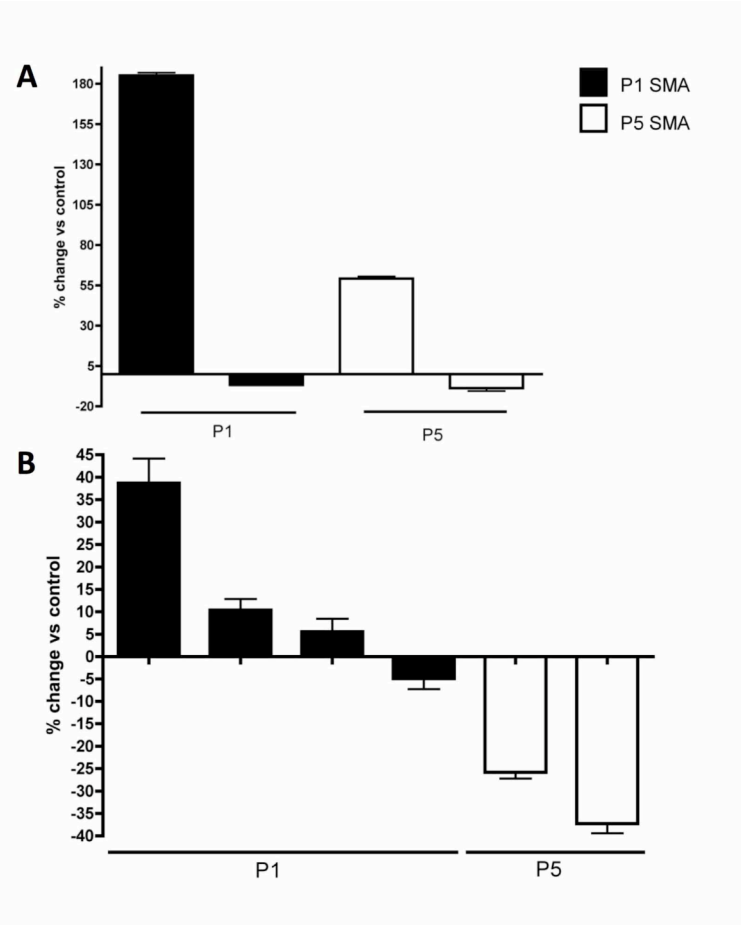

Figure 7.4: Highly variable changes in VDAC1 expression make it an inappropriate candidate biomarker. A,B – Bar charts showing change in expression of VDAC1 in the TVA muscle (A) and skin sample (B) in individual mice compared to control litter mates at both P1 (black bars) and P5 (white bars). Note the high degree of variability in relative levels of this protein in both magnitude and direction observed in both tissues and time-points *(mean ± SEM; Data reflect 3 different scan intensity settings on the same membrane and reflect percentage change compared to control littermate normalised to βactin loading control).*

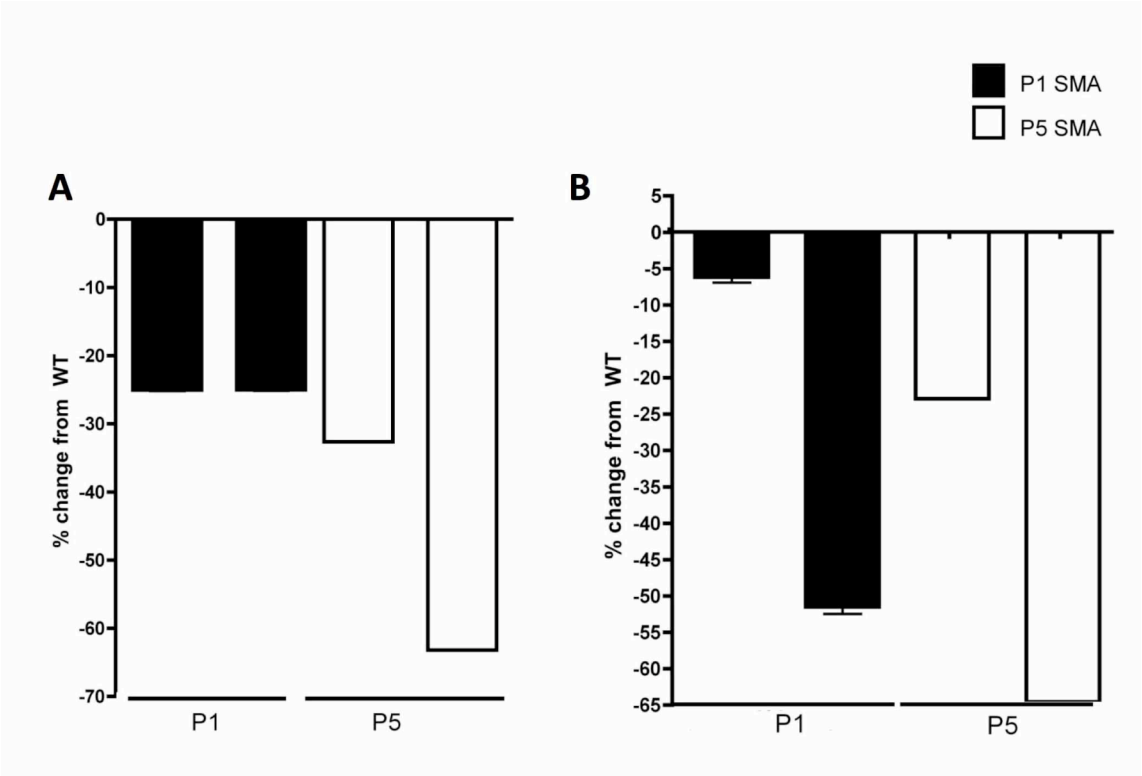

Figure 7.5: Consistent changes in βSNAP expression make it a potential candidate biomarker. A,B – Bar charts showing change in expression of βSNAP in the TVA muscle (A) and skin sample (B) in individual mice compared to control littermates at both P1 (black bars) and P5 (white bars). Note that, although there is some variability in magnitude, especially in skin samples, the direction of change remains consistent. *(mean ± SEM; Data reflect 3 different scan intensity settings on the same membrane and reflect percentage change compared to control littermate normalised to βactin loading control).*

Due to the amount of protein required, sufficient tissue could not obtained for analysis without sacrificing the mouse, making repeated measurements within one individual impossible in the present study. Therefore to determine whether these observed changes have a direct correlation to pathological status, relative changes in protein levels have been compared in differentially affected tissues within 1 individual. Analysis of protein levels of βSNAP and VDAC1, revealed that the greatest magnitude of change was seen in the TVA muscle (175% up regulation VDAC1, 25% down regulation βSNAP compared to control; Figure 7.6). Smaller changes in protein level were also observed in the less affected diaphragm (70% up regulation VDAC1, 5% down regulation βSNAP

compared to control) and skin samples (55% up regulation VDAC1, 0% change βSNAP compared to control). This finding indicates that protein changes occurred in proportion to the pathological state of the tissue i.e. while changes were generally still observed in the diaphragm (a relatively spared muscle in SMA) and skin (a tissue thought to be unaffected in SMA), the magnitude was consistently smaller than the changes observed in the TVA. The minimal changes observed in the diaphragm and skin are to be expected as this analysis was performed at P1. It would therefore be interesting to see if this same correlation remains at later time points.

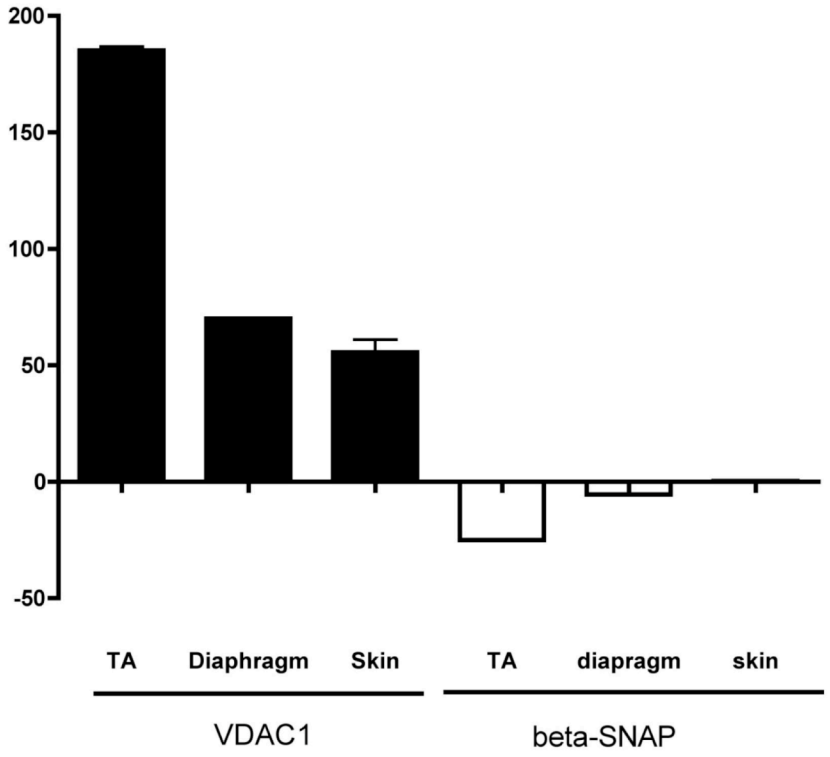

Figure 7.6: Changes in VDAC1 and βSNAP are proportional to the pathological status of the tissue. Bar chart showing change in expression of VDAC1 (black bars) and βSNAP (white bars) in the TVA muscle (which is a vulnerable muscle in *Smn-/-;SMN2* mice), diaphragm (which is relatively spared) and skin (which is thought to be unaffected in SMA) from a single P1 *Smn-/-;SMN2* mouse. Note the change in magnitude is generally proportional to the pathology observed in the associated tissue. *(*mean ± SEM; *Data reflect 3 different scan intensity settings on the same membrane and reflect percentage change compared to control littermate normalised to βactin loading control).*

7.2.3 SmnWld^s mice

From the protein changes described above, it would appear that there may be mechanistic overlap in the pathways conferring synaptic protection on Wld^s mice with those pathways regulating synaptic vulnerability in SMA. In order to directly test whether there is any mechanistic overlap, I have attempted to cross *Smn-/-;SMN2* mice with Wld^s mice. Previous studies attempting to cross Wld^s mice with *Smn-/-;SMN2;Δ7* have concluded that there is no phenotypic benefit (Kariya *et al.*, 2009; Rose *et al.*, 2009), but as they only bred the mice to be heterozygous for the Wld^s mutation, Wld^s proteins levels may have been insufficient for synaptic protection (Mack *et al.*, 2001). The reason that they only reached heterozygosity is perhaps immediately apparent when the challenges of generating this cross are considered, namely the extensive crosses and problematic Wld^s copy number genotyping (Appendix 10.5). For this reason breeding pairs of appropriate genetic combination i.e. Smn+/-;SMN2+/+;Wld^s+/- have only recently been obtained. Litters to date have unfortunately not contained any Smn-/-;SMN2+/+;Wld^s+/+ mice, however data has been obtained from one Smn-/-;SMN2; Wld^s +/- mouse (herein referred to as Smn-/-:Wld^s+/-) and non-Wld^s control littermate (herein referred to as Smn-/-;Wld^s-/-) and compared them to an unaffected littermate (Smn+/+;Wld^s+/+). Due to licensing restrictions, mice must be culled when symptoms become severe, making it difficult to assess any change in life span. However, assessment of body weight at P5 revealed a similar reduction in Smn-/-;Wld^s+/- and Smn-/-;Wld^s-/- mice compared to Smn+/+;Wld^s+/+ littermate (body weight = 1.57g Smn-/-;Wld^s-/- and Smn-/-;Wld^s+/- vs 3.52g Smn+/+;Wld^s+/+). Synaptic degeneration in TVA and LAL muscles was assessed by quantification of the number of fully occupied endplates. Consistent with previous reports, pathology was more advanced in the TVA and LAL caudal band compared to the LAL rostral band, although similar levels of pathology were observed in both Smn-/- mice compared to unaffected littermate (Figure 7.7), indicating that the presence of one copy of Wld^s has no protective effect on synaptic pathology in SMA mice. Subsequent analysis on Smn-/-;Wld^s+/+ mice is clearly required.

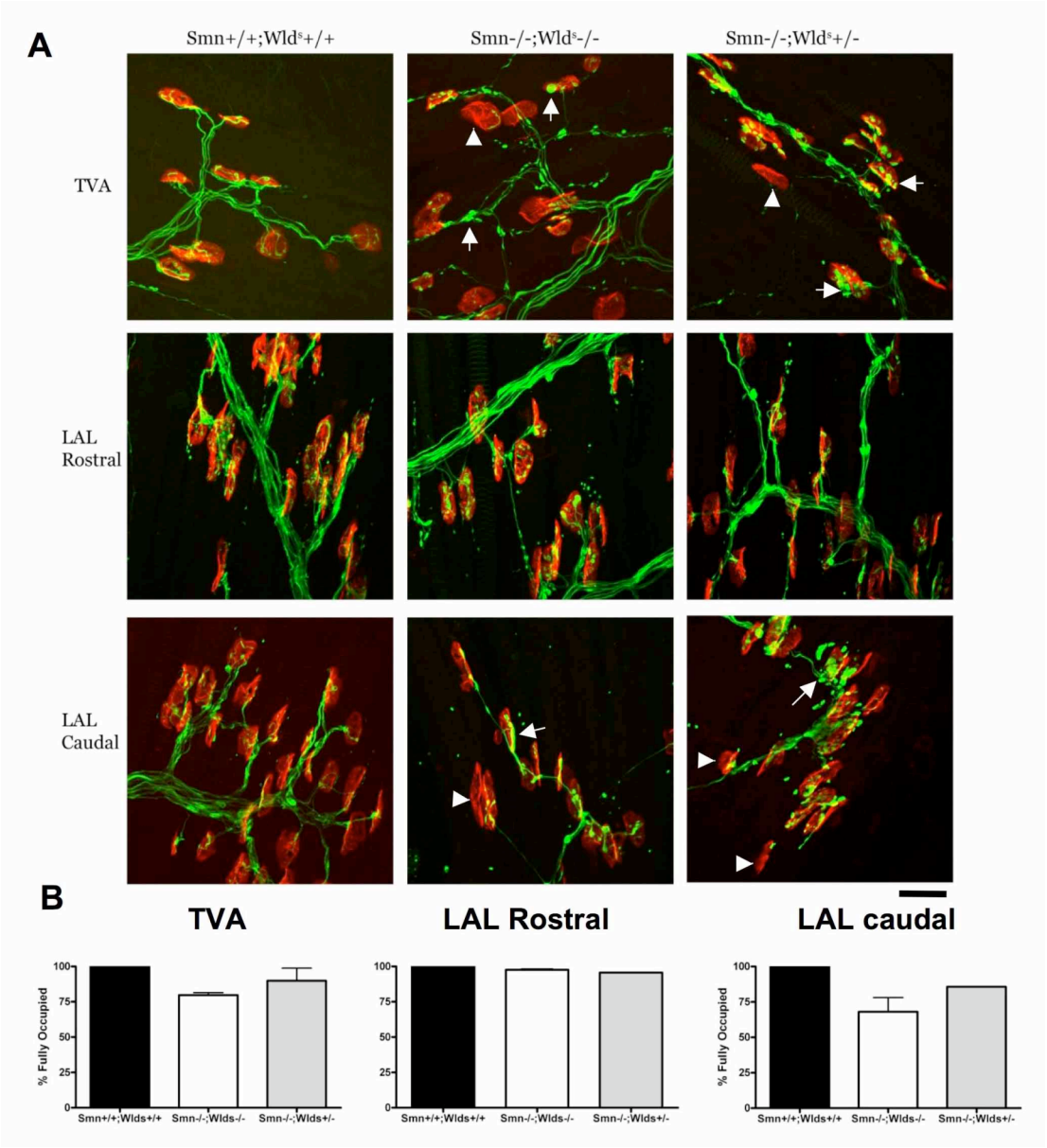

Figure 7.7: NMJ phenotype in SmnWld^s mice. A – confocal micrographs of immunocytochemically labeled TVA and LAL (rostral and caudal bands) muscle preparations (green = 150kDa neurofilaments; red = post-synaptic acetylcholine receptors labelled with TRITC-α-bungarotoxin) from P5 Smn+/+;Wld^s+/+, Smn-/-;Wld^s-/- and Smn-/-;Wld^s+/- mice. As expected, there is no evidence of denervated endplates in Smn+/+;Wld^s+/+ muscles, while significant synaptic pathology is evident in Smn-/-;Wld^s-/- muscles, as evidenced by unoccupied endplates (white arrowhead) and pre-terminal accumulation of neurofilaments (white arrow). In Smn-/-;Wld^s+/- mice, there was also evidence of denervated endplates and accumulation of neurofilaments. B – Bar charts (mean ± SEM) showing the percentage of fully occupied endplates in P5 Smn+/+;Wld^s+/+ (black bars), Smn-/-;Wld^s-/- (white bars) and Smn-/-;Wld^s+/- (grey bars) mice in the TVA muscle, LAL rostral band and LAL caudal band. Note that there was a similar decrease in the number of fully occupied endplates in Smn-/-;Wld^s-/- mice compared to Smn-/-;Wld^s+/- mice, indicating that the presence of one copy of the neuroprotective Wld^s gene does not confer any protection to SMA related NMJ pathology. *(N=2/1 muscles/mice per genotype; N numbers are insufficient for statistical analysis; scale bar = 30μm (A))*

7.3 Discussion

The findings presented above provide preliminary analyses showing that Wld^s can provide mechanistic insights into the pathogenic processes in SMA. Firstly, of a small screen of candidate proteins, I have identified proteins which are changed in the opposite direction in SMA compared to Wld^s thus providing the first evidence that there may be convergent mechanisms regulating synaptic vulnerability in SMA and Wld^s. Secondly, I have demonstrated that such an approach could be used to identify potential biomarkers which may be used to assess pathological status. Finally, I provide preliminary analysis of SmnWld^s mice, which show that one copy of Wlds in Smn-/-;SMN2 mice confers no increase in body weight or synaptic protection.

7.3.1 Proteomic screen to identify biomarkers of SMA

The identification of relevant biomarkers for SMA would be of great benefit to the field. Current measures of pathological progression are based upon assessment of motor function, electrophysiological motor unit assessment, body composition measurement and quantification of Smn levels (Swoboda *et al.*, 2009;). Such measures are generally accepted to be inadequate, partly due to a lack of sensitivity and, in the former case, the questionable relationship between motor ability and disease progression (Swoboda *et al.*, 2005). Recent studies have improved the ability to detect Smn levels in blood samples (Tiziano *et al.*, 2009) however it has been suggested that Smn levels in blood do not correlate to disease severity (Sumner *et al.*, 2006), making this approach only of clinical benefit when the therapeutic approach is to increase Smn levels.

An ideal biomarker which can actively report on the status of the neuromuscular system should have a number of specific characteristics. It should change in a predictable way with the progression of pathology, be highly sensitive (evident at early stages of the disease and be responsive to changes to disease progression) and be evident in clinically accessible material (Turner *et al.*, 2009). The approach utilized here attempts to identify biomarkers by comparing affected tissues in models of neuroprotection and neurodegeneration, and expanding these results to clinically accessible tissue. This

approach has a high probability of discovering useful biomarkers as it highlights proteins which have a high likelihood of reflecting subtle changes in the vulnerability status of the neuromuscular system. From a preliminary screen of only 8 proteins, one was identified which showed the desirable characteristics. Changes could be detected which were proportional to pathological status, apparent in clinical accessible tissue and present at small but noticeable levels at pre-symptomatic time points. The data presented here therefore provide great encouragement that this approach can yield useful biomarkers in the future. Further work is now required to conduct wider proteomic screens on pathologically relevant tissue such as spinal cord, or comparison of unaffected and affected muscle regions, and ultimately assessing whether equivalent changes can also be observed in human tissue.

7.3.2 Mechanistic insight to SMA from Wld^s

Investigation and comparison of Wld^s mice and disease models can provide mechanistic insight into the processes regulating synaptic vulnerability. By using the approach described in this study, e.g. mouse crosses and search for common downstream proteins, we can begin to identify key pathways and events which regulate synaptic vulnerability in a range of conditions. A popular theory regarding neurodegenerative disease is that, although there are distinct pathogenic triggers, there is commonality in the mechanisms regulating neurodegeneration, and by extension, synaptic degeneration (Coleman, 2005; Wishart *et al*. 2006). The findings presented in this chapter are very much in agreement with this hypothesis, as alterations in proteins in SMA tissue were observed, which have previously been shown to be altered in an opposite direction in Wld^s. As equivalent changes have also been identified in mouse models of Batten disease (Kielar *et al.*, 2009), this work suggests that common mechanisms exist to regulate neuronal vulnerability. Results from SmnWld^s mice will also provide further insight into the potential mechanistic overlap between Wld^s and SMA mice. Significant protection might further support the theory that common mechanisms regulate a range of neurodegenerative conditions, while a lack of protection support the idea that distinct pathways control distinct types of synaptic degeneration (e.g. see chapter 6). Regardless

of results, further work is required to begin to tease apart the mechanisms which regulate and perturb synaptic vulnerability in both neuroprotective and neurodegenerative models.

Chapter 8: General discussion

8.1 Overview of results

The work presented in this study has contributed significantly to our understanding of NMJ pathology and disease pathogenesis in SMA. I have shown that NMJs are early and significant targets in mouse models of SMA. Analysis of pre-synaptic and post-synaptic parameters has revealed that pathology can occur independently in both tissues. In depth analysis of pre-synaptic pathology has revealed selectively vulnerable populations of motor units in both slow twitch muscles and in muscle regions conforming to a developmentally distinct FaSyn subtype. Analysis of pre-symptomatic motor neuron connectivity and gene expression has shown that abnormal development of lower motor neuron connectivity is unlikely to underlie pathology in SMA. Micro-array analysis has implicated pathways involved in myelination, growth factor signalling and extracellular matrix integrity in SMA pathology. I have also shown that morphologically distinct types of synaptic degeneration (dying-back neuropathy and Wallerian degeneration) can be mechanistically distinct. Finally, I have shown that protein changes identified in the neuroprotective Wld^s model can be used to give mechanistic insight into molecular processes occurring in SMA and can be used to identify biomarkers to assess pathological status in SMA.

8.2 NMJ pathology in SMA – current thoughts

Following on from the detailed description of NMJ pathology in mouse models of SMA presented here, a number of unrelated papers have subsequently been published focused on the same topic. A study from Umrao Monani's lab has used the *Smn-/-;SMN2*;Δ7 mouse model and the more mild Smn^{A2G} model to conduct a study on NMJ morphology, development and function during disease progression and provides some preliminary reports on NMJ morphology from SMA patients (Kariya *et al*., 2008). Biondi and colleagues have conducted a study looking at NMJ morphology and post-synaptic development in response to exercise training in the SmnΔ7/Δ7;SMN2 model (see Table 1.1; Biondi *et al*., 2008). Charlotte Sumner's group has produced a rigorous study on the

electrophysiological properties on NMJs in differentially affected muscles in the Smn-/-:SMN2;Δ7 model (Kong *et al*., 2009). In this section I will discuss the implications of these recent advances in understanding of SMA related NMJ pathology.

8.2.3 Structural changes at the NMJ

A major question raised by recent publications, is what should we consider 'core' morphological features of NMJ pathology in SMA? Results presented in this study have revealed significant denervation in both *Smn-/-;SMN2* and *Smn-/-;SMN2*;Δ7 mouse models, albeit to a lesser degree in the latter model. However, a study by Kariya *et al.* on the NMJ phenotype in the *Smn-/-;SMN2*;Δ7 model concluded that denervation does not occur at any time point (Kariya *et al.*, 2008). Intriguingly, they did observe a 30% reduction in axon number in ventral roots and in the phrenic nerve, although as they found no evidence of compensatory sprouting or change in poly-innervation it is somewhat paradoxical to suggest that denervation does not occur in this model, unless of course axonal degeneration occurs in a proximal to distal fashion. Regardless of this absurdity, the question of whether denervation is or is not a feature in this model has created a degree of controversy within the field. This controversy is perhaps unnecessary as discrepancies in reported denervation in the *Smn-/-;SMN2*;Δ7 model range from 0% (Kariya *et al.*, 2008), 5-10% (chapter 3) to 3-15% (Kong *et al.*, 2009) and are further compounded by the exclusion or inclusion of partially occupied endplates. Controversy in the field therefore appears based upon the experimenter's definition of 'significant' rather than observed results. Importantly however, given the lack of severe denervation observed in this model, many groups have defined synaptic pathology as observed abnormalities such as thick, swollen nerve terminals, poor terminal arborisation and pre-synaptic accumulation of neurofilaments (Biondi *et al.*, 2008; Kariya *et al.*, 2008). The observation that such morphological defects are also present in the diaphragm of SMA patients has led one group to conclude that this mouse model is an accurate model of human SMA (Kariya *et al.*, 2008), overlooking the fact that the diaphragm is a relatively spared muscle (Farrar *et al.*, 2009). While these changes may be of potential interest, if they do not represent defects observed in affected

muscle groups from human patients, attempts to remedy them may be of limited clinical benefit. Furthermore, potential therapies based upon retrograde transport from muscle are likely to be far less effective in models/patients in which significant denervation has occurred. The fact that such changes are present in pathologically spared muscle groups may suggest that they are not relevant to the pathological process. While the severe denervation observed in other mouse models of SMA may reflect the severe reduction in Smn levels (Cifuentes-diaz *et al.*, 2002; chapter 3), further work will be important to determine whether or not they are of clinical relevance.

The work to date on incidence and prevalence of structural NMJ abnormalities in models of SMA therefore underlines the need for structural NMJ studies in affected muscle groups from SMA patients. It will be crucial to define whether severe NMJ breakdown and denervation is a pathological feature of SMA in humans as it will have a significant impact upon the development of therapeutic strategies. Although obtaining such post-mortem material can be a significant challenge, the development of tissue "biobanks" should greatly facilitate such studies.

8.2.2 *Functional changes at the NMJ*

Recent papers have also indicated that there are significant functional abnormalities at the NMJ in SMA mouse models. Electrophysiological recordings from the mild Smn^{A2G} model (see Table 1.1) have revealed an increase in transmission failures in response to repeated high frequency stimulation (Kariya *et al.*, 2008). This observation may be accounted for by a decrease in synaptic vesicle numbers in the active zone. Equivalent studies in the *Smn-/-;SMN2*;Δ7 model failed to identify transmission failures but did observe equivalent mis-localisation of synaptic vesicles, with a patchy distribution and density throughout the pre-synaptic terminal, and decreased numbers within the active zone (Kong *et al.*, 2009). Electrophysiological recording implied that quantal content was decreased and implied that this is accounted for by a decreased probability of vesicle release, as opposed to changes in post-synaptic response (Kong *et al.*, 2009). These studies might go some way to explaining the severe muscle weakness in the

absence of widespread denervation. These findings are also consistent with observations in *wasted* mice, in which functional deficits occur prior to structural loss. Together these results suggest that synaptic degeneration may occur subsequent to, or in conjunction with functional deficits, and further work into the basis of disruption of synaptic function may yield important information about the initiation of synaptic pathology.

8.2.3 Abnormal development of the NMJ *– cause or effect?*

Although the results presented here strongly suggest that abnormal pre-symptomatic development is not required for pathogenesis in SMA, it remains possible that abnormal development contributes to disease progression. For example, pathology could conceivably be caused by a mis-regulation of developmental synapse elimination pathways. Alternatively, a failure in normal developmental processes might destabilise the NMJ and although initial synaptic formations establish normally, the processes regulating synaptic maintenance and maturation are defective. There are now a number of results which might indicate that developmental processes are not occurring normally. There appears to be a delay in the "plaque to pretzel" process of AChR clustering and endplate maturation. Biondi and colleagues suggested that this delay in maturation correlates with motor neuron pathology (Biondi *et al.*, 2008) and that exercise can accelerate the development of the neuromuscular system in mice and be neuroprotective. There also appears to be a delay in the switch of acetyl choline receptor subunit, with an increase in the embryonic γ subunit with a corresponding decrease in the adult ε subunit (Kariya *et al.*, 2008), and that this delay correlates with the pathology observed in differentially vulnerable muscles (Kong *et al.*, 2009). It has been suggested that this delay in subunit switch accounts for the electophysiological anomalies observed, such as an increased decay time following an endplate potential (Kong *et al.*, 2009). They further suggest that such change in transmission properties may cause the delay in AChR clustering and endplate maturation.

The fundamental problem with investigating development of the neuromuscular system during disease progression is the observation that NMJ development is tightly correlated with synaptic activity. In a pathological neuron, synaptic activity is likely to be affected, and it is therefore difficult to conclude whether abnormal development results in abnormal activity and thus causes synaptic vulnerability, or whether abnormal activity inhibits normal development. Developmental anomalies could therefore simply be a by-product of the pathological processes occurring. The fact that there is a clinical spectrum of SMA severity depending of Smn level, with degenerative and phenotypic onset in milder forms of SMA occurring subsequent to the normal developmental time window, might suggest that developmental processes do not contribute significantly to pathogenesis in all types of SMA. Separating these two events remains a great challenge for researchers however the recent creation of 'TET-On' SMA mice, in which the expression of Smn can be turned on and off by the administration or removal of tetracycline, might present a good opportunity (Le, Burghes, unpublished abstract, Families of Spinal Muscular Atrophy, 2009). Should Smn be turned off in adulthood, and the same degenerative phenotype be observed, we might conclude that SMA is not caused by the mis-regulation of developmental pathways. Future studies are thus likely to produce insightful results relating to the contribution of abnormal development to pathogenesis in SMA.

8.3 Convergent mechanisms of synaptic degeneration in neurodegenerative disease?

This results presented here are in agreement with the hypothesis that synaptic compartments of neurons are vulnerable to pathological insults. We can therefore add SMA to the growing list of neurodegenerative disorders which appear to be 'synaptopathies'. As the list of such diseases grows, the question of mechanistic commonality becomes increasingly important, as this will have significant impact upon the scope of any therapeutics which are developed. An emerging point of view suggests that despite morphological discrepancies, synaptic vulnerability and pathology is regulated by common mechanisms (Coleman, 2005). Although this idea was initially

built upon the ability of the Wld^s mouse to protect against a range of insults, recent reports have added significant weight to this idea, with the identification of proteomic changes identified in Wld^s mice occurring in an opposite direction in mouse models of NCL disorders (Keilar *et al.*, 2009). The work presented in chapter 7 expands upon these findings, showing equivalent changes are also apparent in mouse models of SMA. Together these results suggest that common proteomic changes can occur in opposite directions to regulate synaptic pathology or protection. These findings are in contrast to the results presented in chapter 6, which quite clearly demonstrated that two morphologically distinct types of synaptic degeneration were also mechanistically distinct, with loss of eEF1A2 causing a dying-back neuropathy but inhibiting Wallerian degeneration. This finding might suggest that a range mechanistically distinct pathways can regulate synaptic degeneration. These two possibilities are perhaps not mutually exclusive as it remains possible that independently initiated cascades will ultimately converge upon common downstream mechanisms.

At this stage our knowledge of the mechanisms regulating synaptic vulnerability are somewhat limited. Work in this area is going to be fundamental to address the question not only of mechanistic commonality, but also to develop neuro-protective strategies. Further work investigating the initiating mechanisms of synaptic vulnerability is therefore likely to be crucial. Although, due to it accessibility, the NMJ remains an excellent model to study synaptic vulnerability, its analysis is hampered by the fact that there is not currently a method to study gene expression or to carry out proteomic analysis in specific cellular and subcellular compartments at the NMJ. In the central nervous system, the ability to produce synaptosomes, where the synaptic compartment of the cell can be isolated from the axon and cell body, allow analysis of synaptic responses. Due to the structural stability of the NMJ, no efficient method has been developed to isolate the pre-synaptic terminal from the surrounding muscle, Schwann cell and axonal compartments. The ability to do this would likely prove highly powerful, as it would allow synaptic function to be directly correlated to morphology and give great insight into the mechanisms regulating synaptic function and initiating synaptic

breakdown. Current attempts to isolate the cytoplasmic contents of axonal and synaptic compartments using a polymer based absorption technique may provide an effective alternative to the traditional synaptosome (Broom, Skipp, Perry, unpublished abstract, Molecular and Cellular Mechanisms of Axon Degeneration, 2008). Alternative approaches to physically isolate the synaptic terminal without disrupting the synaptic expression profile face great challenges but would undoubtedly be of great value should efficient methodology be developed.

8.4 Mechanisms regulating neuromuscular vulnerability in SMA?

Work within this study and the broader SMA research field has clearly demonstrated the occurrence and severity of neuromuscular pathology in SMA. Despite this, very little is known about the underlying mechanisms. Results from this study suggest that the pre-symptomatic development of lower motor neurons is normal, and all additional work on neuro-degenerative mechanisms generally suffers from an inability to separate causative mechanisms from neurodegenerative by-product. For example, the identification of widespread splicing defects was subsequently identified to be a late stage event in SMA pathology (Zhang *et al.*, 2008; Baumer *et al.*, under review). Furthermore the identification of abnormal post-synaptic development cannot be separated from the requirement of synaptic function for development (Biondi *et al.*, 2008, Kong *et al.*, 2009). The function of Smn protein is equally undefined as it is not clear whether SMA is a result of a loss of general house keeping function of Smn that neurons are for some reason specifically more vulnerable to, or whether there are specific axon and/or synaptic roles for Smn protein. We are therefore left with a clear and fundamental question: what are the mechanisms regulating neuromuscular pathology in SMA?

8.4.1 Muscle development

Although results here have indicated that lower motor neuron development is normal in SMA mouse models, rigorous studies on the development of muscle in SMA have yet to be performed. Reports from culture models and patient biopsies have suggested that there may be intrinsic abnormalities in muscle development (see introduction section

1.4.4). As neurons and muscle are mutually dependant upon each other survival, defects in muscle could conceivably result in defect in motor neuron survival. Traditional approaches to investigate the contribution of muscle to SMA pathology rely upon conditional loss or gain of Smn expression in specific tissues (Frugier *et al.*, 2000, Cifuentes-diaz *et al.*, 2001; Gavrilina *et al.*, 2008), however such approaches do not account for a requirement for Smn in multiple tissues. It may therefore be of interest to conduct a detailed study of muscle developmental morphology in mouse models of SMA prior to symptom onset. The LAL also presents a convenient opportunity to investigate muscle development, for example by conducting proteomic analysis on affected and unaffected muscle regions at pre-symptomatic time points. This may reveal subtle changes in protein levels in muscle which can be correlated to and occur prior to lower motor neuron breakdown. The creation of mouse models with inducible Smn transgenes will also help define the contribution of abnormal development, as if an equivalent degenerative time course is observed when Smn is turned off in adulthood, the contribution of development to SMA pathogenesis is likely to minimal. Conversely, if Smn can be turned on post-natally and rescue the phenotype, we might conclude that abnormal development does not pre-dispose the nervous system to subsequent pathology.

8.4.2 Contribution of glial cells?

The role of glial cells in SMA pathology has been broadly overlooked over the past decades despite the fact such cells are fundamental to neuronal stability (Feng *et al*., 2008). A role for glial cells in ALS is now well documented (Boillee *et al*., 2006) although it is unknown to what degree both myelinating and terminal Schwann cells might contribute to axonal and synaptic pathology. Intriguingly, the largest single change observed from the microarray analysis on end-stage SMA mice was in the myelin basic protein P0. While this could reflect loss of myelinated axons, it could also be indicative of a disruption in the myelination of axons which would have a significant impact upon their function and stability. In addition, there is currently no data reflecting the accumulation and function of terminal Schwann cells at the NMJ in SMA and hence

further work on the morphology of such cells may be illuminating. Such studies might employ both the electron microscope and fluorescence imaging of both myelinating and terminal Schwann cells during the disease time course and could provide crucial details about the integrity of myelin and the localisation of terminal Schwann cells.

8.4.3 Neurotrophic support

It is well established that growth factors and neurotrophic factors are crucial for the establishment, development and maintenance of motor neurons. They regulate interactions between glial cells, muscle and nerve to direct growth and patterning and provide ongoing trophic support to maintain neuromuscular connections (for review see English *et al*., 2003; Lu and Je, 2003). Neurotrophic factors have been extensively implicated in pathology in ALS, by the identification of aberrant levels in patients and mouse models (Ekestern 2004), single nucleotide polymorphisms associated with a risk of developing ALS (Orrell *et al.*, 1995; Lambrechts *et al.*, 2003), and the observation that viral or exogenous application of growth factors can be neuroprotective (e.g. Kaspar *et al.*, 2003; Azzouz *et al.*, 2004, Pun *et al*, 2006). More recently, increased levels of glial cell-derived growth factor have been identified in the cerebro-spinal fluid of type I SMA patients (Chiaretti *et al.*, 2009), however it is currently unclear whether these changes represent a causative feature or protective response by the induction of nerve sprouting. Result from the micro-array screen also identified a number of genes implicated in growth factor binding and signalling that are mis-regulated in SMA.

Generally, little is known about the specific local requirement for neurotrophic and growth factors i.e. are they required at the NMJ or at the cell body? Therefore, clinical trials applying growth factors to motor neuron disease patients has produced disappointing results. However, the development of viral techniques which can be directed to exclusively muscle, or retrogradely transported presents some excellent opportunities to study the local requirement for growth factors (e.g. Kaspar *et al.*, 2003). Furthermore, future experiments facilitating the ability to locally introduce viruses delivering fluorescent proteins and growth factors, would not only allow tracing of the

destination of such factors, but also allow direct correlation of growth factor expression and NMJ pathology.

8.4.4 Axon transport?

Efficient axon transport is fundamental in delivering organelles and proteins to the periphery, and for the retrograde transport of trophic regulators from the periphery to the cell body. Deficiencies in such processes could conceivably cause significant deficits in energetic and/or functional requirements at the NMJ and put synaptic function under significant stress and there is now significant evidence that defects in axonal transport are present in motor neuron diseases.

Neurofilaments are the most abundant cytoskeletal proteins in motor neurons and are responsible for maintaining axon calibre and the frame work for intracellular transport. The striking accumulation of neurofilament at the NMJ is becoming a hallmark of pathology in SMA (Cifuentes-diaz *et al.*, 2002, Kariya *et al.*, 2008; chapter 3) although equivalent accumulations have been observed in the cell body and proximal axons in ALS patients and models (Mizusawa *et al.*, 1989; Gurney *et al.*, 1994). Mutations in a number of other transport associated machinery, such as the tubulin specific chaperone (Schmalbruch *et al.*, 1991; Bommel *et al.*, 2002; Martin *et al.*, 2002), or molecular motors kinesin or dyenin (Hafezparast *et al.*, 1999; Münch *et al.*, 2004; Puls *et al.*, 2005; Teuling *et al.*, 2008) have also been implicated in motor neuron pathology in mouse models and patients. Axon transport deficits have been noted to be an early event in other models of motor neuron disease (Warrita *et al.*, 1999; Williamson and Cleveland 1999).

Despite reports that β-actin transport to distal axonal compartments and growth cones is disrupted by reduction of Smn levels (Rossoll *et al.*, 2003), additional investigations into the efficiency of axon transport in SMA models are currently lacking. Further work should therefore be dedicated to the tracing of peripherally or centrally delivered markers in SMA models at pre-symptomatic time points. Due to the phenotypic severity

of available models, this may be technically difficult, however work is currently underway to produce new SMA mouse models with a milder phenotype, which may greatly facilitate such studies. Culture systems could also be employed to allow real time imaging of the transport of sub cellular organelles, such as mitochondria, in response to a reduction in Smn levels.

8.4.5 Smn and local protein translation

The role of Smn in pre-mRNA splicing is well established, however it is unclear how this ubiquitous function could result in neuromuscular specific pathology. One possibility is that Smn mediates axonal/synaptic specific protein translation and this function is crucial to maintain synaptic function and stability. Indeed time lapse imaging of Smn localisation has implied that it is transported along axons (Zhang *et al.*, 2003). Mutations in the DNA/RNA binding protein FUS have recently been linked with ALS (Chio *et al.*, 2009; Kwiatkowski *et al.*, 2009; Vance *et al.*, 2009) and this protein has been implicated in the transport of RNA along to axon to peripheral locations for local transcription (Fujii *et al.*, 2005). This hypothesis would therefore create a mechanistic link between ALS and SMA, based upon the requirement for local transcription at the NMJ. The inability to isolate the pre-synaptic compartments of motor neurons (see section 8.3) makes it difficult to define the extent to which local transcription at the NMJ occurs and is required for synaptic maintenance. Future efforts to allow specific and local inhibition of protein synthesis would therefore be of great interest.

8.5. Conclusions

The work described in this study details some of the first steps to understand NMJ pathology in SMA and has begun to address the mechanisms underlying neuromuscular pathogenesis. In Summary, I have shown that

1. NMJs are early and significant targets in mouse models of SMA
2. Pre-symptomatic developmental abnormalities do not underlie vulnerability.

3. Pathways involved in myelination, growth factor signalling and extracellular matrix integrity are mis-regulated in SMA.
4. Wallerian degeneration and dying back neuropathy are mechanistically distinct.
5. Protein changes identified in the neuroprotective Wld^s model can be used to give mechanistic insights into the processes occurring in SMA and assist in identifying novel biomarkers.

This study will hopefully aid future work aimed at defining the mechanisms which regulate and perturb synaptic vulnerability, and be of significant benefit for the development of clinically relevant therapeutic strategies for SMA.

9. References

Anderson M.J., Cohen M.W. (1977) Nerve-induced and spontaneous redistribution of acetylcholine receptors on cultured muscle cells. *J Physiol.* **268**:757-73.

Angaut-Petit, D., Molgo, J., Connold, A.L. and Faille, L. (1987) The levator auris longus muscle of the mouse: A convenient preparation for studies of short- and long-term presynaptic effects of drugs or toxins. *Neurosci Lett*. **82:**83-88.

Arnold A.S., Gueye M., Guettier-Sigrist S., Courdier-Fruh I., Coupin G., Poindron P., Gies J.P. (2004) Reduced expression of nicotinic AChRs in myotubes from spinal muscular atrophy I patients. *Lab Invest.* **84**:1271-1278.

Avila A.M., Burnett B.G., Taye A.A., Gabanella F., Knight M.A., Hartenstein P., Cizman Z., Di Prospero N.A., Pellizzoni L., Fischbeck K.H., Sumner C.J. (2007) Trichostatin A increases SMN expression and survival in a mouse model of spinal muscular atrophy. *J Clin Invest*. **117**:659-671.

Azzouz M., Le T., Ralph G.S., Walmsley L., Monani U.R., Lee D.C., Wilkes F., Mitrophanous K.A., Kingsman S.M., Burghes A.H., Mazarakis N.D. (2004) Lentivector-mediated SMN replacement in a mouse model of spinal muscular atrophy. *J Clin Invest*. **114**:1726-1731

Balabanian S., Gendron N.H., MacKenzie A.E. (2007) Histologic and transcriptional assessment of a mild SMA model. *Neurol Res.* **29**:413-24

Balice-Gordon R.J., Smith D.B., Goldman J., Cork L.C., Shirley A., Cope T.C., Pinter M.J. (2000) Functional motor unit failure precedes neuromuscular degeneration in canine motor neuron disease. *Ann Neurol*. **47**:596-605.

Baughan T., Shababi M., Coady T.H., Dickson A.M., Tullis G.E., Lorson C.L. (2006) Stimulating full-length SMN2 expression by delivering bifunctional RNAs via a viral vector. *Mol Ther*. **14**:54-62

Baughan T.D., Dickson A., Osman E.Y., Lorson C.L. (2009) Delivery of bifunctional RNAs that target an intronic repressor and increase SMN levels in an animal model of spinal muscular atrophy. *Hum Mol Genet.* **18**:1600-1611

Baxter B., Gillingwater T.H., Parson S.H. (2008) Rapid loss of motor nerve terminals following hypoxia-reperfusion injury occurs via mechanisms distinct from classic Wallerian degeneration. *J Anat.* **212**:827-835.

Beirowski B., Adalbert R., Wagner D., Grumme D.S., Addicks K., Ribchester R.R., Coleman M.P. (2005) The progressive nature of Wallerian degeneration in wild-type and slow Wallerian degeneration (WldS) nerves. *BMC Neurosci.* **6**:6

Biondi O., Grondard C., Lécolle S., Deforges S., Pariset C., Lopes P., Cifuentes-Diaz C., Li H., della Gaspera B., Chanoine C., Charbonnier F. (2008) Exercise-induced activation of NMDA receptor promotes motor unit development and survival in a type 2 spinal muscular atrophy model mouse. *J Neurosci*. **28**:953-962

Boillée S., Vande Velde C., Cleveland D.W. (2006) ALS: a disease of motor neurons and their nonneuronal neighbors. *Neuron*. **52**: 39-59.

Bommel H., Xie G., Rossoll W., Wiese S., Jablonka S., Boehm T., Sendtner M. (2002) Missense mutation in the tubulin-specific chaperone E (Tbce) gene in the mouse mutant progressive motor neuronopathy, a model of human motoneuron disease. *J Cell Biol*. **159**: 563-569.

Boon K.L., Xiao S., McWhorter M.L., Donn T., Wolf-Saxon E., Bohnsack M.T., Moens C.B., Beattie C.E. (2009) Zebrafish survival motor neuron mutants exhibit presynaptic neuromuscular junction defects. *Hum Mol Genet.* **in press**

Bradley W.G. (1987) Recent views on amyotrophic lateral sclerosis with emphasis on electrophysiological studies. *Muscle Nerve.* **10**:490-502

Braun S., Croizat B., Lagrange M.C., Warter J.M., Poindron P. (1995) Constitutive muscular abnormalities in culture in spinal muscular atrophy. *Lancet.* **345**:694-695.

Briese M., Esmaeili B., Fraboulet S., Burt E.C., Christodoulou S., Towers P.R., Davies K.E., Sattelle D.B. (2009) Deletion of smn-1, the Caenorhabditis elegans ortholog of the spinal muscular atrophy gene, results in locomotor dysfunction and reduced lifespan. *Hum Mol Genet.* **18**: 97-104

Buffelli M., Busetto G., Bidoia C., Favero M., Cangiano A. (2004) Activity-dependent synaptic competition at mammalian neuromuscular junctions. *News Physiol Sci*. **19**:85-91

Burghes H.M. (2008) Other forms of survival motor neuron protein and spinal muscular atrophy: an opinion. *Neuromuscul Disord*. **18**:82-3

Burghes A.H., Beattie C.E. (2009) Spinal muscular atrophy: why do low levels of survival motor neuron protein make motor neurons sick? *Nat Rev Neurosci*. **10**:597-609

Celio M.R., Spreafico R., De Biasi S., Vitellaro-Zuccarello L. (1998) Perineuronal nets: past and present. *Trends Neurosci.* **21**:510-515

Chai A., Withers J., Koh Y.H., Parry K., Bao H., Zhang B., Budnik V., Pennetta G. (2008) hVAPB, the causative gene of a heterogeneous group of motor neuron diseases in humans, is functionally interchangeable with its Drosophila homologue DVAP-33A at the neuromuscular junction. *Hum Mol Genet.* **17**:266-280

Chambers D.M., Peters J., Abbott C.M. (1998) The lethal mutation of the mouse *wasted* (wst) is a deletion that abolishes expression of a tissue-specific isoform of translation elongation factor 1alpha, encoded by the Eef1a2 gene. *Proc Natl Acad Sci USA*. **95**:4463-4468

Chan, Y.B., Miguel-Aliaga, I., Franks, C., Thomas, N., Trulzsch, B., Sattelle, D.B., Davies, K.E. and van den Heuvel, M. (2003) Neuromuscular defects in a Drosophila survival motor neuron gene mutant. *Hum Mol Genet*. **12:**1367-1376

Chang H.C., Dimlich D.N., Yokokura T., Mukherjee A., Kankel M.W., Sen A., Sridhar V., Fulga T.A., Hart A.C., Van Vactor D., Artavanis-Tsakonas S. (2008) Modeling spinal muscular atrophy in Drosophila. *PLoS One.* **3**:e3209

Chari A., Paknia E., Fischer U. (2009) The role of RNP biogenesis in spinal muscular atrophy. *Curr Opin Cell Biol.* **21**:387-93

Chiaretti A., Leoni C., Barone G., Genovese O., Brahe C., Mariotti P., Conti G. (2009) Increased levels of glial cell-derived neurotrophic factor in CSF of infants with SMA. *Pediatr Neurol.* **41**:195-199.

Chiesa R., Piccardo P., Dossena S., Nowoslawski L., Roth K.A., Ghetti B., Harris D.A. (2005) Bax deletion prevents neuronal loss but not neurological symptoms in a transgenic model of inherited prion disease. *Proc Natl Acad Sci USA* **102**:238-243

Chiò A., Restagno G., Brunetti M., Ossola I., Calvo A., Mora G., Sabatelli M., Monsurrò M.R., Battistini S., Mandrioli J., Salvi F., Spataro R., Schymick J., Traynor B.J., La Bella V. (2009) Two Italian kindreds with familial amyotrophic lateral sclerosis due to FUS mutation. *Neurobiol Aging* **30**:1272-1275

Cifuentes-Diaz, C., Frugier, T., Tiziano, F.D., Lacene, E., Roblot, N., Joshi, V., Moreau, M.H. and Melki, J. (2001) Deletion of murine SMN exon 7 directed to skeletal muscle leads to severe muscular dystrophy. *J. Cell Biol.* **152:**1107-1114

Cifuentes-Diaz C., Nicole S., Velasco M.E., Borra-Cebrian C., Panozzo C., Frugier T., Millet G., Roblot N., Joshi V., Melki J. (2002) Neurofilament accumulation at the motor endplate and lack of axonal sprouting in a spinal muscular atrophy mouse model. *Hum Mol Genet*. **11**: 1439-1447

Cleveland D.W., Rothstein J.D. (2001) From Charcot to Lou Gehrig: deciphering selective motor neuron death in ALS. *Nat Rev Neurosci.* **2**:806-819.

Coady T.H., Shababi M., Tullis G.E., Lorson C.L. (2007) Restoration of SMN function: delivery of a trans-splicing RNA re-directs SMN2 pre-mRNA splicing. *Mol Ther.* **15**:1471-1478

Coleman M.P., Perry V.H. (2002) Axon pathology in neurological disease: a neglected therapeutic target. *Trends Neurosci*. **25**:532-537

Coleman M. (2005) Axon degeneration mechanisms: commonality amid diversity. *Nat Rev Neurosci.* **6**:889-898

Condeelis J. (1995) Elongation factor 1 alpha, translation and the cytoskeleton. *Trends Biochem Sci*. **20**:169-170

Conwit RA, Stashuk D, Tracy B, McHugh M, Brown WF, Metter EJ (1999) The relationship of motor unit size, firing rate and force. *Clin Neurophysiol.* **110**:1270-5

Corcoran J., So P.L., Maden M. (2002) Absence of retinoids can induce motoneuron disease in the adult rat and a retinoid defect is present in motoneuron disease patients. *J Cell Sci.* **15**:4735-41.

Court F.A., Gillingwater T.H., Melrose S., Sherman D.L., Greenshields K.N., Morton A.J., Harris J.B., Willison H.J., Ribchester R.R. (2008) Identity, developmental restriction and reactivity of extralaminar cells capping mammalian neuromuscular junctions. *J Cell Sci.* **121**: 3901-3911

Cunningham C., Deacon R., Wells H., Boche D., Waters S., Diniz C.P., Scott H., Rawlins J.N., Perry V.H. (2003) Synaptic changes characterize early behavioural signs in the ME7 model of murine prion disease. *Eur J Neurosci*. **17**:2147-2155.

Dewil M., dela Cruz V.F., Van Den Bosch L., Robberecht W. (2007) Inhibition of p38 mitogen activated protein kinase activation and mutant SOD1(G93A)-induced motor neuron death. *Neurobiol Dis*. **26**:332-341

Doran B., Gherbesi N., Hendricks G., Flavell R.A., Davis R.J., Gangwani L. (2006) Deficiency of the zinc finger protein ZPR1 causes neurodegeneration. *Proc Natl Acad Sci USA*. **103**:7471-7475

Dubowitz, V. (1999) Very severe spinal muscular atrophy (SMA type 0): an expanding clinical phenotype. *Eur. J. Paediatr. Neurol.* **3:**49-51

Ekestern E. (2004) Neurotrophic factors and amyotrophic lateral sclerosis. *Neurodegener Dis*. **1**:88-100

English A.W. (2003) Cytokines, growth factors and sprouting at the neuromuscular junction. *J Neurocytol*. **32**:943-60.

Erzen I., Cvetko E., Obreza S., Angaut-Petit D., (2000) Fiber types in the mouse levator auris longus muscle: A convenient preparation to study muscle and nerve plasticity. *J Neurosci Res*. **59:**692-697

Fan L., Simard L.R. (2002) Survival motor neuron (SMN) protein: role in neurite outgrowth and neuromuscular maturation during neuronal differentiation and development. *Hum Mol Genet*. **11**:1605-1614

Farrar M.A., Johnston H.M., Grattan-Smith P., Turner A., Kiernan MC. (2009) Spinal Muscular Atrophy: Molecular Mechanisms. *Curr Mol Med* **9**:851-862

Feiguin F., Godena V.K., Romano G., D'Ambrogio A., Klima R., Baralle F.E. (2009) Depletion of TDP-43 affects Drosophila motoneurons terminal synapsis and locomotive behavior. *FEBS Lett.* **583**:1586-1592

Feng G., Mellor R.H., Bernstein M., Keller-Peck C., Nguyen Q.T., Wallace M., Nerbonne J.M., Lichtman J.W., Sanes J.R. (2000) Imaging neuronal subsets in transgenic mice expressing multiple spectral variants of GFP. *Neuron.* **28**:41-51

Feng Z., Koirala S., Ko C.P. (2005) Synapse-glia interactions at the vertebrate neuromuscular junction. *Neuroscientist*. **11**:503-513

Feng Z., Ko C.P. (2008) The role of glial cells in the formation and maintenance of the neuromuscular junction. *Ann N Y Acad Sci.* **1132**:19-28.

Ferguson B., Matyszak M.K., Esiri M.M., Perry V.H. (1997) Axonal damage in acute multiple sclerosis lesions. *Brain.* **120**:393-399

Ferri A., Sanes J.R., Coleman M.P., Cunningham J.M., Kato A.C. (2003) Inhibiting axon degeneration and synapse loss attenuates apoptosis and disease progression in a mouse model of motoneuron disease. *Curr Biol.* **13**: 669-673

Ferri, A., Melki, J. and Kato, A.C. (2004) Progressive and selective degeneration of motoneurons in a mouse model of SMA. *Neuroreport* **15:**275-280

Fischer L.R., Culver D.G., Tennant P., Davis A.A., Wang M., Castellano-Sanchez A., Khan J., Polak M.A., Glass J.D. (2004) Amyotrophic lateral sclerosis is a distal axonopathy in mice and man. *Exp Neurol.* **185**:232-240

Fischer L.R., Culver D.G., Davis A.A., Tennant P., Wang M., Coleman M., Asress S., Adalbert R., Alexander G.M., Glass J.D. (2005) The WldS gene modestly prolongs survival in the SOD1G93A fALS mouse. *Neurobiol Dis*. **19**:293-300.

Foust, K.D., Nurre, E., Montgomery, C.L., Hernandez, A., Chan, C.M. and Kaspar, B.K. (2009) Intravascular AAV9 preferentially targets neonatal neurons and adult astrocytes. *Nat Biotechnol*. **27:**59-65

Fox M.A., Umemori H. (2006) Seeking long-term relationship: axon and target communicate to organize synaptic differentiation. *J Neurochem*. **97**:1215-31

Francis J.W., Sandrock A.W., Bhide P.G., Vonsattel J.P., Brown R.H. Jr. (1998) Heterogeneity of subcellular localization and electrophoretic mobility of survival motor neuron (SMN) protein in mammalian neural cells and tissues. *Proc Natl Acad Sci USA*. **95**: 6492-6497.

Frank E., Fischbach G.D. (1979) Early events in neuromuscular junction formation in vitro: induction of acetylcholine receptor clusters in the postsynaptic membrane and morphology of newly formed synapses. *J Cell Biol.* **83**:143-58

Frey D., Schneider C., Xu L., Borg J., Spooren W., Caroni P. (2000) Early and selective loss of neuromuscular synapse subtypes with low sprouting competence in motoneuron diseases. *J. Neurosci*. **20:**2534-2542

Frischknecht R., Heine M., Perrais D., Seidenbecher C.I., Choquet D., Gundelfinger E.D. (2009) Brain extracellular matrix affects AMPA receptor lateral mobility and short-term synaptic plasticity. *Nat Neurosci*. **12**:897-904

Frugier T., Tiziano F.D., Cifuentes-Diaz C., Miniou P., Roblot N., Dierich A., Le Meur M., Melki J. (2000) Nuclear targeting defect of SMN lacking the C-terminus in a mouse model of spinal muscular atrophy. *Hum Mol Genet.* **9**:849-858.

Fujii R., Okabe S., Urushido T., Inoue K., Yoshimura A., Tachibana T., Nishikawa T., Hicks G.G., Takumi T. (2005) The RNA binding protein TLS is translocated to dendritic spines by mGluR5 activation and regulates spine morphology. *Curr Biol.* **15**:587-593.

Gabanella F., Carissimi C., Usiello A., Pellizzoni L. (2005) The activity of the spinal muscular atrophy protein is regulated during development and cellular differentiation. *Hum Mol Genet*. **14**:3629-3642.

Gangwani L., Mikrut M., Galcheva-Gargova Z., Davis R.J. (1998) Interaction of ZPR1 with translation elongation factor-1alpha in proliferating cells. *J Cell Biol.* **143**:1471-1484

Gangwani L., Mikrut M., Theroux S., Sharma M., Davis R.J. (2001) Spinal muscular atrophy disrupts the interaction of ZPR1 with the SMN protein. *Nat Cell Biol.* **3:**376-383

Gavrilina T.O., McGovern V.L., Workman E., Crawford T.O., Gogliotti R.G., DiDonato C.J., Monani U.R., Morris G.E., Burghes A.H. (2008) Neuronal SMN expression corrects spinal muscular atrophy in severe SMA mice wile muscle specific SMN expression has no phenotypic effect. *Hum Mol Genet*. **17:**1063-1075

Giavazzi A., Setola V., Simonati A., Battaglia G. (2006) Neuronal-specific roles of the survival motor neuron protein: evidence from survival motor neuron expression patterns in the developing human central nervous system. *J Neuropathol Exp Neurol*. **65**:267-277

Gillingwater T.H., Ribchester R.R. (2001) Compartmental neurodegeneration and synaptic plasticity in the Wld^s mutant mouse. *J. Physiol*. **534:**627-639

Gillingwater T.H., Ribchester R.R. (2003) The relationship of neuromuscular synapse elimination to synaptic degeneration and pathology: Insights from Wld^s and other mutant mice. *J. Neurocytol.* **32:**863-881

Gillingwater T.H., Ingham C.A., Coleman M.P., Ribchester R.R. (2003) Ultrastructural correlates of synapse withdrawal at axotomised neuromuscular junctions in mutant and transgenic mice expressing the Wld gene. *J Anat.* **203:**265-276

Gillingwater T.H., Ingham C.A., Parry K.E., Wright A.K., Haley J.E., Wishart T.M., Arbuthnott G.W., Ribchester R.R. (2006a) Delayed synaptic degeneration in the CNS of Wld^s mice after cortical lesion. *Brain.* **129:**1546-1556

Gillingwater T.H., Wishart T.M., Chen P.E., Haley J.E., Robertson K., MacDonald S.H., Middleton S., Wawrowski K., Shipston M.J., Melmed S., Wyllie D.J., Skehel P.A., Coleman M.P., Ribchester R.R. (2006b) The neuroprotective Wld^s gene regulates expression of PTTG1 and erythroid differention regulator 1-like gene in mice and human cells. *Hum Mol Genet*. **15:**625-635

Giustetto M., Hegde A.N., Si K., Casadio A., Inokuchi K., Pei W., Kandel E.R., Schwartz J.H. (2003) Axonal transport of eukaryotic translation elongation factor 1alpha mRNA couples transcription in the nucleus to long-term facilitation at the synapse. *Proc Natl Acad Sci USA*. **100:**13680-13685

Glass J.D., Brushart T.M., George E.B., Griffin J.W. Prolonged survival of transected nerve fibres in C57BL/Ola mice is an intrinsic characteristic of the axon. *J Neurocytol*. **22**:311-321.

Gould T.W., Buss R.R., Vinsant S., Prevette D., Sun W., Knudson C.M., Milligan C.E., Oppenheim R.W. (2006) Complete dissociation of motor neuron death from motor dysfunction by Bax deletion in a mouse model of ALS. *J Neurosci.* **26**: 8774-8786.

Grinnell A.D. (1995) Dynamics of nerve-muscle interaction in developing and mature neuromuscular junctions. *Physiol Rev.* **75**:789-834

Grossman A.W., Aldridge G.M., Weiler I.J., Greenough W.T. (2006) Local protein synthesis and spine morphogenesis: Fragile X syndrome and beyond. *J Neurosci*. **26**:7151-7155

Guettier-Sigrist S., Coupin G., Braun S., Rogovitz D., Courdier I., Warter J.M., Poindron P. (2001) On the possible role of muscle in the pathogenesis of spinal muscular atrophy. *Fundam Clin Pharmacol.* **15**: 31-40

Guettier-Sigrist S., Hugel B., Coupin G., Freyssinet J.M., Poindron P., Warter J.M. (2002) Possible pathogenic role of muscle cell dysfunction in motor neuron death in spinal muscular atrophy. *Muscle Nerve.* **25**:700-8.

Gültner S., Laue M., Riemer C., Heise I., Baier M. (2009) Prion disease development in slow Wallerian degeneration (Wld(S)) mice. *Neurosci Lett.* **456**:93-98.

Gurney M.E., Pu H., Chiu A.Y., Dal Canto M.C., Polchow C.Y., Alexander D.D., Caliendo J., Hentati A., Kwon Y.W., Deng H.X., *et al*. (1994) Motor neuron degeneration in mice that express a human Cu,Zn superoxide dismutase mutation. *Science.* **264**:1772-1775.

Hafezparast M, Klocke R, Ruhrberg C, Marquardt A, Ahmad-Annuar A, Bowen S, Lalli G, Witherden AS, Hummerich H, Nicholson S, Morgan PJ, Oozageer R, Priestley JV, Averill S, King VR, Ball S, Peters J, Toda T, Yamamoto A, Hiraoka Y, Augustin M, Korthaus D, Wattler S, Wabnitz P, Dickneite C, Lampel S, Boehme F, Peraus G, Popp A, Rudelius M, Schlegel J, Fuchs H, Hrabe de Angelis M, Schiavo G, Shima DT, Russ AP, Stumm G, Martin JE, Fisher EM. (2003) Mutations in dynein link motor neuron degeneration to defects in retrograde transport. *Science*. *300*:808-812.

Hasbani D.M., O'Malley K.L. (2006) Wld(S) mice are protected against the Parkinsonian mimetic MPTP. *Exp Neurol.* **202**:93-99

Helmken C., Hofmann Y., Schoenen F., Oprea G., Raschke H., Rudnik-Schöneborn S., Zerres K., Wirth B. (2003) Evidence for a modifying pathway in SMA discordant families: reduced SMN level decreases the amount of its interacting partners and Htra2-beta1. *Hum Genet* **114**:11-21

Hesselmans L.F., Jennekens F.G., Van den Oord C.J., Veldman H., Vincent A. (1993) Development of innervation of skeletal muscle fibers in man: relation to acetylcholine receptors. *Anat Rec*. **236**:553-62

Hinks G.L., Franklin R.J. (2000) Delayed changes in growth factor gene expression during slow remyelination in the CNS of aged rats. *Mol Cell Neurosci.* **16**:542-56

Hoopfer E.D., McLaughlin T., Watts R.J., Schuldiner O., O'Leary D.D.M., Luo L. (2006) Wld^{s} protection distinguishes axon degeneration following injury from naturally occurring developmental pruning. *Neuron*. **50**:883-895

Hua Y., Vickers T.A., Baker B.F., Bennett C.F., Krainer A.R.. (2007) Enhancement of SMN2 exon 7 inclusion by antisense oligonucleotides targeting the exon. *PLoS Biol.* **5**:e73

Hughes B.W., Kusner L.L., Kaminski H.J. (2000) Molecular architecture of the neuromuscular junction. *Muscle Nerve.* **33**:445-61

Hsieh-Li H.M., Chang J.G., Jong Y.J., Wu M.H., Wang N.M., Tsai C.H., Li H. (2000) A mouse model for spinal muscular atrophy. *Nat Genet.* **24**:66-70

Jablonka S, Schrank B, Kralewski M, Rossoll W, Sendtner M. Reduced survival motor neuron (Smn) gene dose in mice leads to motor neuron degeneration: an animal model for spinal muscular atrophy type III. Hum Mol Genet. 2000; 9: 341-346.

Jacob J., Hacker A., Guthrie S. (2001) Mechanisms and molecules in motor neuron specification and axon pathfinding. *Bioessays.* **23**:582-95

Jokic N., Ling Y.Y., Ward R.E., Michael-Titus A.T., Priestley J.V., Malaspina A. (2007) Retinoid receptors in chronic degeneration of the spinal cord: observations in a rat model of amyotrophic lateral sclerosis. *J Neurochem.* **103**:1821-33

Kanekura K., Nishimoto I., Aiso S., Matsuoka M. (2006) Characterization of amyotrophic lateral sclerosis-linked P56S mutation of vesicle-associated membrane protein-associated protein B (VAPB/ALS8). *J Biol Chem.* **281**:30223-30233

Kariya S., Park G.H., Maeno-Hikichi Y., Leykekhman O., Lutz C., Arkovitz M.S., Landmesser L.T., Monani U.R. (2008) Reduced SMN protein impairs maturation of the neuromuscular junctions in mouse models of spinal muscular atrophy. *Hum Mol Genet*. **17**:2552-2569

Kariya S., Mauricio R., Dai Y., Monani U.R. (2009) The neuroprotective factor Wld(s) fails to mitigate distal axonal and neuromuscular junction (NMJ) defects in mouse models of spinal muscular atrophy. *Neurosci Lett.* **449**:246-51

Kaspar B.K., Lladó J., Sherkat N., Rothstein J.D., Gage F.H. (2003) Retrograde viral delivery of IGF-1 prolongs survival in a mouse ALS model. *Science.* **301**:839-842

Keswani S.C., Jack C., Zhou C., Hoke A. (2006) Establishment of a rodent model of HIV-associated sensory neuropathy. *J Neurosci.* **26**:10299-10304

Kielar C., Wishart T.M., Palmer A., Dihanich S., Wong A.M., Macauley S.L., Chan C.H., Sands M.S., Pearce D.A., Cooper J.D., Gillingwater T.H. (2009) Molecular correlates of axonal and synaptic pathology in mouse models of Batten disease. *Hum Mol Genet.* **In press**

Kong L., Wang X., Choe D.W., Polley M., Burnett B.G., Bosch-Marcé M., Griffin J.W., Rich M.M., Sumner C.J. (2009) Impaired synaptic vesicle release and immaturity of neuromuscular junctions in spinal muscular atrophy mice. *J Neurosci*. **29**:842-851

Kühne W. (1888) Croonian Lecture: On the origin and causation of vital movement. *Proceedings of the Royal Society, Series B.* **44**:427–448.

Kwiatkowski T.J. Jr., Bosco D.A., Leclerc A.L., Tamrazian E., Vanderburg C.R., Russ C., Davis A., Gilchrist J., Kasarskis E.J., Munsat T., Valdmanis P., Rouleau G.A., Hosler B.A., Cortelli P., de Jong P.J., Yoshinaga Y., Haines J.L., Pericak-Vance M.A., Yan J., Ticozzi N., Siddique T., McKenna-Yasek D., Sapp P.C., Horvitz H.R., Landers J.E., Brown R.H. Jr. (2009) Mutations in the FUS/TLS gene on chromosome 16 cause familial amyotrophic lateral sclerosis. *Science* **323**:1205-1208

Lambrechts D., Storkebaum E., Morimoto M., Del-Favero J., Desmet F., Marklund S.L., Wyns S., Thijs V., Andersson J., van Marion I., Al-Chalabi A., Bornes S., Musson R., Hansen V., Beckman L., Adolfsson R., Pall H.S., Prats H., Vermeire S., Rutgeerts P., Katayama S., Awata T., Leigh N., Lang-Lazdunski L., Dewerchin M., Shaw C., Moons L., Vlietinck R., Morrison K.E., Robberecht W., Van Broeckhoven C., Collen D., Andersen P.M., Carmeliet P. (2003) VEGF is a modifier of amyotrophic lateral sclerosis in mice and humans and protects motoneurons against ischemic death. *Nat Genet*. **34**:383-394

Le, T.T., Pham, L.T., Butchbach, M.E., Zhang, H.L., Monani, U.R., Coovert, D.D., Gavrilina, T.O., Xing, L., Bassell, G.J. and Burghes, A.H. (2005) SMNΔ7, the major product of the centromeric survival motor neuron (SMN2) gene, extends survival in mice with spinal muscular atrophy and associates with full-length SMN. *Hum Mol Genet*. **14:**845-857

Lee G., Chu T., Shaw C.S. (2009) The primary locus of motor neuron death in an ALS-PDC mouse model. *Neuroreport.* **in press**

Lefebvre S., Burglen L., Reboullet S., Clermont O., Burlet P., Viollet L., Benichou B., Cruaud C. Millasseau P., Zeviani M. (1995) Identification and characterization of spinal muscular atrophy-determining gene. *Cell*. **80:**155-165

Lemmens R., Van Hoecke A., Hersmus N., Geelen V., D'Hollander I., Thijs V., Van Den Bosch L., Carmeliet P., Robberecht W. (2007) Overexpression of mutant superoxide dismutase 1 causes a motor axonopathy in the zebrafish. *Hum Mol Genet*. **16:** 2359-2365

Li J.Y., Plomann M., Brundin P. (2003) Huntington's disease: a synaptopathy? *Trends Mol Med.* **9**:414-420

Lim S.R., Hertel K.J. (2001) Modulation of survival motor neuron pre-mRNA splicing by inhibition of alternative 3' splice site pairing. *J Biol Chem*. **276**:45496-45483

Lu B., Je H.S. (2003) Neurotrophic regulation of the development and function of the neuromuscular synapses. *J Neurocytol.* **32**:931-41

Lunn E.R., Perry V.H., Brown M.C., Rosen H., Gordon S. (1989) Absence of Wallerian degeneration does not hinder regeneration in peripheral nerve. *Eur J Neurosci*. **1**:27-33

Lunn M.R., Wang C.H. (2008) Spinal muscular atrophy. *Lancet.* **371**:2120-2133

Mack T.G.A., Reiner M., Beirowski B., Mi W., Emanuelli M., Wagner D., Thomson D., Gillingwater T., Court F., Conforti L., Fernando F.S., Tarlton A., Andressen C., Addicks K., Magni G., Ribchester R.R., Perry V.H., Coleman M.P. Wallerian degeneration of injured axons and synapses is delayed by a Ube4b/Nmnat chimeric gene. *Nat Neurosci.* **4**:1199-206.

Maden M. (2007) Retinoic acid in the development, regeneration and maintenance of the nervous system. *Nat Rev Neurosci.* 2007 **8**:755-65

Madocsai C., Lim S.R., Geib T., Lam B.J., Hertel K.J. (2005) Correction of SMN2 Pre-mRNA splicing by antisense U7 small nuclear RNAs. *Mol Ther*. **12**:1013-1022

Marques M.J., Conchello J.A., Lichtman J.W. (2000) From plaque to pretzel: fold formation and acetylcholine receptor loss at the developing neuromuscular junction. *J Neurosci.* **20:**3663-3675

Martin N., Jaubert J., Gounon P., Salido E., Haase G., Szatanik M., Guénet J.L. (2002) A missense mutation in Tbce causes progressive motor neuronopathy in mice. *Nat Genet.* **32**: 443-447

Martínez-Hernández R., Soler-Botija C., Also E., Alias L., Caselles L., Gich I., Bernal S., Tizzano E.F. (2009) The developmental pattern of myotubes in spinal muscular atrophy indicates prenatal delay of muscle maturation. *J Neuropathol Exp Neurol*. **68**:474-481

Martinou J.C., Merlie J.P. (1991) Nerve-dependent modulation of acetylcholine receptor epsilon-subunit gene expression. J Neurosci. **11**:1291-1299

Masaki T., Matsumura K., Saito F., Sunada Y., Shimizu T., Yorifuji H., Motoyoshi K., Kamakura K. (2000) Expression of dystroglycan and laminin-2 in peripheral nerve under axonal degeneration and regeneration. *Acta Neuropathol.* **99**:289-95

Masaki T., Matsumura K., Saito F., Yamada H., Higuchi S., Kamakura K., Yorifuji H., Shimizu T. (2003) Association of dystroglycan and laminin-2 coexpression with

myelinogenesis in peripheral nerves. *Med Electron Microsc.* **36**:221-39

Maselli R.A., Wollman R.L., Leung C., Distad B., Palombi S., Richman D.P., Salazar-Grueso E.F., Roos R.P. (1993) Neuromuscular transmission in amyotrophic lateral sclerosis. *Muscle Nerve.* **16**:1193-1203

McCann C.M., Nguyen Q.T., Santo Neto H., Lichtman J.W. (2007) Rapid synapse elimination after postsynaptic protein synthesis inhibition in vivo. *J Neurosci.* **27**:6064-6067.

McGovern V.L., Gavrilina T.O., Beattie C.E., Burghes A.H. (2008). Embryonic motor axon development in the severe SMA mouse. *Hum Mol Genet.* **17**:2900-2909

McWhorter, M.L., Monani, U.R., Burghes, A.H.M. and Beattie, C.E. (2003) Knockdown of the survival motor neuron (Smn) protein in zebrafish causes defects in motor axon outgrowing and pathfinding. *J. Cell Biol*. **162:**919-931

Mi W., Beirowski B., Gillingwater T.H., Adalbert R., Wagner D., Grumme D., Osaka H., Conforti L., Arnhold S., Hangoc V., Celik A., Addicks K., Wada K., Ribchester R.R., Coleman M.P. (2005) The slow Wallerian degeneration gene, *Wld*^{S}, inhibits axonal spheroid pathology in gracile axonal dystrophy mice. *Brain*. **128**:405-416

Miledi R, Slater CR. (1970) On the degeneration of rat neuromuscular junctions after nerve section. J Physiol. **207**:507-528

Mishra V.N., Kalita J., Kesari A., Mitta B., Shankar S.K., Misra U.K. (2004) A clinical and genetic study of spinal muscular atrophy. *Electromyogr Clin Neurophysiol*. **44**:307-312

Mishra A.K., Gangwani L., Davis R.J., Lambright D.G. (2007) Structural insights into the interaction of the evolutionarily conserved ZPR1 domain tandem with eukaryotic EF1A, receptors, and SMN complexes. *Proc Natl Acad Sci USA* **104**:13930-13935

Missias A.C., Mudd J., Cunningham J.M., Steinbach J.H., Merlie J.P., Sanes J.R. (1997) Deficient development and maintenance of postsynaptic specializations in mutant mice lacking an 'adult' acetylcholine receptor subunit. *Development*. **124**:5075-86

Mizusawa H., Matsumoto S., Yen S.H., Hirano A., Rojas-Corona R.R., Donnenfeld H. (1989) Focal accumulation of phosphorylated neurofilaments within anterior horn cell in familial amyotrophic lateral sclerosis. *Acta Neuropathol*. **79**:37-43

Monani U.R., Sendtner M., Coovert D.D., Parsons D.W., Andreassi C., Le T.T., Jablonka S., Schrank B, Rossoll W, Prior TW, Morris GE, Burghes AH. (2000) The human centromeric survival motor neuron gene (SMN2) rescues embryonic lethality in Smn(-/-) mice and results in a mouse with spinal muscular atrophy. *Hum Mol Genet*. **9**:333-339

Monani U.R., Pastore M.T., Gavrilina T.O., Jablonka S., Le T.T., Andreassi C., DiCocco J.M., Lorson C., Androphy E.J., Sendtner M., Podell M., Burghes A.H. (2003) A transgene carrying an A2G missense mutation in the SMN gene modulates phenotypic severity in mice with severe (type I) spinal muscular atrophy. *J Cell Biol.* **160:**41-52

Monani, U.R. (2005) Spinal muscular atrophy: A deficiency in a ubiquitous protein; a motor neuron-specific disease. *Neuron* **48:**885-896

Morrison B.M., Lachey J.L., Warsing L.C., Ting B.L., Pullen A.E., Underwood K.W., Kumar R., Sako D., Grinberg A., Wong V., Colantuoni E., Seehra J.S., Wagner K.R. (2009) A soluble activin type IIB receptor improves function in a mouse model of amyotrophic lateral sclerosis. *Exp Neurol.* **217**:258-268

Münch C., Sedlmeier R., Meyer T., Homberg V., Sperfeld A.D., Kurt A., Prudlo J., Peraus G., Hanemann C.O., Stumm G., Ludolph A.C. (2004) Point mutations of the p150 subunit of dynactin (DCTN1) gene in ALS. *Neurology.* **63**:724-726

Murray L.M., Thomson D., Conklin A., Wishart T.M., Gillingwater T.H. (2008) Loss of translation elongation factor (eEF1A2) expression in vivo differentiates between Wallerian degeneration and dying-back neuronal pathology. *J Anat.* **213**:633-45

Nagai M., Aoki M., Miyoshi I., Kato M., Pasinelli P., Kasai N., Brown R.H. Jr., Itoyama Y. (2001) Rats expressing human cytosolic copper-zinc superoxide dismutase transgenes with amyotrophic lateral sclerosis: associated mutations develop motor neuron disease. *J Neurosci.* **21**:9246-9254

Navarrette R., Vrbová G. (1993) Activity-dependent interactions between motoneurones and muscles: their role in the development of the motor unit. *Prog Neurobiol*. 41:93-124

Newbery H.J., Gillingwater T.H., Dharmasaroja P., Peters J., Wharton S.B., Thomson D., Ribchester R.R., Abbott, C.M. (2005) Progressive loss of motor neuron function in wasted mice: Effects of a spontaneous null mutation in the gene for the eEF1A2 translation factor. *J. Neuropathol. Exp. Neurol.* **64:**295-303

Newbery H.J., Loh D.H., O'Donoghue J.E., Tomlinson V.A., Chau Y.Y., Boyd J.A., Bergmann J.H., Brownstein D., Abbott C.M. (2007) Translation elongation factor eEF1A2 is essential for post-weaning survival in mice. *J Biol Chem* **282:**28951-28959

Nishimura A.L., Mitne-Neto M., Silva H.C., Richieri-Costa A., Middleton S., Cascio D., Kok F., Oliveira J.R., Gillingwater T., Webb J., Skehel P., Zatz M. (2004) A mutation in the vesicle-trafficking protein VAPB causes late-onset spinal muscular atrophy and amyotrophic lateral sclerosis. *Am J Hum Genet*. **75**:822-831

Oprea G.E., Kröber S., McWhorter M.L., Rossoll W., Müller S., Krawczak M., Bassell G.J., Beattie C.E., Wirth B. (2008) Plastin 3 is a protective modifier of autosomal

recessive spinal muscular atrophy. *Science.* **320**:524-527

Orrell R.W., King A.W., Lane R.J., de Belleroche J.S. (1995) Investigation of a null mutation of the CNTF gene in familial amyotrophic lateral sclerosis. *J Neurol Sci.* **132**:126-128

Pan J., Ruest L.B., Xu S., Wang E. (2004) Immuno-characterization of the switch of peptide elongation development. *Brain Res Dev Brain Res* **149:**1-8

Parson S.H., Mackintosh C.L., Ribchester R.R. (1997) Elimination of motor nerve terminals in neonatal mice expressing a gene for slow wallerian degeneration (C57Bl/Wlds). *Eur J Neurosci.* **9**:1586-92

Pearn J. (1978) Incidence, prevalence, and gene frequency studies of chronic childhood spinal muscular atrophy. *J. Med. Genet*. **15:**409-413

Pegoraro E., Marks H., Garcia C.A., Crawford T., Mancias P., Connolly A.M., Fanin M., Martinello F., Trevisan C.P., Angelini C., Stella A., Scavina M., Munk R.L., Servidei S., Bönnemann C.C., Bertorini T., Acsadi G., Thompson C.E., Gagnon D., Hoganson G., Carver V., Zimmerman R.A., Hoffman E.P. (1998) Laminin alpha2 muscular dystrophy: genotype/phenotype studies of 22 patients. *Neurology.* **51**:101-1

Perry V.H., Brown M.C., Lunn E.R., Tree P., Gordon S. (1990) Evidence that Very Slow Wallerian Degeneration in C57BL/Ola Mice is an Intrinsic Property of the Peripheral Nerve. *Eur J Neurosci.* **2**:802-808

Perry V.H., Anthony D.C. (1999) Axon damage and repair in multiple sclerosis. *Philos Trans R Soc Lond B Biol Sci.* **354**:1641-1647

Piper M., Holt C. (2004) RNA translation in axons. *Annu Rev Cell Dev Biol* **20**:505-523

Prasarnpun S., Walsh J., Awad S.S., Harris J.B. (2005) Envenoming bites by kraits: the biological basis of treatment-resistant neuromuscular paralysis. *Brain*. **128**: 2987-2996

Puls I., Oh S.J., Sumner C.J., Wallace K.E., Floeter M.K., Mann E.A., Kennedy W.R., Wendelschafer-Crabb G., Vortmeyer A., Powers R., Finnegan K., Holzbaur E.L., Fischbeck K.H., Ludlow C.L. (2005) Distal spinal and bulbar muscular atrophy caused by dynactin mutation. Ann Neurol. **57**:687-694

Pun S., Sigrist M., Santos A.F., Ruegg M.A., Sanes J.R., Jessell T.M., Arber S., Caroni, P. (2002) An intrinsic distinction in neuromuscular junction assembly and maintenance in different skeletal muscles. *Neuron* **34:**357-370

Pun S., Santos A.F., Saxena S., Caroni, P. (2006) Selective vulnerability and pruning of phasic motoneuron axons in motoneuron disease alleviated by CNTF. *Nat. Neurosci.* **9:**408-419

Raff M.C., Whitmore A.V., Finn J.T. (2002) Axonal self-destruction and neurodegeneration. *Science* **296:**868-871

Rajendra T.K., Gonsalvez G.B., Walker M.P., Shpargel K.B., Salz H.K., Matera, A.G. (2007) A Drosophila melanogaster model of spinal muscular atrophy reveals a function for SMN in striated muscle. *J. Cell Biol.* **176:**831-841

Ranvier L. (1889) Traité Technique D'Histologie. *Libraire F. Savy 2nd edn.* 613–637

Ratnaparkhi A., Lawless G.M., Schweizer F.E., Golshani P., Jackson G.R. (2008) A Drosophila model of ALS: human ALS-associated mutation in VAP33A suggests a dominant negative mechanism. *PLoS One.* 3:e2334

Ribchester R.R., Tsao J.W., Barry J.A., Asgari-Jirhandeh N., Perry V.H., Brown M.C. (1995) Persistence of neuromuscular junctions after axotomy in mice with slow Wallerian degeneration (C57BL/WldS). *Eur J Neurosci.* **7**:1641-50.

Rich M.M., Wang X., Cope T.C., Pinter M.J. (2002) Reduced neuromuscular quantal content with normal synaptic release time course and depression in canine motor neuron disease. *J Neurophysiol.* 88: 3305-3314

Robertson J.D. 1956 The ultrastructure of a reptilian myoneural junction. *J Biophys Biochem Cytol.* **2**:381-94.

Rose F.F. Jr, Meehan P.W., Coady T.H., Garcia V.B., Garcia M.L., Lorson C.L. (2008) The Wallerian degeneration slow (Wld^S) gene does not attenuate disease in a mouse model of spinal muscular atrophy. *Biochem Biophys Res Commun*. **375**:119-123

Rosen D.R., Siddique T., Patterson D., Figlewicz D.A., Sapp P., Hentati A., Donaldson D., Goto J., O'Regan J.P., Deng H.X., Rahmani Z., Krizus A., McKenna-Yasek D., Cayabyab A., Gaston S.M., Berger R., Tanzi R.E., Halperin J.J., Herzfeldt B., Van den Bergh R., Hung W.Y., Bird T., Deng G., Mulder D.W., Smyth C., Laing N.G., Soriano E., Pericak–Vance M.A., Haines J., Rouleau G.A., Gusella J.S., Horvitz H.R., Brown R.H. (1993) Mutations in Cu/Zn superoxide dismutase gene are associated with familial amyotrophic lateral sclerosis. *Nature*. **362**:59-62

Rossoll W., Jablonka S., Andreassi C., Kroning A-K., Karle K., Monani U.R., Sendtner M. (2003) Smn, the spinal muscular atrophy-determining gene product, modulates axon growth and localization of β-actin mRNA in growth cones of motoneurons. *J. Cell Biol*. **163:**801-812

Rothstein J.D. (2009) Current hypotheses for the underlying biology of amyotrophic lateral sclerosis. *Ann Neurol*. **65**:S3-9

Rouaux C., Panteleeva I., René F., Gonzalez de Aguilar J.L., Echaniz-Laguna A., Dupuis L., Menger Y., Boutillier A.L., Loeffler J.P. (2007) Sodium valproate exerts neuroprotective effects in vivo through CREB-binding protein-dependent mechanisms but does not improve survival in an amyotrophic lateral sclerosis mouse model. *J Neurosci*. **27**:5535-5545

Russman B.S. (2007) Spinal muscular atrophy: clinical classification and disease heterogeneity. *J Child Neurol.* **22**:946-51

Sagot Y., Dubois-Dauphin M., Tan S.A., de Bilbao F., Aebischer P., Martinou J.C., Kato A.C. (1995) Bcl-2 overexpression prevents motoneuron cell body loss but not axonal degeneration in a mouse model of a neurodegenerative disease. *J Neurosci.* **15**:7727-7733

Samsam M., Mi W., Wessig C., Zielasek J., Toyka K.V., Coleman M.P., Martini R. (2003) The Wlds mutation delays robust loss of motor and sensory axons in a genetic model for myelin-related axonopathy. *J Neurosci.* **23**:2833-9

Sanes J.R., Lichtman J.W. (1999) Development of the vertebrate neuromuscular junction. *Annu Rev Neurosci.* **22**:389-442

Schaefer A.M., Sanes J.R., Lichtman J.W. (2005) A compensatory subpopulation of motor neurons in a mouse model of amyotrophic lateral sclerosis. *J. Comp. Neurol.* **490:**209-219

Schmalbruch H., Jensen H.J., Bjaerg M., Kamieniecka Z., Kurland L. (1991) A new mouse mutant with progressive motor neuronopathy. *J Neuropathol Exp Neurol.* **50**:192-204

Schrank B, Götz R, Gunnersen JM, Ure JM, Toyka KV, Smith AG, Sendtner M. (1997) Inactivation of the survival motor neuron gene, a candidate gene for human spinal muscular atrophy, leads to massive cell death in early mouse embryos. *Proc Natl Acad Sci U S A*. **94**:9920-9925.

Shultz L.D., Sweet H.O., Davisson M.T., Coman D.R. (1982) 'Wasted', a new mutant of the mouse with abnormalities characteristic to ataxia telangiectasia. *Nature.* **297**:402-4

Schymick J.C., Talbot K., Traynor B.J. (2007) Genetics of sporadic amyotrophic lateral sclerosis. Hum Mol Genet. **16**:R233-42

Selkoe D.J. (2002) Alzheimer's disease is a synaptic failure. *Science.* 298: 789-791

Setola V., Terao M., Locatelli D., Bassanini S., Garattini E., Battaglia G. (2007) Axonal-SMN (a-SMN), a protein isoform of the survival motor neuron gene, is specifically involved in axonogenesis. *Proc Natl Acad Sci USA*. **104**:1959-1964

Shafey D., MacKenzie A.E., Kothary R. (2008) Neurodevelopmental abnormalities in neurosphere-derived neural stem cells from SMN-depleted mice. *J Neurosci Res*. **86**:2839-2847

Shamovsky I., Ivannikov M., Kandel E.S., Gershon D., Nudler E. (2006) RNA-mediated response to heat shock in mammalian cells. *Nature* **440**:556-560

Shiina N., Gotoh Y., Kubomura N., Iwamatsu A., Nishida E. (1994) Microtubule severing by elongation factor 1 alpha. *Science.* **266**:282-285

Shultz L.D., Sweet H.O., Davisson M.T., Coman D.R. (1982) 'Wasted', a new mutant of the mouse with abnormalities characteristic to ataxia telangiectasia. *Nature.* **297**:402-404

Singer M.A., Statland J.M., Wolfe G.I., Barohn R.J. (2006) Primary lateral sclerosis. *Muscle Nerve.* **35**:291-302

Soubrouillard C., Pellissier J.F., Lepidi H., Mancini J., Rougon G., Figarella-Branger D. (1995) Expression of developmentally regulated cytoskeleton and cell surface proteins in childhood spinal muscular atrophies. *J. Neurol. Sci.* **133:**155-163

Sreedharan J., Blair I.P., Tripathi V.B., Hu X., Vance C., Rogelj B., Ackerley S., Durnall J.C., Williams K.L., Buratti E., Baralle F., de Belleroche J., Mitchell J.D., Leigh P.N., Al-Chalabi A., Miller C.C., Nicholson G., Shaw C.E. (2008) TDP-43 mutations in familial and sporadic amyotrophic lateral sclerosis. *Science.* **319:**1668-1672

Stavisky R.C., Britt J.M., Zuzek A., Pham T., Marzullo T.C., Bittner G.D. (2003) Degeneration of mammalian PNS and CNS axons is accelerated by incubation with protein synthesis inhibitors. *Neurosci Res.* **47**:445-9

Sumner C.J., Kolb S.J., Harmison G.G., Jeffries N.O., Schadt K., Finkel R.S., Dreyfuss G., Fischbeck K.H. (2006) SMN mRNA and protein levels in peripheral blood: biomarkers for SMA clinical trials. *Neurology.* **66**:1067-73

Suzuki M., McHugh J., Tork C., Shelley B., Klein S.M., Aebischer P., Svendsen C.N. (2007) GDNF secreting human neural progenitor cells protect dying motor neurons, but not their projection to muscle, in a rat model of familial ALS. *PLoS One.* **2**:e689

Swoboda K.J., Prior T.W., Scott C.B., McNaught T.P., Wride M.C., Reyna S.P., Bromberg M.B. (2005) Natural history of denervation in SMA: Relation to age, SMN2 copy number, and function. *Ann. Neurol.* **57:**704-712

Swoboda K.J., Kissel J.T., Crawford T.O., Bromberg M.B., Acsadi G., D'Anjou G., Krosschell K.J., Reyna S.P., Schroth M.K., Scott C.B., Simard L.R. (2007) Perspectives on clinical trials in spinal muscular atrophy. *J Child Neurol.* **22:**957-66

Teuling E., van Dis V., Wulf P.S., Haasdijk E.D., Akhmanova A., Hoogenraad C.C., Jaarsma D. (2008) A novel mouse model with impaired dynein/dynactin function develops amyotrophic lateral sclerosis (ALS)-like features in motor neurons and improves lifespan in SOD1-ALS mice. *Hum Mol Genet*. **17**:2849-2862

Ting C.H., Lin C.W., Wen S.L., Hsieh-Li H.M., Li H. (2007) Stat5 constitutive activation rescues defects in spinal muscular atrophy. *Hum Mol Genet*. **15**:499-514

Tiziano F.D., Pinto A.M., Fiori S., Lomastro R., Messina S., Bruno C., Pini A., Pane M., D'Amico A., Ghezzo A., Bertini E., Mercuri E., Neri G., Brahe C. (2009) SMN transcript levels in leukocytes of SMA patients determined by absolute real-time PCR. *Eur J Hum Genet.* **In Press**

Tsujihata M., Hazama R., Yoshimura T., Satoh A., Mori M., Nagataki S. (1984) The motor end-plate fine structure and ultrastructural localization of acetylcholine receptors in amyotrophic lateral sclerosis. *Muscle Nerve*. **7**:243-249

Turner M.R., Kiernan M.C., Leigh P.N., Talbot K. (2009) Biomarkers in amyotrophic lateral sclerosis. *Lancet Neurol.* **8**:94-109

Vance C., Rogelj B., Hortobágyi T., De Vos K.J., Nishimura A.L., Sreedharan J., Hu X., Smith B., Ruddy D., Wright P., Ganesalingam J., Williams K.L., Tripathi V., Al-Saraj S., Al-Chalabi A., Leigh P.N., Blair I.P., Nicholson G., de Belleroche J., Gallo J.M., Miller C.C., Shaw C.E. (2009) Mutations in FUS, an RNA processing protein, cause familial amyotrophic lateral Sclerosis type 6. *Science* **323**:1208-1211

Vande-Velde C., Garcia M.L., Yin X., Trapp B.D., Cleveland D.W. (2004) The neuroprotective factor Wlds does not attenuate mutant SOD1-mediated motor neuron disease. *Neuromolecular Med*. **5**:193-203

Vrbová G. (2008) Spinal muscular atrophy: motoneurone or muscle disease? *Neuromuscul Disord.* **18**: 81-82

von Gontard A., Zerres K., Backes M., Laufersweiler-Plass C., Wendland C., Melchers P., Lehmkuhl G., Rudnik-Schöneborn S. (2002) Intelligence and cognitive function in children and adolescents with spinal muscular atrophy. *Neuromuscul Disord.* **12**:130-6

Walker M.P., Rajendra T.K., Saieva L., Fuentes J.L., Pellizzoni L., Matera A.G. (2008) SMN complex localizes to the sarcomeric Z-disc and is a proteolytic target of calpain. Hum Mol Genet. **17**:3399-3410

Wang M.S., Fang G., Culver D.G., Davis A.A., Rich M.M., Glass J.D. (2001) The WldS protein protects against axonal degeneration: a model of gene therapy for peripheral neuropathy. Ann Neurol.**50**:773-9

Wang J., Farr G.W., Hall D.H., Li F., Furtak K., Dreier L., Horwich A.L. (2009a) An ALS-linked mutant SOD1 produces a locomotor defect associated with aggregation and synaptic dysfunction when expressed in neurons of Caenorhabditis elegans. *PLoS Genet*. **5**:e1000350

Warita H., Itoyama Y., Abe K. (1999) Selective impairment of fast anterograde axonal transport in the peripheral nerves of asymptomatic transgenic mice with a G93A mutant SOD1 gene. *Brain Res.* **819**:120-131

Williamson T.L., Cleveland D.W. (1999) Slowing of axonal transport is a very early event in the toxicity of ALS-linked SOD1 mutants to motor neurons. *Nat Neurosci*. **2**:50-56

Willison H.J. (2005) The immunobiology of Guillain-Barré syndromes. *J Peripher Nerv Syst*. **10**:94-112

Winkler C., Eggert C., Gradl D., Meister G., Giegerich M., Wedlich D., Laggerbauer B., Fischer U. (2005) Reduced U snRNP assembly causes motor axon degeneration in an animal model for spinal muscular atrophy. *Genes Dev*. **19**:2320-2330

Winlow W., Usherwood P.N. (1975) Ultrastructural studies of normal and degenerating mouse neuromuscular junctions. *J Neurocytol.* **4**:377-394

Wirth B., Brichta L., Hahnen E. (2006) Spinal muscular atrophy: From gene to therapy. *Sem. Pediatric Neurol*. **13:**121-131

Wishart T.M., Parson S.H., Gillingwater T.H. (2006) Synaptic vulnerability in neurodegenerative disease. *J Neuropathol Exp Neurol.* **65:**733-739

Wishart T.M., Macdonald S.H., Chen P.E., Shipston M.J., Coleman M.P., Gillingwater T.H., Ribchester R.R. (2007a) Design of a novel quantitative PCR (QPCR)-based protocol for genotyping mice carrying the neuroprotective Wallerian degeneration slow (Wlds) gene. *Mol Neurodegener.* **2**:21

Wishart T.M., Paterson J.M., Short D.M., Meredith S., Robertson K.A., Sutherland C., Cousin M.A., Dutia M.B., Gillingwater T.H. (2007b) Differential proteomics analysis of synaptic proteins identifies potential cellular targets and protein mediators of synaptic neuroprotection conferred by the slow Wallerian degeneration (*Wld*^{s}) gene. *Mol Cell Proteomics.* **6:**1318-1330.

Wishart T.M., Pemberton H.N., James S.R., McCabe C.J., Gillingwater T.H. (2008) Modified cell cycle status in a mouse model of altered neuronal vulnerability (slow Wallerian degeneration; Wlds). *Genome Biol.* **9**: R101

Woldeyesus M.T., Britsch S., Riethmacher D., Xu L., Sonnenberg-Riethmacher E., Abou-Rebyeh F., Harvey R., Caroni P., Birchmeier C. (1999) Peripheral nervous system defects in erbB2 mutants following genetic rescue of heart development. *Genes Dev.* **13**:2538-48

Wolpowitz D., Mason T.B., Dietrich P., Mendelsohn M., Talmage D.A., Role L.W. (2000) Cysteine-rich domain isoforms of the neuregulin-1 gene are required for maintenance of peripheral synapses. *Neuron.* **25**:79-91

Wong F., Fan L., Wells S., Hartley R., Mackenzie F.E., Oyebode O., Brown R., Thomson D., Coleman M.P., Blanco G., Ribchester R.R. (2009) Axonal and neuromuscular synaptic phenotypes in Wld(S), SOD1(G93A) and ostes mutant mice identified by fiber-optic confocal microendoscopy. *Mol Cell Neurosci.* **In Press**

Wyatt R.M., Balice-Gordon R.J. (2003) Activity-dependent elimination of neuromuscular synapses. *J Neurocytol*. **32**: 777-794

Yang F., Demma M., Warren V., Dharmawardhane S., and Condeelis J. (1990) Identification of an actin-binding protein from Dictyostelium as elongation factor 1a. *Nature*. **347**:494-496

Yang W., Burkhart W., Cavallius J., Merrick W.C., Boss W.F. (1993) Purification and characterization of a phosphatidylinositol 4-kinase activator in carrot cells. *J Biol Chem* **268**: 392-398

Ymlahi-Ouazzani Q., J Bronchain O., Paillard E., Ballagny C., Chesneau A., Jadaud A., Mazabraud A., Pollet N. (2009) Reduced levels of survival motor neuron protein leads to aberrant motoneuron growth in a Xenopus model of muscular atrophy. *Neurogenetics.* **In press**

Zhang H.L., Pan F., Hong D., Shenoy S.M., Singer R.H., Bassell G.J. (2003) Active transport of the survival motor neuron protein and the role of exon-7 in cytoplasmic localization. *J Neurosci*. **23**:6627-6637

Zhang Z., Lotti F., Dittmar K., Younis I., Wan L., Kasim M., Dreyfuss G. (2008) SMN deficiency causes tissue-specific perturbations in the repertoire of snRNAs and widespread defects in splicing. *Cell.* 133:585-600

10. Appendices

Appendix 10.1 Validation of axon counting methods

Quantifying axon numbers in intramuscular nerves presents a significant challenge in order to obtain reliable results. I have therefore dedicated some effort to determining the most accurate system for measuring axons in whole mount nerve/muscle preparations. As it was clear that axon number could not be evaluated accurately by looking down the standard fluorescent microscope, efforts were dedicated to using confocal images. The first consideration, therefore, was as what point on the intramuscular nerve to acquire the image. Regions were chosen and carefully defined in order to standardise the number of endplates included and to minimise the incidence of axon branching (Figure 10.1.1).

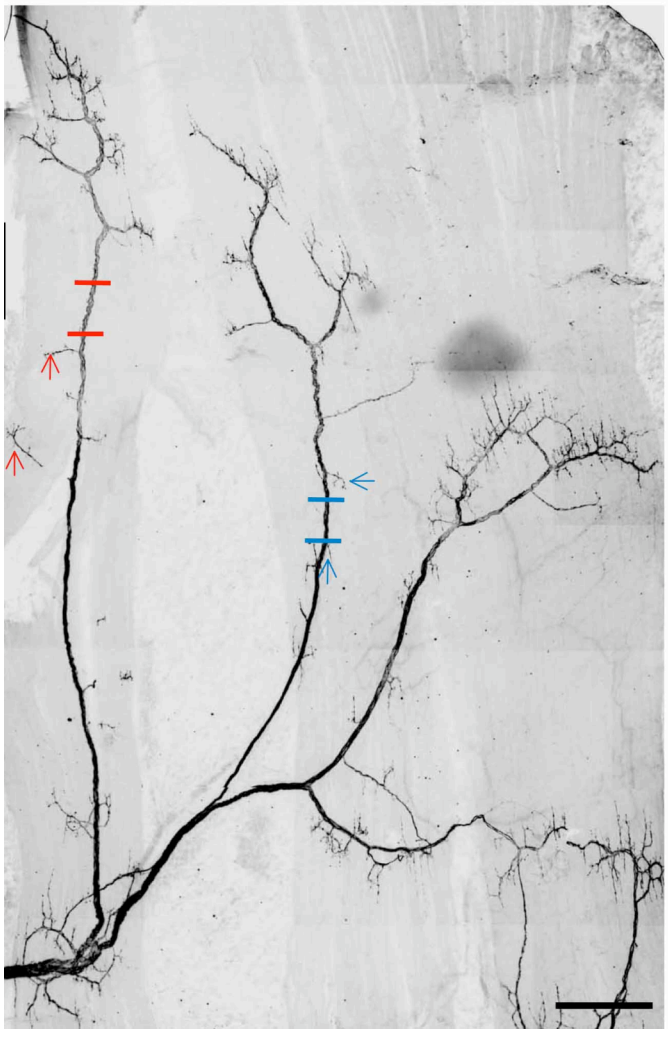

Figure 10.1.1: Position of images used for axon quantification. Images taken to quantify axon number in the caudal band were taken at least 200μm from the endplate band to minimise branching but not more than 500μm to standardise the number of endplates included by excluding small branches (red arrow) (red lines show limits of region used). Images taken to quantify axons in the rostral band were taken in a region in which there were no small collateral branches (blue arrows) that was at least 200μm from the main R3/R4 endplate band (blue lines show limits of region used). *(Scale bar = 500μm).*

Initial attempts to quantify axon number focused on counting axons from raw confocal Z stacks. As it became apparent that it was commonly difficult to identify individual axon profiles, raw images were subject to deconvolution analysis. The process of deconvolution uses an algorithm based on the intrinsic noise introduced by the imaging system and attempts to reverse this noise and therefore increase the image clarity. In order to determine the most accurate method of axon quantification, a random sample of 8 axon bundle images were visualised and quantified in 3 different ways: visualisation in grey scale and scanned up and down through the z series; pseudo-colouring images by signal intensity and scanning up and down through z series; pseudo-colouring images by signal intensity and visualisation in cross section (Figure 10.1.2). In order to determine the variability in counting methods, each image was quantified at three pre-defined points (top, middle and bottom) and each count was compared to the average of the three counts (Figure 10.1.3). To prevent experimenter bias, each image was quantified at one point (i.e. top) and then re-blinded before repeat counts. Results imply that the least variability in axon quantification is seen when axons are counted in x-y sections in grey scale on deconvolved images (Figure 10.1.3 B). It was clear deconvolution decreased the variability seen, and that in both raw and deconvolved images, the highest variability was seen when axons were counted in cross section.

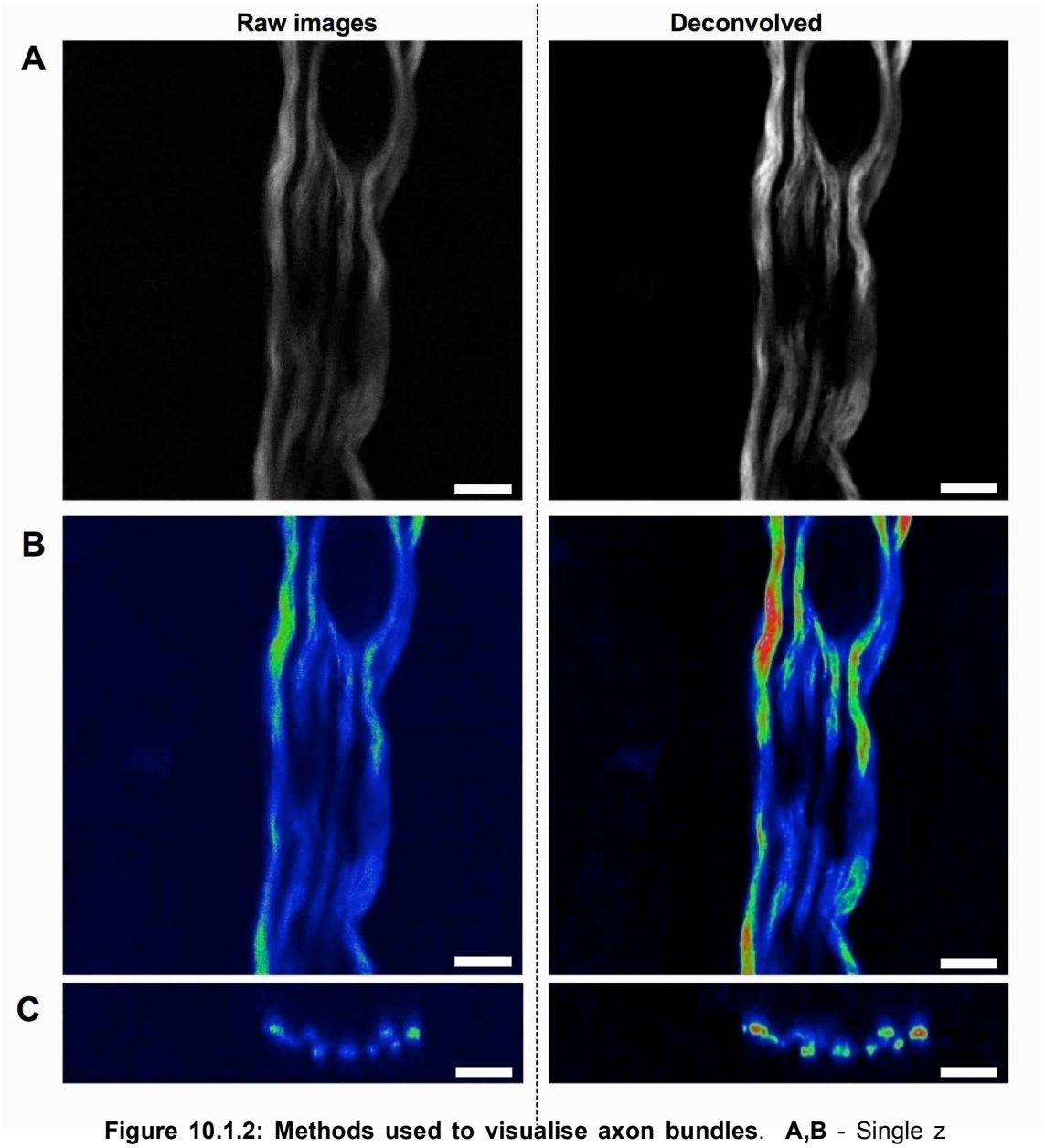

Figure 10.1.2: Methods used to visualise axon bundles. **A,B** - Single z slices of confocal images of intramuscular axon bundle labeled with 150KDa neurofilaments, which reflect raw images (left) or deconvolved images (left). Axon were visualised in grey scale (A) or pseudocoloured by signal intensity (B). **C -** cross sectional pseudocoloured slices through raw images (left) or deconvolved images (right) of axon bundles. *(Scale bar = 10μm).*

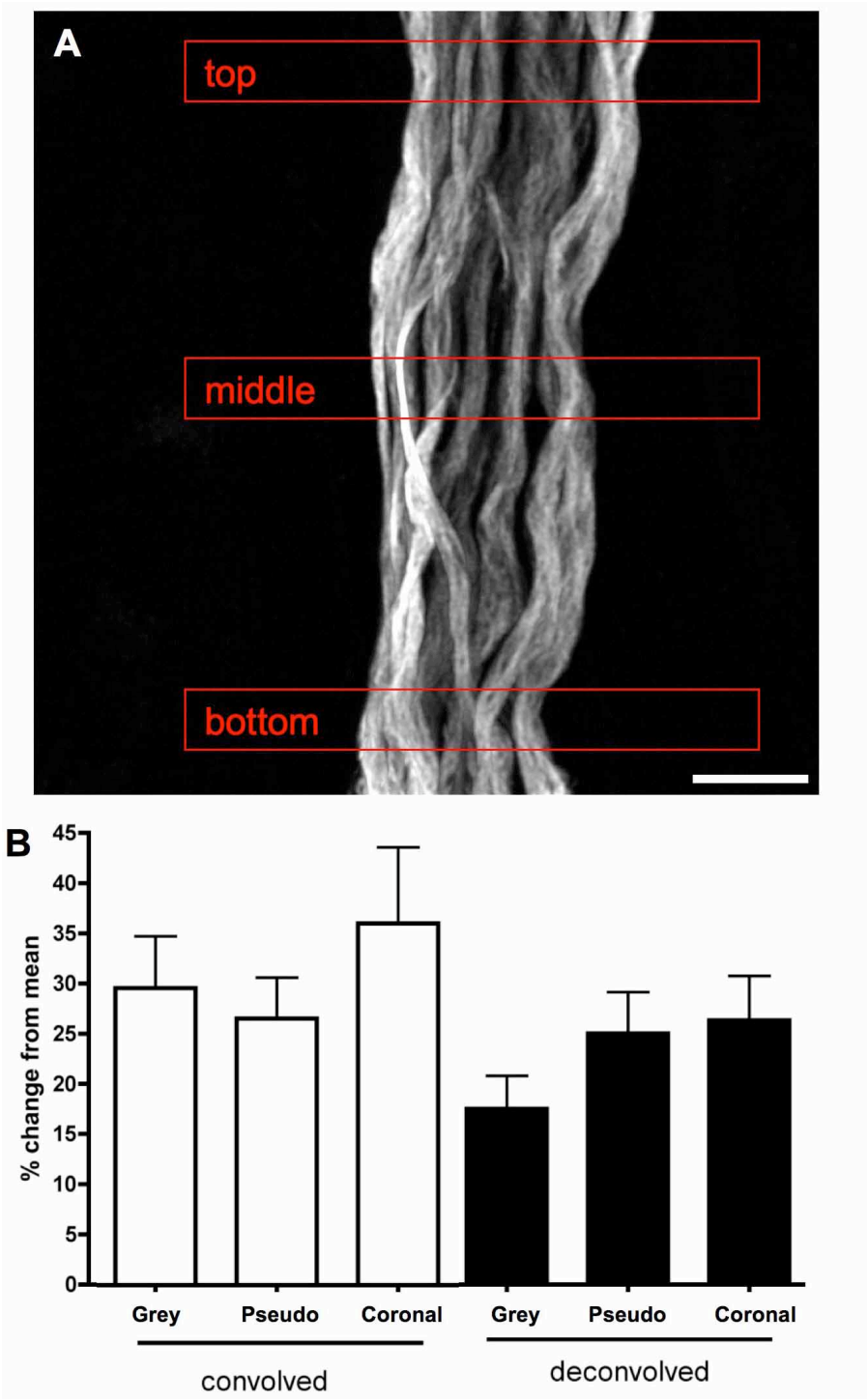

Figure 10.1.3: Variability in different axon counting methods. A - example confocal micrograph illustrating the three points at which axon number was quantified. Axons were visualized using three different methods on both deconvolved and convolved images (see figure 10.1.2). B - Bar chart (Mean ± SEM) showing the average percentage variability between the three individual measurements taken from each image for the three different counting methods (grey, pseudo, coronal) on both raw images and deconvolved images. Data acquired from 8 randomly selected axons bundles. Note the lowest levels of variability is seen by counting in the grey channel on deconvolved images. *(Scale bar - 15μm (A))*

All experimental muscles were therefore quantified using the X-Y deconvolved images in gray scale. When the variability observed was compared between caudal and rostral bands there was a general tendency for decreased variability in the caudal band in all genotypes investigated (Figure 10.1.4). Additionally there was trend for increased variability in *Smn-/-;SMN2* muscles compared to control muscles. While this finding could simply reflect natural variability, it does raise the possibility that increased variability could reflect an increase in axon branching. This therefore questions whether it is justified to use low variability as an indication of a reliable quantification technique. It is possible that systems producing high variability may reflect an increase in sensitivity in the technique, in which new axons branches are becoming visible. Should this be the case, I would expect a progressive change in the number of axons when comparing the 3 independent counts i.e. the 'middle' should rarely be the highest. In contrast, comparison of the 3 individual counts revealed the 'middle' count was the highest in 10/21 cases (Figure 10.1.5). This would strongly suggest that axon branching does not account for the variability seen and therefore justifies using low variability as an indicator of a reliable counting method making the chosen method an appropriate choice.

Results imply that variability of approximately 15-25% can be reasonably expected when quantifying axons in intramuscular nerves. While this is clearly not ideal, we must remember that in most cases this reflects discrepancy of approximately only 1-3 axons. The methodology chosen here should therefore defect any changes in axon distribution of over 1-3 axons but will not identify more subtle changes in axon number.

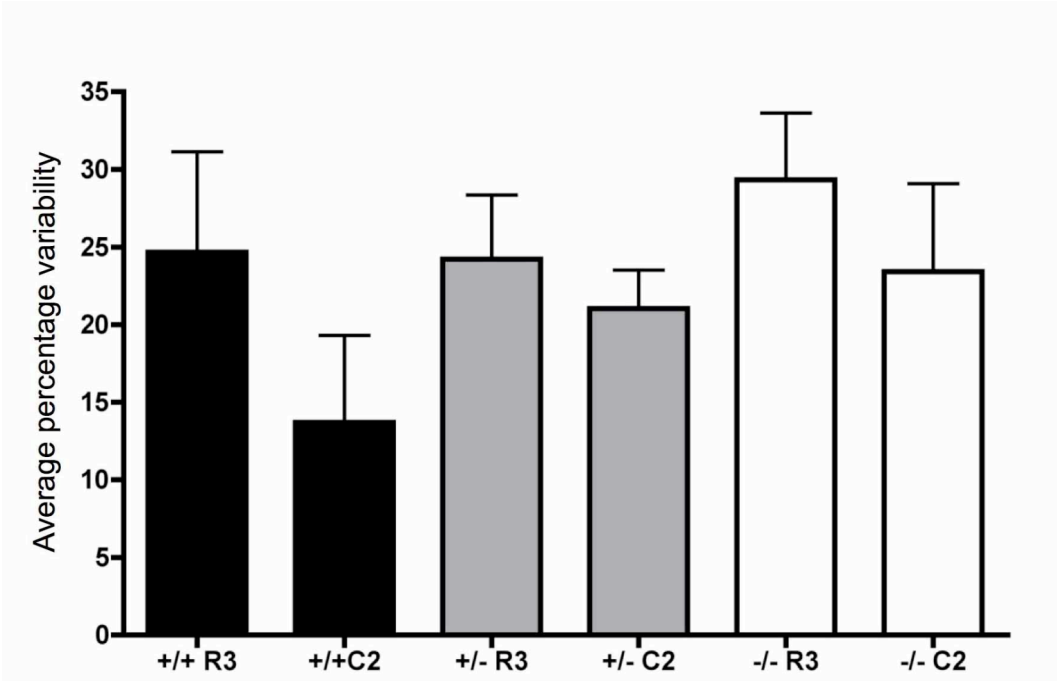

Figure 10.1.4: Average percentage variability between three individual axons counts. Bar chart (mean ± SEM) showing the average percentage variability (range between three individual counts on the same axon bundle, divided by the average of the three values and multiplied by 100%) supplying regions R3 and C2 in wildtype (black bars), heterozygote (grey bars) and Smn-/-;SMN2 (white bars) mice. Note the general trend for less variabilty in region C2 which may be accounted for by increased axon branching in region R3. *(N=4/5 per wildtype rostral/caudal band; N=7/5 per heterozygote rostral/caudal band; N=10/10 per knock-out rostral/caudal band.)*

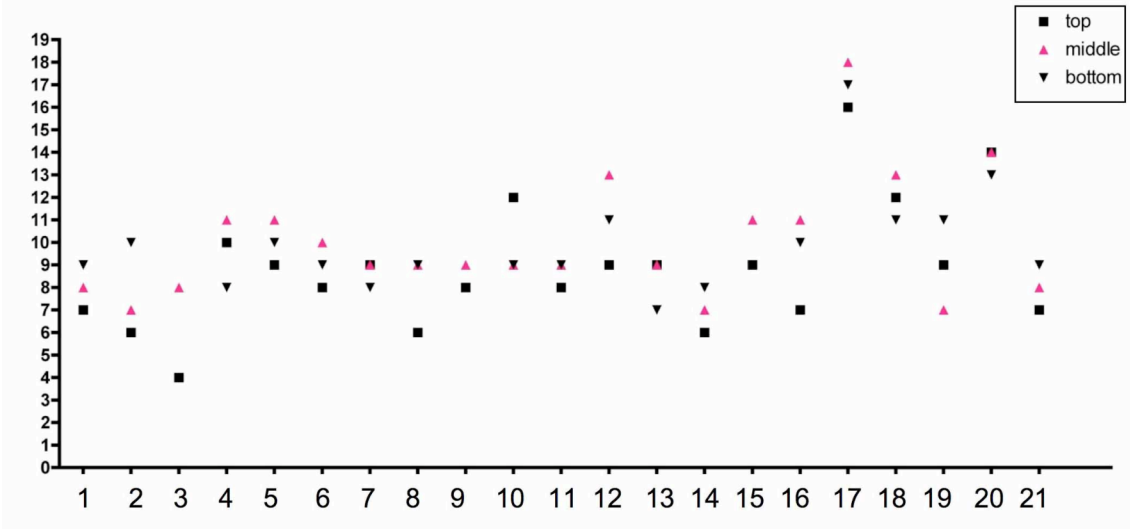

Figure 10.1.5: Axon branching does not account for the variability seen in axon counts. Scatter plot showing the value for each of the three counts on 21 axon bundles counted. The 'middle' count (see figure 3) is shown in pink. Note the middle value is the highest 10/21 times indicating axon branching does not account for the variability seen and we are therefore justified in using minimal variability as a reliable measure of a good counting technique.

Appendix 10.2 Maintenance of *wasted* mice on a heat-mat mildly ameliorates neuromuscular pathology and abolishes protection from Wallerian degeneration.

10.2.1 Maintenance on a heat-mat can ameliorate pathology in wasted mice.

During the course of these experiments, it was observed that maintaining particularly sick mice on a heat mat appeared to mildly ameliorate symptoms and increase expected life span by up to 12 hours. For this reason, a number of litters from the *wasted* colony were maintained on a heat-mat from the point of weaning. To investigate whether the heat-mat had any affect on NMJ pathology, endplate occupancy was compared in mice maintained on a heat-mat *(wasted HM)* to those maintained at normal room temperature *(wasted)*. In the LAL muscle, significant denervation was evident in muscles from both groups, however there was a significant increase in the number of fully occupied endplates in *wastedHM* mice (Figure 10.2). A similar trend was evident in the TVA muscle although this did not reach statistical significance (Figure 10.2 B). I also observed a significant increase in the body weight in *wasted*HM mice (Figure 10.2 C).

It is currently unclear whether this apparent protection from *wasted* pathology is due to an increase in temperature or an increase in physical activity. Maintaining mice on a heat mat increases their physical activity and conversely physical activity tends to increase body temperature. It is therefore experimentally very difficult to separate these two processes to determine whether it is the warmth or activity which exerts the neuroprotective affect, delaying the progression of dying-back pathology. Nonetheless, this finding perhaps warrants further study as if heat and/or exercise can be of therapeutic value, both would be relatively simply to apply and therefore be of potential clinical interest.

10.2.2 Maintenance on a heat-mat reduces protection from Wallerian degeneration seen in wasted mice.

The mice which were maintained on a heat-mat also underwent a tibial nerve cut and the NMJ phenotype was analysed 24 hours later. Interestingly, in stark contrast to the significant protection observed in *wasted* mice with around 90% of endplates remaining

innervated, only around 15% of NMJs remained in *wastedHM* mice (Figure 10.2 D). This result suggests that maintaining mice on a heat-mat dramatically reduces the protection of Wallerian degeneration observed in *wasted* mice.

As discussed above, it is unclear whether this is a result of increased activity or an increase in temperature. However, as all *wasted* mice are maintained on a heat mat post operatively, this finding suggests that it is not due to altered temperature or activity during the course of Wallerian degeneration, and rather due to an intrinsic alteration in the neuromuscular system occurring prior to the nerve axotomy. These findings may be in line with the suggestion that the protection from Wallerian degeneration seen in *wasted* mice is due to a delay in the maturation of the neuromuscular system and retention of a immature phenotype in which distal extremities are protected while proximal nerve stumps are subject to degeneration. An increase in activity due to the heat-mat may accelerate neuromuscular development and therefore result in the normal adult progression of Wallerian degeneration. Alternatively, it is also possible that the heat-mat can in some way, either by direct temperature affect or via physical activity, increase or prolong the expression of other eEF1A isoforms which can then compensate for the loss of eEF1A2. This might explain the observed reduction in neuromuscular pathology and indicate a requirement for eEF1A isoforms for the normal initiation and progression of Wallerian degeneration. This phenomenon clearly required further investigation but may give important insight into the mechanisms of both *wasted* pathology and neuromuscular degeneration.

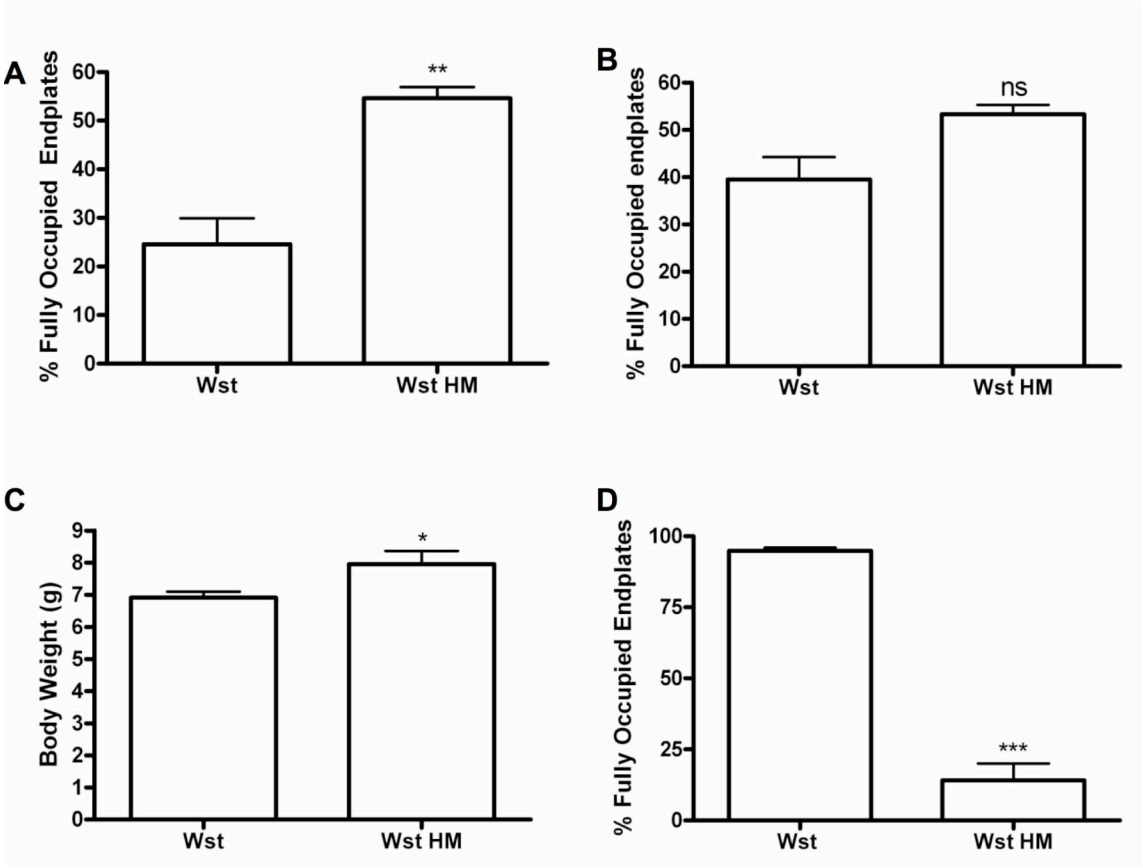

Figure 10.2: Mice maintained on a heat-mat show modest amelioration from NMJ pathology and reduced protection from Wallerian Degeneration. A,B - Bar chart showing the percentage of fully occupied endplates the LAL (A) and TVA (B) muscles of P25 wild-type mice, *wasted* mice (Wst) and *wasted* mice maintained on a heat mat from weaning (WstHM). C - Bar chart (mean ± SEM) showing body weight of *wasted* mice compared to *wasted* mice maintained on a heat mat from weaning (Wst HM). **D** - Bar chart (mean ± SEM) showing the percentage of fully innervated endplates in lumbrical muscles 24 hours post nerve cut from *Wasted* mice compared to *wasted* mice maintained on a heatmat from weaning. Note protections from denervation seen in *wasted* mice is significantly reduced in those time maintained on a heatmat. *(mean ± SEM; Mann Whitney U test (A,B,D) or Students T test (C); ns – non significant, *P<0.05, **P<0.01, ***P<0.001); A-C: N=6 mice/12 muscles wasted, 4 mice/8 muscles wasted HM. D: N=6 mice/12 muscles wasted, 3 mice/8 muscles wasted HM)*.

Appendix 10.3 Delay in Wallerian degeneration in heterozygous *wasted*;YFP-H mice.

In order to maximise N number for this study, tibial nerve cuts were performed on *wasted*;YFP-H mice alongside mice from non-fluorescent *wasted* strains. However during this study there was an increase in the number of fully occupied endplates after axotomy in heterozygous mice from the YFP-H background (Figure 10.3). This finding is somewhat preliminary, and unfortunately was not corroborated by including wild-type YFP-H mice. However this finding does indicate that mice on a YFP-H background display a delay in Wallerian degeneration. While these mice were excluded from results for the current study they do raise important considerations for the study of the neuromuscular system.

It is not clear whether this result is due to an alteration in genetic background or as a direct consequence of the YFP present in motor neurons. Should the effect be due to the presence of YFP, this would have rather major consequences for research, as 'inert' fluorescent markers are commonly used to visualise many different cell types and structures, including motor neurons. It is therefore important to determine whether YFP can have an affect on normal neuronal homeostasis and/or degenerative pathways. These experiments are on going in the Gillingwater lab and could potentially yield important results for a wide range of research fields.

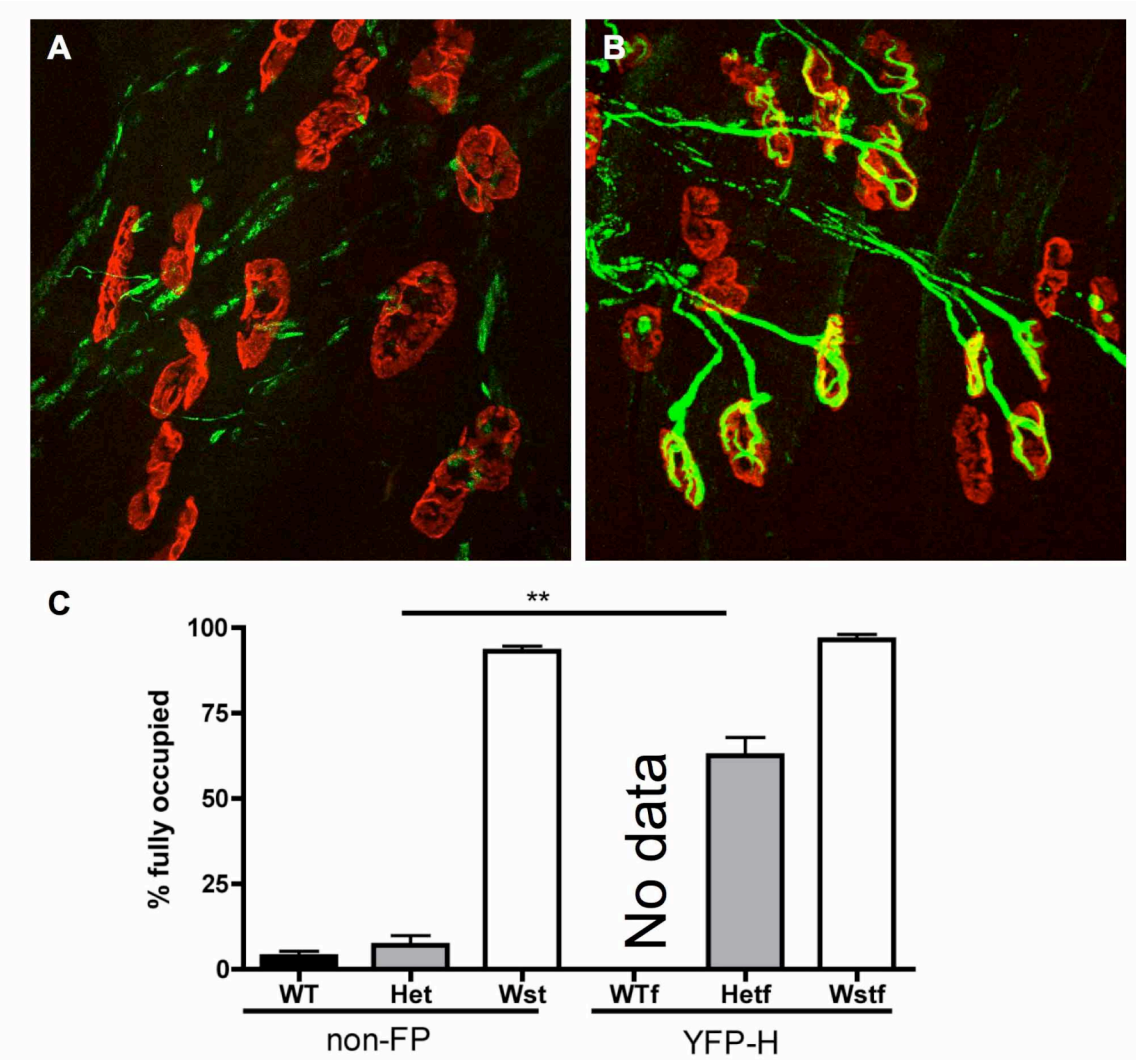

Figure 10.3: A delay in Wallerian degeneration was observed in *wasted* heterozygote mice crossed with YFP-H. A,B - confocal micrographs from immunocytochemcally labelled lumbrical muscles from heterozygote *wasted* and *wasted;YFP-H* mice (Green = 150KDa Neurofilaments; Red = post-synaptic acetylcholine receptors). C – Bar chart (mean ± SEM) showing the percentage of fully occupied endaplates in wild-type, *wasted* heterozygote and *wasted* homozygote lumbrical muscles from both non-YFP strains and YFP-H strains. Note an increase in the percentage of fully occupied endplates in heterozygous *wasted;YFP-H* mice compared to non YFP-H heterozygous *wasted* mice. *(Kruskal Wallis with Dunn's multiple comparison test; ** P<0.01; N=32/33/14 muscles WT/Het/wasted non YFP-H, N=0/9/15 WT/Het/wasted YFP-H).*

Appendix 10.4 Background fluorescence intensity measurement methodology in quantitative western blotting.

In this study, I have used quantitative fluorescent blotting to measure protein levels as it is thought to give greater sensitivity than densitometry analysis on conventional western blots. This system employs secondary antibodies labelled with infra-red dyes which can be detected using an infrared imaging system (Oddysey ®). Laser levels can be altered to optimum conditions to detect faint bands while avoiding saturation of strong bands. Oddysey imaging software can be used to visualise bands and by subtracting background fluorescence levels from fluorescence intensity of the band, it gives a measure of relative protein levels in neighbouring bands. This system offers many advantages over traditional western blotting with densitometric analysis, including greater sensitivity and a wider dynamic range.

Within this system, several different methods are available to calculate background intensity levels. To define the area for background measurement either a 'lane' (which measures the signal intensity within the lane of the band) or a box (which measures the signal intensity under the box outline) can be used. For the latter method, the background levels can reflect either the whole outline, left and right or the top and bottom of the box, and can reflect either mean or median values. As this measurement will clearly have a great impact upon results, I felt it was important to determine whether the method of background measurement had any bearing on the reliability of results. I therefore measured the signal intensity on a number of blots using a variety of methods to calculate background: lane, box with mean intensity value, box with median from all 4 sides or box with median from just the left and right sides. To give an indication of how much variability is introduced by use of a different background measurement method, the following formula was applied:

$$\% \text{ variability} = [(i_{B1L1}/i_{B2L1}) - ((i_{B1L1}/i_{B2L1} + i_{B1L2}/i_{B2L2} + i_{B1L3}/i_{B2L3})/3)]*100\%$$

where i = fluorescence intensity; B = band (1 or 2); L = laser level settings (1, 2 or 3).

By making resultant values positive, the percentage that each measurement deviates from the average of three measurements at different laser settings can eb determined and thus measure the variability introduced by the quantification methodology

The above analysis was applied to western blot membranes labelled for COX1, which give a strong signal with a high signal to noise ration. This revealed that there was very little variability between different scan settings and the method of background quantification has little bearing upon the result (Figure 10.4 A). I next applied this analysis to a membrane labelled for VDAC1, an antibody which gives a distinct, but none the less faint band, with a low signal to noise ratio. In this event, method of background quantification had a significant impact upon the observed variability, with the lane method producing the highest degree of variability between laser settings, of up to 15% (Figure 10.4 B). Measuring background using mean background levels, as oppose to median values marginally decreased the variability. Due to the sensitivity of the system, some antibodies, such as β-Actin, label a variety of non-specific products thus producing a laddering type effect. Quantification of blots labelled with β-Actin again indicated that background quantification method has a significant bearing on the reliability of results, with the method using the box outline to measure the mean signal intensity producing significantly less variability than the other three methods (Figure 10.4 C).

From this analysis, I conclude that the method used to quantify background fluorescence levels has little affect on result reliability when measuring a strong band with a high signal to noise ratio but can have significant effects when measuring blots with a low signal to noise ratio or multiple bands. The consistently most reliable method of background measurement was using the box outline to measure the mean signal intensity and I have therefore employed this method for the western blot quantification for thus study.

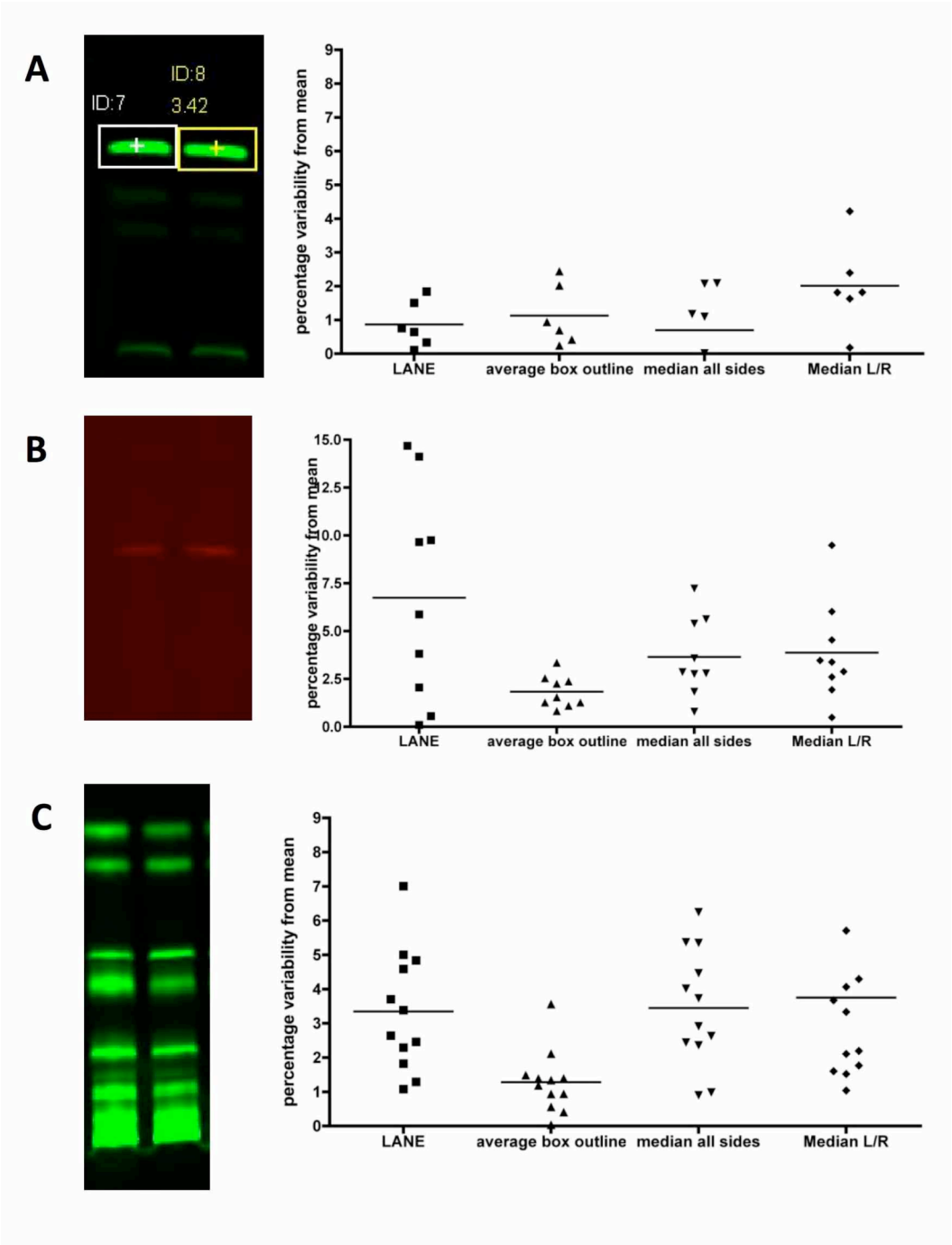

Figure 10.4 – Variability in signal intensity levels by different measuring methods. A – Example image from a COX1 antibody showing a high signal to noise ratio (left). Scatter plot showing that quantification of these bands at different scan settings by use of any of the 4 methods available to calculate background intensity (lane, average box outline, the median of all sides or median of left and right sides) gives relatively similar variability. B,C quantification of bands from blots which have either a low signal to noise ratio (B left) or multiple bands present (C left) reveals different methods of background calculation produce significantly different levels of variability (B,C right). Use of the average box outline to calculate background gives consistently lower variability. *(Data for scatterplots acquired by subtracting the average percentage difference in band intensity between 2 bands across 3 different scan intensity settings, from the percentage change seen at a single scan intensity setting. Data was obtained from 3 different scan settings from 2(A), 3(B) or 4(C) separate blots.*

Appendix 10.5 SmnWld^s breeding strategy and genotyping

Although relatively simple in concept, obtaining homozygous SmnWld^s (*Smn-/-;SMN2*;Wld^s+/+) mice, along with relevant littermate controls, has become a significant challenge. The breeding strategy firstly involved a cross between a Smn+/-;SMN2 mouse and a homozygous Wld^s mouse (Wld^s+/+; Figure 10.5.1). Interbreeding offspring from this initial cross which were which were heterozygous for Smn (Smn+/-;SMN2+/-;Wld^s+/-) could then potentially produce 27 genetic combinations (Figure 10.5.1, stage 2). Smn heterozygotes could be readily identified by conventional PCR protocols. Conventional PCR could also be used to identify mice carrying the SMN2 transgene and as the insertion site of the SMN2 transgene had not yet been mapped, quantitative real-time PCR was required to determine SMN2 copy number to distinguish between SMN2+/- and SMN2+/+ mice (Figure 10.5.2; protocol courtesy of Nick Parkinson). At this point, the preferable breeding strategy would have been to interbreed Smn+/-;SMN2+/+;Wld^s+/- mice to produce litters which contain both *Smn-/-;SMN2*+/+;Wld^s+/+ mice along with *Smn-/-;SMN2*+/+;Wld^s-/- littermate controls. Unfortunately at this point, problematic Wld^s genotyping made it difficult to accurately distinguish between genotypes, making heterozygotes particularly difficult to identify (Figure 10.5.3 A). This protocol relies on simultaneous amplification of the NMNAT portion of the Wld^s gene and tubulin in a single well with different fluorophores indicating relative levels of NMNAT compared to endogenous tubulin control (Wishart *et al.*, 2007b). Although amplification was successful, and all controls generally grouped by cycle number, a slight overlap at the boundaries of each genotype meant I could not confidently genotype animals of unknown Wld^s status. After many unsuccessful attempts at protocol optimisation, I decided to back cross mice which consistently had a high cycle number difference, and were therefore likely to be Wld^s homozygotes, with *Smn-/-;SMN2* mice. All resultant mice should therefore be Wld^s heterozygotes. This step had the added benefit of increasing genetic similarity to the original *Smn-/-;SMN2* strain thereby minimising effects of genetic modifiers. Concurrently with this, new attempts were made to genotype for Wld^s copy number by using real-time PCR protocol used for SMN2 genotyping (Figure 10.5.3 B). This method

uses amplification of Wld^s and endogenous control uses the same fluorophore in separate wells and has thus far given much better separation between genotypes, allowing identification of Wld^s homozygote, heterozygote and wild-type mice. Unfortunately, due to the time consuming nature of these problems, appropriate genetic mice have only very recently become available and I are therefore at the very early stages of phenotypic analysis.

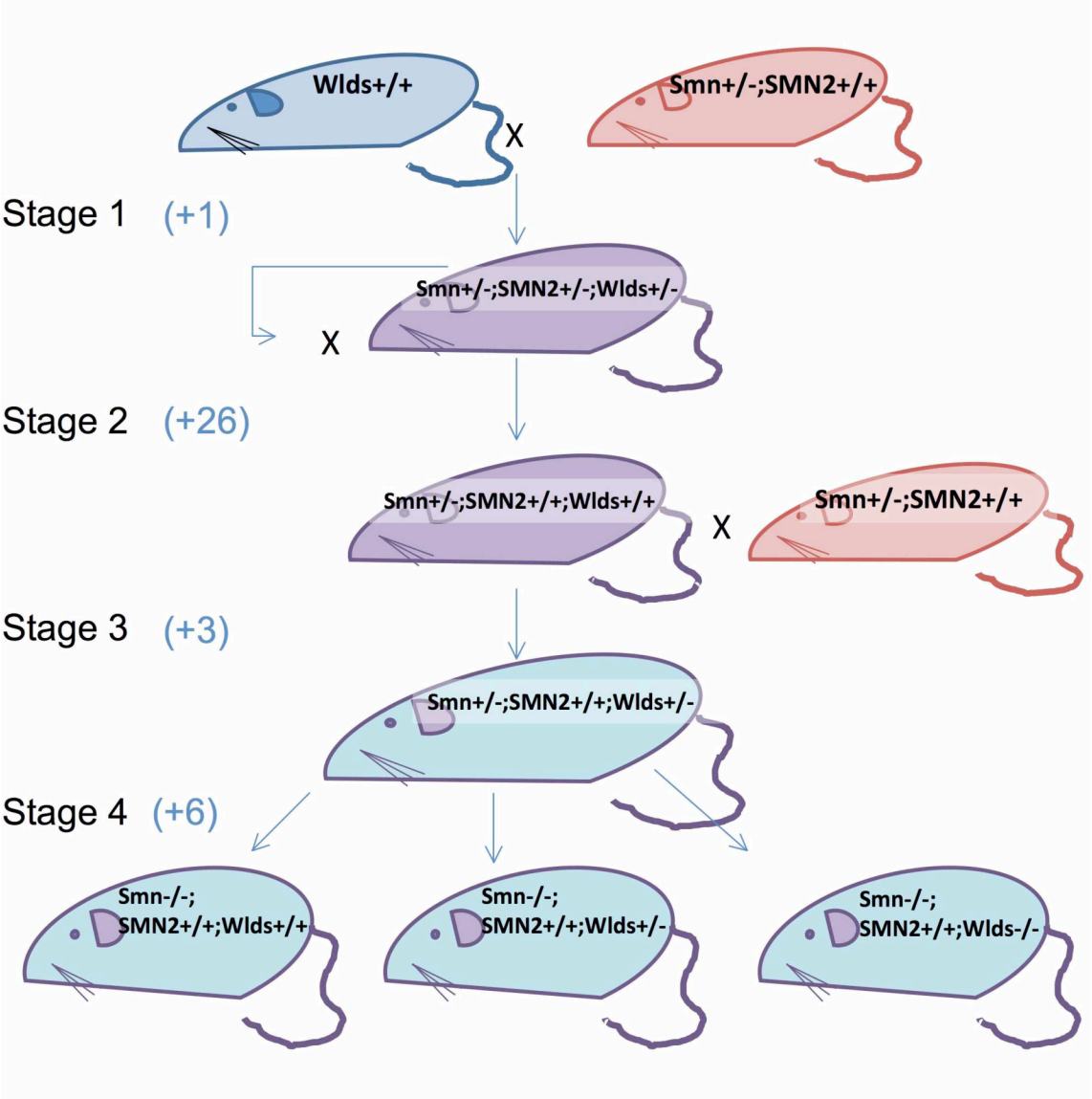

Figure 10.5.1: Breeding strategy to produce experimental SmnWld^s mice. To obtain *Smn-/-;SMN2*;*Wld*^{s} mice, the above breeding plan was employed. Number in blue denote the number of additional undesirable genetic combinations produced at each breeding stage. Due to problems with Wld^s genotyping, resulting in homozygous mice being easiest to identify, stage 3 was employed to ensure the production of Wld^s heterozygous mice until genotyping issues could be resolved.

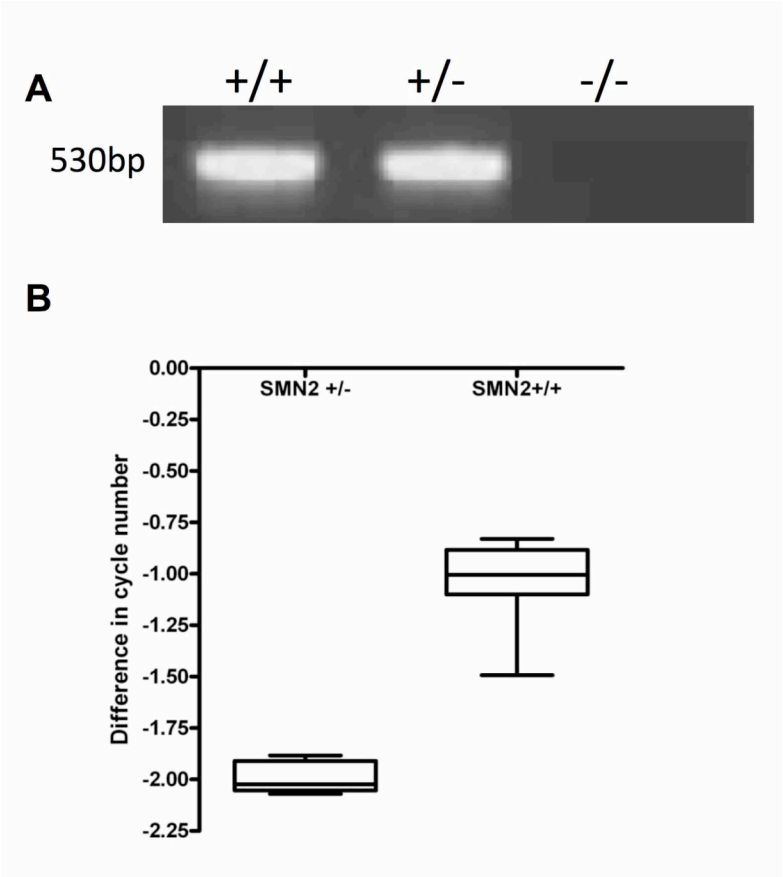

Figure 10.5.2: Conventional and quantitative methods of PCR genotyping for SMN2. A – Conventional PCR and gel electrophoresis allowed identification of mice which carried the SMN2 transgene by presence of absence of a product at 530bp however this method does not distinguish between 1 or 2 copies of the transgene. B – Box and whisker plot showing the expected cycle number differences produced from analysis of real-time quantitative PCR curves. Note SMN2 homozygotes and hetoerozygotes can be easily distinguished.

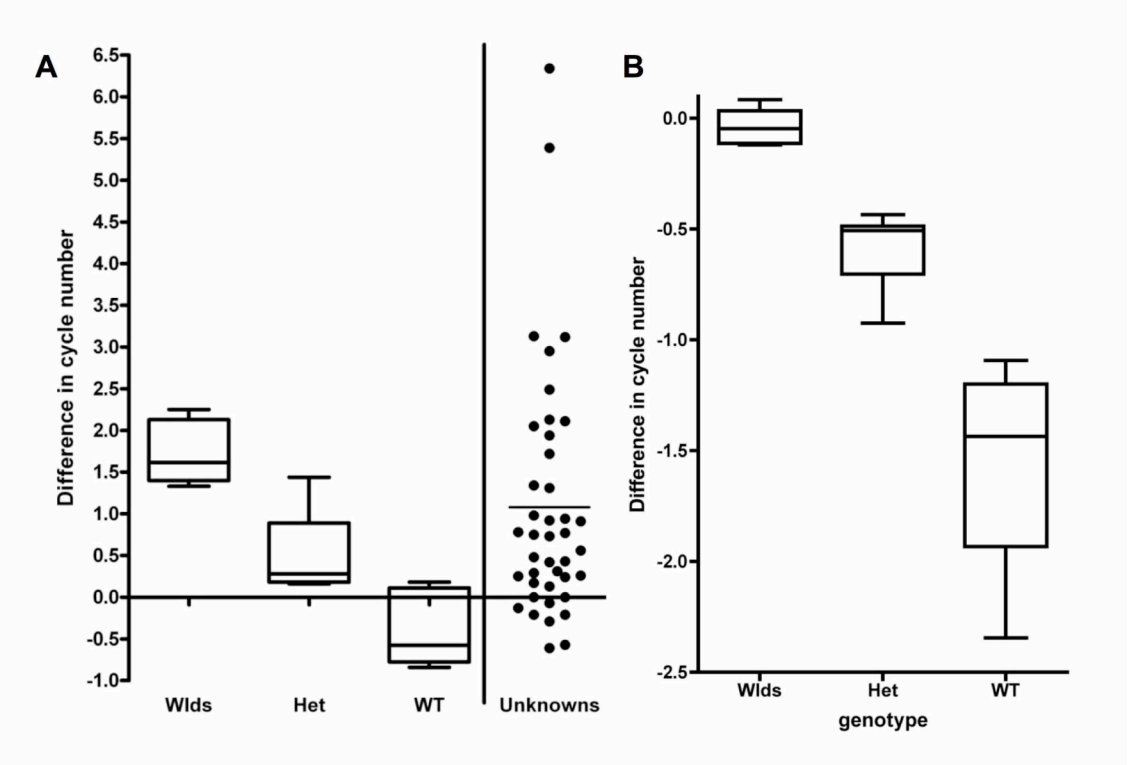

Figure 10.4.3: Real-time quantitative PCR results for assessing Wld^s copy number. A - Box and whisker plot showing the difference in cycle number produced when using the original real-time PCR protocol. Note that although, in general, genotypes separate by difference cycle number, there is modest overlap at the boundary between genotypes. This makes it difficult to definitively genotype animals of unknown genotype. B - Box and whisker plot showing the difference in cycle number produced when using the modified real-time PCR protocol, with different primer sets in different wells. Note genotypes group by cycle number with significant separation between each genotype.

Appendix 10.6 Publications

10.6.1 Papers: published and under review

Murray LM, Comley LH, Thomson D, Parkinson N, Talbot K, Gillingwater TH. Selective vulnerability of motor neurons and dissociation of pre- and post-synaptic pathology at the neuromuscular junction in mouse models of spinal muscular atrophy. Hum Mol Genet. 2008; 17: 949-962.

Murray LM, Thomson D, Conklin A, Wishart TM, Gillingwater TH. Loss of translation elongation factor (eEF1A2) expression in vivo differentiates between Wallerian degeneration and dying-back neuronal pathology. J Anat. 2008; 213: 633-645.

Soriano FX, Baxter P, **Murray LM**, Sporn MB, Gillingwater TH, Hardingham GE. Transcriptional regulation of the AP-1 and Nrf2 target gene sulfiredoxin. Molecules and Cells. 2009; **27**:279-282

Murray LM, Talbot K, Gillingwater TH. Neuromuscular Synaptic Vulnerability in Motor Neuron Disease: Amyotrophic Lateral Sclerosis and Spinal Muscular Atrophy. Neuropathol Appl Neurobiol. *In Press*

Murray LM, Lee S, Bäumer D, Parson SH, Talbot K, Gillingwater TH. Pre-symptomatic development of lower motor neuron connectivity in a mouse model of severe spinal muscular atrophy. Hum Mol Genet. *In Press*

Bäumer D, Lee S, Davies J, Nicholson G, Parkinson NJ, **Murray LM**, Gillingwater TH, Davies KE, Talbot K. Alternative splicing events are a late feature of pathology in a mouse model of Spinal Muscular Atrophy. PLoS Genetics. *In Press*

10.6.2 Conference abstracts

Edinburgh neuroscience day - 2007 - Poster

"Synaptic Pathology in Childhood Motor Neuron Disease (Spinal Muscular Atrophy)."

Anatomical Society of Great Britain and Northern Ireland, 2007, Durham - Poster

"Synaptic Pathology in Childhood Motor Neuron Disease (Spinal Muscular Atrophy)."

Society for Neuroscience, 2007, San Diego - Poster

"Synaptic Pathology at the Neuromuscular Junction in Childhood Motor Neuron Disease."

UK SMA, 2007, Oxford - Poster

"Synaptic Pathology at the Neuromuscular Junction in a Mouse Model of Childhood Motor Neuron Disease."

Edinburgh Neuroscience Day, 2008 - Poster

"Synaptic pathology at the neuromuscular junction in childhood motor neuron disease (Spinal Muscular Atrophy; SMA)"

Anatomical Society of Great Britain and Northern Ireland, 2008, Nottingham - Poster

"Loss of translation elongation factor eEF1A2 differentially affects pathways responsible for dying-back neuropathy and Wallerian degeneration *in vivo*."

UK SMA, 2008, Sheffield – Poster and Talk

*"*Loss of translation elongation factor eEF1A2 differentially affects pathways responsible for dying-back neuropathy and Wallerian degeneration *in vivo."*

Anatomical Society of Great Britain and Northern Ireland, 2009, Oxford - Talk

"Synaptic Vulnerability in Spinal Muscular Atrophy."

Families of Spinal Muscular Atrophy, 2009, Cincinnati – Poster and Talk

*"*Does abnormal neuromuscular development underlie selective vulnerability of motor units in mouse models of Spinal Muscular Atrophy?"